Title

Fullerene-porphyrin cocrystallization, the varied reactivity of titanium (IV) chloride, and the metal-mediated oxidative coupling of tertiary arylamines

Permalink

Author

Roy, Mrittika

Publication Date

2021

Peer reviewed|Thesis/dissertation

Fullerene-porphyrin co-crystallization, the varied reactivity of titanium (IV) chloride, and the metal-mediated oxidative coupling of tertiary arylamines

By

MRITTIKA ROY
DISSERTATION

Submitted in partial satisfaction of the requirements for the degree of

DOCTOR OF PHILOSOPHY

in

Chemistry

in the

OFFICE OF GRADUATE STUDIES

of the

UNIVERSITY OF CALIFORNIA

DAVIS

Approved:

_____
Alan L. Balch, Chair

_____
Philip P. Power

_____
R. David Britt

Committee in Charge

2021

To my mother Sucharita Roy, and Professor Marilyn M. Olmstead.

Abstract

This dissertation attempts to summarize two of the author's several research projects – in separate, broadly disparate areas of chemistry. Chapters I, II and III discuss the structural chemistry of fullerenes while chapters IV, V, VI and VII discuss metal-mediated chemistry focusing on the oxidative coupling of tertiary amines. All of the doctoral research performed during the author's time in the Balch group is not covered in this dissertation. Instead, two representative areas of chemistry have been chosen.

In Chapter I, we discuss the relationship between the shape and geometry of fullerenes, and the arduousness of their structural characterization. An elegant solution to this problem is the technique of cocrystallization, which is discussed in this chapter. Chapter II explores the use of this technique of cocrystallization in the analysis of two endohedral metallofullerenes. The two compounds are isostructural and their crystal structure is discussed in detail, paying special heed to peculiarities in porphyrin conformation. This and other variations in the nature of porphyrin-fullerene association leads us to a systematic study of the phenomenon of cocrystallization, which is discussed in Chapter III. The variation in the ratio of porphyrins binding each fullerene, as well as how conformational changes in the porphyrin affects the quality of "ordering" experienced by the fullerene, is explained in this Chapter. We look at two separate parameters – metal-ion effects, and solvent/solvate effects. We do not delve into the C-C bond activation chemistry of fullerenes and the various strategies employed in the functionalization of C_{60}, but a recent positive outcome of our efforts to synthesize a metal-inserted heterofullerene is briefly mentioned in the conclusion to Chapters I, II and III.

Chapter IV discusses *some* of the various reactivity shown by titanium (IV) chloride in the coordination chemistry performed with it. Titanium (IV) chloride has been demonstrated over the course of this project to act as a halogenating agent, halogen abstraction agent, oxidizing agent, radical stabilizer (in form of a noncoordinating anion), in addition to its pedestrian role as a small, hard metal center capable of ordinary coordination chemistry. We discuss two different behaviors it exhibits towards tertiary phosphines, and then examine its behavior towards tertiary amines.

Chapter V explores the direct crystallization of radical cations of amines, through one-electron oxidation, by using titanium (IV) chloride as oxidant. This process for isolating crystalline forms of tertiary amine radicals is unprecedented. Simultaneously, we compare two other closed-shell metal halides, antimony (V) chloride and tin (IV) chloride, in similar systems. All three metal halides are shown to perform direct crystallization of suitable tertiary amine radicals. However, we begin to see variation in the behavior of these metal halides in Chapters VI and VII, where we deliberately choose tertiary amines that are capable of further association to form diamines. A metal-dependent selectivity of the diamine product formed is observed. This is not only novel but also remarkably significant to the field of triarylamine-based charge transfer materials, where the nature of the π-system bridging the nitrogen centers in di- or polyamines massively influences the redox properties of the system. Our technique for metal-mediated "tuning" of the diamine product leaves room for a great deal of future work in exploiting oxidative coupling reactions for preferential formation of charged diamine species. We have also demonstrated a time-dependent product conversion that, with more refinement of kinetic control, can be established as a second metric for diamine selectivity.

Acknowledgments

I am thankful to have joined the Balch Group in my first quarter as a graduate student at UC Davis and to have had Professor Alan L. Balch as an advisor and mentor. Being part of his group has afforded me the tremendous mentorship of not only Professor Balch himself, but also my co-advisor, the late Professor Emerita Marilyn Olmstead. Professor Balch has a unique advising style where he calibrates his involvement and instruction to the needs of his students, and I was allowed more freedom than I would have been in any other laboratory. He provided me with direct mentorship wherever needed, such as to strengthen my skills in academic writing, teaching and science communication, while leaving me free to make my own mistakes in the laboratory and learn from them. I gained an immense amount of knowledge about the fields of fullerene chemistry, coordination chemistry, the inception of electrochemistry, and modern spectroscopy techniques from simply our day-to-day conversations, where I hung on to each word. I am in awe of his expertise and experience and could not have asked for a better mentor. Thank you for being a reservoir of knowledge and advice than I could call upon whenever I was stuck on a problem – from using an abderhalden drying pistol to finetuning my understanding of peak-splitting, I could always turn to you.

I wish I could personally thank Professor Marilyn M. Olmstead, who tragically will not get to see me accomplish this milestone. Although she started out as a mentor, she became my friend at some point during our hours-long sessions of trying to refine refractory fullerene structures. Thank you for your gifts of pomegranate jelly and infinite wisdom, and for being a steadfast source of support, enthusiasm and joy during our three years together. I can only hope to be half the mentor you were to me, to a future student someday.

I learnt a great deal from him about teaching large classes and engaging students, and I hope to put that training to good use someday. I would like to express my sincerest thanks to Dr Jeff Walton for partnering with me on the EPR section of this dissertation as well as other projects, and for lending his immense expertise on a subject I was initially entirely unfamiliar with. Lastly, I would like to thank Professor Dave Britt for stepping in to replace Marilyn on this dissertation committee.

I am also immensely grateful to my immediate predecessors in the Balch lab, Dr Xian Powers, Dr Daniel Walters and Dr Lucy Luong. To Xian, in particular, I owe a lot of my success as a fullerene chemist and crystallographer. Amongst my friends in this department, I am particularly grateful to Cary Stennett from the Power Lab, for being a great friend, an exceptional peer, and a helping hand whenever I needed one. I want to thank Kathleen Becker from the Osterloh group for being someone I could always share my academic woes with, and for keeping me sane during the crushing loneliness of quarantine. My amazing undergraduate researchers, Isaac and Merissa, make me proud every day and I am so glad to have been able to work alongside them. Finally, I want to thank my lab mates in the Balch Lab, as well as the various excellent friends I have made in this department – Chris, Kasey, Brian and Steven.

Lastly, I would love to thank my friends and family outside of this institution, for seeing me through to the end. My parents – for letting me dream big when I was precocious twelve-year-old on the wrong side of the globe, with opinions on the special theory of relativity. If you hadn't fanned the flames of that curiosity and made sacrifices to help me follow through every step of the way, I would not be here. My grandma – for being the kindest and smartest women I have ever known, who could just as easily have been a scientist as anyone I work with. I hope your dreams and the dreams of generations of my exceptional female ancestors are somewhat vicariously realized through me. My extended family who supported me when I landed in a big, foreign

Table of Contents

Chapter I. An Introduction to the Structural Chemistry of Fullerenes: History, Geometry and Crystallography

Fullerenes (also known as Buckminsterfullerenes or buckyballs) are a molecular, crystalline allotrope of carbon and the only form of pure carbon to exhibit solubility in organic solvents. The most popular and abundant fullerene, C_{60}, adopts the shape of a truncated icosahedron formed entirely out of carbon atoms. The molecule belongs to the point group I_h and is thus highly symmetrical – a feature that informs its structural and chemical peculiarities. Due to each atom on C_{60} being symmetrically interchangeable with any other arbitrary atom on it, C_{60} contains only one kind of carbon atom and possesses a ^{13}CNMR signal with one single peak[1]: a feature promptly undone by any kind of functionalization that lowers the molecule's symmetry. The chemical properties of fullerenes are directly related to their structure – regions of flatness on the surface of the higher buckyballs correspond to greater aromaticity[2], while regions of increased pyramidalization or "bumpiness" correspond to more sp^3 nature[2]. While there is only one type of carbon atom on C_{60}[3], it forms two types of bonds: that at the junction of a hexagon and pentagon (5:6 junction, 1.45 ± 0.015Å) and that at the junction of two hexagons (6:6 junction, 1.40 ± 0.015 Å)[4], as shown in Figure 1. The 6:6 junction bond in C_{60} is of olefinic type by both bond length and as well as reactivity; the most common instance of fullerene-metal coordination involves η^2 complexation to molecules analogous to ethylene, occurring almost exclusively from the 6:6 junction bond[5,6]. The absence of a 5:5 junction bond in C_{60} is a matter dictated by solid geometry and enthalpy, which we shall examine shortly.
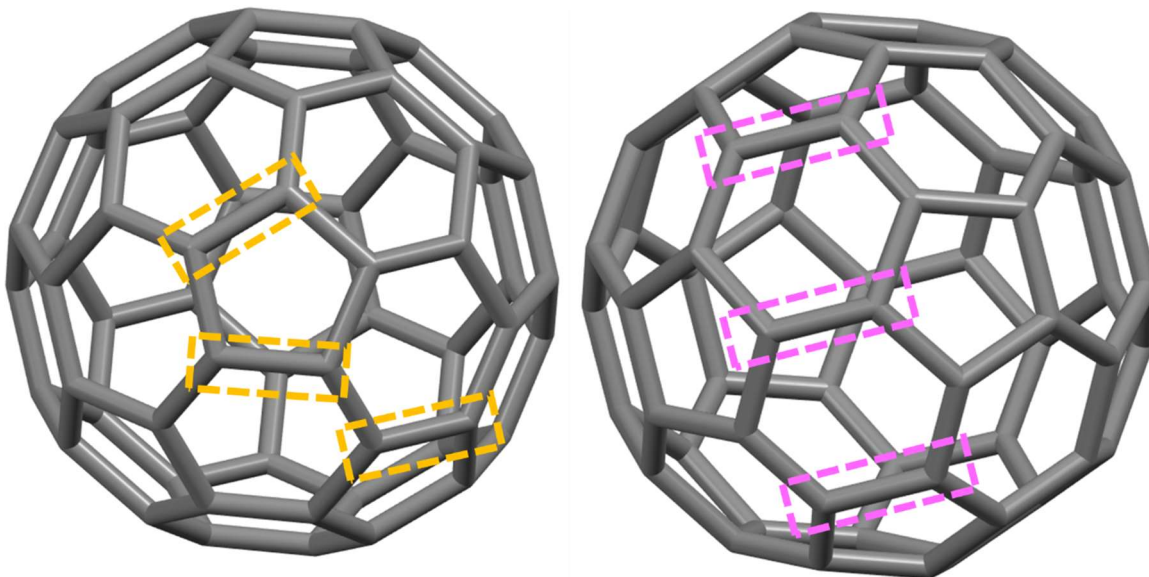
Fig 1. Two views of the C$_{60}$ molecule, down a C_5 axis (left) showing the 5:6 junction bonds in orange; offset from a σ_h (right) showing the 6:6 junction bonds in pink.

The truncated icosahedron is a shape that has been known to mankind for centuries – and studied extensively by during that time. Theorems pertaining to polyhedra (such as Euler's formula V+F-E=2 where V = vertex, F = face and E = edge) can be applied to the shapes formed by empty-cage fullerenes[7], which conform remarkably to principles of solid geometry. For instance, regardless of size and number of constituent carbon atoms, empty-cage fullerenes may only contain 12 pentagons (in keeping with Euler's formula), and any increase in size is accounted for by adding hexagons into the scaffolding[8]. This, unsurprisingly, affects the "roundedness" of the resulting shape (in our case, the fullerene)[9], and has great bearing on the nature of the carbon-carbon bond on any region of the fullerene's surface. A detailed analysis of the structure of a fullerene is thus imperative to fully comprehend its function.

Figure 2 shows Leonardo Da Vinci's illustrations of three crucial polyhedra for Italian mathematician Lucas Pacioli's sixteenth century book, The Divine Proportions. Platonic,

Archimedean, and Catalan solids are related through symmetry groups and operations as well as the operation of "truncation". When one truncates an icosahedron, each triangular face is transformed into a hexagon and each vertex where five triangles unite is turned into a pentagon – very similar to the phenomenon of disintegrating a pentagonal dodecahedron into its twelve constituent polygons, and then gluing it back together but with a belt of hexagons separating each pentagon from the others. Not only does this simple operation explain the relationship between three polyhedra belonging to the point group I_h, it sets up a premise for the Isolated Pentagon Rule. We must now turn our attention from regular polyhedra, towards polyhedra that can reasonably be constructed out of carbon.
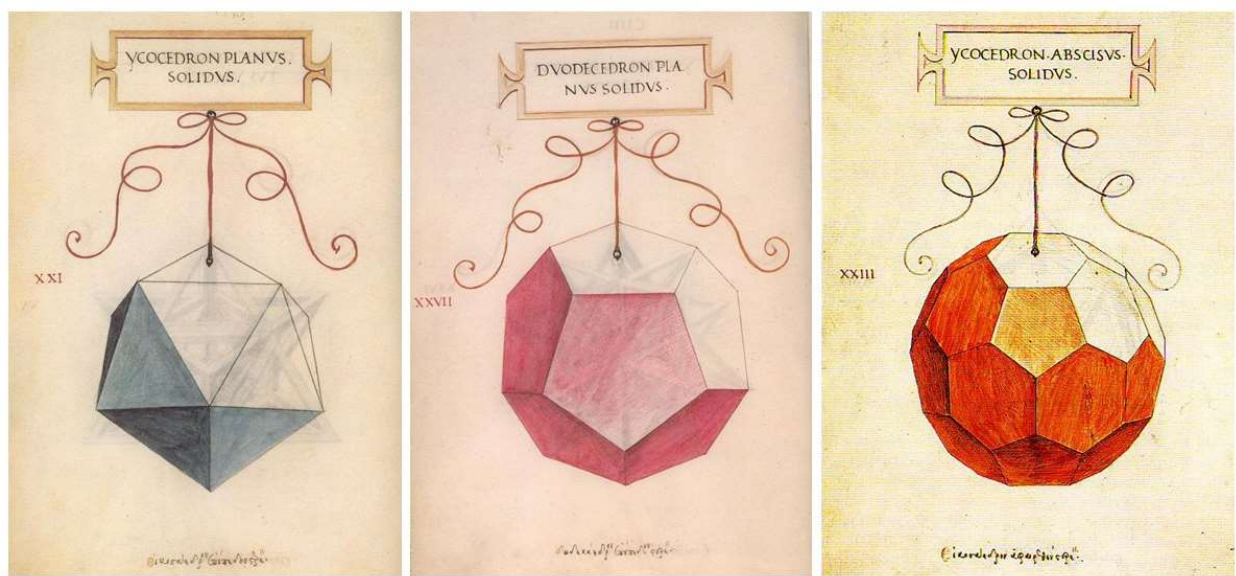
Fig 2. Da Vinci's illustrations of the solid forms of an icosahedron, a pentagonal dodecahedron and a truncated icosahedron from Luca Pacioli's *De Divina Proportione* (pictures sourced from "Luca & Leonardo – The Divine Proportion and a life-long Renaissance friendship" by Daryl Green).

The minimum number of vertices required to form a closed, regular polyhedron out of ≥ 5 membered rings is 20 – corresponding to a pentagonal dodecahedron. A vertex on a pentagonal

dodecahedral carbon cage is too pyramidalized to be stable as a variant of the sp^2 bonding type required in a pure fullerene, rendering the C_{20} fullerene unstable and non-isolable[10]. However, while pentagons give us curvature and "closing", hexagons supply flatness – and separating pentagons with a singular belt of hexagons softens up the bumpiness of C_{20} to just the right extent for thermodynamic stability of the resulting solid. It is no coincidence that the first member of the fullerene series to be discovered (and in such relative abundance) is C_{60} – which would be the smallest closed polyhedron constructed out of the same twelve pentagons, but with an adequate squashing of the dihedral angles owing to the hexagons. From C_{60} onwards, larger empty fullerenes are constructed out of the same twelve pentagons, but a varying number of hexagons to enlarge the size.[11]

C_{60} was discovered in 1985 by Harold Kroto, Richard Smalley and their team[12], who used laser vaporization of graphite and observed the masses of the resultant gas-phase molecules. Once the material proved isolable, the mathematical conjecture that its shape must be a truncated icosahedron found support in characterization by $^{13}CNMR$[1]. However, structural evidence eluded crystallographers for years. The first structure of C_{60} was obtained, quite arduously, in 1991 – only after osmylation of the molecule to lower its icosahedral symmetry so as to obtain an ordered crystal structure[13]. Attempts to grow crystals of C_{60} alone, or simply solvates, result in severe orientational disorder to the point that atoms and bonds are indiscernible[14–16]. The approach of lowering of symmetry by functionalization led to the first structure of C_{60} – and was followed by several instances of dihapto-coordination from the 6:6 junction bond in C_{60} to low-valent metal centers[17]. These coordination complexes point to crucial information regarding the chemical behavior of C_{60}, especially as a ligand, and ultimately help understand its electronic nature.[2] However, coordination or functionalization also fundamentally alters the very molecule that is

being studied. A more elegant solution to the problem of disorder can be found in deliberate cocrystallization – the phenomenon of adding a second molecule into the crystallization setup that can adequately interact or associate with a fullerene to cause significant ordering of the round molecule. A massive field of research has been dedicated to the design and synthesis of ideal cocrystallization agents for C_{60} – molecules that harvest its gentle curvature and pockets of aromaticity. Organic molecules with the ability to enter into pi-pi interactions, such as calixarenes, bowl-shaped molecules such as corranulene and its derivatives, substituted fulvalenes, calixarenes, phosphangulenes and porphyrins are all demonstrably capable of cocrystallizing C_{60} with sufficiently strong interaction to be able to order it[18–25]. Unlike simple solvates, neat C_{60}, or C_{60} cocrystallized with non-interacting molecules (Figure 3), cocrystals containing these molecules show clean, ordered C_{60} molecules with discernible bonds and atoms (Figure 4).
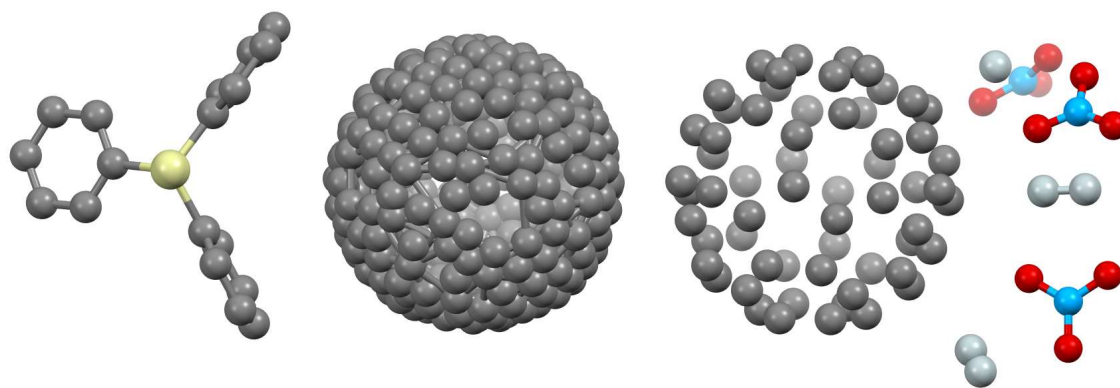
Fig 3. Severe disorder in C_{60} fullerene due to inadequate interaction and ordering influence[26]
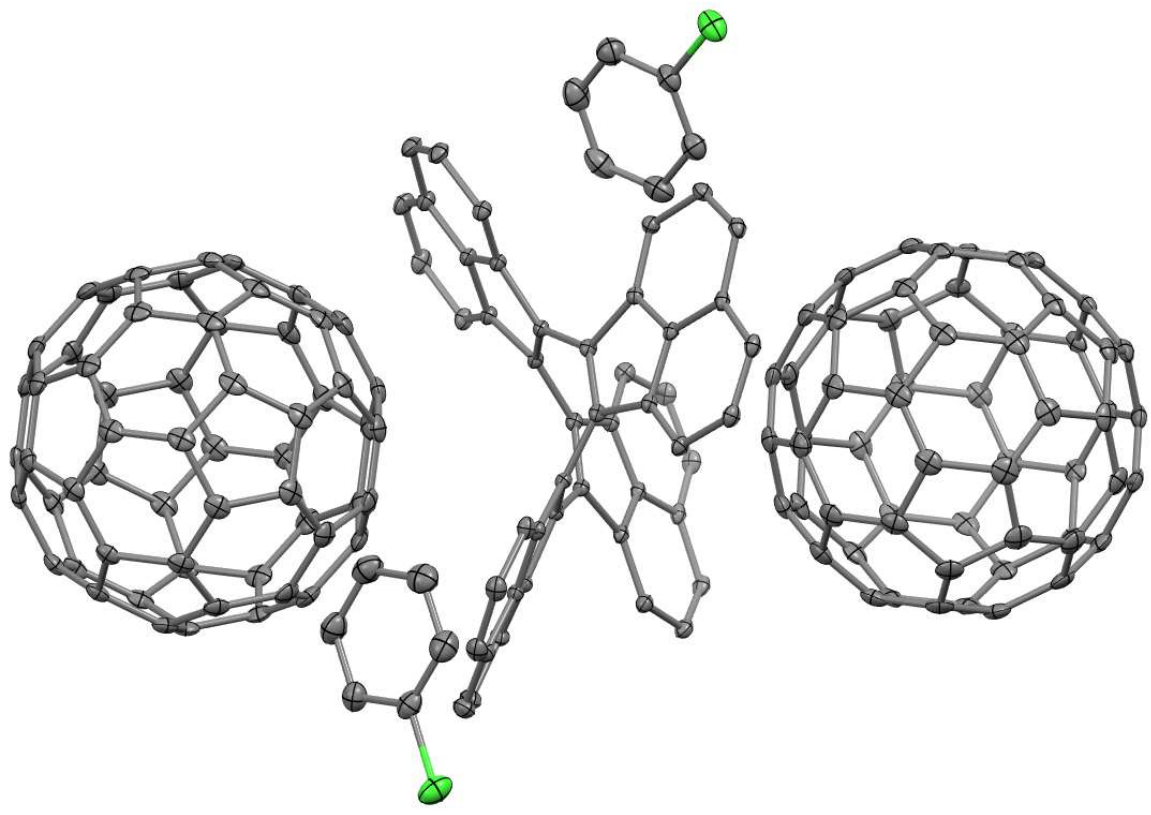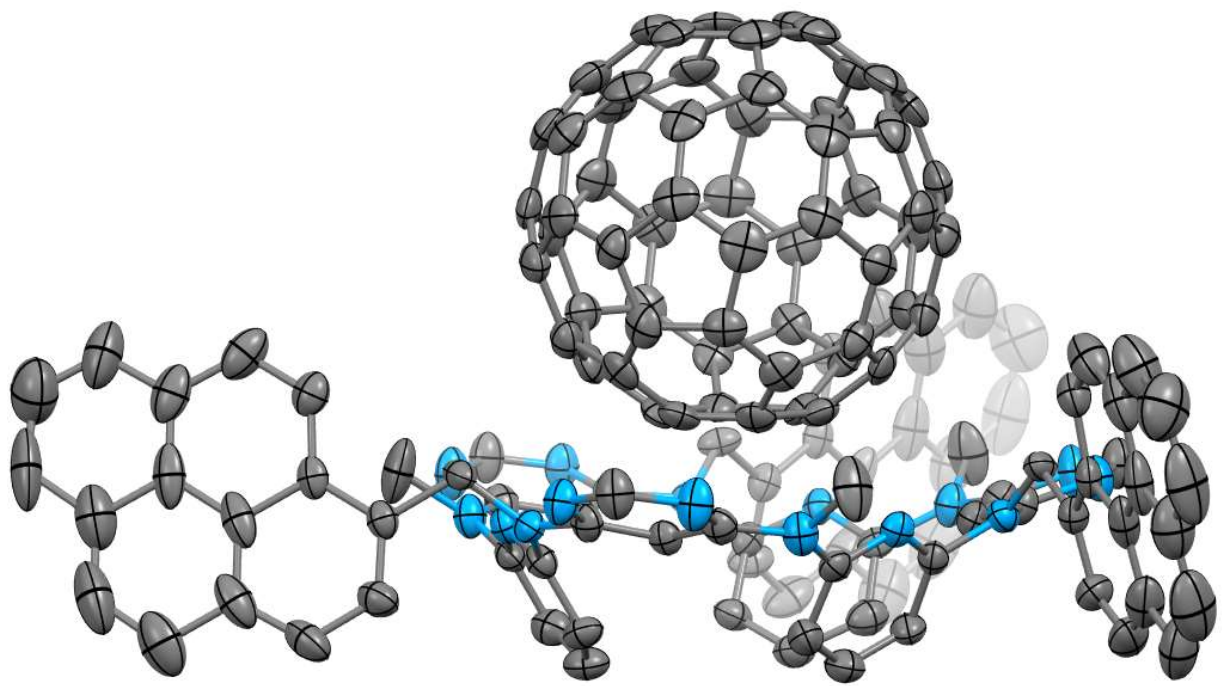
Fig 4. C$_{60}$ cocrystallized with adequate (top)[20] and pleasantly effective (bottom)[27] degrees of interaction between the fullerene and the cocrystallization agent.

Of the plethora of successful cocrystallization agents available, we focus on metalloporphyrins – specifically, M^{II} salts of octaethylporphyrin. Metal octaethylporphyrins have exhibited exceptional success cocrystallizing not only C$_{60}$ (Figure 5) and other round, empty fullerenes[28], but also curiously shaped higher fullerenes, endohedral metallofullerenes, and even functionalized fulleroids. Metal octaethylporphyrin cocrystallization agents were responsible for the characterization of the first endohedral fullerene[29], egg-shaped endohedrals that disobey the isolated pentagon rule[30], tubular higher fullerenes[31], fullerenes containing a heptagonal moiety on the cage[32], endohedrals containing metal nitrides[30], sulfides, carbides[33] and oxides[34] encapsulated inside of them, and fullerenes with an artificially created orifice on their surface surrounded by heteroatoms and aryl substituents[35]. These are all molecules of interest – studying the host-guest chemistry of larger fullerenes containing encapsulated molecules is a field in and of itself. Isolating small molecules such as formaldehyde or hydrogen cyanide inside a functionalized fullerene enables us to study a single molecule of a substance completely isolated from its bulk components[36]. Endohedrals containing metal complexes trapped inside them, particularly paramagnetic metals such as lanthanides[37], may be the key to developing safer alternatives to MRI contrast agents than the current practice of injection or ingestion of ferromagnetic salts. Scalable synthetic strategies towards high-yield endohedral metallofullerenes, as well as understanding the properties of endohedrals hosting nonmetallic small molecules, may face the common issue of difficulty in obtaining reliable structural data.
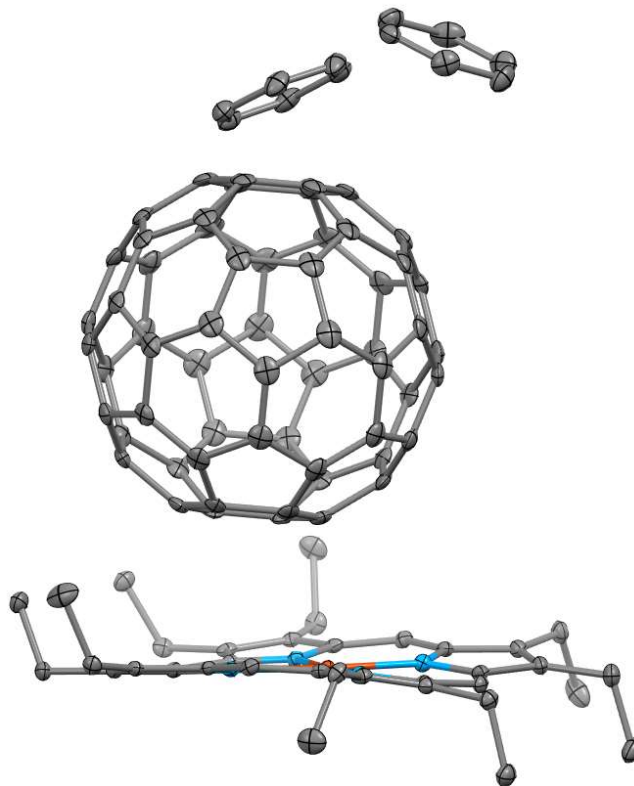
Fig 5. The structure of $Cu^{II}(OEP)·C_{60}.2C_6H_6$[38] showing successful ordering of the fullerene molecule

In the following two chapters, we will examine three distinct but related topics involving fullerene behavior: 1) the isolation and crystallographic characterization of two isostructural endohedral metallofullerenes and 2) a systematic look at fullerene-porphyrin cocrystallization, and briefly glimpse at the structural characterization of two functionalized fullerenes.

References

(1)   Taylor, R.; Hare, J. P.; Abdul-Sada, A. K.; Kroto, H. W. Isolation, Separation and Characterisation of the Fullerenes C_{60} and C_{70}: The Third Form of Carbon. *Journal of the Chemical Society, Chemical Communications* **1990**, No. 20. https://doi.org/10.1039/C39900001423.

(2)   Lichtenberger, D. L.; Wright, L. L.; Gruhn, N. E.; Rempe, M. E. Electronic Structure and Bonding of C_{60} to Metals. *Synthetic Metals* **1993**, *59* (3). https://doi.org/10.1016/0379-6779(93)91167-Z.

(3)   Diana, N.; Yamada, Y.; Gohda, S.; Ono, H.; Kubo, S.; Sato, S. Carbon Materials with High Pentagon Density. *Journal of Materials Science* **2021**, *56* (4). https://doi.org/10.1007/s10853-020-05392-x.

(4)   Friedrich, M.; Piovano, P.; Stefanelli, U. The Geometry of C_{60}: A Rigorous Approach via Molecular Mechanics. *SIAM Journal on Applied Mathematics* **2016**, *76* (5). https://doi.org/10.1137/16M106978X.

(5)   Balch, A. L.; Catalano, V. J.; Lee, J. W.; Olmstead, M. M.; Parkin, S. R. $(H_2$-$C_{70})Ir(CO)Cl(PPh_3)_2$: The Synthesis and Structure of an Organometallic Derivative of a Higher Fullerene. *Journal of the American Chemical Society* **1991**, *113* (23). https://doi.org/10.1021/ja00023a057.

(6)   Fagan, P. J.; Calabrese, J. C.; Malone, B. The Chemical Nature of Buckminsterfullerene (C_{60}) and the Characterization of a Platinum Derivative. *Science* **1991**, *252* (5009). https://doi.org/10.1126/science.252.5009.1160.

(7)   Euler's Gem: The Polyhedron Formula and the Birth of Topology. *Choice Reviews Online* **2009**, *46* (06). https://doi.org/10.5860/choice.46-3313.

(8)   Kroto, H. W. The Stability of the Fullerenes C_n, with n = 24, 28, 32, 36, 50, 60 and 70. *Nature* **1987**, *329* (6139). https://doi.org/10.1038/329529a0.

(9) Beer, F.; Gügel, A.; Martin, K.; Räder, J.; Müllen, K. High-Yield Reactive Extraction of Giant Fullerenes from Soot. *Journal of Materials Chemistry* **1997**, *7* (8). https://doi.org/10.1039/a608186j.

(10) Baei, M. T.; Koohi, M.; Shariati, M. Characterization of C_{20} Fullerene and Its Isolated C20-NGe_n Derivatives (n = 1-5) by Alternating Germanium Atom(s) in Equatorial Position: A DFT Survey. *Heteroatom Chemistry* **2018**, *29* (1). https://doi.org/10.1002/hc.21410.

(11) Rodríguez-Fortea, A.; Alegret, N.; Balch, A. L.; Poblet, J. M. The Maximum Pentagon Separation Rule Provides a Guideline for the Structures of Endohedral Metallofullerenes. *Nature Chemistry* **2010**, *2* (11). https://doi.org/10.1038/nchem.837.

(12) Kroto, H. W.; Heath, J. R.; O'Brien, S. C.; Curl, R. F.; Smalley, R. E. C_{60}: Buckminsterfullerene. *Nature* **1985**, *318* (6042). https://doi.org/10.1038/318162a0.

(13) Hawkins, J. M.; Meyer, A.; Lewis, T. A.; Loren, S.; Hollander, F. J. Crystal Structure of Osmylated C_{60}: Confirmation of the Soccer Ball Framework. *Science* **1991**, *252* (5003). https://doi.org/10.1126/science.252.5003.312.

(14) Li, B.; Zhen, J.; Wan, Y.; Lei, X.; Jia, L.; Wu, X.; Zeng, H.; Chen, M.; Wang, G. W.; Yang, S. Steering the Electron Transport Properties of Pyridine-Functionalized Fullerene Derivatives in Inverted Perovskite Solar Cells: The Nitrogen Site Matters. *Journal of Materials Chemistry A* **2020**, *8* (7). https://doi.org/10.1039/c9ta12188a.

(15) Heskia, A.; Maris, T.; Aguiar, P. M.; Wuest, J. D. Building Large Structures with Curved Aromatic Surfaces by Complexing Metals with Phosphangulene. *Journal of the American Chemical Society* **2019**, *141* (47). https://doi.org/10.1021/jacs.9b08179.

(16)   Lawrence, S. R.; Ohlin, C. A.; Cordes, D. B.; Slawin, A. M. Z.; Stasch, A. Hydrocarbon-Soluble, Hexaanionic Fulleride Complexes of Magnesium. *Chemical Science* **2019**, *10* (46). https://doi.org/10.1039/c9sc03857d.

(17)   Balch, A. L.; Olmstead, M. M. Reactions of Transition Metal Complexes with Fullerenes (C_{60}, C_{70}, Etc.) and Related Materials. *Chemical Reviews* **1998**, *98* (6). https://doi.org/10.1021/cr960040e.

(18)   Fukui, N.; Kim, T.; Kim, D.; Osuka, A. Porphyrin Arch-Tapes: Synthesis, Contorted Structures, and Full Conjugation. *Journal of the American Chemical Society* **2017**, *139* (26). https://doi.org/10.1021/jacs.7b05332.

(19)   Heskia, A.; Maris, T.; Wuest, J. D. Putting Fullerenes in Their Place: Cocrystallizing C_{60} and C_{70} with Phosphangulene Chalcogenides. *Crystal Growth and Design* **2019**, *19* (9). https://doi.org/10.1021/acs.cgd.9b00954.

(20)   Fa, S. X.; Wang, L. X.; Wang, D. X.; Zhao, L.; Wang, M. X. Synthesis, Structure, and Fullerene-Complexing Property of Azacalix[6]Aromatics. *Journal of Organic Chemistry* **2014**, *79* (8). https://doi.org/10.1021/jo5003714.

(21)   Konarev, D. v.; Litvinov, A. L.; Neretin, I. S.; Drichko, N. v.; Slovokhotov, Y. L.; Lyubovskaya, R. N.; Howard, J. A. K.; Yufit, D. S. Formation of Coordination Porphyrin Pentamers in New Supramolecular Complex of Fullerene: {(ZnTPP)$_4$·4-TPyP}·(C_{60}) 2·(C_6H_5CN)$_{3.5}$. *Crystal Growth and Design* **2004**, *4* (4). https://doi.org/10.1021/cg034259f.

(22)   Andrews, P. C.; Atwood, J. L.; Barbour, L. J.; Croucher, P. D.; Nichols, P. J.; Smith, N. O.; Skelton, B. W.; White, A. H.; Raston, C. L. Supramolecular Confinement of C_{60}, S_8, P_4Se_3

and Toluene by Metal(II) Macrocyclic Complexes. *Journal of the Chemical Society - Dalton Transactions* **1999**, No. 17. https://doi.org/10.1039/a903669e.

(23) Sun, Y.; Cui, Z.; Chen, L.; Lu, X.; Wu, Y.; Zhang, H. L.; Shao, X. Aryl-Fused Tetrathianaphthalene (TTN): Synthesis, Structures, Properties, and Cocrystals with Fullerenes. *RSC Advances* **2016**, *6* (83). https://doi.org/10.1039/c6ra18945h.

(24) Lu, R. Q.; Wu, S.; Bao, Y. H.; Yang, L. L.; Qu, H.; Saha, M.; Wang, X. Y.; Zhuo, Y. Z.; Xu, B.; Pei, J.; Zhang, H.; Weng, W.; Cao, X. Y. Cocrystallization of Imide-Fused Corannulene Derivatives and C_{60}: Guest-Induced Conformational Switching and 1:1 Segregated Packing. *Chemistry - An Asian Journal* **2018**, *13* (19). https://doi.org/10.1002/asia.201801086.

(25) van Raden, J. M.; Leonhardt, E. J.; Zakharov, L. N.; Pérez-Guardiola, A.; Pérez-Jiménez, A. J.; Marshall, C. R.; Brozek, C. K.; Sancho-García, J. C.; Jasti, R. Precision Nanotube Mimics via Self-Assembly of Programmed Carbon Nanohoops. *Journal of Organic Chemistry* **2020**, *85* (1). https://doi.org/10.1021/acs.joc.9b02340.

(26) Olmstead, M. M.; Maitra, K.; Balch, A. L. ChemInform Abstract: Formation of a Curved Silver Nitrate Network That Conforms to the Shape of C60 and Encapsulates the Fullerene-Structural Characterization of $C_{60}\{Ag(NO_3)\}_5$. *ChemInform* **2010**, *30* (14). https://doi.org/10.1002/chin.199914007.

(27) Sumy, D. P.; Dodge, N. J.; Harrison, C. M.; Finke, A. D.; Whalley, A. C. Tridecacyclene: A Cyclic Tetramer of Acenaphthylene. *Chemistry - A European Journal* **2016**, *22* (14). https://doi.org/10.1002/chem.201600165.

(28)   Olmstead, M. M.; Costa, D. A.; Maitra, K.; Noll, B. C.; Phillips, S. L.; van Calcar, P. M.; Balch, A. L. Interaction of Curved and Flat Molecular Surfaces. The Structures of Crystalline Compounds Composed of Fullerene (C_{60}, $C_{60}O$, C_{70}, and $C_{120}O$) and Metal Octaethylporphyrin Units. *Journal of the American Chemical Society* **1999**, *121* (30). https://doi.org/10.1021/ja990618c.

(29)   Stevenson, S.; Rice, G.; Glass, T.; Harlch, K.; Cromer, F.; Jordan, M. R.; Craft, J.; Hadju, E.; Bible, R.; Olmstead, M. M.; Maltra, K.; Fisher, A. J.; Balch, A. L.; Dorn, H. C. Small-Bandgap Endohedral Metallofullerenes in High Yield and Purity. *Nature* **1999**, *401* (6748). https://doi.org/10.1038/43415.

(30)   Stevenson, S.; Phillips, J. P.; Reid, J. E.; Olmstead, M. M.; Rath, S. P.; Balch, A. L. Pyramidalization of Gd_3N inside a C_{80} Cage. The Synthesis and Structure of $Gd_3N@C_{80}$. *Chemical Communications* **2004**, No. 24. https://doi.org/10.1039/b412338g.

(31)   Yang, H.; Beavers, C. M.; Wang, Z.; Jiang, A.; Liu, Z.; Jin, H.; Mercado, B. Q.; Olmstead, M. M.; Balch, A. L. Isolation of a Small Carbon Nanotube: The Surprising Appearance of $D_{5h}(1)$-C_{90}. *Angewandte Chemie - International Edition* **2010**, *49* (5). https://doi.org/10.1002/anie.200906023.

(32)   Zhang, Y.; Ghiassi, K. B.; Deng, Q.; Samoylova, N. A.; Olmstead, M. M.; Balch, A. L.; Popov, A. A. Synthesis and Structure of $LaSc_2N@C_s$(Hept)-C_{80} with One Heptagon and Thirteen Pentagons. *Angewandte Chemie - International Edition* **2015**, *54* (2). https://doi.org/10.1002/anie.201409094.

(33)   Pan, C.; Bao, L.; Yu, X.; Fang, H.; Xie, Y.; Akasaka, T.; Lu, X. Facile Access to Y_2C_{2n} (2n = 92-130) and Crystallographic Characterization of $Y_2C_2@C_1(1660)$-C_{108}: A Giant

Nanocapsule with a Linear Carbide Cluster. *ACS Nano* **2018**, *12* (2). https://doi.org/10.1021/acsnano.8b00384.

(34) Feng, L.; Hao, Y.; Liu, A.; Slanina, Z. Trapping Metallic Oxide Clusters inside Fullerene Cages. *Accounts of Chemical Research* **2019**, *52* (7). https://doi.org/10.1021/acs.accounts.9b00206.

(35) Futagoishi, T.; Murata, M.; Wakamiya, A.; Sasamori, T.; Murata, Y. Expansion of Orifices of Open C_{60} Derivatives and Formation of an Open $C_{59}S$ Derivative by Reaction with Sulfur. *Organic Letters* **2013**, *15* (11). https://doi.org/10.1021/ol401083c.

(36) Chen, C. S.; Kuo, T. S.; Yeh, W. Y. Encapsulation of Formaldehyde and Hydrogen Cyanide in an Open-Cage Fullerene. *Chemistry - A European Journal* **2016**, *22* (26). https://doi.org/10.1002/chem.201601737.

(37) Ghiassi, K. B.; Olmstead, M. M.; Balch, A. L. Gadolinium-Containing Endohedral Fullerenes: Structures and Function as Magnetic Resonance Imaging (MRI) Agents. *Dalton Transactions*. 2014. https://doi.org/10.1039/c3dt53517g.

(38) Ishii, T.; Aizawa, N.; Yamashita, M.; Matsuzaka, H.; Kodama, T.; Kikuchi, K.; Ikcmoto, I.; Iwasa, Y. First Syntheses of Cocrystallites Consisting of anti-Formed Metal Octaethylporphyrins with Fullerene C_{60}. *Journal of the Chemical Society, Dalton Transactions* **2000**, No. 23. https://doi.org/10.1039/b006593p.

Chapter II. The isolation and crystallographic characterization of Ho$_3$N@C_2(22010)-C$_{78}$ and Tb$_3$N@C_2(22010)-C$_{78}$

Introduction

In the previous chapter we have examined the unique structural properties of C$_{60}$ fullerene, a truncated icosahedral molecule with high symmetry and a tendency for crystallographic disorder. The structural features of endohedral metallofullerenes are even more wide-ranging and remarkable. Endohedral metallofullerenes consist of a closed carbon cage encapsulating metal atoms, metal ions, or complexes and clusters of metal atoms and main group elements. [1–5] Unique motifs such as the completely planar M$_3$N^{3+} unit can be isolated as well as characterized inside of endohedral fullerenes of various sizes, whilst it does not exist outside a fullerene.[6–10] The trapping of highly magnetic metals (such as lanthanides) inside endofullerenes can find a variety of potential applications, such as single molecule magnets[11,12] and as contrast agents for magnetic resonance imagining.[13,14] While empty cage fullerenes obey the isolated pentagon rule (IPR), based on pyramidalization factors discussed in Chapter 1, endohedral fullerenes may exhibit exceptions to the IPR – which is made possible by significant metal-cage interaction stabilizing the extra-pyramidalized pentalene region (region of fused pentagons). [15–17] Thus, motifs that do not exist outside a fullerene, and motifs on the cage that are not otherwise chemically feasible, may converge to supplement one another and make a joint appearance in the form of non-IPR obeying endohedral metallofullerenes. Structural studies of trends in endohedrals of homologous type, such as all characterized members of the M$_3$N@I_h-C$_{80}$ species, the shape of the M$_3$N group changes from completely planar for small metal ions,[18] to increasingly pyramidal around the N atom with an increase in the size of M ions.[19] For the slightly smaller fullerene C$_{78}$, the M$_3$N@C$_{78}$ series

looks quite different. With the smallest metal ion, scandium, the cage takes the form of an IPR-obeying isomer, $Sc_3N@D_{3h}$-C_{78} encasing a planar Sc_3N unit[20,21] while $Gd_3N@C_2(22010)C_{78}$, a member of the series containing a much larger metal ion, adopts a non-IPR cage[22] which has two regions of IPR-violating fused pentagons (or pentalenes) with a gadolinium ion caressing each pentalene from the inside of the cage. Computation predicts that other $M_3N@C78$ with large M atoms such as Y, Lu, La, Gd, Dy and Tm should also utilize the $M_3N@C_2(22010)C_{78}$.[23] In this work, two isomorphous crystal structures were obtained for the Ho and Tb members of the series, both of which are larger than scandium, and adopt the $C_2(22010)$-C_{78} cage isomer.

Results and Discussions

To synthesize these endohedral fullerenes, carbon soot was made using established Krätschmer-Huffman method of electric-arc synthesis using cored, graphite rods packed with Ho_2O_3 powder.[24] The carbon soot that formed was extracted with carbon disulfide, filtered and evaporated to dryness, and a mass spectrum of the xylene extract of this is shown in Figure 1. Further purification of the sample was achieved by selective Lewis acid precipitation of $Ho_3N@C_2(22010)$-C_{78} along with some of the other endohedral fullerenes, followed by further selective precipitation by magnesium chloride, redissolution, and two rounds of recycling HPLC. In case of the Tb endohedral, a 3-phase electric arc discharge evaporation of graphite rods was employed on cored rods containing Tb_4O_7 powder in a pure N_2 atmosphere. After extracting the soot with toluene, the sample was subjected to the usual amino functionalized silica chemical separation and further HPLC.
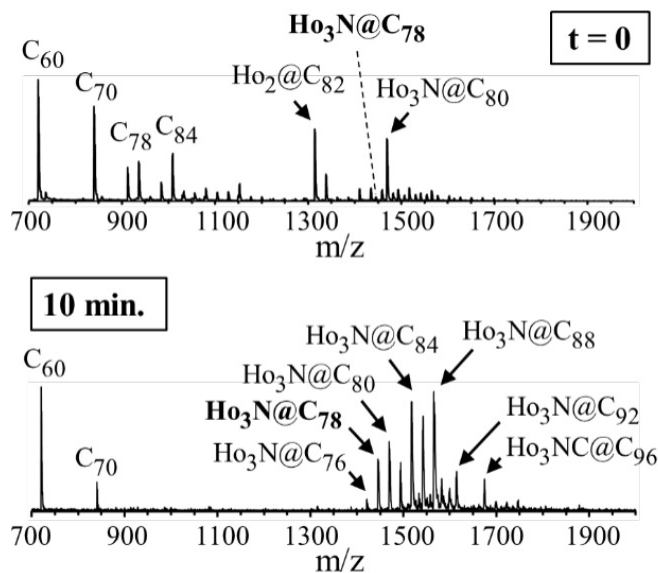
Fig 1. LDI mass spectra of Ho extract in xylenes. Top - initial spectrum, bottom - after 10 min. of reaction with 3-amino-1-propanol

The pure samples of $Ho_3N@C_2(22010)-C_{78}$ and $Tb_3N@C_2(22010)-C_{78}$ exhibit very similar UV/Vis absorption spectra (Figure 2) to one another and other $C_2(22010)-C_{78}$ cage isomers of this M_3N series, especially contrasted with the Sc member of this series that appears as a different cage isomer.
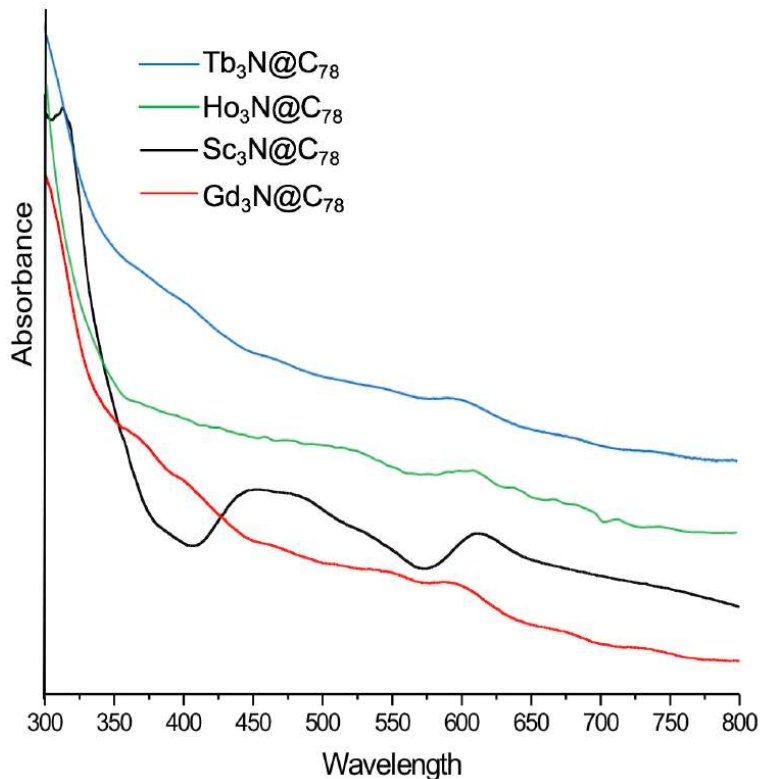
Fig 2. Optical spectra comparing various M₃N@C₇₈ endohedrals, of which the Sc₃N member is a different isomer (Sc and Gd spectra from Ref 25[25]

The Ho and Tb containing compounds are exactly isomorphous, including fullerene-porphyrin interaction, porphyrin morphology, solvate, and cell dimensions. We will thus discuss only the Ho₃N species, whose crystal structure is shown in Figure 3A as a POVRAY graphic including toluene solvate molecules. Figure 3B shows the ORTEP representation with only one cage enantiomer. The cage is chiral, and crystallizes with both enantiomers in the same crystallographic site, shown in Figure 3C. Figure 3D highlights the regions of the cage which interact with the Ho atoms on the inside.

(A)

(B)

19
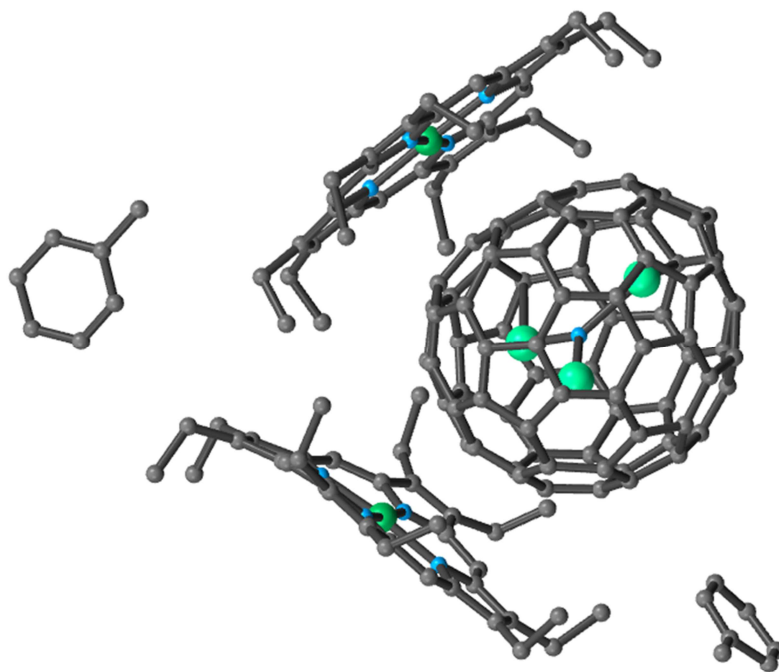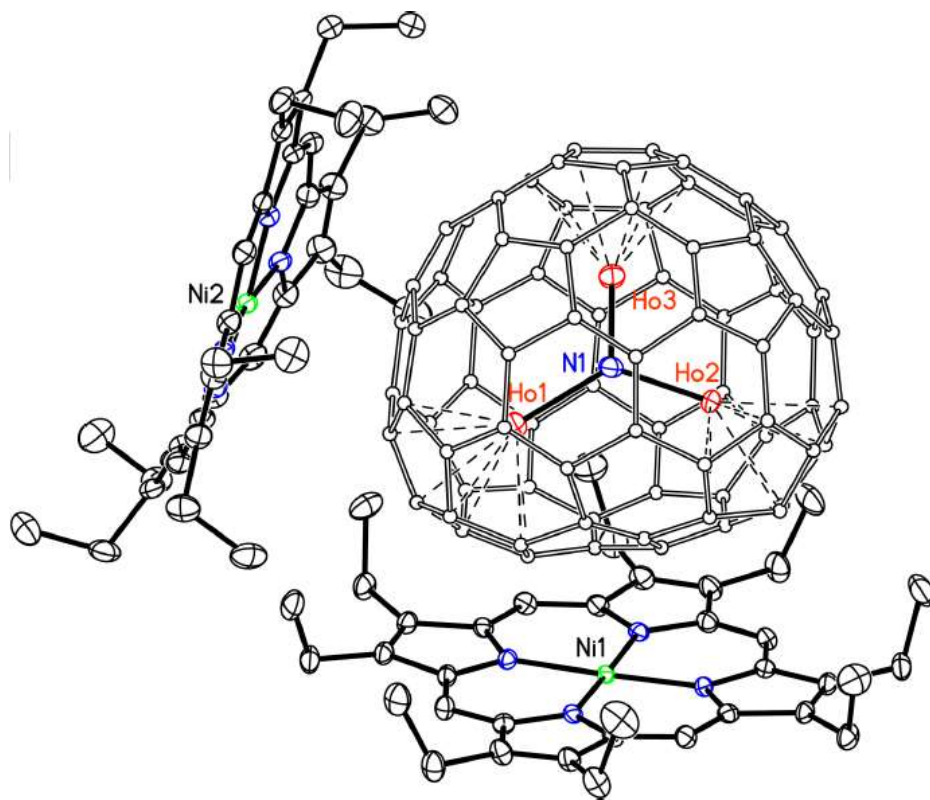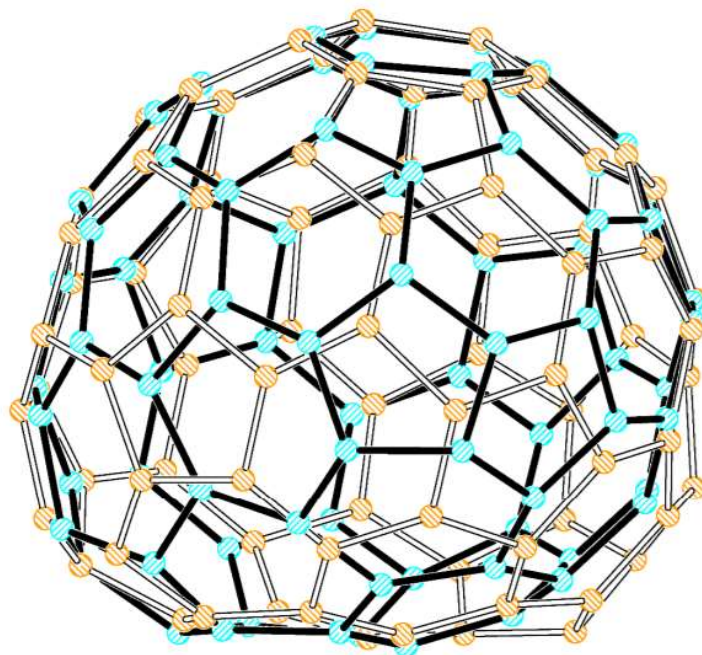
(C)

(D)

Fig 3. (A) A representation of the Ho₃N endohedral exhibiting one orientation of the fullerene, the two associated porphyrins, and solvate molecules. (B) A representation containing thermal ellipsoids showing where the Ho₃N unit sits inside the cage. (C) The two hands of the chiral cage,

sorted by color. (D) Metal-cage interactions: two sets of pentalene-Ho interactions and one

hexagon-Ho interaction.

The crystals of both endohedrals were grown by diffusion of a toluene solution of

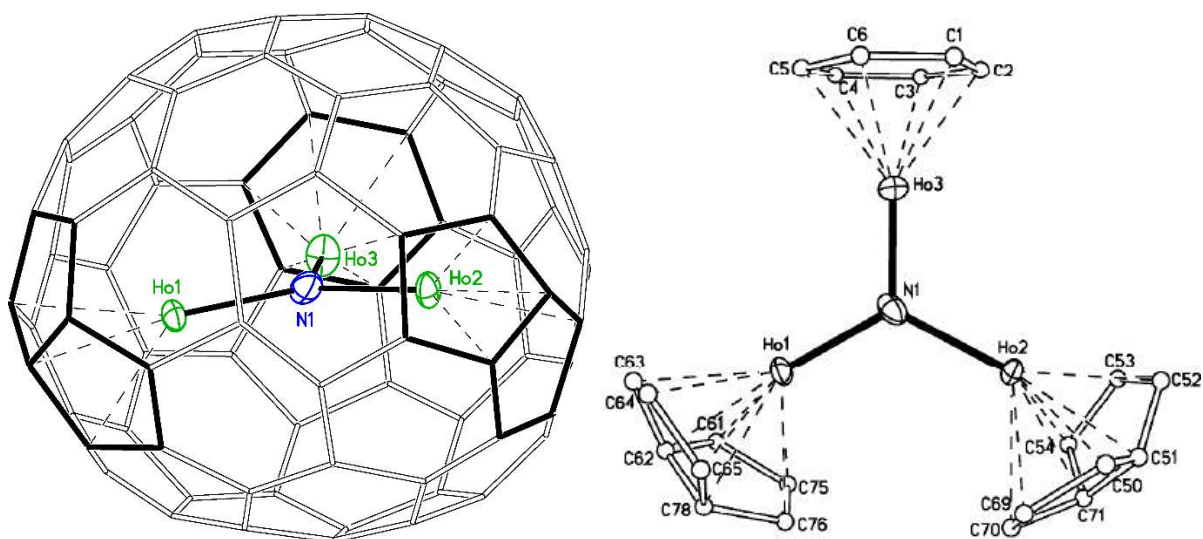$Ni^{II}(OEP)$ (where OEP is the dianion of octaethylporphyrin) into a toluene solution of

$Ho_3N@C_2(22010)$-C_{78} or $Tb_3N@C_2(22010)$-C_{78}. In both compounds, the trimetallic nitride cluster

is located inside a C_2-C_{78} cage. The cage is rnumbered 22010 by the spiral algorithm out of 24109

possible combinations of pentagons and hexagons for the C_{78} cage size – the spiral algorithm

increases by factorial when violating the IPR. for a cage this size. The two separate pentalenes are

related by C_2 symmetry. The two hands of the chiral cage are present at 50:50 occupancy and

occupy the same region in the unit cell, as shown in Figure 3C. The metal nitride unit exhibits

rotational disorder about the nitrogen where the metals appear to circulate in 15 holmium atom

positions around one nitrogen position. Each set of three holmiums can be assigned to major

positions associated with each enantiomer. At these major sites, the N atom deviates only 0.008(4)

Å from Ho1 Ho2 Ho3 plane indicating near-perfect planarity of the cluster. Considering only

major sites, Ho1 and Ho2 are each adjacent to a pentalene region, while Ho3 is in an η^6 interaction

with a hexagon.

Figure 4 shows the packing diagram for the Ho and Tb structures, which, one may recall,

is crystallized from toluene. It is contrasted with the packing diagram for the identical cage isomer

of Gd3N@C78, which crystallizes from benzene and forms a completely distinct porphyrin-

fullerene interaction with only one kind of Ni(OEP) molecule in the structure. The nature of the

solvents used to grow the crystals brings about this difference. The Ho/Tb structure also contains

two dissimilar Ni(OEP) molecules that form a clam-shell like environment about each fullerene

cage. One Ni(OEP) molecules is relatively flat with all eight ethyl pointing towards the fullerene,

while the other porphyrin is not as well centered on the cage and has a distorted conformation with two ethyl arms pointed away from the fullerene. The relative "distortion" and out-of-plane displacement of each porphyrin is depicted in a linearized fashion in Figure 5.
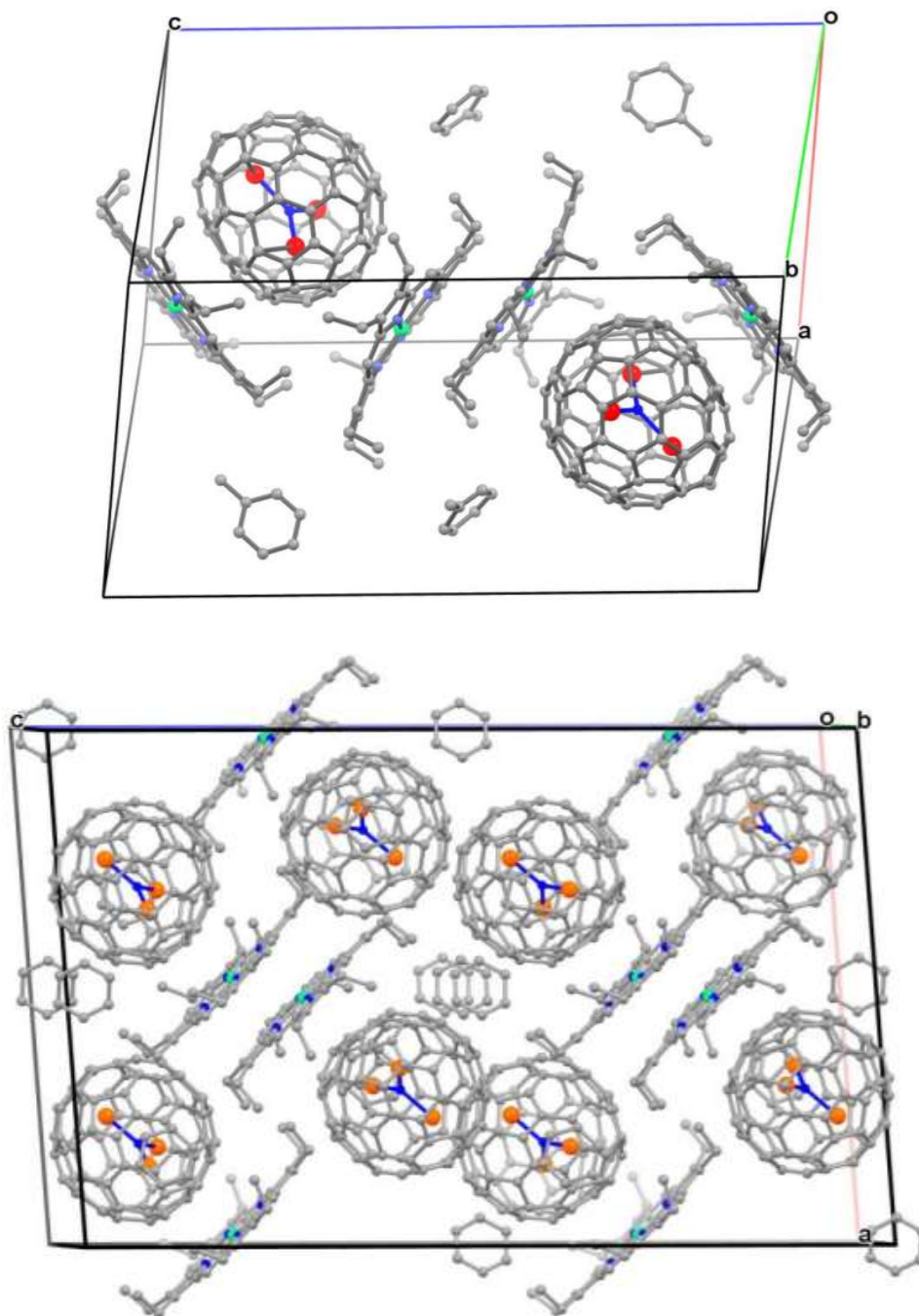
Fig 4. The packing in Ho₃N@C₂(22010)-C₇₈•2Ni(OEP)•2C₇H₈ (top) vs Gd₃N@C₂(22010)-C₇₈•Ni(OEP) •1.5 C₆H₆ (bottom)
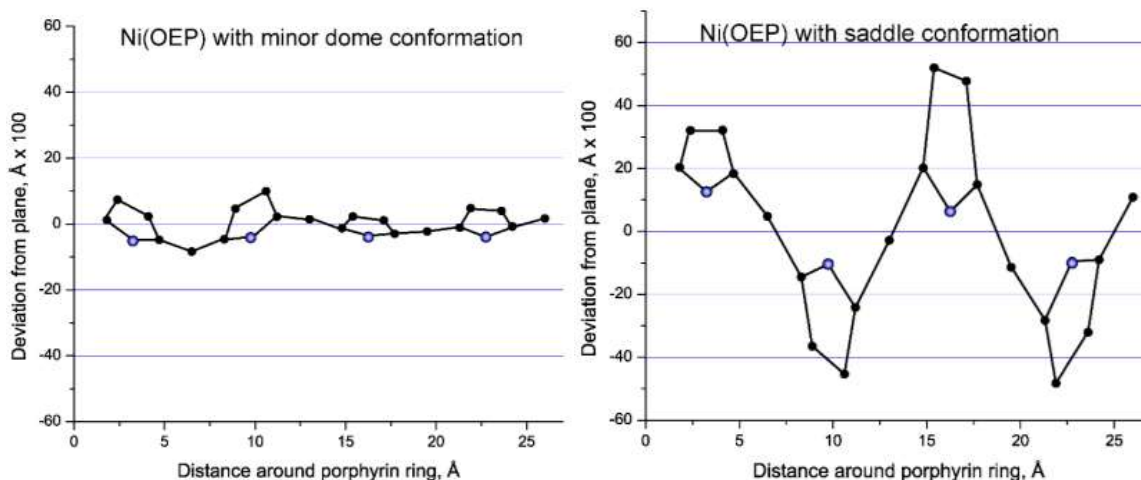

Fig 5. Deviation from planarity in the all-syn pointing Ni(OEP) (left) and the more-distorted, partly anti pointing Ni(OEP) (right)

Conclusion

The results reported above add to previous studies discussing the clear difference in how the internal M_3N units and bonds/atoms on the fullerene cages interact in the $M_3N@C78$ series as opposed to the $M3N@C80$ the series. In the larger cage, two cage isomers that have been observed: I_h-C_{80} and D_{5h}-C_{80}, both of which follow the IPR, and do not appear to be directly influencing the geometry in the M_3N unit, which is more often pyramidalized for this cage size.[19] In the smaller cage, C_{78}, the isomer we see in our structures (and previous ones besides Sc) is predicted to be the second most stable by computation.[23] The most stable (and IPR-obeying) D_{3h} isomer can accommodate the smallest member of the series, Sc_3N, but not larger metal nitride clusters. A relationship between cage isomer, metal ion size, and metal nitride geometry can be established and fortified by this work. In addition, the correlation between crystallization solvent and crystal

structure, porphyrin-fullerene stoichiometry, as well as porphyrin morphology, justify the necessity for more systematic investigations into those parameters.

References

(1) Mercado, B. Q.; Chen, N.; Rodríguez-Fortea, A.; MacKey, M. A.; Stevenson, S.; Echegoyen, L.; Poblet, J. M.; Olmstead, M. M.; Balch, A. L. The Shape of the Sc2(M2-S) Unit Trapped in C_{82}: Crystallographic, Computational, and Electrochemical Studies of the Isomers, Sc$_2$(μ2-S)@C_s(6)-C$_{82}$ and Sc$_2$(μ2-S)@C_{3v}(8)-C$_{82}$. *Journal of the American Chemical Society* **2011**, *133* (17). https://doi.org/10.1021/ja200289w.

(2) Yang, S.; Wei, T.; Jin, F. When Metal Clusters Meet Carbon Cages: Endohedral Clusterfullerenes. *Chemical Society Reviews*. **2017.** https://doi.org/10.1039/c6cs00498a.

(3) Cong, H.; Yu, B.; Akasaka, T.; Lu, X. Endohedral Metallofullerenes: An Unconventional Core-Shell Coordination Union. *Coordination Chemistry Reviews*. 2013. https://doi.org/10.1016/j.ccr.2013.05.020.

(4) Lu, X.; Feng, L.; Akasaka, T.; Nagase, S. Current Status and Future Developments of Endohedral Metallofullerenes. *Chemical Society Reviews* **2012**, *41* (23). https://doi.org/10.1039/c2cs35214a.

(5) Rodríguez-Fortea, A.; Balch, A. L.; Poblet, J. M. Endohedral Metallofullerenes: A Unique Host–Guest Association. *Chemical Society Reviews* **2011**, *40* (7). https://doi.org/10.1039/c0cs00225a.

(6)   Rodríguez-Fortea, A.; Campanera, J. M.; Cardona, C. M.; Echegoyen, L.; Poblet, J. M. Dancing on a Fullerene Surface: Isomerization of $Y_3N@(N-$ Ethylpyrrolidino-C80) from the 6,6 to the 5,6 Regioisomer. *Angewandte Chemie - International Edition* **2006**, *45* (48). https://doi.org/10.1002/anie.200604052.

(7)   Aroua, S.; Garcia-Borràs, M.; Osuna, S.; Yamakoshi, Y. Essential Factors for Control of the Equilibrium in the Reversible Rearrangement of $M_3N@I_h$-C_{80} Fulleropyrrolidines: Exohedral Functional Groups versus Endohedral Metal Clusters. *Chemistry - A European Journal* **2014**, *20* (43). https://doi.org/10.1002/chem.201403743.

(8)   Shen, W.; Hu, S.; Lu, X. Endohedral Metallofullerenes: New Structures and Unseen Phenomena. *Chemistry - A European Journal*. 2020. https://doi.org/10.1002/chem.201905306.

(9)   Stevenson, S.; Arvola, K. D.; Fahim, M.; Martin, B. R.; Ghiassi, K. B.; Olmstead, M. M.; Balch, A. L. Isolation and Crystallographic Characterization of $Gd_3N@D_2(35)$-C_{88} through Non-Chromatographic Methods. *Inorganic Chemistry* **2016**, *55* (1). https://doi.org/10.1021/acs.inorgchem.5b01814.

(10)   Cerón, M. R.; Izquierdo, M.; Garcia-Borràs, M.; Lee, S. S.; Stevenson, S.; Osuna, S.; Echegoyen, L. Bis-1,3-Dipolar Cycloadditions on Endohedral Fullerenes $M_3N@I_h$-C_{80} (M = Sc, Lu): Remarkable Endohedral-Cluster Regiochemical Control. *Journal of the American Chemical Society* **2015**, *137* (36). https://doi.org/10.1021/jacs.5b07207.

(11)   Schlesier, C.; Spree, L.; Kostanyan, A.; Westerström, R.; Brandenburg, A.; Wolter, A. U. B.; Yang, S.; Greber, T.; Popov, A. A. Strong Carbon Cage Influence on the Single

Molecule Magnetism in Dy-Sc Nitride Clusterfullerenes. *Chemical Communications* **2018**, *54* (70). https://doi.org/10.1039/c8cc05029e.

(12) Liu, F.; Krylov, D. S.; Spree, L.; Avdoshenko, S. M.; Samoylova, N. A.; Rosenkranz, M.; Kostanyan, A.; Greber, T.; Wolter, A. U. B.; Büchner, B.; Popov, A. A. Single Molecule Magnet with an Unpaired Electron Trapped between Two Lanthanide Ions inside a Fullerene. *Nature Communications* **2017**, *8*. https://doi.org/10.1038/ncomms16098.

(13) Mikawa, M.; Kato, H.; Okumura, M.; Narazaki, M.; Kanazawa, Y.; Miwa, N.; Shinohara, H. Paramagnetic Water-Soluble Metallofullerenes Having the Highest Relaxivity for MRI Contrast Agents. *Bioconjugate Chemistry* **2001**, *12* (4). https://doi.org/10.1021/bc000136m.

(14) Ghiassi, K. B.; Olmstead, M. M.; Balch, A. L. Gadolinium-Containing Endohedral Fullerenes: Structures and Function as Magnetic Resonance Imaging (MRI) Agents. *Dalton Transactions*. 2014. https://doi.org/10.1039/c3dt53517g.

(15) Wang, D. L.; Sun, X. P.; Zhai, Y. C. DFT Studies on Non-IPR C_{68} and Endohedral Fullerene $Sc_3N@C_{68}$. *Jiegou Huaxue* **2007**, *26* (3).

(16) Yang, S.; Popov, A. A.; Dunsch, L. Violating the Isolated Pentagon Rule (IPR): The Endohedral Non-IPR C_{70} Cage of $Sc_3N@C70$. *Angewandte Chemie - International Edition* **2007**, *46* (8). https://doi.org/10.1002/anie.200603281.

(17) Guo, M.; Li, X.; Yao, Y. R.; Zhuang, J.; Meng, Q.; Yan, Y.; Liu, X.; Chen, N. A Non-Isolated Pentagon Rule C_{82} cage Stabilized by a Stretched Sc_3N Cluster. *Chemical Communications* **2021**, *57* (34). https://doi.org/10.1039/d1cc00328c.

(18)   Stevenson, S.; Lee, H. M.; Olmstead, M. M.; Kozikowski, C.; Stevenson, P.; Balch, A. L. Preparation and Crystallographic Characterization of a New Endohedral, $Lu_3N@C_{80}\cdot5$ (o-Xylene), and Comparison with $Sc_3N@C_{80}\cdot5$ (o-Xylene). *Chemistry - A European Journal* **2002**, *8* (19). https://doi.org/10.1002/1521-3765(20021004)8

(19)   Olmstead, M. M.; Zuo, T.; Dorn, H. C.; Li, T.; Balch, A. L. Metal Ion Size and the Pyramidalization of Trimetallic Nitride Units inside a Fullerene Cage: Comparisons of the Crystal Structures of $M_3N@I_h\text{-}C_{80}$ (M = Gd, Tb, Dy, Ho, Er, Tm, Lu, and Sc) and Some Mixed Metal Counterparts. *Inorganica Chimica Acta* **2017**, *468*. https://doi.org/10.1016/j.ica.2017.05.046.

(20)   Mercado, B. Q.; Chaur, M. N.; Echegoyen, L.; Gharamaleki, J. A.; Olmstead, M. M.; Balch, A. L. A Single Crystal X-Ray Diffraction Study of a Fully Ordered Cocrystal of Pristine $Sc_3N@D_{3h}(5)\text{-}C_{78}$. *Polyhedron* **2013**, *58*. https://doi.org/10.1016/j.poly.2012.08.035.

(21)   Olmstead, M. M.; de Bettencourt-Dias, A.; Duchamp, J. C.; Stevenson, S.; Marciu, D.; Dorn, H. C.; Balch, A. L. Isolation and Structural Characterization of the Endohedral Fullerene $Sc_3N@C_{78}$. *Angewandte Chemie International Edition* **2001**, *40* (7). https://doi.org/10.1002/1521-3773(20010401)40:7<1223::aid-anie1223>3.3.co;2-2.

(22)   Beavers, C. M.; Chaur, M. N.; Olmstead, M. M.; Echegoyen, L.; Balch, A. L. Large Metal Ions in a Relatively Small Fullerene Cage: The Structure of $Gd_3N@C_2(22010)\text{-}C_{78}$ Departs from the Isolated Pentagon Rule. *Journal of the American Chemical Society* **2009**, *131* (32). https://doi.org/10.1021/ja903741r.

(23) Popov, A. A.; Krause, M.; Yang, S.; Wong, J.; Dunsch, L. C78 Cage Isomerism Defined by Trimetallic Nitride Cluster Size: A Computational and Vibrational Spectroscopic Study. *Journal of Physical Chemistry B* **2007**, *111* (13). https://doi.org/10.1021/jp068661r.

(24) Stevenson, S.; Mackey, M. A.; Thompson, M. C.; Coumbe, H. L.; Madasu, P. K.; Coumbe, C. E.; Phillips, J. P. Effect of Copper Metal on the Yield of $Sc_3N@C_{80}$ Metallofullerenes. *Chemical Communications* **2007**, No. 41. https://doi.org/10.1039/b706859j.

(25) Campanera, J. M.; Bo, C.; Olmstead, M. M.; Balch, A. L.; Poblet, J. M. Bonding within the Endohedral Fullerenes $Sc_3N@C_{78}$ and $Sc_3N@C_{80}$ as Determined by Density Functional Calculations and Reexamination of the Crystal Structure of $\{Sc_3N@C_{78}\cdot Co(OEP)\}\cdot 1.5(C_6H_6)\cdot 0.3(CHCl_3)$. *Journal of Physical Chemistry A* **2002**, *106* (51). https://doi.org/10.1021/jp021882m.

Chapter III. A systematic study of porphyrin-fullerene interactions in M^{II}(OEP)-C_{60} cocrystals

The technique of cocrystallization with M^{II}(OEP) stands out as being one of the most successful ways to determine the structures of fullerenes, endohedral fullerenes and fulleroids.[1–6] Studying the wide variety of porphyrin-fullerene interactions in these structures can lead us to notice poorly-understood aspects of the supramolecular interactions within these. For instance, porpyrin-C_{60} cocrystals can contain C_{60} molecules surrounded by one, two, or three porphyrins[7,8]. Porphyrin molecules can append a fullerene on only one side, two porphyrins can surround a fullerene, or the porphyrin itself can be sandwiched between two fullerenes.[9,10] As discussed in Chapter 2, crystallization solvent alters M^{II}(OEP) stoichiometry towards the fullerene it associates with,[11,12] while other variations of structure and stoichiometry were observed in Ref 10. To further investigate these variations and the parameters they depend on, a systematic study was performed using C_{60} as the model fullerene.

Part I. Metal on effects on fullerene-porphyrin cocrystallization[13]

In this section we report some systematic studies of the cocrystallization of C_{60} with M^{II}(OEP) with M = Co, Ni, Cu, and Zn that probe the effects of altering the metal ion on the nature of the cocrystals that form.

Crystals of $6Co^{II}$(OEP)$\cdot 5C_{60} \cdot 5CH_2Cl_2$, $6Co^{II}$(OEP)$\cdot 5C_{60} \cdot 5C_2H_4Cl_2$, $6Zn^{II}$(OEP)$\cdot 5C_{60} \cdot 5CH_2Cl_2$, $6Zn^{II}$(OEP)$\cdot 5C_{60} \cdot 5C_2H_4Cl_2$, Cu^{II}(OEP)$\cdot C_{60} \cdot CH_2Cl_2$, Cu^{II}(OEP)$\cdot C_{60} \cdot C_2H_4Cl_2$ and Ni^{II}(OEP)$\cdot C_{60} \cdot 0.1CH_2Cl_2 \cdot 1.9C_6H_6$ were prepared by a common procedure that involved layering a solution of C_{60} in benzene over an equimolar solution of each M^{II}(OEP) in dichloromethane or

dichloroethane. The order of layering was reversed to ensure this had no bearing on crystal structure. Crystals were allowed to grow for about two weeks to achieve appropriate size for X-Ray Crystallography. Only one type of cocrystal was found for each of the four different metalloporphyrins for each solvate combination. Efforts to obtain crystals with different compositions by increasing the $M^{II}(OEP)/C_{60}$ ratio produced the same cocrystals reported, with concomitant crystallization of pristine $M^{II}(OEP)$ when the porphyrin was used in excess.

Table 1 shows all the eight structures (seven of them novel) obtained for the four metal ions, using dichloromethane and dichloroethane as solvate. The ratios expressed in the table indicate the porphyrin:fullerene stoichiometry, the color-coding reflects isostructurality of more than one structure, and the table also contains also contains the CCDC refcode for each structure.

|	$Co^{II}(OEP)$	$Zn^{II}(OEP)$	$Cu^{II}(OEP)$	$Ni^{II}(OEP)$
Dichloromethane	6 to 5 $P\bar{1}$ NOZFEQ	6 to 5 $P\bar{1}$ NOZFIU	1 to 1 $P2_1/c$ NOZDUE	1 to 1 $P\bar{1}$ NOZFAM
Dichloroethane	6 to 5 $C2/m$ NOZFUG	6 to 5 $P\bar{1}$ NOZGAN	1 to 1 $P2_1/c$	1 to 1 $P\bar{1}$

Table 1. Comparing the structures obtained with 4 $M^{II}(OEP)$ and C_{60} in two chlorinated solvents

Discussion and comparison of cocrystal structures

Structures of $6Co^{II}(OEP) \cdot 5C_{60} \cdot 5CH_2Cl_2$ and $6Co^{II}(OEP) \cdot 5C_{60} \cdot 5C_2H_4Cl_2$

Although occurring in different space groups, the two CoII(OEP) cocrystals of C_{60} in dichloromethane and dichloroethane contain the same (and unprecedented) 6 porphyrin, 5

fullerene motif shown in Figure 1A as its asymmetric unit. The difference in space group can be

visualized in Figure 1B (dichloromethane solvate) vs Figure 1C (dichloroethane solvate).
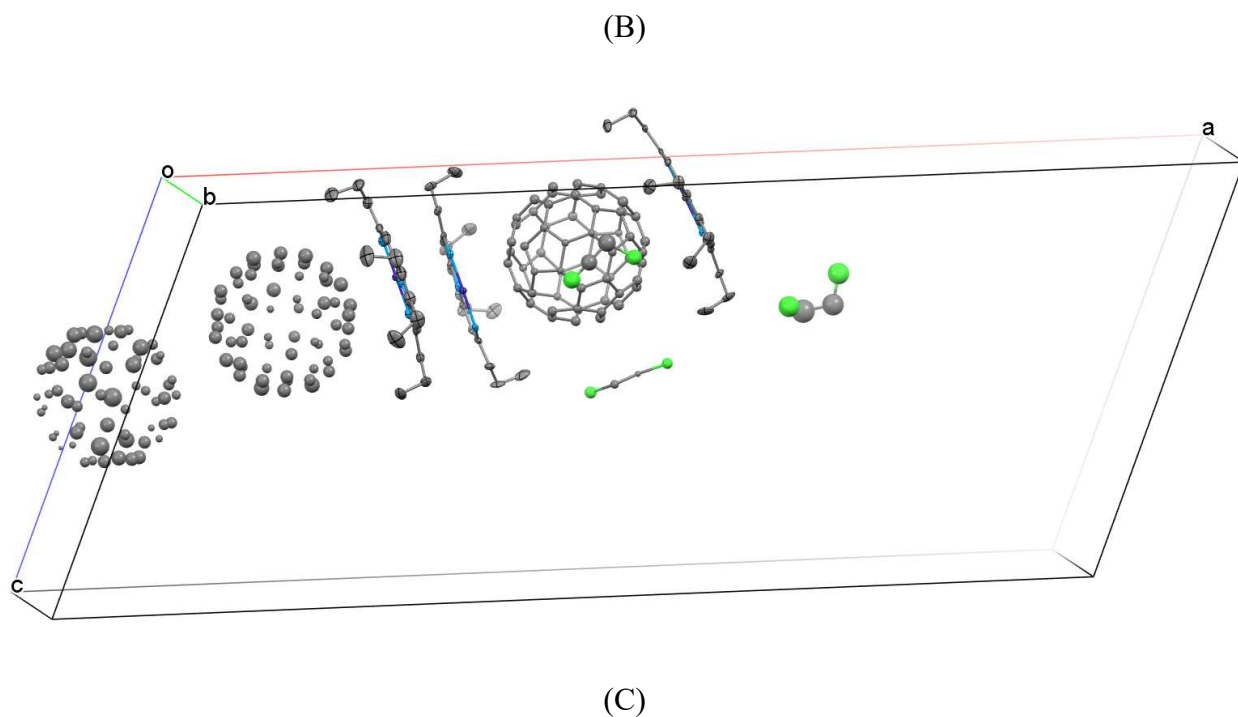

(A)

(B)

(C)
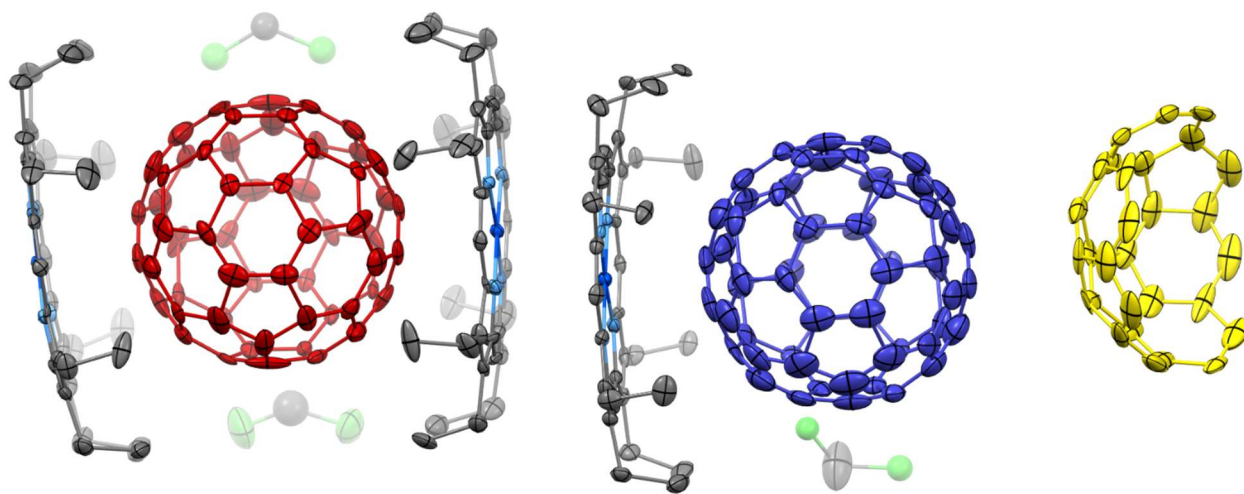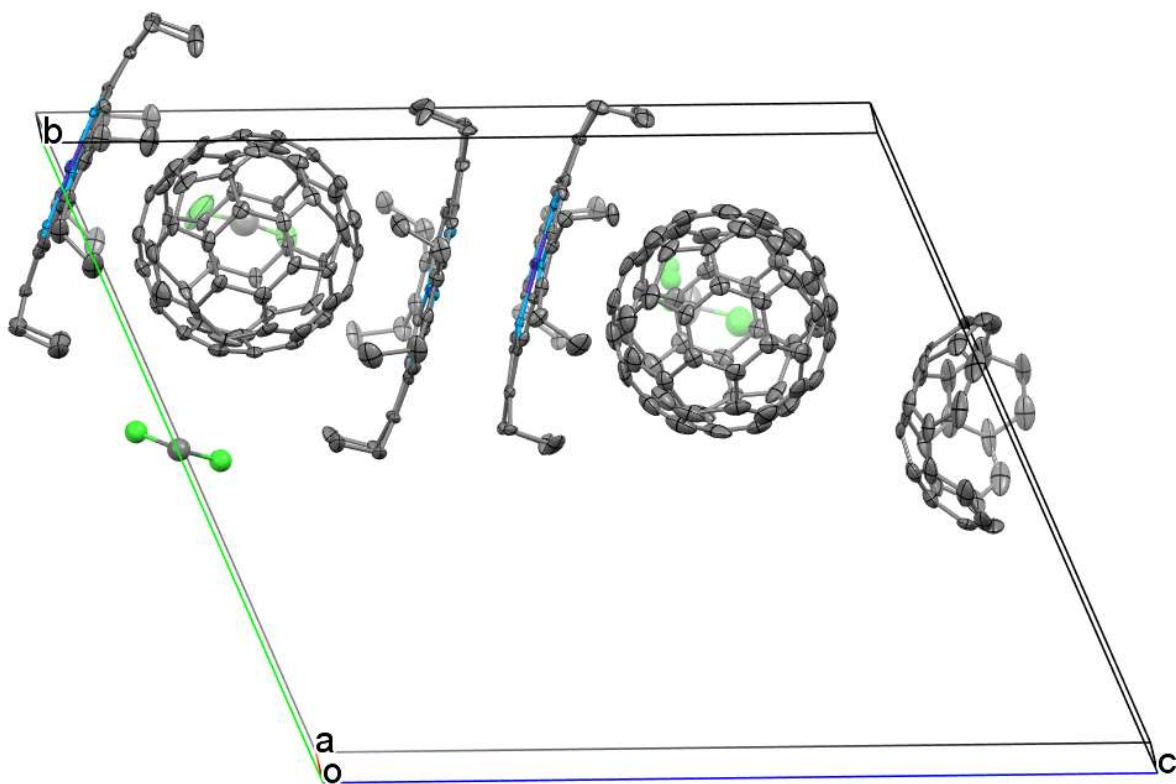
Fig 1. (A) The asymmetric unit in $6Co^{II}(OEP) \cdot 5C_{60} \cdot 5CH_2Cl_2$ depicting three symmetry environments for the C60 molecule: red, a fullerene surrounded by two porphyrins, blue, a fullerene bound by one porphyrin, and yellow, a fullerene with no adjacent porphyrin. (B) and (C) show the cell axes for $6Co^{II}(OEP) \cdot 5C_{60} \cdot 5CH_2Cl_2$ and $6Co^{II}(OEP) \cdot 5C_{60} \cdot 5C_2H_4Cl_2$ respectively.

The DCM solvated crystals form in the space group $P\bar{1}$ and its asymmetric unit contains three molecules of $Co^{II}(OEP)$ in general positions, two molecules of C_{60} in general positions, with another half molecule of C_{60} residing on a crystallographic inversion center, and disordered molecules of dichloromethane at three sites. Because of partial occupancies, the formula only designates five molecules of dichloromethane, although six sites are in use. Part A of Figure 1 shows a drawing of the asymmetric unit with each fullerene color-coded to represent the three different environments for C_{60} in this crystal. The red-colored fullerene is seated between two porphyrins; the blue-colored fullerene is capped at one end by a porphyrin (suggestive of the commonly seen 1:1 fullerene/porphyrin stoichiometry) and abuts another fullerene on the opposite

side; the yellow-colored fullerene, which is located on a center of symmetry, has no neighboring porphyrin. Surprisingly, all three fullerenes are completely ordered at 90 K for the DCM solvated structure. The fullerene and porphyrin molecules in the DCM solvate structure are arranged into chains as shown in Figure 2. Within this chain, there are two crystallographic centers of symmetry, one situated between two $Co^{II}(OEP)$ molecules and the other at the center of the yellow-colored C_{60} molecule. The packing may be envisioned as a 3-D arrangement of the rows that are shown in Figure 2A, shifted such that a yellow cage always faces the "open" side of a red cage. It is quite unusual to find a fullerene yellow-colored fullerene, which is situated on a crystallographic symmetry element that coincides with a symmetry element within the fullerene itself. It is much more common to find a fullerene that is positioned on a crystallographic mirror plane that does not coincide with a mirror plane of the carbon cage. In such a case, the fullerene suffers from disorder with two molecules occupying a common site.
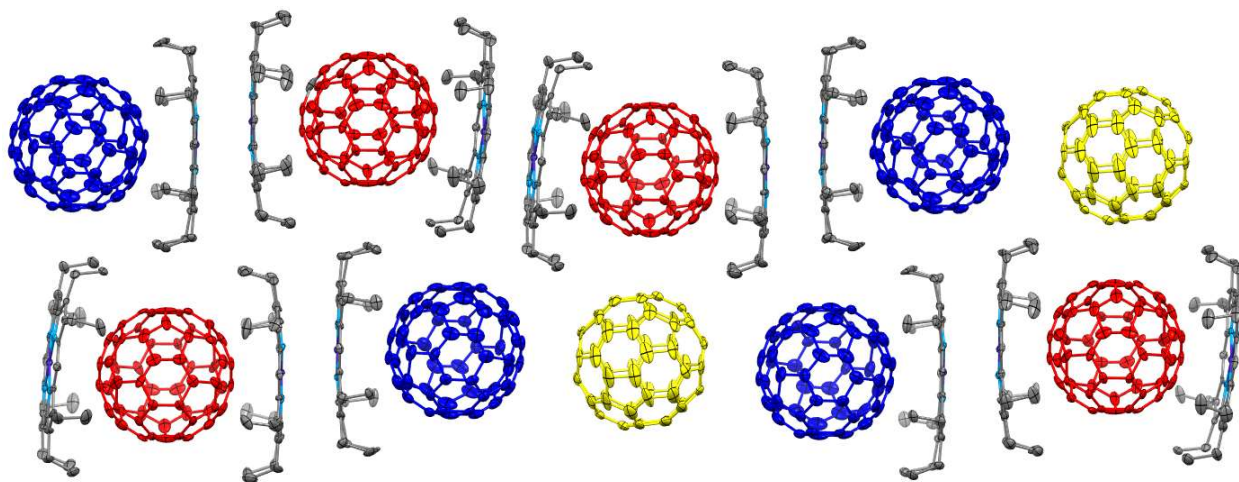

Fig 2. The one-dimensional propagation of the asymmetric unit of the Co^{II} DCM and DCE cocrystals (of which, the better DCM structure is shown here) and how it stacks in two dimensions.

The thermal ellipsoids of the three different C_{60} molecules show a noteworthy trend. The average isotropic thermal ellipsoid for the red fullerene in Figure 1, which is sandwiched between

33

two porphyrins, is 0.0388 Å^2, while that for the blue fullerene that is encapsulated by only on porphyrin is larger, 0.0521 Å2. The yellow C_{60} molecule, which does not interact with a porphyrin, has an even larger average thermal ellipsoid, 0.0636 Å2. These differences indicate that the adjacency of the porphyrin acts to restrict the thermal motion of the neighboring fullerene. This is consistent with computational studies that have shown that complementary regions of surface charge on the porphyrin and the fullerene are involved in producing ordered fullerene molecules in cocrystals of higher fullerenes[14,15] – a phenomenon also applicable to our system.

The structure of the dichloroethane (DCE) solvate retains the vast majority of symmetry properties exhibited by the DCM solvate. However, as apparent from the unit cell, this compound crystallizes in a monoclinic space group. Additionally, the fullerenes in this crystal exhibit more disorder – particularly in case of the "yellow" or unbound C_{60}. Some aspects of this structure become clearer when making a temperature-dependent observation about the DCM solvate crystals. During data collection, it was apparent that the crystal of $6Co^{II}(OEP) \cdot 5C_{60} \cdot 5CH_2Cl_2$ underwent a phase change upon cooling. At 140 K, the crystal was monoclinic (space group $C2/m$) like the DCE solvate, and also displayed disorder that was particularly pronounced for the unbound C_{60}. On cooling to 90 K, the crystal transformed into the twinned, triclinic form as reported in Table 1. In this form, all of the fullerenes are ordered. These are telltale signs of a temperature-dependent phase transition, and appears to be reversible upon warming (although this causes some loss to the structural integrity of the crystal). This helps us hypothesize that the DCE solvate, observed in its monoclinic, disordered and non-twinned state, may have the potential to also phase-transition into a twinned, ordered and lower symmetry form upon further cooling than was possible under the instrumental settings available to us. One final observation to make about the two

CoII(OEP) cocrystals is that throughout the entire asymmetric unit and its one dimensional propagation, the Co^{II}(OEP) molecules have all eight ethyl groups arranged to embrace the C_{60}.

Structures of $6Zn^{II}(OEP)\cdot5C_{60}\cdot5CH_2Cl_2$ and $6Zn^{II}(OEP)\cdot5C_{60}\cdot5C_2H_4Cl_2$

Crystals of $6Zn^{II}$(OEP)$\cdot5C_{60}\cdot5CH_2Cl_2$ (which we will refer to as DCM solvate) are nominally isostructural with those of $6Co^{II}$(OEP)$\cdot5C_{60}\cdot5CH_2Cl_2$ (1) as seen from the color-coding in Table 1. However, in a slight difference from the Co^{II} set, the two Zn^{II} cocrystals (DCM and DCE solvate) both adopt a triclinic space group and are isomorphous to one another. Figure 3 shows the structure of the DCE solvate, consisting of three molecules of Zn^{II}(OEP) and two molecules of C_{60} in general positions along with a half molecule of C_{60} residing on a crystallographic inversion center. There are also 2.5 molecules of dichloroethane in three sites. The thermal ellipsoids of the three different C_{60} molecules again show the same trend as discussed before. The yellow C_{60} molecule, which does not interact with a porphyrin, exhibits the highest average isotropic thermal sphere, 0.0637 $Å^2$ while the red C_{60} molecule has an average isotropic thermal parameter of 0.0461 $Å^2$, and the blue fullerene has an average isotropic thermal parameter of 0.0436 $Å^2$. Additionally, there is some disorder in the yellow C_{60} molecule that appears to result from incomplete conversion from the high temperature monoclinic form into the twinned, triclinic form.
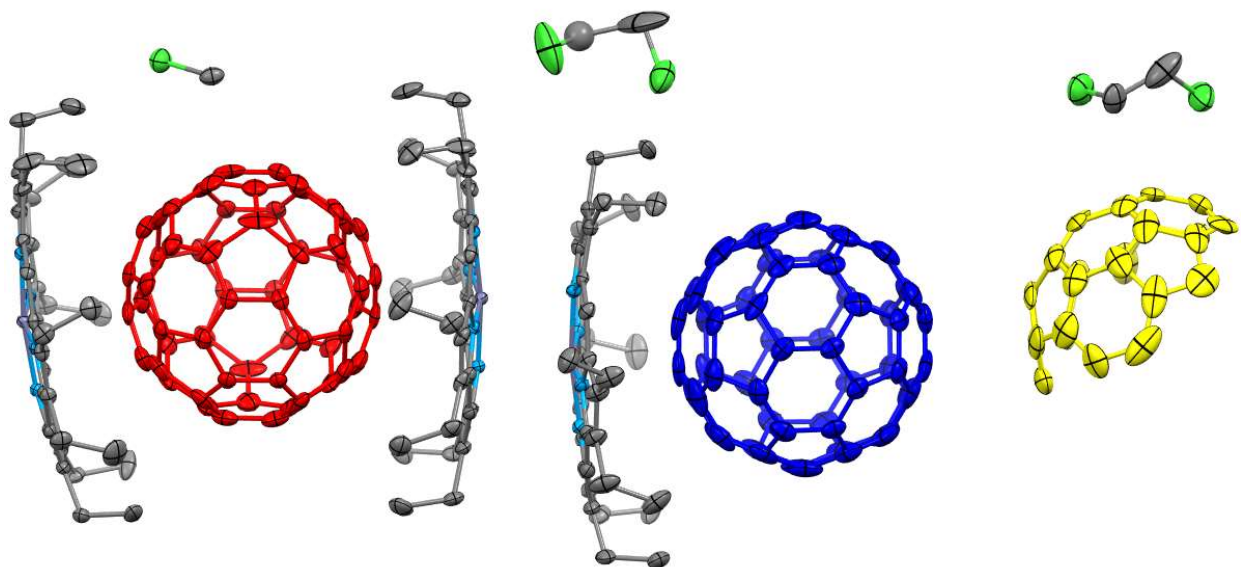
Fig 3. The asymmetric unit (with a similar color coding as Figure 1A) of $6Zn^{II}(OEP)\cdot5C_{60}\cdot5C_2H_4Cl_2$

There are two significant differences between the structures of the zinc and cobalt crystals. In case of the Zn-DCM and Zn-DCE combinations, one of the 24 ethyl groups is pointing away from the adjacent fullerene, while the others encapsulate a C_{60} molecule. The unique ethyl group is colored green and highlighted with a box in Figure 4A. The second difference involves the pairwise interactions of $M^{II}(OEP)$ molecules in the two different sets of crystals. In the Zn^{II} structures, back-to-back porphyrins approach each other much more closely than is the case in the cobalt crystal. Figure 4B shows both sets of adjacent $Zn^{II}(OEP)$ molecules in the crystal. The first set is generated by a center of inversion. For comparison the Co$\cdots$N distances are 2.939(6) and 2.936(6) Å in one pair and 2.876(6) Å in the other pair in $6Co^{II}(OEP)\cdot5C_{60}\cdot5CH_2Cl_2$. Analogous pairwise intermolecular Zn$\cdots$N distances occur in the structures of $Zn^{II}(OEP)\cdot C_{60}\cdot2C_6H_4Cl_2$ (2.613 Å)[16] and in $2Zn^{II}(OEP)\cdot C_{60}\cdot CHCl_3$ (2.592 and 2.674 Å).[10] These Zn$\cdots$N distances may be related to the tendency of Zn porphyrins to expand its coordination number. However, the Zn$\cdots$N distances remain significantly longer than the out-of-plane Zn$-$N(pyridine) distance of 2.200(3) Å in (pyridine)ZnII(OEP).[17]
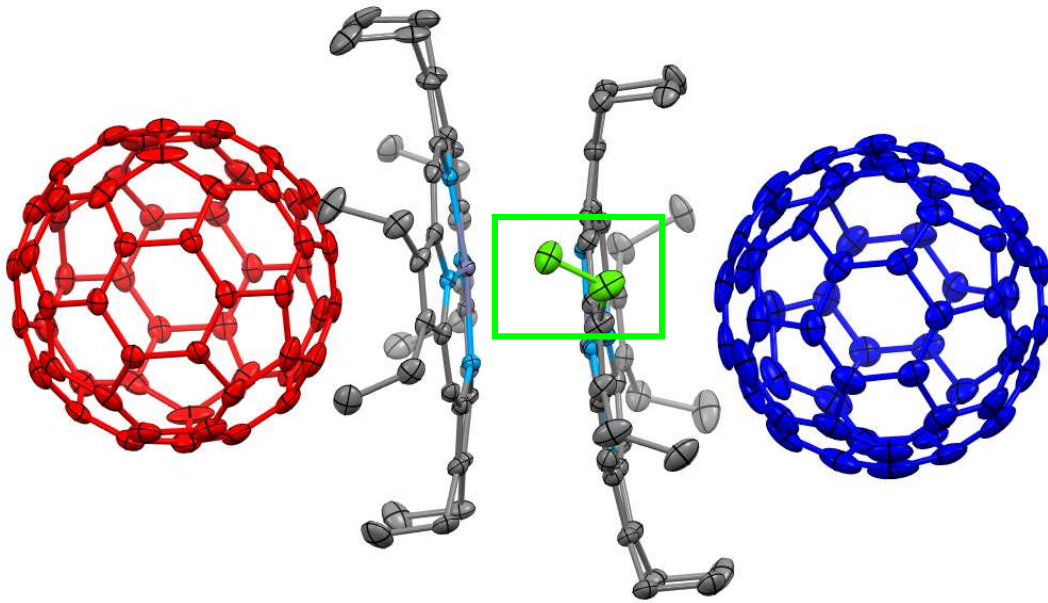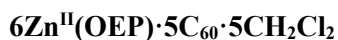
(A)
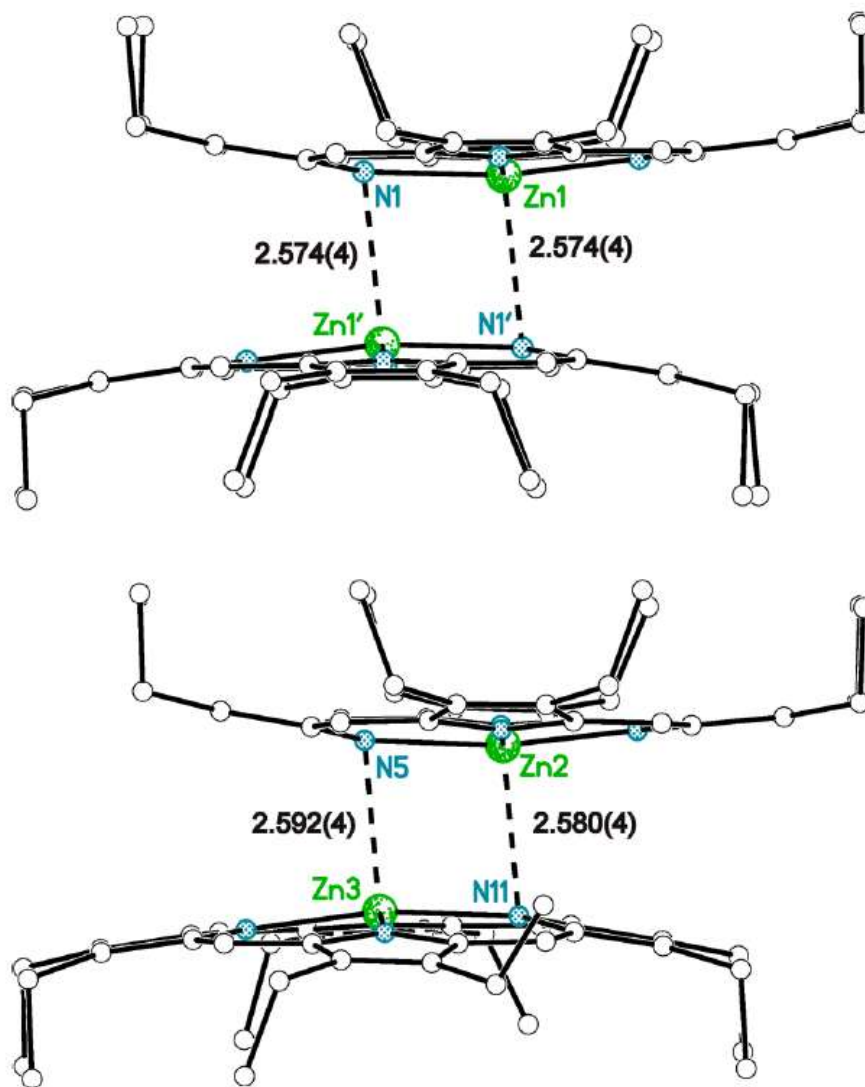
(B)

Fig 4. (A) A closer inspection of one porphyrin in the 6:5 Zn structures showing one anti ethyl group highlighted in green. (B) Interaction of two Zn^{II}(OEP) molecules in crystalline 6Zn^{II}(OEP)·5C$_{60}$·5CH$_2$Cl$_2$

Structures of Cu^{II}(OEP)·C$_{60}$·CH$_2$Cl$_2$ and Cu^{II}(OEP)·C$_{60}$·C$_2$H$_4$Cl$_2$

Under the exact conditions which produced 6:5 crystals in case of Zn^{II} and Co^{II}, Cu^{II}(OEP) produces 1:1, all-syn cocrystals with C$_{60}$ with one mol each of fullerene, porphyrin and solvating molecule (DCM or DCE) in the asymmetric unit. Figure 5 shows how the C$_{60}$ and

Cu^{II}(OEP)molecules are arranged into chains. All eight ethyl groups of the porphyrin embrace the fullerene in both structures. The Cu^{II}(OEP) molecules form back-to-back pairs that do not interact significantly with one another. The centroid···centroid distance between adjacent C$_{60}$ cages is 9.898 Å for the DCM solvate. Zigzag chains of C$_{60}$ also pack along the b direction with centroid···centroid separations of 10.132 Å. DCM and DCE molecules occupy interstitial positions.

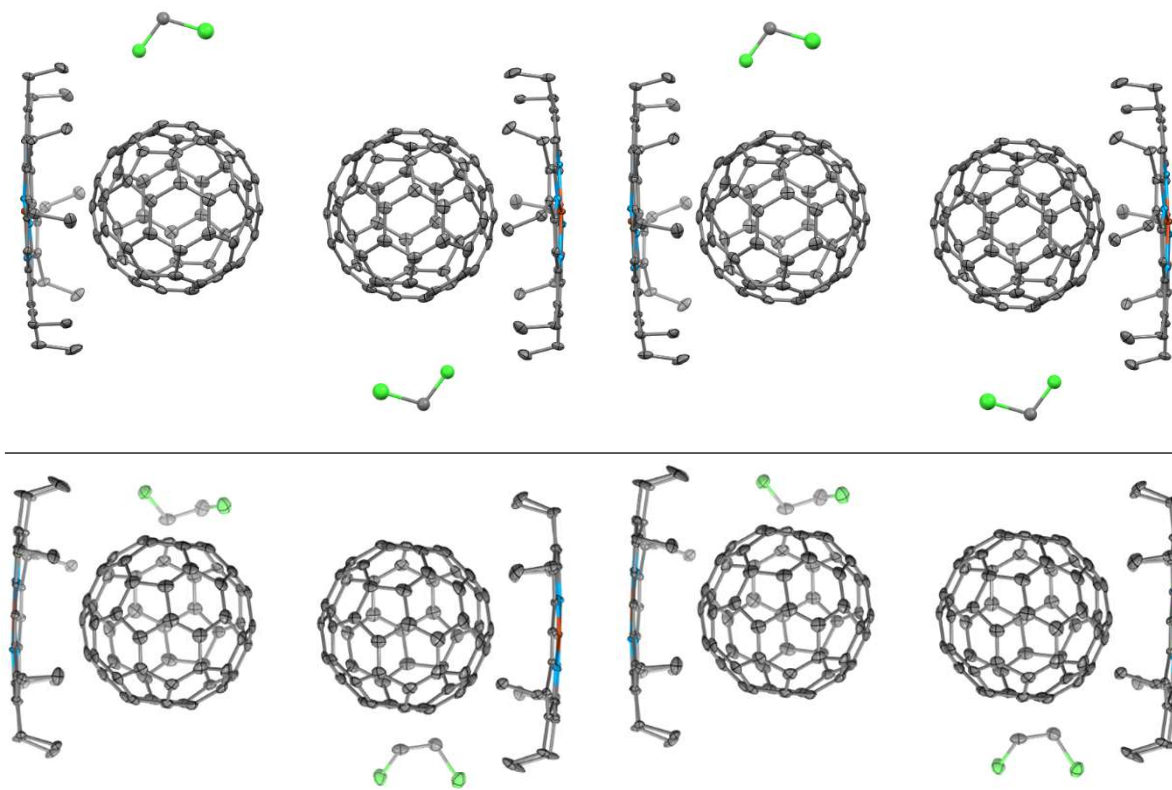**Fig 5. The isostructural DCM (left) and DCE (right) solvated Cu^{II}(OEP)-C$_{60}$ cocrystals exhibiting a 1:1 porphyrin-fullerene ratio and an all-syn conformation of the porphyrin ethyl arms towards the fullerene.**
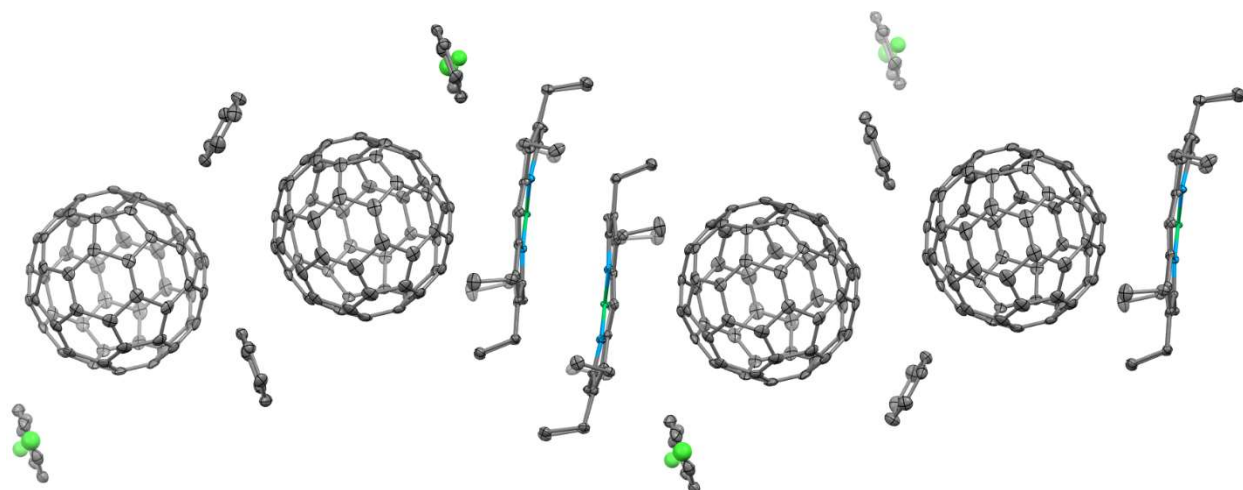
Structure of Ni^{II}(OEP)·C$_{60}$·0.1CH$_2$Cl$_2$·1.9C$_6$H$_6$

We may recall that the crystallization technique for all cocrystals involves slow diffusion of solutions of the fullerene in benzene and the porphyrin in DCM or DCE. While in case of Co, Zn and Cu, the solvate observed is the chlorinated solvent and not benzene, in case of the Ni

cocrystal an exception occurs. In the DCE crystallization setup, no DCE is incorporated into the cocrystal and a previously characterized benzene solvate[18] with 4 syn and 4 anti ethyl groups is obtained. In the DCM crystallization setup, the compound shown as an ORTEP in Figure 6A is observed. Its asymmetric unit consists of an ordered C_{60} molecule, a $Ni^{II}(OEP)$ molecule, a molecule of benzene, and a second site that is fractionally occupied by 0.1 dichloromethane/0.9benzene. Of the cocrystals reported here, this is the only one to incorporate benzene. Only four of the ethyl groups of a $Ni^{II}(OEP)$ molecule engage the fullerene. The other four reside on the opposite side of the porphyrin plane. This is, in every way except for the partial occupance of DCM, isostructural to the structure in Ref X[18]. Figure 6B shows how the C_{60} and NiII(OEP) molecules and the solvate molecules are arranged in the solid. The $Ni^{II}(OEP)$ molecules still adopt a back-to-back arrangement the Ni⋯Ni separation and the lateral shift of the porphyrins are much greater than in any of the other cocrystals reported here.

(A)

40
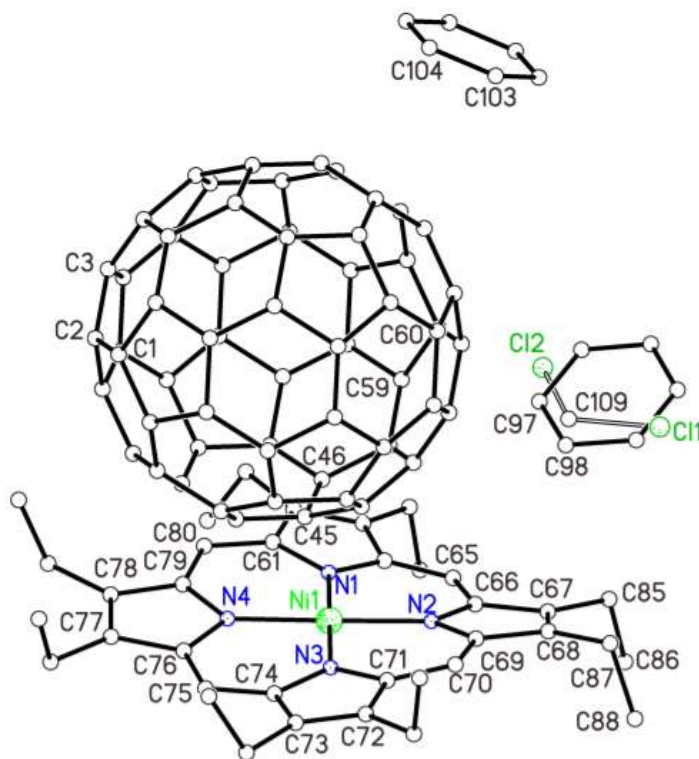
(B)

Fig 6. (A) An ORTEP diagram showing the components of the $Ni^{II}(OEP) \cdot C_{60} \cdot 0.1CH_2Cl_2 \cdot 1.9C_6H_6$ cocrystal. (B) Its one-dimensional propagation showing an offset back-to-back porphyrin stacking

The porphyrin in Figure 6 has a ruffled distortion that has the largest deviation from planarity of any of the porphyrins reported here. This can be compared in a displacement plot shown in Figure 7. $Pd^{II}(OEP) \cdot C_{60} \cdot 1.5C_6H_6$ and $Cu^{II}(OEP) \cdot C_{60} \cdot 2C_6H_6$[19] have similar structures with only four ethyl groups of the porphyrin contacting the fullerene and with an analogous back-to-back arrangement of two porphyrins.
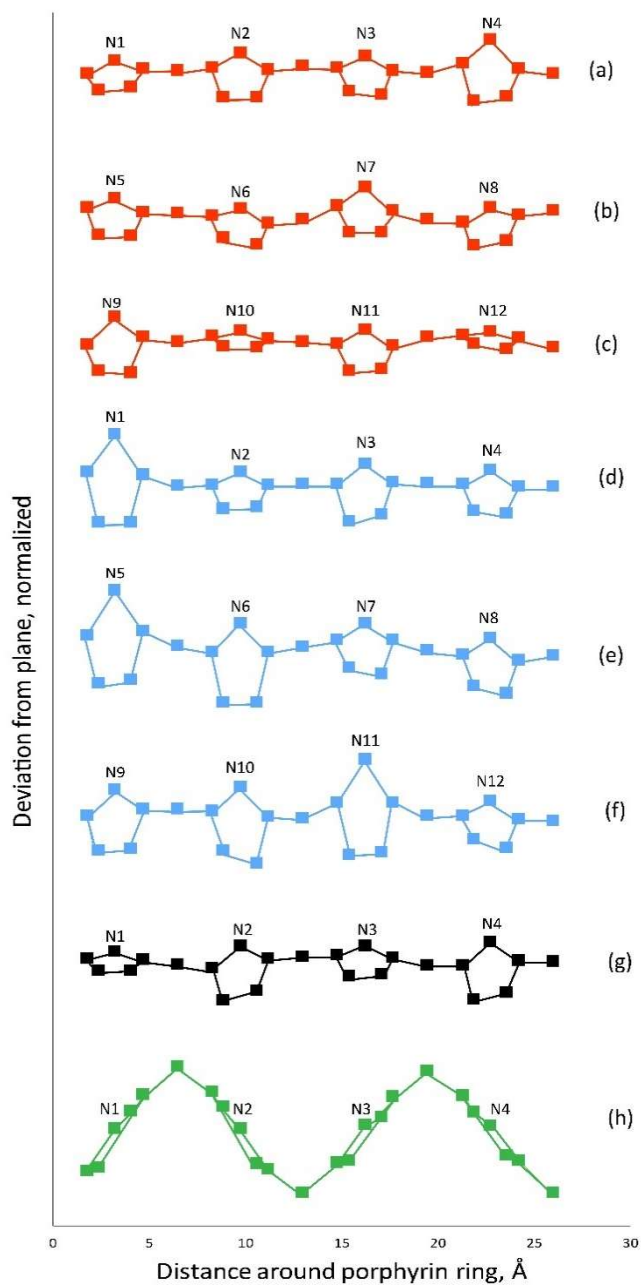
Fig 7. Diagrams comparing the out-of-plane displacements of the porphyrin core atoms from the mean plane of the porphyrin for the three porphyrins in $6Co^{II}(OEP) \cdot 5C_{60} \cdot 5CH_2Cl_2$, (a, b, c) in red; the three porphyrins in $6Zn^{II}(OEP) \cdot 5C_{60} \cdot 5CH_2Cl_2$ (d, e, f) in blue; $Cu^{II}(OEP) \cdot C_{60} \cdot CH_2Cl_2$ (g) in black and $Ni^{II}(OEP) \cdot C_{60} \cdot 0.1CH_2Cl_2 \cdot 1.9C_6H_6$ (h) in green.

Conclusions

Mixing of solutions of M^{II}(OEP) with M = Co, Ni, Cu dissolved in dichloromethane or dichloroethane and C_{60} in benzene produced four different types of cocrystals with each metal ion producing a different structure. In all cases, the M^{II}(OEP) molecules crystallize as back-to-back pairs, but varying numbers of ethyl groups embracing the adjacent C_{60} molecule. Nevertheless, in the structures reported here, all of the fullerene molecules are ordered at 90 K (with the exception of the unbound fullerene in the higher-symmetry $6Co^{II}$(OEP)·$5C_{60}$·$5C_2H_4Cl_2$). In the 6:5 crystals of Co^{II}(OEP) and Zn^{II}(OEP), the thermal parameters for the fullerenes show that thermal motion is the least when the fullerene is surrounded by two porphyrins and the greatest when there is no porphyrin near the C_{60} cage. Cocrystallization produces changes in the planarity of the M^{II}(OEP) molecules with the zinc, cobalt, and copper porphyrins undergoing a dome distortion that puts the metal further from the fullerene. The Ni^{II}(OEP) molecule in Ni^{II}(OEP)·C_{60}·$0.1CH_2Cl_2$·$1.9C_6H_6$ (4) shows a ruffled distortion that is the largest out-of-plane distortion seen in these cocrystals but is smaller than that found in the tetragonal polymorph of pristine Ni^{II}(OEP).[20] The incorporation of only 5% of the chlorinated solvent in case of the Ni(OEP)-DCM combination, and none at all in case of the DCE crystallization setup, represents a deviation from the solvation behavior exhibited in case of the other metal porphyrins. The similarity in the 6:5 structures containing Co^{II} and Zn^{II} and their distinction from the 1:1 combinations observed for Cu^{II} and Ni^{II} points at minor electrostatic and geometric variations massively affecting the overall association of porphyrins and fullerenes and their crystallization. These variations are further explored in Part II.

Part II: Solvent and solvate effects on fullerene-porphyrin cocrystallization[21]

The previous study demonstrated how similar, planar $M^{II}(OEP)$ molecules clear differences between in cocrystal composition and structure. In the following work we address a separate issue: the effect of solvent on cocrystal composition and structure. The crystals in the DCM/DCE series were grown from a mixture of benzene and the chlorinated solvent, but only the chlorinated solvent was found in the cocrystal. This fact is noteworthy since benzene is known to display both π-type face-to-face and C−H−π(C_{60}) interactions with C_{60} in solvated crystals[22] – leading us to think it would incorporate into all cocrystal structures the way it did in the Ni^{II} case. We thus attempted the same crystallization technique as before and replaced the chlorinated solvents with a few more candidates. Crystals were grown using the slow diffusion technique as in Part I.

Discussion and comparison of cocrystal structures

Comparison of the Structures of $Co^{II}(OEP) \cdot C_{60} \cdot CS_2$ and $Zn^{II}(OEP) \cdot C_{60} \cdot CS_2$

$Co^{II}(OEP) \cdot C_{60} \cdot CS_2$ crystallizes in the space group $P\bar{1}$, while $Co^{II}(OEP) \cdot C_{60} \cdot CS_2$ crystallizes in $I2/a$. However, as seen in Figure 7, C_{60} and $M^{II}(OEP)$ molecules are identically organized in both structures: into columns with the carbon disulfide molecules situated off to the sides of these columns. In the Co^{II} case, two porphyrin molecules pack about a center of symmetry to produce a back-to-back array and each porphyrin cups an adjacent C_{60} molecule. Finally, there is close contact between two C_{60} molecules, which pack about a center of symmetry with a centroid-to-centroid distance of 9.889 Å. In $Zn^{II}(OEP) \cdot C_{60} \cdot CS_2$ we still see this back-to-back arrangement; however, it arises from 2-fold crystallographic rotational symmetry. In contrast to the situation in $Co^{II}(OEP) \cdot C_{60} \cdot CS_2$ where all eight ethyl groups embrace the adjacent fullerene, in $Zn^{II}(OEP) \cdot C_{60} \cdot CS_2$ only seven of the ethyl arms surround the neighboring C_{60} molecule. The

unique ethyl group is colored green in Figure 8 and highlighted with a rectangle. It is worthwhile to recall that one ethyl arm in one of the three porphyrins in 6:5Zn is also turned away from embracing the adjacent fullerene, while in the cobalt analogues, 6:5Co, all ethyl arms in all three porphyrins in the asymmetric unit embrace the adjacent C_{60} molecule.
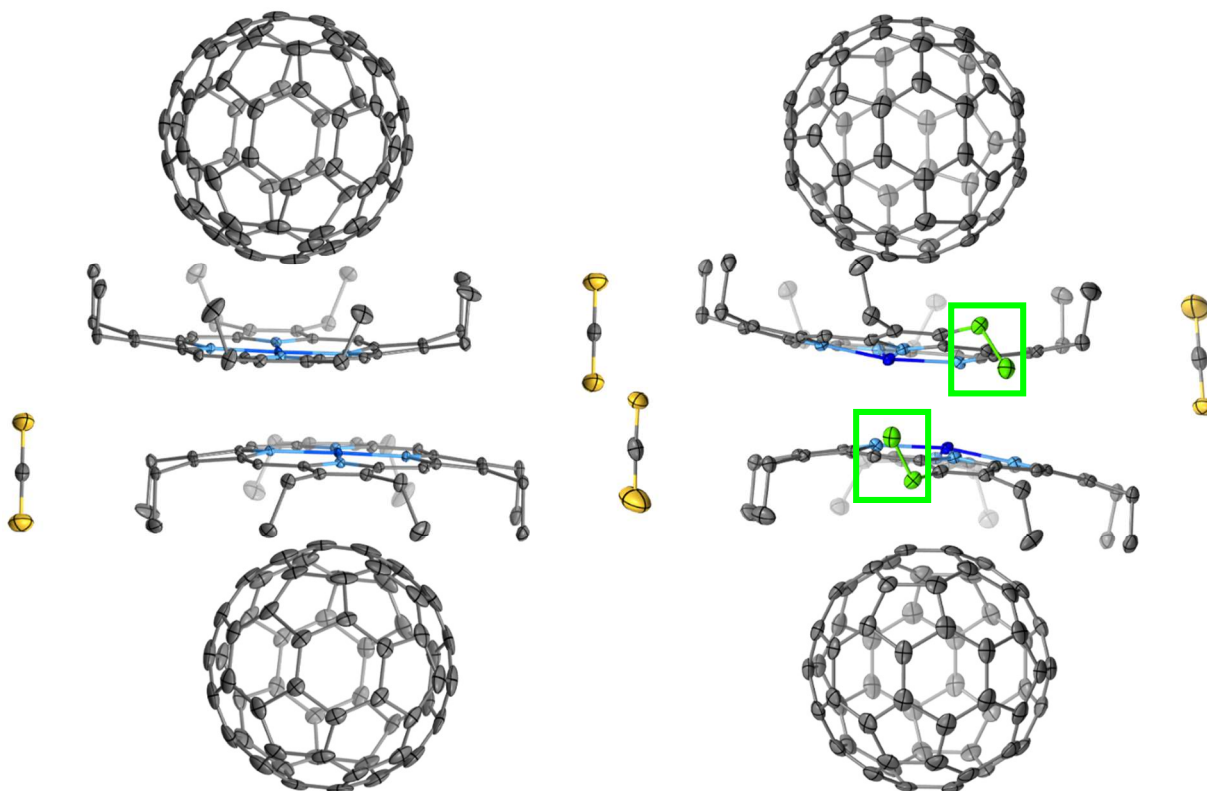

Fig 8. The columnar structure of $P\bar{1}$ $Co^{II}(OEP)\cdot C_{60}\cdot CS_2$ (left) and a portion of the columnar structure of $I2/a$ $Zn^{II}(OEP)\cdot C_{60}\cdot CS_2$ (right). The ethyl arms of the $Zn^{II}(OEP)$ molecules that point away from the C_{60} molecule are colored green.

The molecular packing in $Co^{II}(OEP)\cdot C_{60}\cdot CS_2$ in $P\bar{1}$ and $Zn^{II}(OEP)\cdot C_{60}\cdot CS_2$ in $I2/a$ shares other similarities beyond the columnar organization seen in Figure 8. Both structures reveal a pattern of infinite zigzag chains. The Co structure shows two alternating centroid-to-centroid distances between the C_{60} molecules in each zigzag, 10.029 and 10.297 Å, and a third such distance in between two sets of stacked chains, 9.889 Å. The Zn structure has only one such distance,
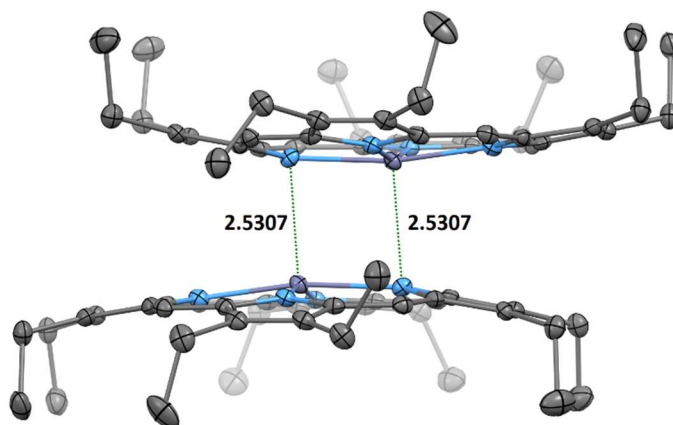
10.101 Å. Molecules of carbon disulfide occupy the cavities produced by the angular arrangement. Within the pair of adjacent porphyrins in the Zn structure, the molecules pack closely and the interplanar Zn−N distance of 2.531(2) Å (Figure 9C).
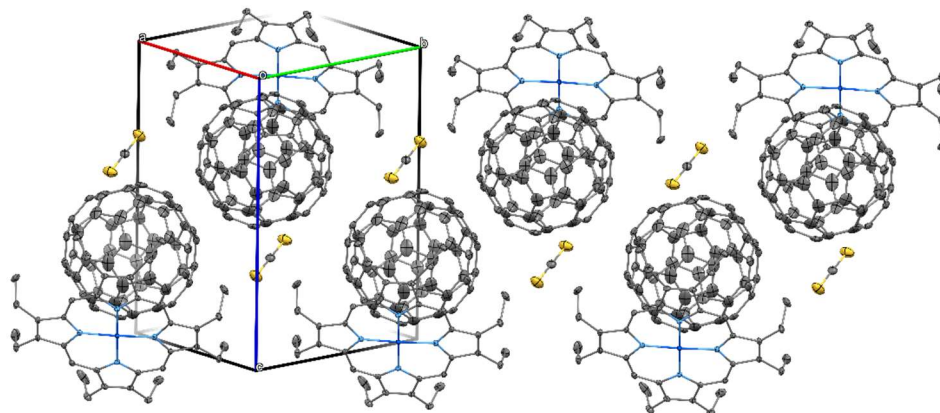
(A)
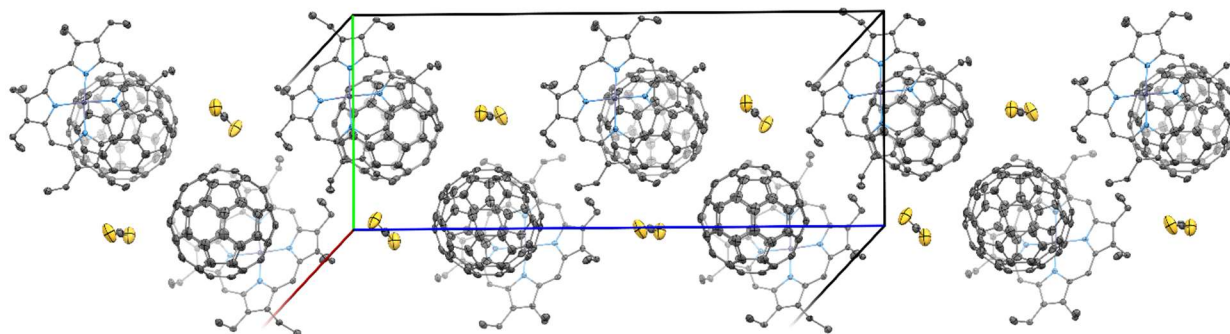
(B)

(C)

Fig 9. Molecular packing and unit cells in $P\overline{1}$ Co^{II}(OEP)·C$_{60}$·CS$_2$ (A) and $I2/a$ Zn^{II}(OEP)·C$_{60}$·CS$_2$

(B) showing the similar zigzag arrangements of fullerenes in each. (C) The short, out-of-plane

Zn−N distance between two adjacent porphyrins in Zn^{II}(OEP)·C$_{60}$·CS$_2$

Comparison of the Structures of ClCoIII(OEP)·C$_{60}$·CCl$_4$ and 2Zn^{II}(OEP)·C$_{60}$·0.75CCl$_4$

With carbon tetrachloride as the solvent for Co^{II}(OEP), crystals of ClCo^{III}(OEP)·C$_{60}$·CCl$_4$

formed. In this case, the cobalt complex was oxidized in a process that does not seem to have

precedent but may involve adventitious dioxygen as the oxidant. The structure of the molecules

within the cocrystal are shown in Figure 10 with disorder removed. All eight ethyl groups in the

ClCo^{III}(OEP) molecule cup the fullerene, while the cobalt ion is drawn away from the fullerene

toward the axial chloride ion. While the porphyrin is ordered, there is crystallographic disorder in

the fullerene and the carbon tetrachloride molecule since they reside on sites with symmetry *m2m*

in the space group *Cmcm*. In contrast, when a benzene solution of C$_{60}$ was allowed to diffuse into

a solution of Zn^{II}(OEP) in carbon tetrachloride, 2Zn^{II}(OEP)·C$_{60}$·0.75CCl$_4$ formed. In this case, two

crystallographically independent Zn^{II}(OEP) molecules surrounded each fully ordered fullerene in

a clamshell arrangement. All eight ethyl groups of each porphyrin surround the adjacent C$_{60}$

molecule and the carbon tetrachloride molecule has only 0.75 fractional occupancy.
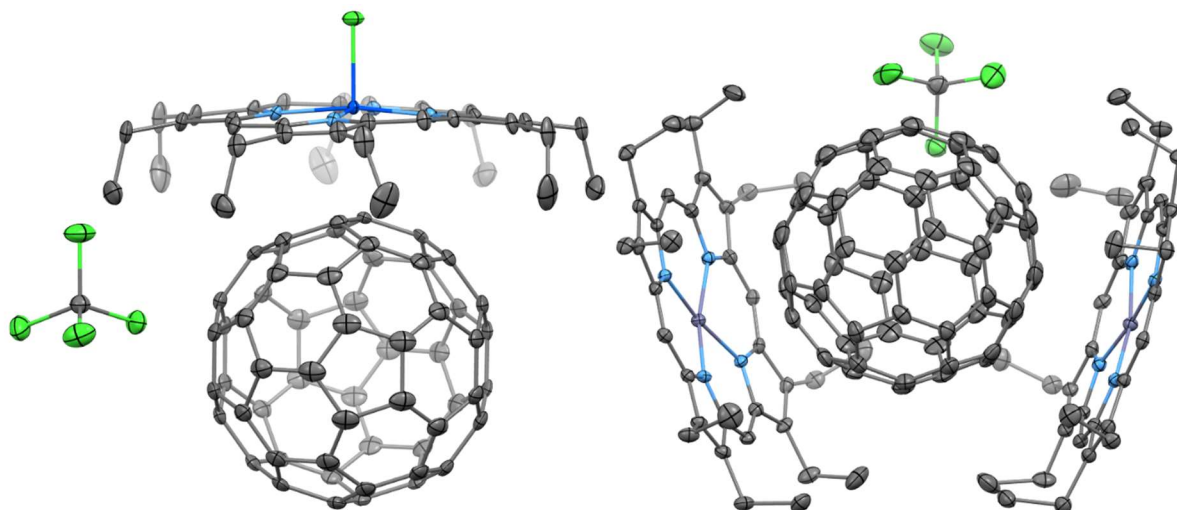
Fig 10. Structures of ClCo^{III}(OEP)·C$_{60}$·CCl$_4$ (left) and 2Zn^{II}(OEP)·C$_{60}$·0.75CCl$_4$ (right), with disorder removed for the Zn structure.

Figure 11 shows the molecular packing for ClCo^{III}(OEP)·C$_{60}$·CCl$_4$ and 2Zn^{II}(OEP)·C$_{60}$·0.75CCl$_4$. Because of the presence of the axial chloride ligand, there is no back-to-back arrangement of the porphyrins in the five-coordinate C structure. However, a zigzag pattern of C$_{60}$ molecules (similar to the CS$_2$ solvated structures) is clearly present. The 2Zn^{II}(OEP)·C$_{60}$ units are organized into columns in which there is back-to-back contact between two porphyrins as seen in Figure 11. However, the Zn−N distance (2.609(3) Å) between adjoining porphyrins is much longer than the corresponding distance (2.531(2) Å) in Zn^{II}(OEP)·C$_{60}$·CS$_2$. The carbon tetrachloride molecules are situated to the sides of these columns. The cell parameters and structure of 2Zn^{II}(OEP)·C$_{60}$·0.75CCl$_4$ are similar to those of the previously reported 2Co^{II}(OEP)·C$_{60}$·CHCl$_3$,[10] which has an analogous clamshell arrangement with two porphyrins surrounding each C$_{60}$ molecule.
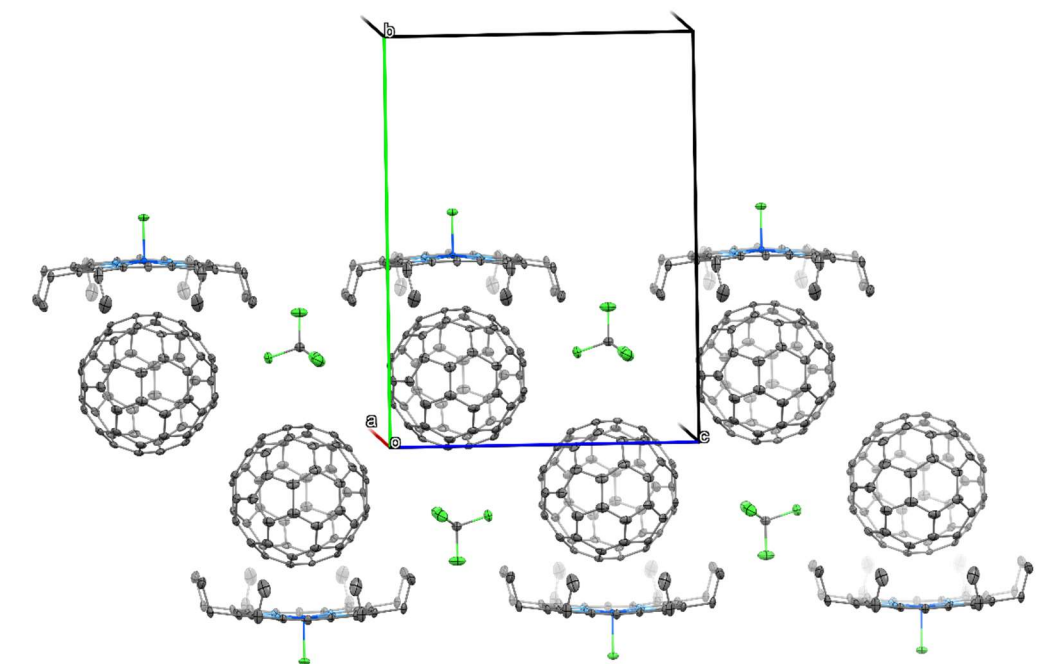
(A)
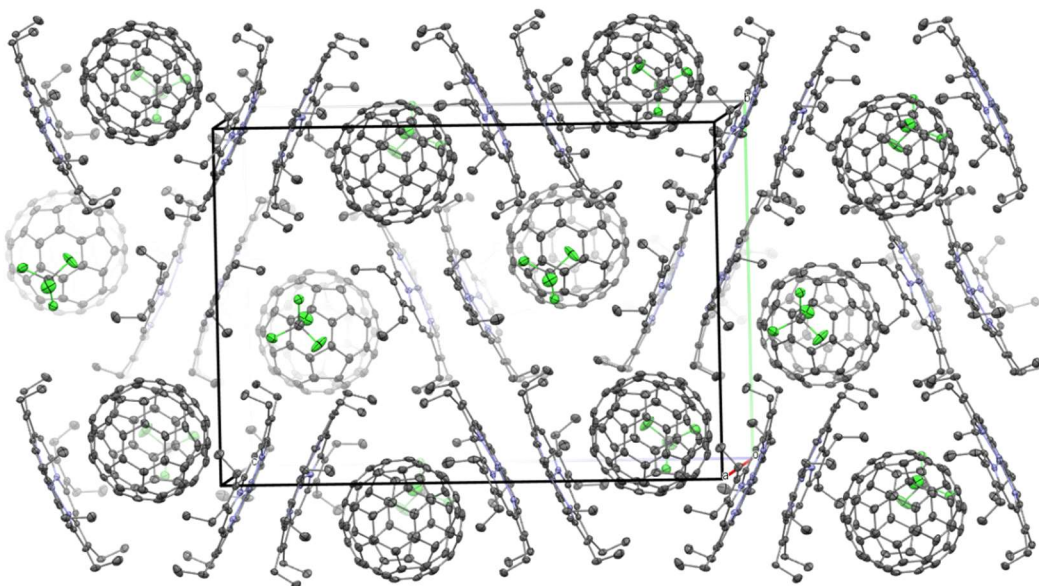
(B)

**Fig 11. Molecular packing and unit cell for ClCo^{III}(OEP)·C$_{60}$·CCl$_4$ (A) showing the zigzag arrangements of the fullerene molecules. The disorder in the positions of the C60 and carbon**

**tetrachloride molecules is not shown for simplicity. (B) Molecular packing for**

$2Zn^{II}(OEP) \cdot C_{60} \cdot 0.75CCl_4$
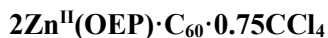
Comparisons of the Dioxane Solvates $Co^{II}(OEP) \cdot C_{60} \cdot C_4H_8O_2$ and $(C_4H_8O_2)Zn^{II}(OEP) \cdot C_{60} \cdot C_4H_8O_2$

$Co^{II}(OEP) \cdot C_{60} \cdot C_4H_8O_2$ and $(C_4H_8O_2)$-$Zn^{II}(OEP) \cdot C_{60} \cdot C_4H_8O_2$, are produced when dioxane

is used as the solvent for the porphyrin. The structure of $Co^{II}(OEP) \cdot C_{60} \cdot C_4H_8O_2$ which crystallizes

in the space group $P2_1/c$ and contains one cobalt porphyrin, one fullerene, and one dioxane

molecule in the asymmetric unit, is shown in (A) of Figure 12. The structure of

$Co^{II}(OEP) \cdot C_{60} \cdot C_4H_8O_2$ bears considerable similarity to the CO and Zn CS_2 solvates, although each

cocrystal belongs to a different space group. The zigzag arrangement is shown in (C) of Figure 12.

The fullerene is fully ordered with the eight ethyl groups of the porphyrin surrounding it. The

structure of $(C_4H_8O_2)$-$Zn^{II}(OEP) \cdot C_{60} \cdot C_4H_8O_2$ shown in Figure 12B involves a fullerene that is

disordered over two positions, an ordered $Zn^{II}(OEP)$ molecule that is coordinated by a disordered

dioxane molecule, which occupies two sites, and an ordered dioxane molecule as a solvate. The

zinc ion is located away from the fullerene, since it is coordinated to the axial dioxane ligand. The

$Zn-O$ distance is 2.277(3) Å. All eight ethyl groups surround the C_{60} molecule. The molecular

packing for $(C_4H_8O_2)$ $Zn^{II}(OEP) \cdot C_{60} \cdot C_4H_8O_2$ is shown in Figure 12D. Zigzag arrangements of

fullerene molecules are apparent and similar to those found in the five-coordinate porphyrin

cocrystal, $ClCo^{III}(OEP) \cdot C_{60} \cdot CCl_4$.
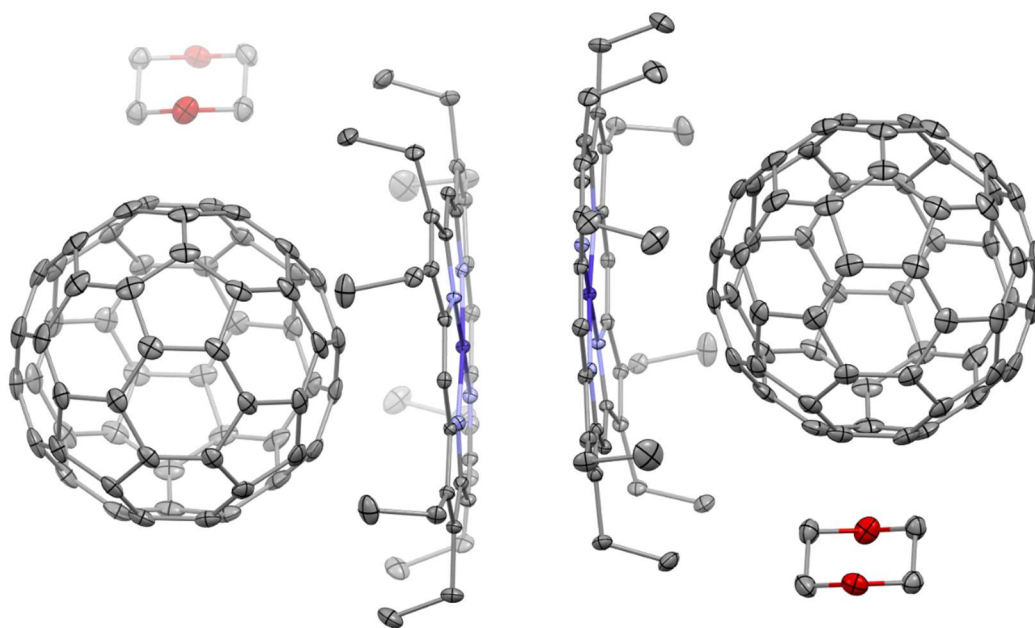
(A)
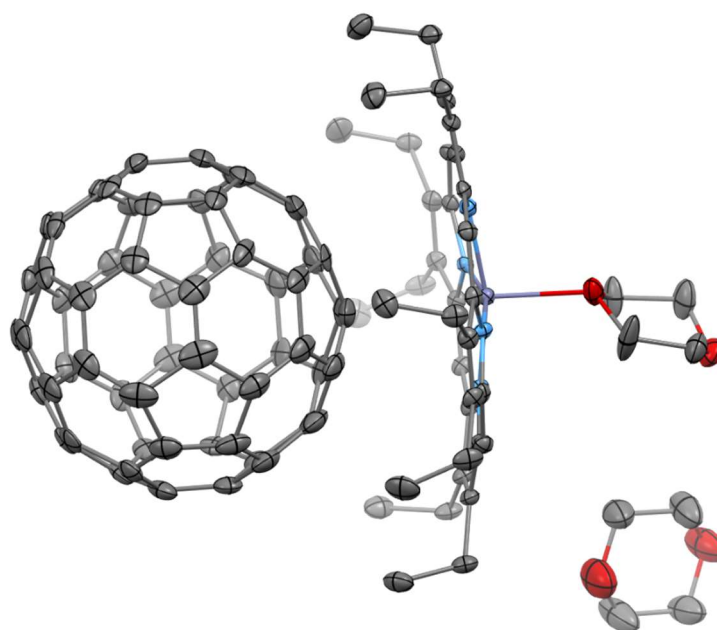
(B)
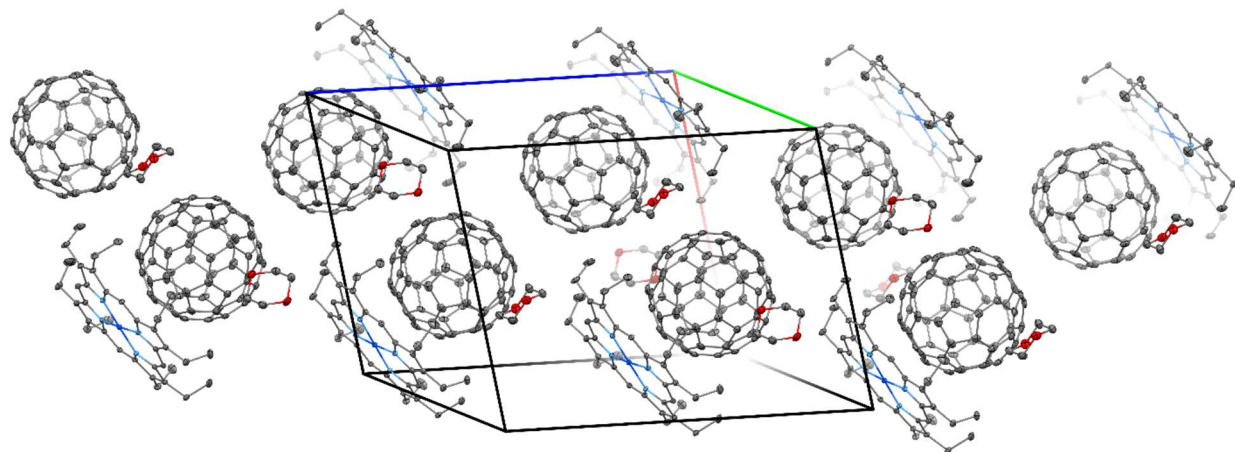
(C)
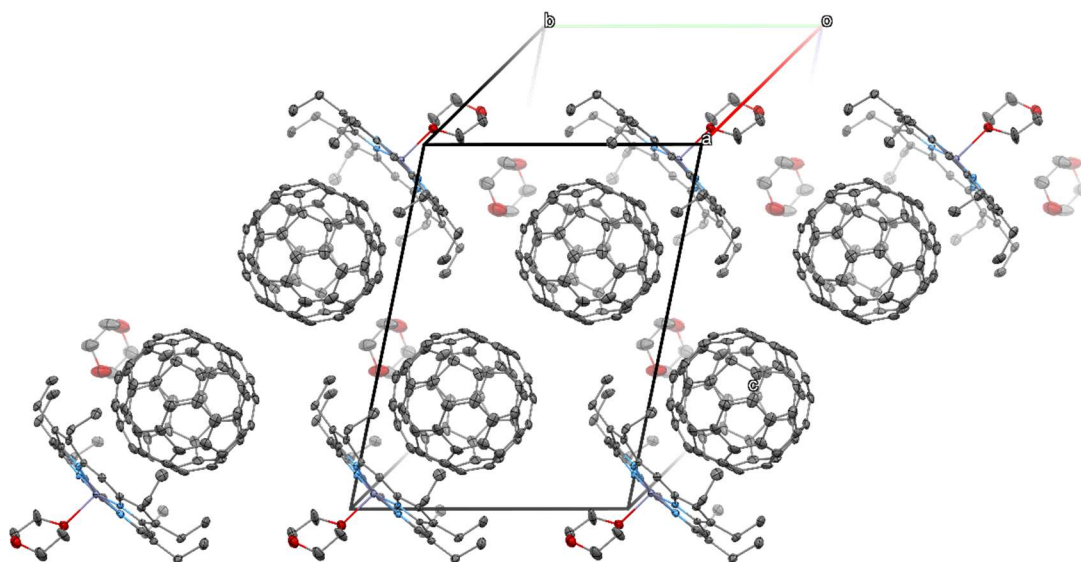
(D)

Fig 12. portion of the columnar structure Co^{II}(OEP)·C$_{60}$·C$_4$H$_8$O$_2$, which crystallizes in the space group P21/c, showing the back-to-back arrangements of the porphyrins and the locations of the solvate molecules beside the fullerene. (B) The structure of (C$_4$H$_8$O$_2$) Zn^{II}(OEP)·C$_{60}$·C$_4$H$_8$O$_2$ (C) Molecular packing for Co^{II}(OEP)·C$_{60}$·C$_4$H$_8$O$_2$ showing the zigzag arrangements of the fullerene molecules (D) Molecular packing for (C$_4$H$_8$O$_2$) Zn^{II}(OEP)·C$_{60}$·C$_4$H$_8$O$_2$ showing the zigzag arrangements of the fullerene molecules

The Tetrahydrofuran Solvates, Cu^{II}(OEP)·C$_{60}$·C$_4$H$_8$O and 2Co^{II}(OEP)·C$_{60}$·C$_4$H$_8$O

An analogous structure to the $Co^{II}(OEP) \cdot C_{60} \cdot C_4H_8O_2$ compound discussed above is obtained by combining C_{60} in benzene and $Cu^{II}(OEP)$ in tetrahydrofuran (THF). It exhibits a very similar columnar structure (Figure 13A) with C_{60} and the porphyrin both forming back-to-back interactions, and has a similar zigzag arrangement in two dimensions (Figure 13B). Figure 13C shows a side by side comparison of $Co^{II}(OEP) \cdot C_{60} \cdot C_4H_8O_2$ and $Cu^{II}(OEP) \cdot C_{60} \cdot C_4H_8O$.
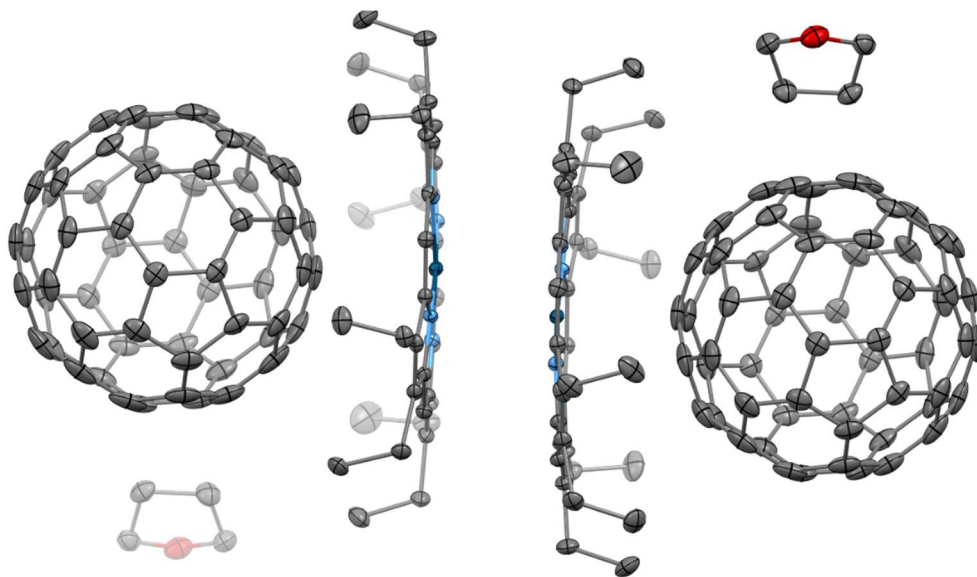
(A)
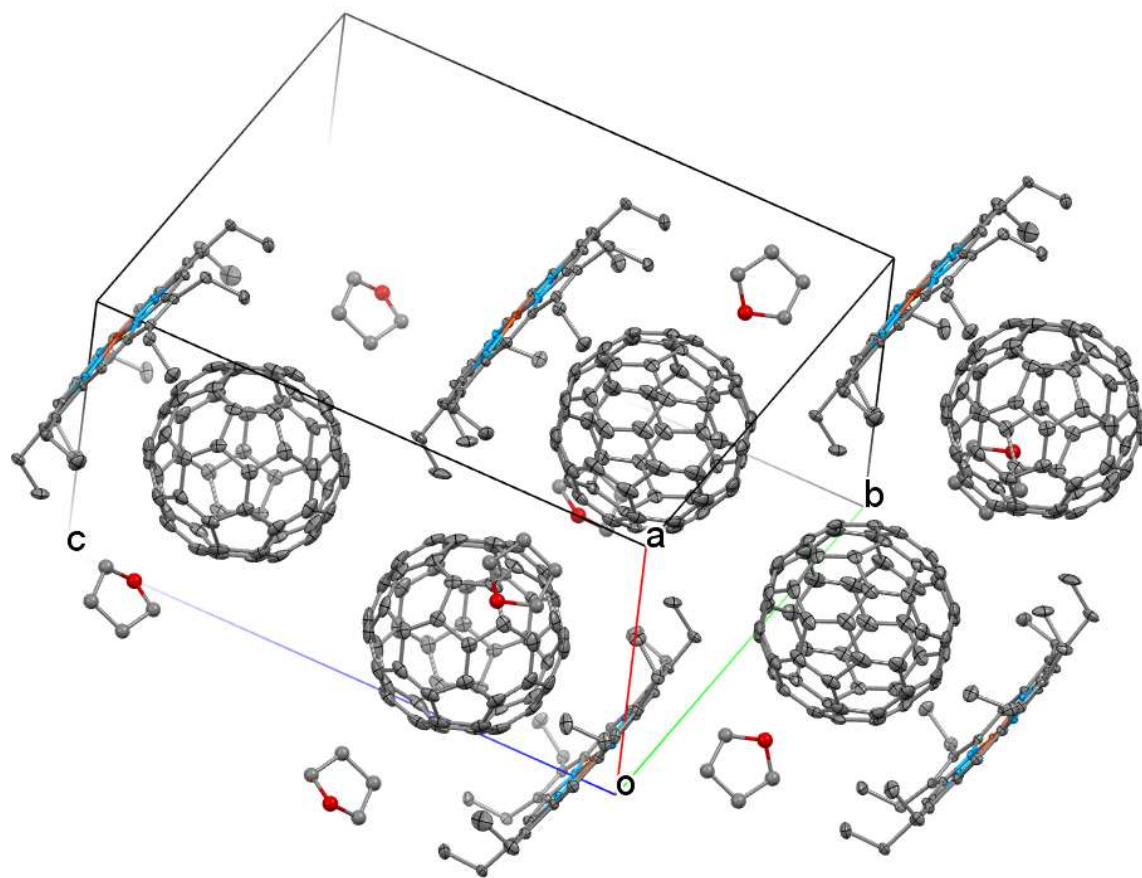
(B)
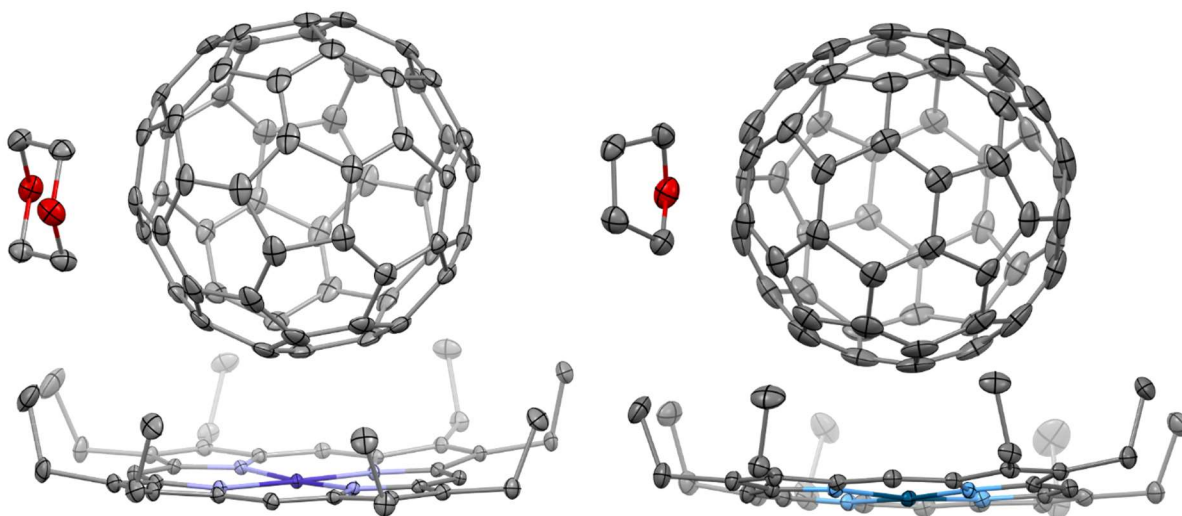
(C)

Fig 13. (A) The columnar arrangement of Cu^{II}(OEP)·C$_{60}$·C$_4$H$_8$O. (B) The zigzag arrangement of fullerenes in Cu^{II}(OEP)·C$_{60}$·C$_4$H$_8$O. (C) a comparison of Co^{II}(OEP)·C$_{60}$·C$_4$H$_8$O$_2$ (left) and Cu^{II}(OEP)·C$_{60}$·C$_4$H$_8$O (right).

When a solution of C$_{60}$ in benzene was allowed to diffuse into a solution of Co^{II}(OEP) in tetrahydrofuran, a THF-containing 2:1 solvate, 2Co^{II}(OEP)·C$_{60}$·C$_4$H$_8$O formed. A view of the asymmetric unit, which contains a molecule of each of the components, is shown in Figure 14A. The clamshell structure of 2Co^{II}(OEP)·C$_{60}$·C$_4$H$_8$O is similar to that of 2Zn^{II}(OEP)·C$_{60}$·0.75CCl$_4$ (4) described above. Both of these cocrystals are found in the same space group, $P2_12_12_1$ and the molecular packing for 2Co^{II}(OEP)·C$_{60}$·C$_4$H$_8$O (Figure 14B) is similar to that shown in Figure 11B for 2Zn^{II}(OEP)·C$_{60}$·0.75CCl$_4$. Under similar crystallization conditions using Zn^{II}(OEP), only low-quality crystals of a tetrahydrofuran solvate of C$_{60}$ formed instead of a cocrystal.
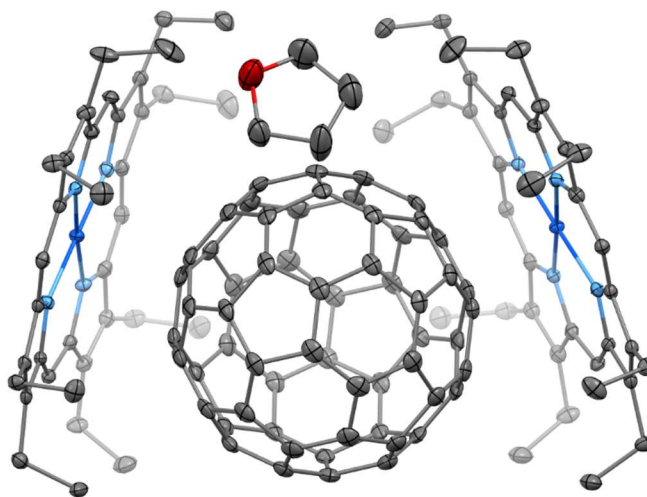
(A)
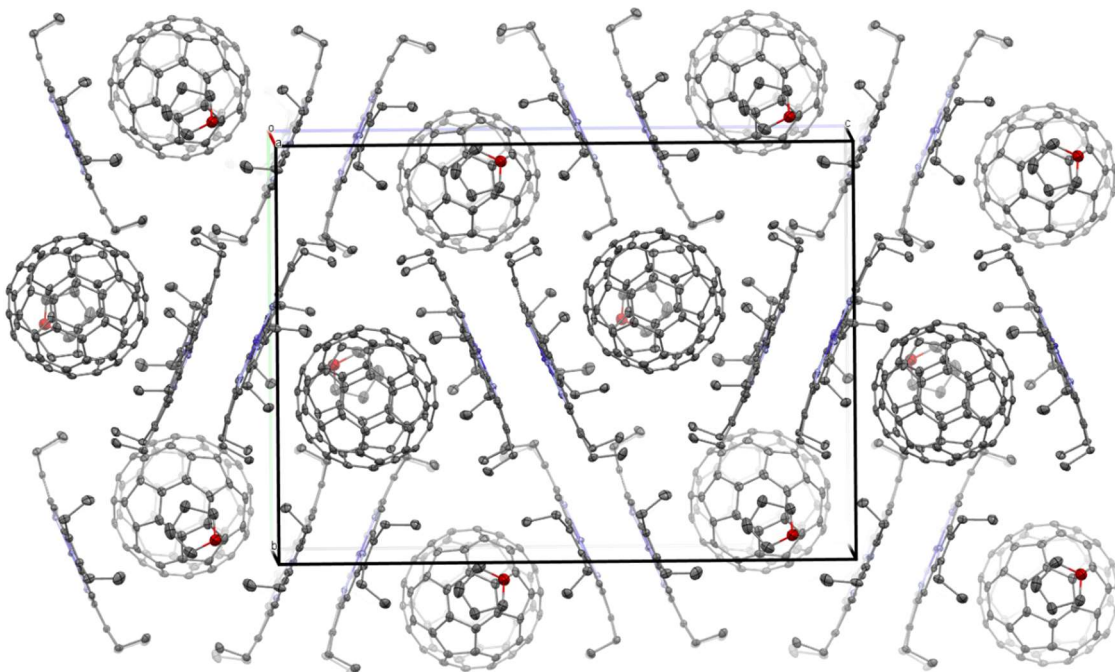
(B)

Fig 14. (A) The asymmetric unit of $2Co^{II}(OEP) \cdot C_{60} \cdot C_4H_8O$. (B) The packing in

$2Co^{II}(OEP) \cdot C_{60} \cdot C_4H_8O$

The porphyrin macrocycles in these cocrystals show some deviations from planarity as is common with such cocrystals. The various types of porphyrin distortions have been classified as ruffed, saddled, domed, waved (wav-(x) or wav-(y)), or pyrrole propellered. Figure 15 shows diagrams representing the out-of-plane displacements of the porphyrin core atoms from the mean plane of the porphyrin for the structures discussed above, in addition to the benzene solvate, $Co^{II}(OEP).C_{60}.1.5C_6H_6$. The y-axis represents deviation or departure from planarity, which is calculated in each case by setting the plane to be the average of the four nitrogen and 20 sp2 hybridized carbon atoms constructing the aromatic system, and then mapping the positive or negative deviation of each individual atom from the plane average. The x-axis represents a "linearized" form of a porphyrin macrocycle. Most of the porphyrins in this series show a dome distortion. The exception is five-coordinate $ClCo^{III}(OEP) \cdot C_{60} \cdot CCl_4$ which has a wav-(y) distortion.

56

This is in contrast to $(C_4H_8O_2)Zn^{II}(OEP)\cdot C_{60}\cdot C_4H_8O_2$ in (g), where the steric bulk and flapping in the axial ligand affects the four pyrroles unequally and causes the porphyrin to be severely domed.
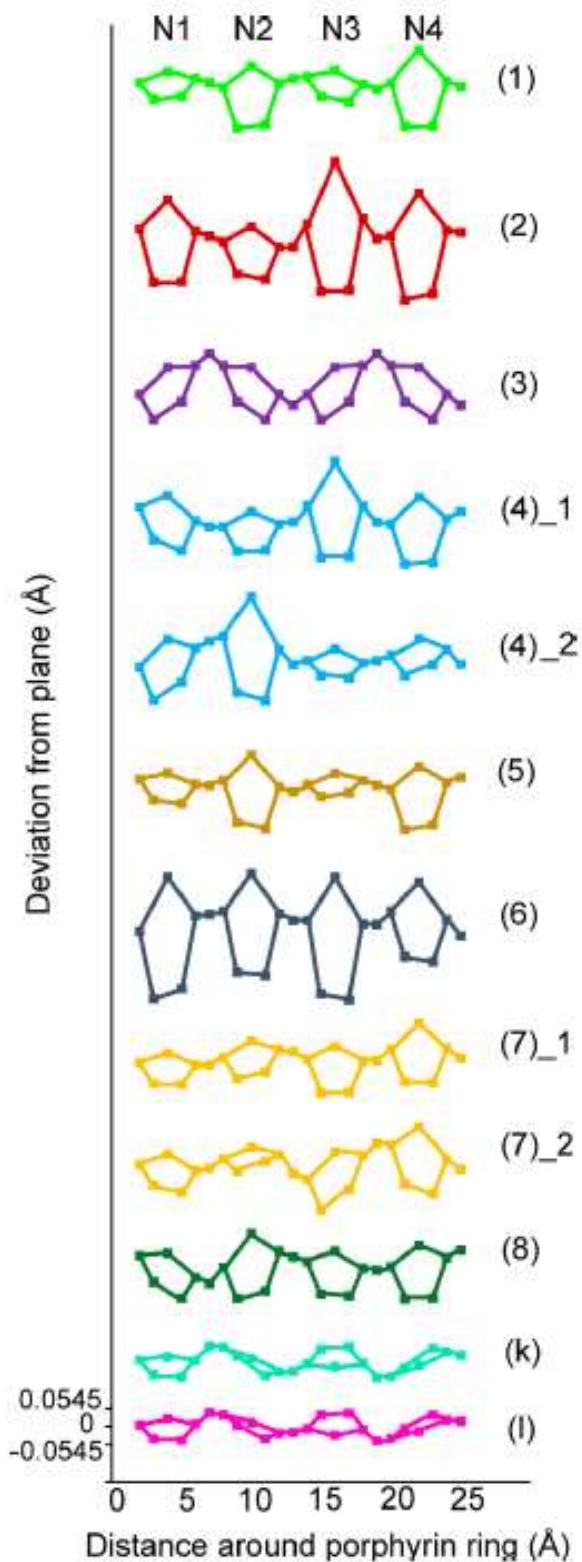
Fig 15. Comparison of the out-of-plane displacements of the porphyrin core atoms from the mean porphyrin plane as visualized in a linear fashion, for (Co^{II}(OEP)·C$_{60}$·CS$_2$ (1); Zn^{II}(OEP)·C$_{60}$·CS$_2$ (2); ClCo^{III}(OEP)·C$_{60}$·CCl$_4$ (3); the two symmetrically unrelated porphyrins in 2Zn^{II}(OEP)·C$_{60}$·0.75CCl$_4$ (4)_1 and (4)_2; Co^{II}(OEP)·C$_{60}$·C$_4$H$_8$O$_2$ (5); (C$_4$H$_8$O$_2$)Zn^{II}(OEP)·C$_{60}$·C$_4$H$_8$O$_2$ (6); the two symmetrically unrelated porphyrins in 2Co^{II}(OEP)·C$_{60}$·C$_4$H$_8$O(7)_1 and (7)_2; Co^{II}(OEP)·C$_{60}$·1.5C$_6$H$_6$ (8); (k) Co^{II}(OEP) (from data in Ref 22);[23] (l) Zn^{II}(OEP) (from data in Ref 23).[24]

Conclusions: The Solvent Dependence of Cocrystal Formation with M^{II}(OEP)

Table 2 presents a survey of the types of cocrystals found for Co^{II} and Zn^{II} using eight different solvents to dissolve the porphyrin (with the fullerene always) in benzene solution. Different colors are used to identify different structural types. As these data indicate, crystals with the 6:5 ratio only form when dichloromethane or 1,2-dichloroethane is the solvent. Three other classes of new cocrystals have been prepared: Class 1 with ordered crystals with a 1:1 porphyrin/fullerene ratio including Co^{II}(OEP)·C$_{60}$·CS$_2$, Zn^{II}(OEP)·C$_{60}$·CS$_2$, Co^{II}(OEP)·C$_{60}$·C$_4$H$_8$O$_2$, Co^{II}(OEP)·C$_{60}$·1.5C$_6$H$_6$; Class 2 with ordered crystals with a 2:1 porphyrin/fullerene ratio including 2Zn^{II}(OEP)·C$_{60}$·0.75CCl$_4$ and 2Co^{II}(OEP)·C$_{60}$·C$_4$H$_8$O; and Class 3 with a five-coordinate metal and a disordered fullerene cage including ClCo^{III}(OEP)·C$_{60}$·CCl$_4$ and (C$_4$H$_8$O2)Zn^{II}(OEP)·C$_{60}$·C$_4$H$_8$O$_2$. Class 1 involves cocrystals forming in three different space groups, $P1$, $I2/a$, and $P2_1/c$. Nevertheless, cocrystals in this class possess common structural features: the formation of extended columns zigzag arrays of fullerenes. However, the inclusion of different solvate molecules results in crystallization of Class 1 cocrystals in different space groups with different symmetry elements generating the common patterns of intermolecular interactions. All of the cocrystals in Class 2, which include some previously

identified members isostructural and crystallize in the space group $P2_12_12_1$ and have the clam-shell arrangements. The two members of Class 3 crystallize in different space groups, but both cocrystals show a zigzag pattern of fullerene cages as seen in the packing diagrams. Cocrystallization of a five-coordinate porphyrin, LM(OEP), with C_{60} seems to be always accompanied by disorder in the fullerene, as seen in other axially ligated porphyrins such as $ClFe^{III}(OEP) \cdot C_{60} \cdot CHCl_3$,[10] $ClIn^{III}(OEP) \cdot C_{60} \cdot C_6H_6$,[25] and $Zn^{II}(OEP)$-4,4′-bipyridine-$Zn^{II}(OEP) \cdot 2C_{60} \cdot 2CHCl_3$.[17] Consequently, five-coordinate LM(OEP) complexes would be poor choices to use if one wanted to produce cocrystals with ordered fullerenes.

Our results indicate that the choice of solvents utilized to grow cocrystals of $M^{II}(OEP)$ with C_{60} directs the composition and structure of the cocrystal that forms. The information in Table 2 also demonstrates the importance of the solvent and solvate molecules in determining the type of cocrystal that forms. Solvent, not the solution stoichiometry, determines the composition of the cocrystal that forms. In particular, our efforts to prepare crystals of Class 2 with a clamshell structure by altering the ratio of porphyrin to fullerene in the growth solution have not been successful. Although all of the cocrystals reported here have been obtained from a mixture of two solvents, it is remarkable that only one type of solvate molecule is found in each cocrystal. Despite the fact that the benzene-containing cocrystals $Co^{II}(OEP) \cdot C_{60} \cdot 1.5C_6H_6$ and $Zn^{II}(OEP) \cdot C_{60} \cdot 2C_6H_6$ could have formed in the cases where carbon disulfide, carbon tetrachloride, dioxane, tetrahydrofuran, dichloromethane, 1,2-dichloroethane, or chloroform were used to dissolve the porphyrin, benzene was not incorporated into any of the cocrystals that formed. In cases where cocrystallization of a fullerene or endohedral fullerene with $M^{II}(OEP)$ leads to a disordered structure as sometimes occurs, redissolving the sample in a different solvent mixture followed by slow evaporation may produce an entirely different cocrystal, which may not suffer from disorder.

Additionally, it may be beneficial in such a case to utilize a different $M^{II}(OEP)$ that is likely to form another type of cocrystal that may not suffer from disorder. Because of the reoccurrence of the clamshell structure type with $Zn^{II}(OEP)$ and the unusually clean ordering of all fullerenes (even that unbound by a porphyrin) in the 6:5Zn columnar structures, we have come to accept the confluence of $Zn^{II}(OEP)$ and chlorinated solvents as the most favorable combination when attempting to obtain well-ordered C_{60}, and this situation may pertain for other fullerenes.

	$Co^{II}(OEP)$	$Zn^{II}(OEP)$
Carbon disulfide	1:1 $P\bar{1}$ LUTQAV	1:1 $I2/a$ LUTQEZ
Carbon Tetrachloride	1:1 $Cmcm$ LUTRUQ	2:1 $P2_12_12_1$ LUTQID
Dioxane	1:1 $P2_1/c$ LUTSAX	1:1 $P\bar{1}$ LUTQOJ
Tetrahydrofuran	2:1 $P2_12_12_1$ LUTSEB	None
Chlorobenzene	1:1 $P\bar{1}$ **(9)**	1:1 $P\bar{1}$ **(10)**
1,1,2-trichloroethane	1:1 $P\bar{1}$	None
Dichloromethane	6:5 $P\bar{1}$ NOZFEQ	6:5 $P\bar{1}$ NOZFIU
Dichloroethane	6:5 $C2/m$ NOZFUG	6:5 $P\bar{1}$ NOZGAN
	2:1	2:1

Chloroform	$P2_12_12_1$ CELTIW	$P2_12_12_1$ CELVAQ
Benzene	1:1 $P\bar{1}$ LUTSIF	2:1 $P2_12_12_1$ QARQIJ

Table 2. Structures color-coded to represent 2:1 clamshell, all-syn 1:1, 6:5 column, axially coordinated, 1:1 with one anti ethyl group

References

(1) Zhang, R.; Murata, M.; Aharen, T.; Wakamiya, A.; Shimoaka, T.; Hasegawa, T.; Murata, Y. Synthesis of a Distinct Water Dimer inside Fullerene C_{70}. *Nature Chemistry* **2016**, *8* (5). https://doi.org/10.1038/nchem.2464.

(2) Krylov, D. S.; Liu, F.; Brandenburg, A.; Spree, L.; Bon, V.; Kaskel, S.; Wolter, A. U. B.; Büchner, B.; Avdoshenko, S. M.; Popov, A. A. Magnetization Relaxation in the Single-Ion Magnet $DySc_2N@C_{80}$: Quantum Tunneling, Magnetic Dilution, and Unconventional Temperature Dependence. *Physical Chemistry Chemical Physics* **2018**, *20* (17). https://doi.org/10.1039/c8cp01608a.

(3) Bloodworth, S.; Gräsvik, J.; Alom, S.; Kouřil, K.; Elliott, S. J.; Wells, N. J.; Horsewill, A. J.; Mamone, S.; Jiménez-Ruiz, M.; Rols, S.; Nagel, U.; Rõõm, T.; Levitt, M. H.; Whitby, R. J. Synthesis and Properties of Open Fullerenes Encapsulating Ammonia and Methane. *ChemPhysChem* **2018**, *19* (3). https://doi.org/10.1002/cphc.201701212.

(4) Pan, C.; Shen, W.; Yang, L.; Bao, L.; Wei, Z.; Jin, P.; Fang, H.; Xie, Y.; Akasaka, T.; Lu, X. Crystallographic Characterization of Y_2C_{2n} (2 n = 82, 88-94): Direct Y-Y Bonding and Cage-Dependent Cluster Evolution. *Chemical Science* **2019**, *10* (17). https://doi.org/10.1039/c9sc00941h.

(5) Konarev, D. v.; Khasanov, S. S.; Otsuka, A.; Saito, G.; Lyubovskaya, R. N. Peculiarities of C_{60}- Coordination to Cobalt(II) Octaethylporphyrin in Ionic Multicomponent Complexes: Observation of the Reversible Formation of Co-C(C60-) Coordination Bonds. *Chemistry - A European Journal* **2006**, *12* (20). https://doi.org/10.1002/chem.200600132.

(6)   Futagoishi, T.; Murata, M.; Wakamiya, A.; Sasamori, T.; Murata, Y. Expansion of Orifices of Open C_{60} Derivatives and Formation of an Open $C_{59}S$ Derivative by Reaction with Sulfur. *Organic Letters* **2013**, *15* (11). https://doi.org/10.1021/ol401083c.

(7)   Filatov, A. S.; Ferguson, M. v.; Spisak, S. N.; Li, B.; Campana, C. F.; Petrukhina, M. A. Bowl-Shaped Polyarenes as Concave-Convex Shape Complementary Hosts for C_{60}- and C_{70}-Fullerenes. *Crystal Growth and Design* **2014**, *14* (2). https://doi.org/10.1021/cg401616j.

(8)   Karunanithi, K.; Bhyrappa, P. Structural Elucidation of a Few Electron-Deficient Porphyrin/Fullerene Cocrystallates: Effect of Fullerene on the Porphyrin Ring Conformation. *Inorganica Chimica Acta* **2015**, *427*. https://doi.org/10.1016/j.ica.2014.12.003.

(9)   Konarev, D. v.; Neretin, I. S.; Slovokhotov, Y. L.; Yudanova, E. I.; Drichko, N. v.; Shul'ga, Y. M.; Tarasov, B. P.; Gumanov, L. L.; Batsanov, A. S.; Howard, J. A. K.; Lyubovskaya, R. N. New Molecular Complexes of Fullerenes C_{60} and C_{70} with Tetraphenylporphyrins [M(Tpp)], in Which M = H_2, Mn, Co, Cu, Zn, and FeCl. *Chemistry - A European Journal* **2001**, *7* (12). https://doi.org/10.1002/1521-3765(20010618)7:12<2605::AID-CHEM26050>3.0.CO;2-P.

(10)   Olmstead, M. M.; Costa, D. A.; Maitra, K.; Noll, B. C.; Phillips, S. L.; van Calcar, P. M.; Balch, A. L. Interaction of Curved and Flat Molecular Surfaces. The Structures of Crystalline Compounds Composed of Fullerene (C_{60}, $C_{60}O$, C_{70}, and $C_{120}O$) and Metal Octaethylporphyrin Units. *Journal of the American Chemical Society* **1999**, *121* (30). https://doi.org/10.1021/ja990618c.

(11)   Stevenson, S.; Rothgeb, A. J.; Tepper, K. R.; Duchamp, J.; Dorn, H. C.; Powers, X. B.; Roy, M.; Olmstead, M. M.; Balch, A. L. Isolation and Crystallographic Characterization of Two, Nonisolated Pentagon Endohedral Fullerenes: $Ho_3N@C_2(22010)$-C_{78} and $Tb_3N@C_2(22010)$-C_{78}. *Chemistry - A European Journal* **2019**, *25* (54). https://doi.org/10.1002/chem.201902559.

(12)   Beavers, C. M.; Chaur, M. N.; Olmstead, M. M.; Echegoyen, L.; Balch, A. L. Large Metal Ions in a Relatively Small Fullerene Cage: The Structure of $Gd_3N@C_2(22010)$-C_{78} Departs from the Isolated Pentagon Rule. *Journal of the American Chemical Society* **2009**, *131* (32). https://doi.org/10.1021/ja903741r.

(13)   Roy, M.; Olmstead, M. M.; Balch, A. L. Metal Ion Effects on Fullerene/Porphyrin Cocrystallization. *Crystal Growth and Design* **2019**, *19* (11). https://doi.org/10.1021/acs.cgd.9b01092.

(14)   Dubrovin, V.; Gan, L. H.; Büchner, B.; Popov, A. A.; Avdoshenko, S. M. Endohedral Metal-Nitride Cluster Ordering in Metallofullerene-Ni^{II}(OEP) Complexes and Crystals: A Theoretical Study. *Physical Chemistry Chemical Physics* **2019**, *21* (16). https://doi.org/10.1039/c9cp00634f.

(15)   Yang, H.; Beavers, C. M.; Wang, Z.; Jiang, A.; Liu, Z.; Jin, H.; Mercado, B. Q.; Olmstead, M. M.; Balch, A. L. Isolation of a Small Carbon Nanotube: The Surprising Appearance of D 5h(1)-C90. *Angewandte Chemie - International Edition* **2010**, *49* (5). https://doi.org/10.1002/anie.200906023.

(16)   Konarev, D. v.; Khasanov, S. S.; Saito, G.; Lyubovskaya, R. N. Design of Molecular and Ionic Complexes of Fullerene C_{60} with Metal(II) Octaethylporphyrins, M^{II}OEP (M = Zn,

Co, Fe, and Mn) Containing Coordination M-N(Ligand) and M-C(C60-) Bonds. *Crystal Growth and Design* **2009**, *9* (2). https://doi.org/10.1021/cg8010184.

(17)   Cullen, D. L.; Meyer Jnr, E. F. The Crystal and Molecular Structure of 2,3,7,8,12,13,17,18-Octaethylporphinatomonopyridinezinc(II). *Acta Crystallographica Section B Structural Crystallography and Crystal Chemistry* **1976**, *32* (8). https://doi.org/10.1107/s0567740876007565.

(18)   Lee, H. M.; Olmstead, M. M.; Suetsuna, T.; Shimotani, H.; Dragoe, N.; Cross, R. J.; Kitazawa, K.; Balch, A. L. Crystallographic Characterization of $Kr@C_{60}$ in $(0.09Kr@C_{60}/0.91C_{60})\cdot(Ni^{II}(OEP))\cdot2C_6H_6$. *Chemical Communications* **2002**, *2* (13). https://doi.org/10.1039/b202925c.

(19)   Ishii, T.; Aizawa, N.; Yamashita, M.; Matsuzaka, H.; Kodama, T.; Kikuchi, K.; Ikcmoto, I.; Iwasa, Y. First Syntheses of Cocrystallites Consisting of anti-Formed Metal Octaethylporphyrins with Fullerene C_{60}. *Journal of the Chemical Society, Dalton Transactions* **2000**, No. 23. https://doi.org/10.1039/b006593p.

(20)   Meyer, E. F. The Crystal and Molecular Structure of Nickel(II)Octaethylporphyrin. *Acta Crystallographica Section B Structural Crystallography and Crystal Chemistry* **1972**, *28* (7). https://doi.org/10.1107/s0567740872005722.

(21)   Roy, M.; Diaz Morillo, I. D.; Carroll, X. B.; Olmstead, M. M.; Balch, A. L. Solvent and Solvate Effects on the Cocrystallization of C_{60} with $Co^{II}(OEP)$ or $Zn^{II}(OEP)$ (OEP = Octaethylporphyrin). *Crystal Growth and Design* **2020**, *20* (8). https://doi.org/10.1021/acs.cgd.0c00793.

(22)   Chancellor, C. J.; Bowles, F. L.; Franco, J. U.; Pham, D. M.; Rivera, M.; Sarina, E. A.; Ghiassi, K. B.; Balch, A. L.; Olmstead, M. M. Single-Crystal X-Ray Diffraction Studies of Solvated Crystals of C_{60} Reveal the Intermolecular Interactions between the Component Molecules. *Journal of Physical Chemistry A* **2018**, *122* (50). https://doi.org/10.1021/acs.jpca.8b08740.

(23)   Garcia, T. Y.; Olmstead, M. M.; Fettinger, J. C.; Balch, A. L. Crystallization of Chloroindium(III)Octaethylporphyrin into a Clamshell Motif to Engulf Guest Molecules. *CrystEngComm* **2010**, *12* (3). https://doi.org/10.1039/b911180h.

(24)   Scheidt, W. R.; Turowska-tyrk, I. Crystal and Molecular Structure of (Octaethylporphinato)Cobalt(II). Comparison of the Structures of Four-Coordinate M(TPP) and M(OEP) Derivatives (M = Fe-Cu). Use of Area Detector Data. *Inorganic Chemistry* **1994**, *33* (7). https://doi.org/10.1021/ic00085a017.

(25)   Ozarowski, A.; Lee, H. M.; Balch, A. L. Crystal Environments Probed by EPR Spectroscopy. Variations in the EPR Spectra of Co^{II}(Octaethylporphyrin) Doped in Crystalline Diamagnetic Hosts and a Reassessment of the Electronic Structure of Four-Coordinate Cobalt(II). *Journal of the American Chemical Society* **2003**, *125* (41). https://doi.org/10.1021/ja030221f.

A brief conclusion to Chapters I, II and III

In the first half of this dissertation, we have discussed and explored the phenomenon of porphyrin-fullerene cocrystallization – first as an analytical tool for the study of the structures of two endohedrals, and then in more detail as a systematic study involving a model system. While cocrystallization is not the only way to obtain fullerene structures, it provides a reliability to the crystallographic technique. We have recently published the synthesis and characterization of a novel open-cage heterofullerene with a $(Ph_3P)_2Pt$ unit inserted into an activated C-C bond.[1] This compound proved rather cumbersome to crystallize and solve, despite containing a heavy atom and being of intrinsically lower symmetry than pristine fullerenes. Unlike pristine fullerenes, functionalized or open-cage compounds have been characterized with far less success using the cocrystallization technique. For instance, out of several dozen open-cage fullerene synthesized by the Murata group, only a handful have been cocrystallized.[2] A possible explanation for this would be that a large percentage of the cage surface is rendered unsuitable for the porphyrin-fullerene interaction, making it more difficult for the groups to associate in the correct orientation for cocrystal formation. The crystal structure of the open-cage Pt-containing heterofullerene is shown below and was obtained through a simpler technique involving antisolvent layering over a very dilute solution of the open-cage fullerene. A second functionalized fullerene (synthesized by the Pla Quintana group and the University of Girona, Spain) was also laboriously crystallized by this technique and is also shown below, and is (at present) ahead of publication.
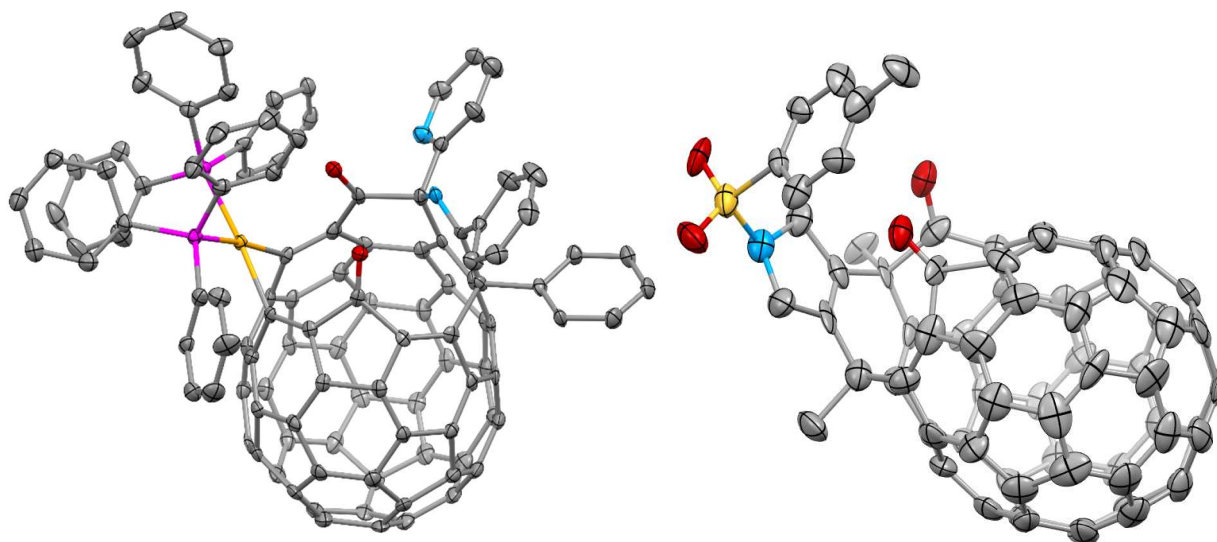
The structures of a Pt-containing heterofullerene (left) and a tosylated open-cage fullerene (right)

The design of intelligent cocrystallization agents for any system prone to disorder is largely dependent on understanding the factors that affect successful crystallization, and being able to predict the same. We believe that the in-depth study described earlier may be able to supply some correlation in case of closed fullerene systems, to aid the crystallization techniques used by fullerene chemists worldwide. A previous study published in this lab exhibited how replacing four out of the eight ethyl groups in octaethylporphyrin renders the resulting porphyrin (etioporphyrin) much less potent in its cocrystallization ability.[84] The dramatic effects of seemingly small changes (such as, in our study, solvent or metal) on the crystal structure directs attention towards the need to study, analyze and better understand the ramifications of small electrostatic effects, volume of molecules in interstitial sites, slight variation in bond lengths and angles, other non-covalent forces, and variations in solubility – to accentuate the crystallography community's ability to control and tune these parameters for improved crystal design.

References

(1)   Gralinski, S. R.; Roy, M.; Baldauf, L. M.; Olmstead, M. M.; Balch, A. L. Introduction of a (Ph$_3$P)$_2$Pt Group into the Rim of an Open-Cage Fullerene by Breaking a Carbon–Carbon Bond . *Chemical Communications* **2021**, *57* (79). https://doi.org/10.1039/d1cc04336f.

(2)   Futagoishi, T.; Murata, M.; Wakamiya, A.; Sasamori, T.; Murata, Y. Expansion of Orifices of Open C$_{60}$ Derivatives and Formation of an Open C$_{59}$S Derivative by Reaction with Sulfur. *Organic Letters* **2013**, *15* (11). https://doi.org/10.1021/ol401083c.

(3)   Ghiassi, K. B.; Powers, X. B.; Wescott, J.; Balch, A. L.; Olmstead, M. M. Crystal Engineering Gone Awry. What a Difference a Few Methyl Groups Make in Fullerene/Porphyrin Cocrystallization. *Crystal Growth and Design* **2016**, *16* (1). https://doi.org/10.1021/acs.cgd.5b01449.

Chapter IV. The chemistry of titanium tetrachloride towards tertiary group 15 species and an introduction to tertiary amine radical cation chemistry

Arsine and Phosphine Chemistry

The coordination chemistry of Ti(IV) is filled with peculiarities. Despite being a very small cation (ionic radius 0.61 Å), Ti(IV) tends to attain unexpectedly high coordination numbers.[1,2] These coordination numbers do not always require the design of specialized ligands – for instance, Ti(IV) halides, particularly $TiCl_4$, frequently accommodates neutral ligands in addition to retaining all four chloride ligands up to a coordination number of 8,[3,4] occasionally reorganizing its four terminal chlorides into a chloride-bridged bimetallic[5] or trimetallic[6] species to do so. We concerned ourselves with complexes of tertiary group 15 ligands – due to there being precedent that these complexes can participate in organotitanium metathesis with some degree of success.[5,7] The structural characterization of the L_2TiX_4 or $(L^{\wedge}L)TiX_4$ type complexes of tertiary phosphines and arsines is sadly incomplete – their air-sensitivity, instability in solution state, and propensity to hydrolyze make recrystallization very cumbersome. We were able to find success by slowing down the reaction rate and forming coordination complexes in single-crystal form through slow diffusion of dilute solutions of ligand and metal halide into one another. Figure 1A shows the crystals obtained through such a technique, while the rest of Figure 1 shows the crystal structures of some simple, novel coordination complexes of Ti(IV) obtained thusly.
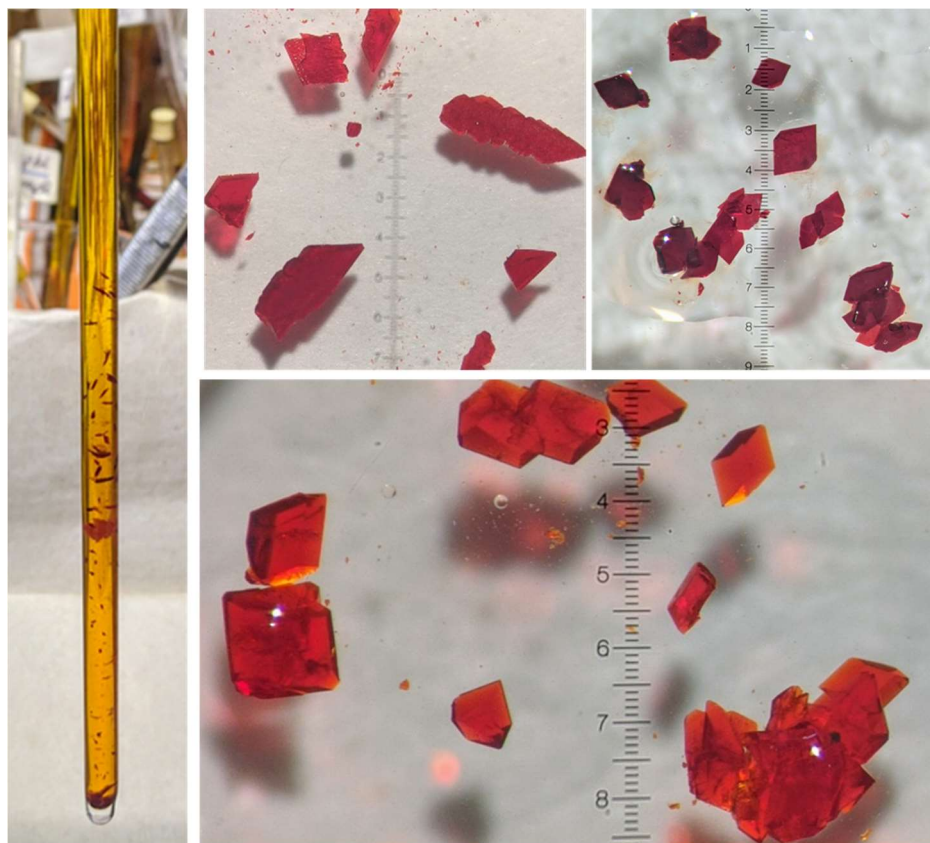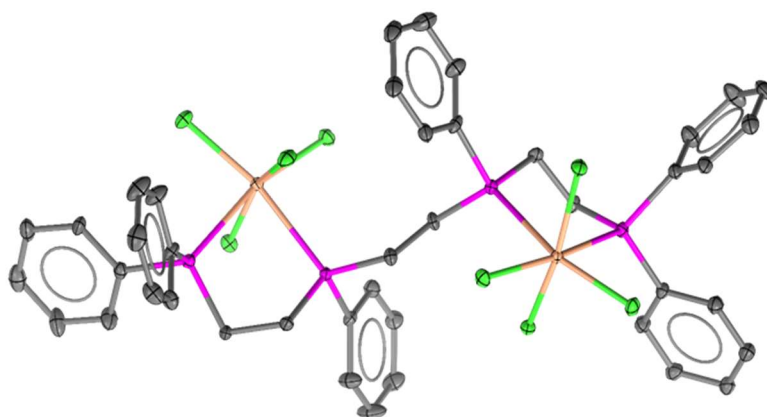
(A)
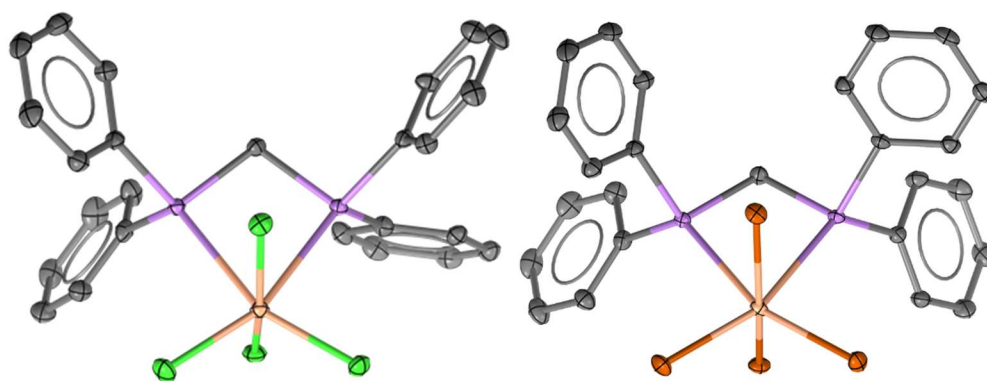
(B)
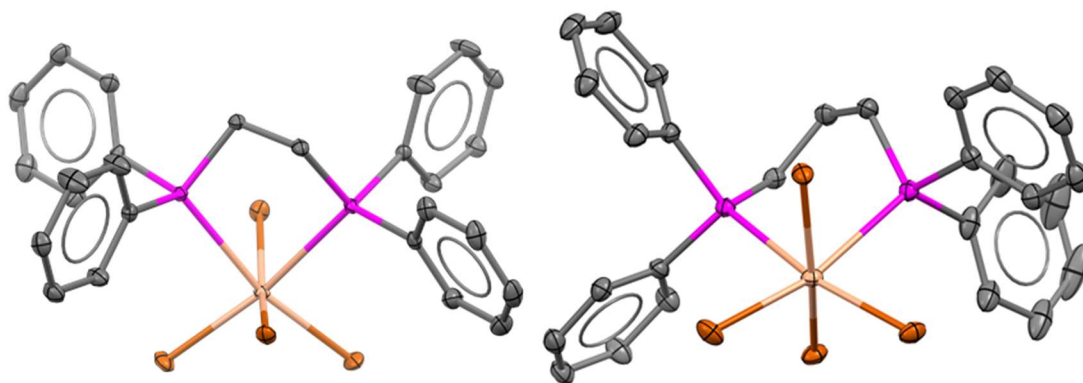
(C)

(D)

Figure 1. (A) Crystals of sensitive coordination complexes of TiX4 obtained by direct ligand-metal slow diffusion. (B). Six-coordinate complexes of (Ph₂AsCH₂AsPh₂)TiX₄ (C) Six coordinate complexes of (Ph₂P(CH₂)₂PPh₂)TiBr₄ and (Ph₂P(CH₂)₃PPh₂)TiBr₄ (D) A six coordinate complex containing Tetraphos I in two binding modes. Color code: Ti, Br, Cl, P, As, C.

The performance of these group 15 complexes of Ti(IV) towards organometallic reagents (in our experimental attempts) was woefully inadequate. Figure 2 shows the scheme for a simple test reaction and the two crystalline species involved, a 6-coordinate starting material and a 5-coordinate complex obtained at the end, with concomitant formation of the $(Ph_3P)^+(CH_2Ph)^-$ ylide.

The activation of the tertiary P-atom towards attack by PhCH$_2^-$ could be attributed to its coordination to hard, electrophilic Ti(IV). This led us to try and investigate the extent of electron-withdrawal that can be performed by Ti(IV) on tertiary phosphine species. Would Ti(IV) succeed in performing a full one-electron oxidation on them?
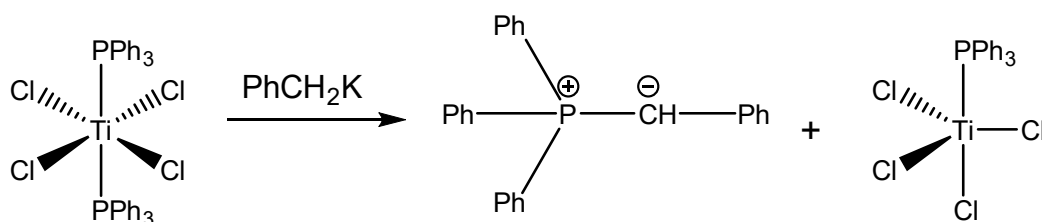

(A)
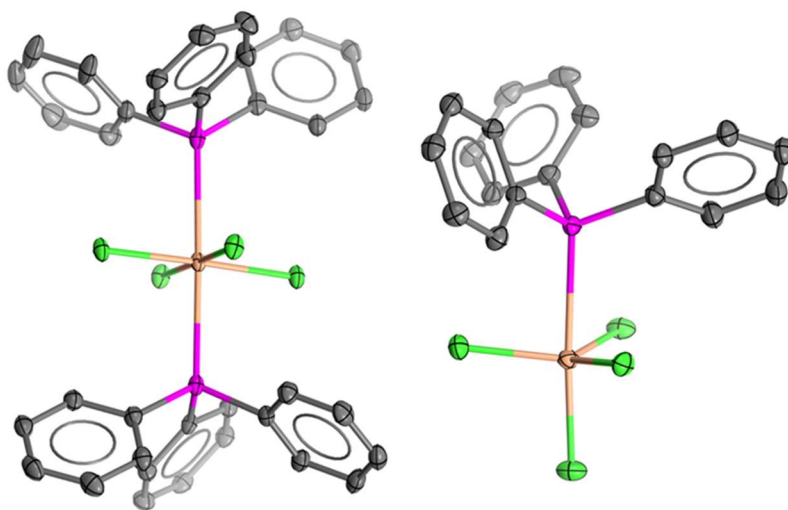
(B)

Figure 2. (A) Formation of a phosphonium ylide from six-coordinate Ti^{IV} complex and benzyl carbanion. (B) The two Ti^{IV} complexes involved. Color code: Ti, Cl, P, C.

Figure 3 shows the structure of red-green dichroic crystals obtained from a reaction mixture containing (F$_3$C-Ph)$_3$P and TiCl$_4$ in toluene. From simple inspection, we can observe that the

phosphine vs metal halide species form a charge pair. The question, of course, arises – is the phosphine in its radical form? Tertiary phosphines continue to be pyramidalized when oxidized[8], and there seems to be no solid structural metric to distinguish Ar_3P^+ and Ar_3PH^+ type species. What we could say for certain, from the structure, was that Ti(IV) formed two different anions. This is better visualized in 3C where one anion shows a polymer expansion, and one does not. The discrete anion, $Ti_2Cl_9^-$, has been reported before and believed to contain Ti(IV), while this polymeric anion has not been reported before. It can be formulated as $[Ti_3Cl_{10}]_n^{n-}$ and shows alternation between two sets of three bridging chlorides, and then one set of two bridging chlorides and one terminal chloride. The anion is suspected to be Ti(III) based on structural factors observed in some Ti^{III} chloride anions before.[9] These anions will be revisited in Chapters 6, 7 and 8.

(A)

(B)

(C)

75
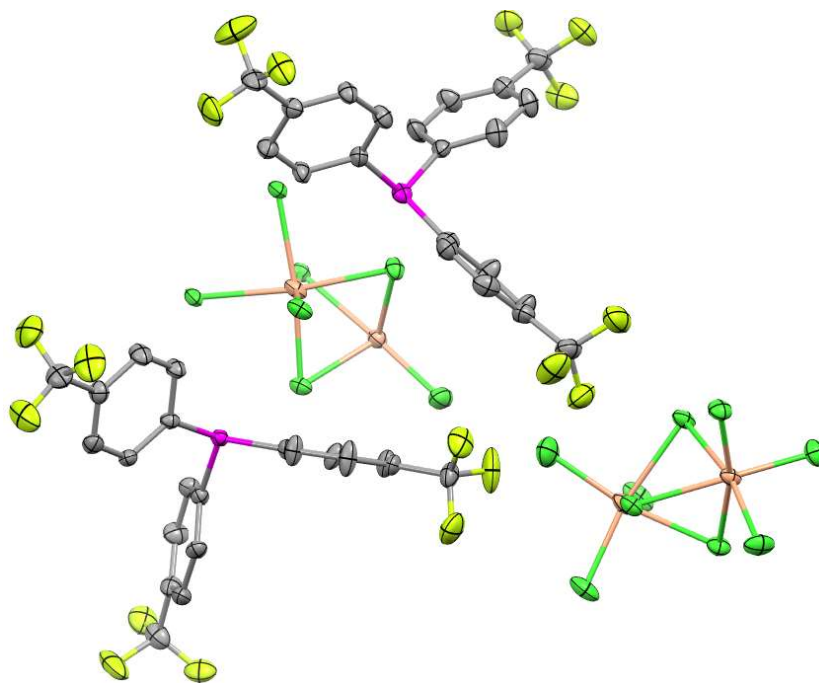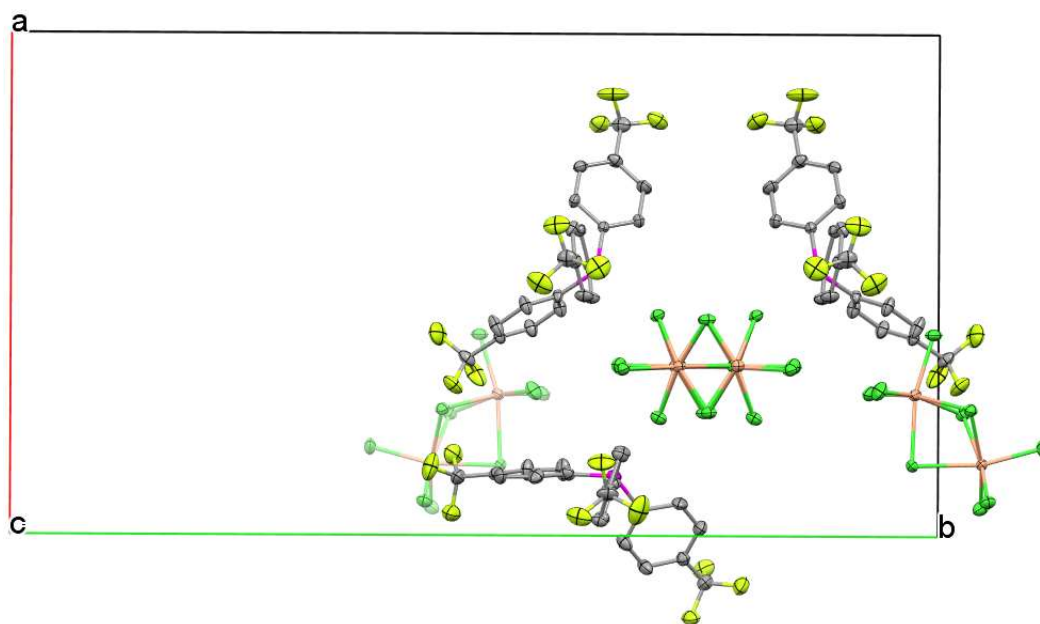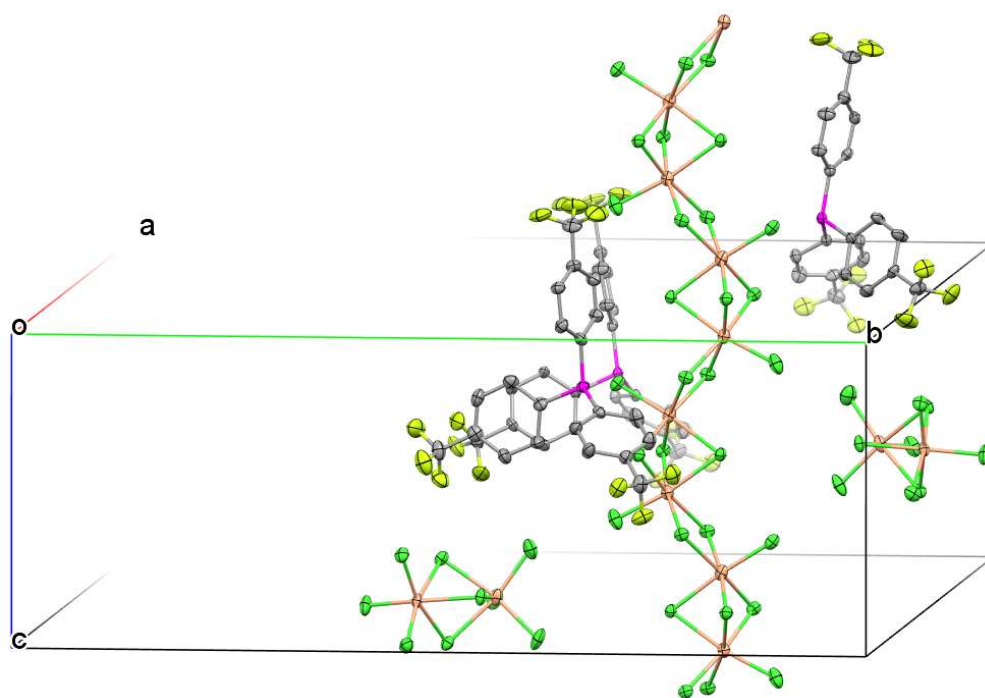
Figure 3. The crystal structure obtained from combination of (F₃CPh)₃P and TiCl₄ in toluene, exhibiting the asymmetric unit (A), the arrangement of phosphine species around the polymer anion (B) and the chain-like propagation of the polymer anion (C). Color code: Ti, Cl, P, F, C.

Using EPR spectroscopy to examine this reaction mixture in solution as well as solid state led to some peculiar findings. Figure 4A shows the solution state spectrum and 4B shows a spectrum obtained from crushed, washed and dried crystals. In 4A, there is no EPR-activity in the g = 2.002 region that would be expected to be inhabited by an organic radical. Rather, a singlet at g = 1.946 is strongly suggestive of Ti(III) being formed, and the same region appears to show a signal in the crushed solids (Figure 4B) that supplied us with the structure shown in Figure 3.
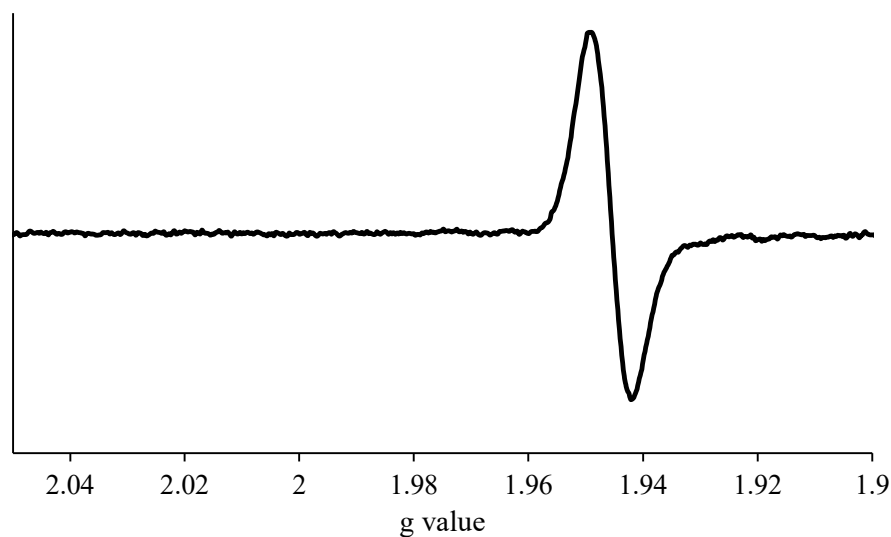
(A)
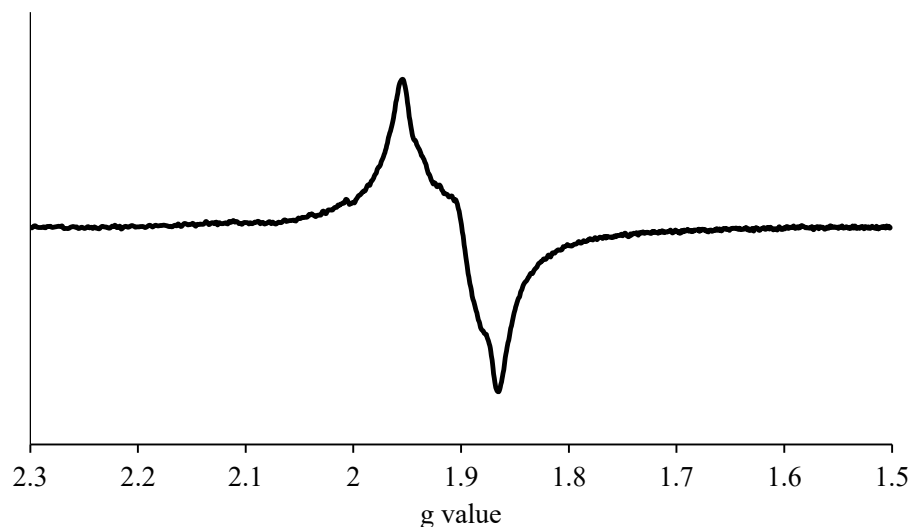
(B)

Figure 4. (A) The solution-state EPR spectrum of an aliquot from the reaction mixture containing (F$_3$CPh)$_3$P and TiCl$_4$ in toluene. (B) The solid-state EPR spectrum obtained from the crushed crystals whose contents are shown in Figure 3.

This leaves us with a peculiar scenario – one where the metal halide reagent appears to have itself undergone reduction, but the oxidized species that must have simultaneously formed (i.e., a phosphine cation) was not captured alongside Ti^{III}, nor detected in solution form. After a few more unsuccessful attempts to either obtain phosphine complexes of Ti^{IV} that would be more amenable to organometallic metathesis, or to capture radical cations of bulkier phosphines using TiCl$_4$ (despite obtaining Ti^{III} in almost all cases), we turned our attention to another member of the Group 15 series – tertiary amines.

Turning to amine chemistry

Tertiary arylamines tend to be associated with lower inner-sphere reorganization energy during radical formation,[10] due to their already existing in a planarized conformation. Figure 5 shows the side-by-side comparison of neutral triphenylamine and triphenylphosphine.
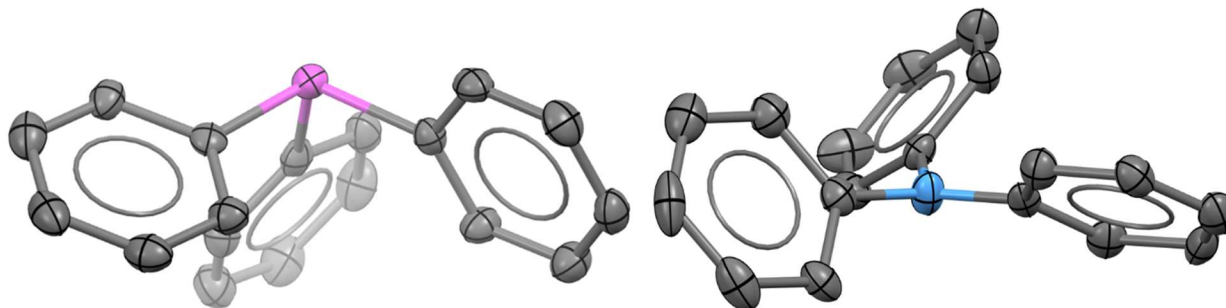

Figure 6. Triphenylphosphine (left)[11] and triphenylamine (right)[12]

The intrinsic planarity of triarylamines is associated with their non-basic nature and sets their chemistry apart from that of alkylamines (primary, secondary or tertiary). Triphenylamine and its derivatives are readily utilized for charge-transfer chemistry and associated applications – optoelectronic materials, organic light-emitting diodes, conductive materials, and dye-sensitized solar cells.[13–20] The ease of oxidation of triphenylamine derivatives makes them crucial to hole transport[21,22] and formation of Farbe centers and unpaired spins in complex materials containing triarylamine templates.[23] Triphenylamine or triarylamines are often grouped into the same category as macrocycles or oligomeric species containing multiple N-centers when it comes to discussions about the aforementioned materials. However, the chemical behavior of isolated triphenylamine or triarylamine species and their radical cations is distinct from the properties of radical cations of polyamines that include the triphenylamine template. The delocalization of unpaired spins across multiple N-centers[24] is automatically associated with structural stability – while these species participate in charge-transport and can undergo one or more rounds of oxidation,[25–27] they rarely

78

undergo bond formation or breakage. On the other hand, a simple triphenylamine or triarylamine is not only oxidizable to a radical cation, but also capable of coupling or dimerization chemistry involving the forging of new bonds, as demonstrated in the oxidative coupling processes where triphenylamine can be converted to N,N,N',N'-tetraphneylbenzidine.[28–31]

The use of metal halides in amine radical formation is not entirely unprecedented,[32] but typically does not explore Ti^{IV} as a mediator or radical stabilizer. Additionally, directly synthesis of diamine products in their radical form from simpler triarylamine starting materials has not been demonstrated. In the following three chapters, we explore the use of $TiCl_4$ and other Lewis acidic metal halides to generate and crystallize cation radicals of tertiary arylamines. The work explores both in situ direct crystallization of amines after simple oxidation, as well as the capture of products of coupling chemistry in their charged form, and leads to the formation of some unexpected compounds.

References

(1) Kayal, A.; Kuncheria, J.; Lee, S. C. Bis[Hydrotris(Pyrazol-1-Yl)Borato]Titanium(III): A Stable Tp+M Complex of Singular Reactivity. *Chemical Communications* **2001**, *1* (23). https://doi.org/10.1039/b108115b.

(2) Yélamos, C.; Gust, K. R.; Baboul, A. G.; Heeg, M. J.; Schlegel, H. B.; Winter, C. H. Early Transition Metal Complexes Containing 1,2,4-Triazolato and Tetrazolato Ligands: Synthesis, Structure, and Molecular Orbital Studies. *Inorganic Chemistry* **2001**, *40* (25). https://doi.org/10.1021/ic0109389.

(3) Hart, R.; Levason, W.; Patel, B.; Reid, G. Synthesis, Spectroscopic and Structural Studies on Six- and Eight-Coordinate Phosphane and Arsane Complexes of Titanium(IV) Halides.

European Journal of Inorganic Chemistry **2001**, No. 11. https://doi.org/10.1002/1099-0682(200111)2001:11<2927::AID-EJIC2927>3.0.CO;2-3.

(4)   Clark, R. J. H.; Lewis, J.; Nyholm, R. S. 471. Diarsine Complexes of Quadrivalent-Metal Halides. *Journal   of   the   Chemical   Society   (Resumed)* **1962**. https://doi.org/10.1039/jr9620002460.

(5)   Kurogi, T.; Kuroki, K.; Moritani, S.; Takai, K. Structural Elucidation of a Methylenation Reagent of Esters: Synthesis and Reactivity of a Dinuclear Titanium(III) Methylene Complex. *Chemical Science* **2021**, *12* (10). https://doi.org/10.1039/d0sc06366e.

(6)   Edema, J. J. H.; Duchateau, R.; Gambarotta, S.; Bensimon, C. Labile Triangulo-Trititamum(II) and -Trivanadium(II) Clusters. *Inorganic Chemistry* **1991**, *30* (19). https://doi.org/10.1021/ic00019a001.

(7)   Cotton, F. A.; Murillo, C. A.; Petrukhina, M. A. Reactions of TiCl4 with Phosphines and Alkylating Reagents: An Organometallic Route to a Titanium(II) Cluster Compound1. *Journal of Organometallic Chemistry* **1999**, *573* (1–2). https://doi.org/10.1016/S0022-328X(98)00655-X.

(8)   Pan, X.; Chen, X.; Li, T.; Li, Y.; Wang, X. Isolation and X-Ray Crystal Structures of Triarylphosphine Radical Cations. *Journal of the American Chemical Society* **2013**, *135* (9). https://doi.org/10.1021/ja4012113.

(9)   Chen, L.; Cotton, F. A. Synthesis, Reactivity, and X-Ray Structures of Face-Sharing Ti(III) Complexes; The New Trinuclear Ion, $[Ti_3Cl_{12}]^{3-}$. *Polyhedron* **1998**, *17* (21). https://doi.org/10.1016/s0277-5387(98)00171-5.

(10) Quiroz-Guzman, M.; Brown, S. N. Tris(4-Bromo-Phenyl)Aminium Hexa-Chloridoantimonate (Magic Blue): A Strong Oxidant with Low Inner-Sphere Reorganization. *Acta Crystallographica Section C: Crystal Structure Communications* **2010**, *66* (7). https://doi.org/10.1107/S0108270110019748.

(11) Dunne, B. J.; Orpen, A. G. Triphenylphosphine: A Redetermination. *Acta Crystallographica Section C Crystal Structure Communications* **1991**, *47* (2). https://doi.org/10.1107/s010827019000508x.

(12) Sobolev, A. N.; Belsky, V. K.; Romm, I. P.; Chernikova, N. Yu.; Guryanova, E. N. Structural Investigation of the Triaryl Derivatives of the Group V Elements. IX. Structure of Triphenylamine, $C_{18}H_{15}N$. *Acta Crystallographica Section C Crystal Structure Communications* **1985**, *41* (6). https://doi.org/10.1107/s0108270185006217.

(13) Krug, M.; Fröhlich, N.; Fehn, D.; Vogel, A.; Rominger, F.; Meyer, K.; Clark, T.; Kivala, M.; Guldi, D. M. Pre-Planarized Triphenylamine-Based Linear Mixed-Valence Charge-Transfer Systems. *Angewandte Chemie - International Edition* **2021**, *60* (12). https://doi.org/10.1002/anie.202014567.

(14) Wang, M. Q.; Gao, L. X.; Yang, Y. F.; Xiong, X. N.; Zheng, Z. Y.; Li, S.; Wu, Y.; Ma, L. L. A Triphenylamine Derivative as a Naked-Eye and Light-up Fluorescent Probe for G-Quadruplex DNA. *Tetrahedron Letters* **2016**, *57* (46). https://doi.org/10.1016/j.tetlet.2016.09.100.

(15) Selby, T. D.; Kim, K. Y.; Blackstock, S. C. Patterned Redox Arrays of Polyarylamines I. Synthesis and Electrochemistry of a p-Phenylenediamine and Arylamino-Appended p-

Phenylenediamine Arrays. *Chemistry of Materials* **2002**, *14* (4). https://doi.org/10.1021/cm0106769.

(16)   Coropceanu, V.; Lambert, C.; Nöll, G.; Brédas, J. L. Charge-Transfer Transitions in Triarylamine Mixed-Valence Systems: The Effect of Temperature. *Chemical Physics Letters* **2003**, *373* (1–2). https://doi.org/10.1016/S0009-2614(03)00553-0.

(17)   Wu, Z. S.; Song, X. C.; Liu, Y. D.; Zhang, J.; Wang, H. S.; Chen, Z. J.; Liu, S.; Weng, Q.; An, Z. W.; Guo, W. J. New Organic Dyes with Varied Arylamine Donors as Effective Co-Sensitizers for Ruthenium Complex N719 in Dye Sensitized Solar Cells. *Journal of Power Sources* **2020**, *451*. https://doi.org/10.1016/j.jpowsour.2020.227776.

(18)   Wan, Z.; Jia, C.; Zhou, L.; Huo, W.; Yao, X.; Shi, Y. Influence of Different Arylamine Electron Donors in Organic Sensitizers for Dye-Sensitized Solar Cells. *Dyes and Pigments* **2012**, *95* (1). https://doi.org/10.1016/j.dyepig.2012.03.028.

(19)   Kar, S.; Roy, J. K.; Leszczynska, D.; Leszczynski, J. Power Conversion Efficiency of Arylamine Organic Dyes for Dye-Sensitized Solar Cells (DSSCs) Explicit to Cobalt Electrolyte: Understanding the Structural Attributes Using a Direct QSPR Approach. *Computation* **2017**, *5* (1). https://doi.org/10.3390/computation5010002.

(20)   Liang, M.; Chen, J. Arylamine Organic Dyes for Dye-Sensitized Solar Cells. *Chemical Society Reviews* **2013**, *42* (8). https://doi.org/10.1039/c3cs35372a.

(21)   Agarwala, P.; Kabra, D. A Review on Triphenylamine (TPA) Based Organic Hole Transport Materials (HTMs) for Dye Sensitized Solar Cells (DSSCs) and Perovskite Solar Cells (PSCs): Evolution and Molecular Engineering. *Journal of Materials Chemistry A*. 2017. https://doi.org/10.1039/c6ta08449d.

(22)   Heckmann, A.; Lambert, C. Organic Mixed-Valence Compounds: A Playground for Electrons and Holes. *Angewandte Chemie - International Edition*. 2012. https://doi.org/10.1002/anie.201100944.

(23)   Sindt, A. J.; Dehaven, B. A.; McEachern, D. F.; Dissanayake, D. M. M. M.; Smith, M. D.; Vannucci, A. K.; Shimizu, L. S. UV-Irradiation of Self-Assembled Triphenylamines Affords Persistent and Regenerable Radicals. *Chemical Science* **2019**, *10* (9). https://doi.org/10.1039/c8sc04607g.

(24)   Lazrak, M.; Toufik, H.; Bouzzine, S. M.; Lamchouri, F. Bridge Effect on the Charge Transfer and Optoelectronic Properties of Triphenylamine-Based Organic Dye Sensitized Solar Cells: Theoretical Approach. *Research on Chemical Intermediates* **2020**, *46* (8). https://doi.org/10.1007/s11164-020-04184-x.

(25)   Bailey, S. E.; Zink, J. I.; Nelsen, S. F. Contributions of Symmetric and Asymmetric Normal Coordinates to the Intervalence Electronic Absorption and Resonance Raman Spectra of a Strongly Coupled P-Phenylenediamine Radical Cation. *Journal of the American Chemical Society* **2003**, *125* (19). https://doi.org/10.1021/ja021343v.

(26)   Chiu, K. Y.; Su, T. H.; Huang, C. W.; Liou, G. S.; Cheng, S. H. Substituent Effects on the Electrochemical and Spectral Characteristics of N,N,N′,N′-Tetraaryl-*p*-Phenylenediamine Derivatives. *Journal of Electroanalytical Chemistry* **2005**, *578* (2). https://doi.org/10.1016/j.jelechem.2005.01.010.

(27)   Li, B.; Zhen, J.; Wan, Y.; Lei, X.; Jia, L.; Wu, X.; Zeng, H.; Chen, M.; Wang, G. W.; Yang, S. Steering the Electron Transport Properties of Pyridine-Functionalized Fullerene

Derivatives in Inverted Perovskite Solar Cells: The Nitrogen Site Matters. *Journal of Materials Chemistry A* **2020**, *8* (7). https://doi.org/10.1039/c9ta12188a.

(28) Xi, C.; Jiang, Y.; Yang, X. Remarkably Efficient Oxidative Coupling of N,N-Dialkylarylamines in Water Mediated by Cerium(IV) Ammonium Nitrate. *Tetrahedron Letters* **2005**, *46* (22). https://doi.org/10.1016/j.tetlet.2005.03.173.

(29) Ling, X.; Xiong, Y.; Huang, R.; Zhang, X.; Zhang, S.; Chen, C. Synthesis of Benzidine Derivatives via $FeCl_3 \cdot 6H_2O$-Promoted Oxidative Coupling of Anilines. *Journal of Organic Chemistry* **2013**, *78* (11). https://doi.org/10.1021/jo4002504.

(30) Bharathi, P.; Periasamy, M. Metalation of Iminium Ions Formed in the Reaction of Tertiary Amines with $TiCl_4$. *Organic Letters* **1999**, *1* (6). https://doi.org/10.1021/ol990745d.

(31) Svejstrup, T. D.; Ruffoni, A.; Juliá, F.; Aubert, V. M.; Leonori, D. Synthesis of Arylamines via Aminium Radicals. *Angewandte Chemie - International Edition* **2017**, *56* (47). https://doi.org/10.1002/anie.201708693.

(32) Ganzorig, C.; Suga, K.; Fujihira, M. P-Type Semiconductors of Aromatic Diamines Doped with $SbCl_5$. *Chemistry Letters* **2000**, No. 9. https://doi.org/10.1246/cl.2000.1032.

Chapter V: Part I of tertiary amine radical chemistry – the synthesis of radical cations from their corresponding neutral forms

A brief introduction

Direct crystallization of radical cations from neutral tertiary amine may occur in cases where the oxidizing agent is used in excess and is capable of reorganizing into a non-coordinating anion. For instance, magic blue may be crystallized directly by mixing neutral tris(p-bromophenyl)amine with excess $SbCl_5$ in toluene or dichloromethane. This phenomenon may also be extended to diamines where an unpaired electron is delocalized across two nitrogen centers separated by a phenylene or benzidine type species. The diamines tend not to participate in further bond-formation chemistry and may thus be thought of as "terminal" radical cations. They can be generated and crystallized in a similar fashion, either by oxidation of the corresponding neutral amine and then ion-exchange, or by direct crystallization of the radical cation from the neutral diamine species. Other "terminal" radical cations include amines where an unpaired electron may experience even further delocalization, i.e., those containing 3 or more nitrogen centers, as well as amines where further dimerization chemistry is effectively prevented by a substituent that does not serve as a leaving group (such as tri-p-tolylamine or tris(p-t-butylphenyl)amine).

Separately from the above phenomena, Lewis acids have shown themselves capable of generating the radical cations of tertiary amines in order to couple two moles of the same, giving rise to the formation of a carbon-carbon bond through an overall process of oxidative coupling (as discussed in the introduction). The accepted route for the formation of this C-C bond can be shown in Scheme 1 and proceeds through activation of the para-position on one phenyl group and coupling. These diamine products are obtained in their neutral state after standard organic

extraction/purification techniques; while the mechanism is accepted to involve radical formation, the radicals themselves are rarely found to be isolable.
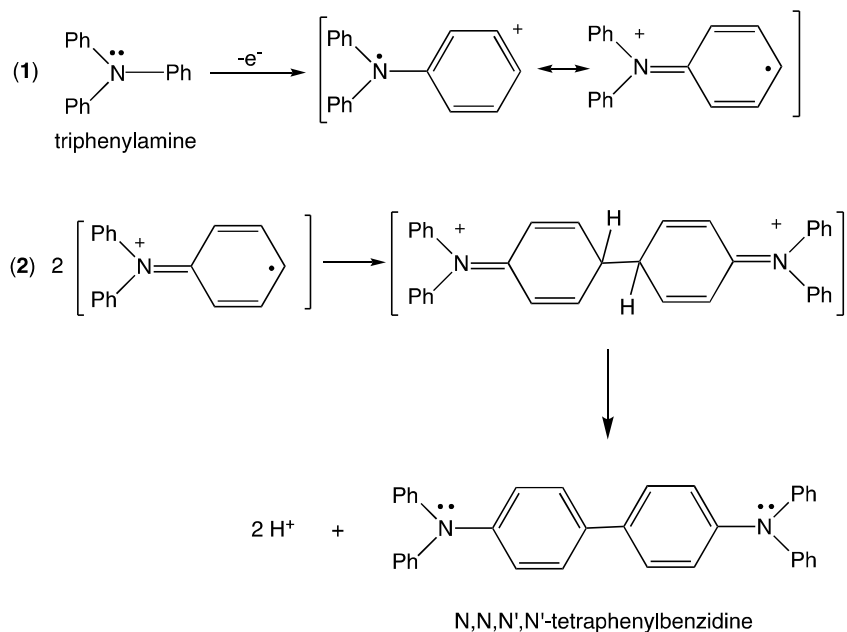

Scheme 1, the formation of neutral N,N,N',N'-tetraphenylbenzidine from neutral triphenylamine[1]

The two concepts discussed above, i.e., the formation of stable, persistent, and isolable radical cations through one-electron oxidation, and the coupling of tertiary amine radical cations to give rise to diamines through *p*-position coupling, can find their confluence in a well-studied phenomenon: the aging of magic blue. Pure commercial magic blue, upon aging, begins to show the appearance of additional bands in its optical spectrum that have curious features, such as extending well into the NIR region (a characteristic of the more "delocalized" unpaired electron). A comparison of pure vs aged magic blue (taken from ref 1) can be seen in Figure 1A. Mass spectrometry and optical spectroscopy have confirmed this "impurity" to be the radical monocation of the amine shown in in Fig 1B[2].
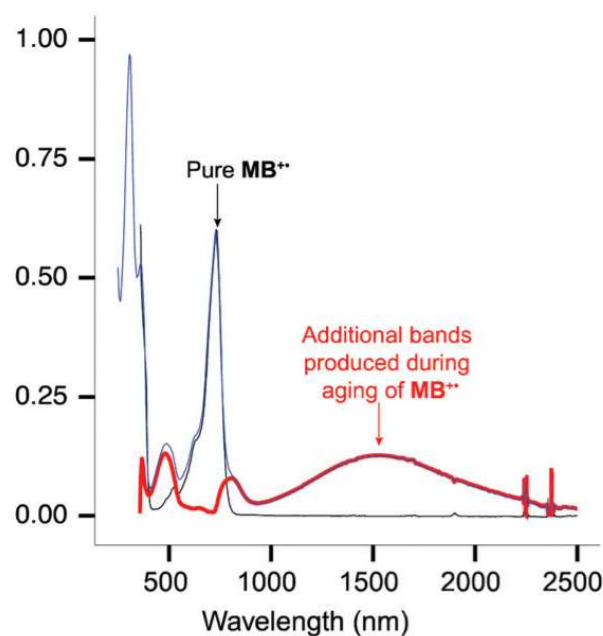
(A)
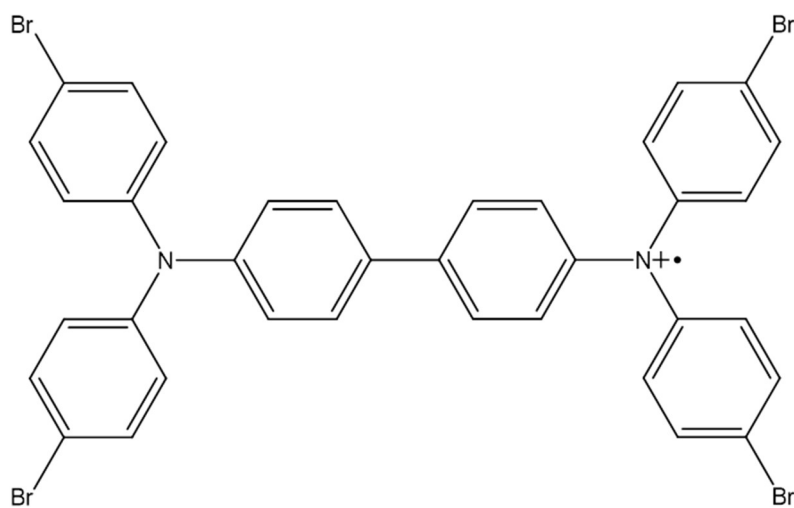
(B)

Fig 1: (A) the optical spectra of pure magic blue, denoted as MB·⁺, and impurities formed during its aging; (B) the diamine radical monocation believed to be responsible for the red trace in 1A.

The formation of the diamine shown in Fig 1B must proceed through a coupling similar to that which produces N,NN',N'-tetraphenylbenzidine in Lewis acid-mediated oxidative couplings

discussed above – with the distinction of also eliminating Br_2. However, while it can be demonstrated that magic blue does indeed convert into the radical cation of N,N,N',N'-tetrakis(*p*-bromophenyl)benzidine when left to its own devices for a few months, a direct synthesis of N,N,N',N'-tetrakis(p-bromophenyl)benzidine in it radical *or* neutral form from neutral tris(*p*-bromophenyl)amine has not been performed, to our knowledge.

Here, we attempt to demonstrate several unique phenomena with regards to the metal-mediated one-electron oxidation chemistry of tertiary amines: 1) the formation of strongly colored, persistent radical cations of starting neutral amines, 2) the subsequent coupling of *some* of these tertiary amine radical cations into other species and their capture in *charged,* crystalline state, and 3) the evidence (spectroscopic or crystallographic) of deviation from the expected C-C coupling scheme and formation of unprecedented C-N bonds. The Lewis acids and oxidants used are titanium tetrachloride ($TiCl_4$), titanium tetrabromide ($TiBr_4$), tin tetrachloride ($SnCl_4$) and antimony pentachloride ($SbCl_5$). Not all combinations of metal halide and amine resulted in crystalline data, in which case they will be examined purely spectroscopically.

Results and discussions

In this section, we will discuss amines that underwent no further dimerization or coupling chemistry from their starting (neutral amine) state to the crystalline or solution form they were obtained in, i.e., amines that simply underwent one electron oxidation, and were crystallized as the corresponding radical cation accompanied by a non-coordinating anion formed from reorganization of the Lewis acid used as oxidant. $SbCl_5$ has shown itself to be capable crystallizing, in one step, the radical cation of an appropriate amine counterbalanced by the weakly-coordinating $SbCl_6^-$ anion. However, to date, titanium (IV) chloride and tin (IV) chloride have not been used to

directly crystallize "terminal" amine radicals counterbalanced by an appropriate metal-halide anionic species. To test the feasibility of using Ti^{IV} as an oxidant as well as counterion generator, we chose 1,3,5-tris(diphenylamino)benzene, a polycyclic tertiary arylamine that would be unlikely to undergo further radical-coupling chemistry, and performed reactions between the amine and an excess of $TiCl_4$ or $TiBr_4$ in toluene under carefully controlled air and water-free conditions. A radical monocation of the amine, accompanied by a $Ti_2X_9^-$ counterion (where X is Cl or Br) was obtained as a toluene solvate in case of both Ti^{IV} compounds, the structures themselves being isomorphous. The structure of the chloride-containing compound is shown below in Figure 2.
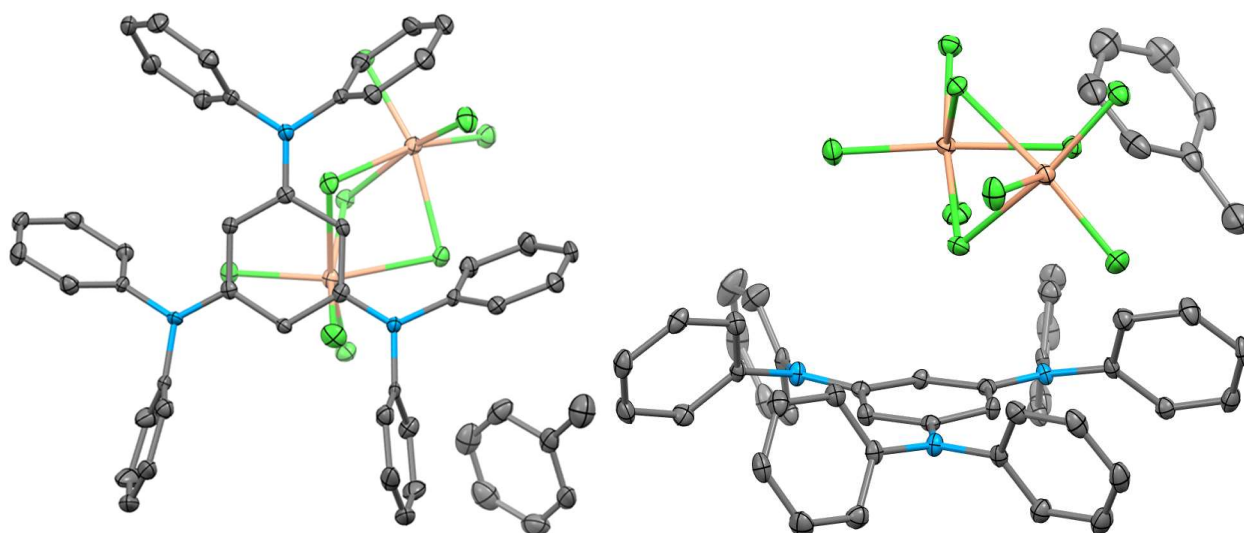

**Fig 2. Two views of the radical cation of tris(diphenylamino)benzene counterbalanced by $Ti_2Cl_9^-$.**

Color code: C, N, Cl, Ti.

The counterion each structure contains is a $Ti_2X_9^-$ unit. While the $Ti_2Cl_9^-$ anion has been previously characterized, no previous instance of the $Ti_2Br_9^-$ counterion could be found in the Cambridge Structural Database. To confirm that the charge balance was being identified correctly, the anion observed in the crystal structure discussed above was compared to literature occurrences of the same. Two such anions of the same composition, $Ti^{IV}_2Cl_9^-$ and $Ti^{III}_2Cl_9^{3-}$, are known and

have been previously crystallographically characterized. However, simply comparing the bond

distances in the structure we obtained to those observed in pre-existing instances[3,4] of both anions

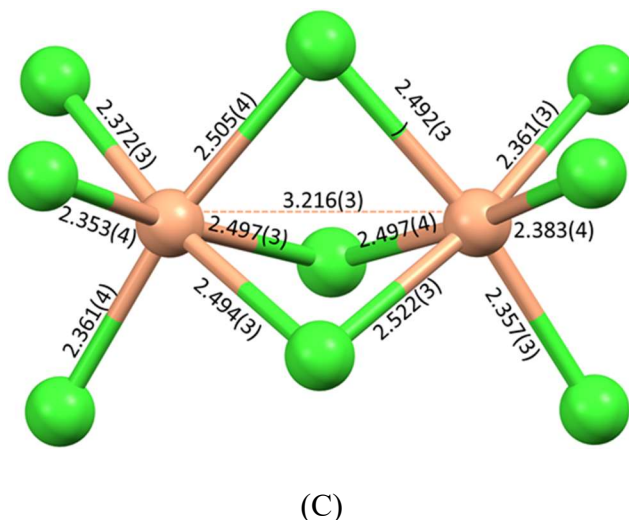clarifies that our structure contains $Ti^{IV}_2Cl_9^-$.

(A)

(B)

(C)
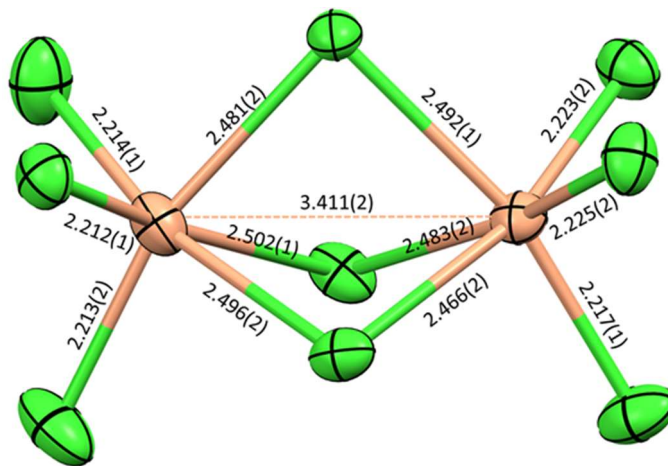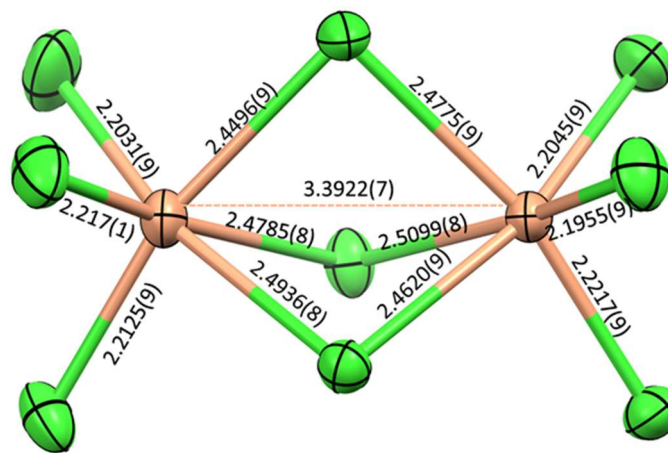
Fig 3. Comparisons of Ti-Cl and Ti-Ti bond distances in the $Ti_2Cl_9^{2-}$ anion present in structure of (1,3,5-tris(diphneylamino)benzene$^+$)(Ti$^{IV}_2Cl_9^-$)•toluene (A) with those exhibited by Ti$^{IV}_2Cl_9^-$ anion in ((Ph$_3$P)$_2$N$^+$)(Ti$^{IV}_2Cl_9^-$) (B)[3] as well as the (Ti$^{III}_2Cl_9^{3-}$) anion in (Ph$_4$P)$_3$(Ti$^{IV}_2Cl_9^{3-}$)•2CH$_2$Cl$_2$ (C)[4]

Although the above oxidation reactions are unremarkable due to their lack of interesting further chemistry with the radical cation, they establish that Ti^{IV} halides are capable of reorganizing into a noncoordinating anion and aiding an in-situ, direct crystallization of the oxidized form of the amine despite themselves not undergoing reduction. A one-electron transfer process can only logically be assumed; however, in the event of excess metal halide, the counterion that forms precipitously (pun unintended) appears to contain Ti^{IV}. Armed with this information, we sought to accomplish the following:

- crystallize a series of diamines with Ti^{IV} as oxidant, to serve as "standards" against tris-arylamine coupling reactions,

- compare Ti^{IV} with other closed-shell metal halide oxidants such as Sb^V and Sn^{IV},

- isolate or detect a reduced form of the metal to confirm that electron transfer does indeed occur.

To that end, we synthesized and crystallographically characterized the following compounds.

The Formation of Green, Crystalline (N,N,N',N'-tetraphenyl-1,4-benzenediamine$^+$)(Ti$^{IV}_2$Cl$_9^-$)•toluene from Neutral N,N,N',N'-tetraphenyl-1,4-benzenediamine.

Mixing of toluene or acetonitrile solutions of TiCl$_4$ with solutions of N,N,N',N'-tetraphenyl-1,4-benzenediamine in the same solvent produces deep green solutions corresponding to the radical cation of the diamine. The UV/Vis/NIR spectrum of this radical cation is shown below.
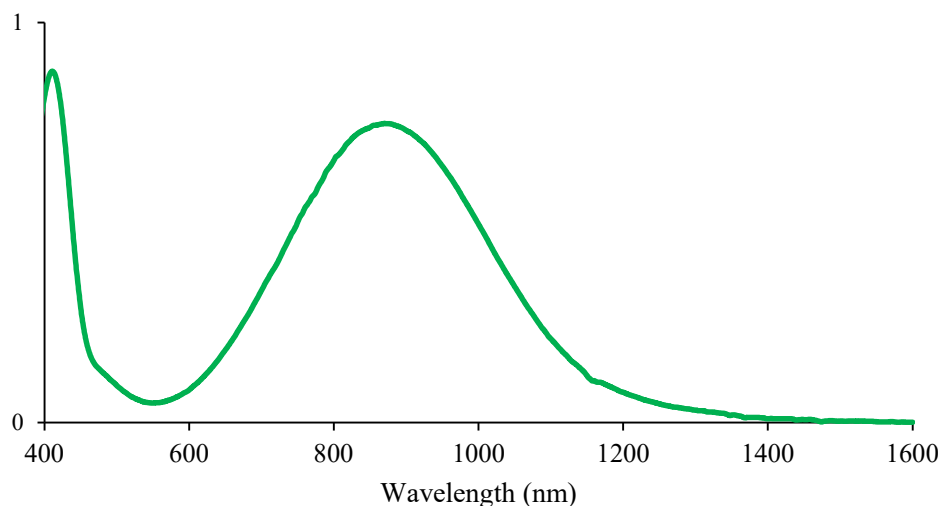

Fig 4. The UV/Vis/NIR spectrum of a mixture of TiCl$_4$ and N,N,N',N'-tetraphenyl-1,4-benzenediamine in toluene

Upon standing, the toluene solutions of TiCl$_4$ and N,N,N',N'-tetraphenyl-1,4-benzenediamine produced identical, deep green crystals of (N,N,N',N'-tetraphenyl-1,4-benzenediamine$^+$)(Ti$^{IV}_2$Cl$_9^-$)•toluene which form in the space group $P\bar{1}$. The asymmetric unit contains two half cations, one anion and a disordered molecule of toluene. The other halves of the cation are generated by inversion through centers of symmetry. The crystals under a microscope

and its structural components are shown in Fig 5. Because of the crystallographic center of symmetry in the center of the cation, it is surrounded by anions on either face and toluene molecules along the sides, features that isolate the radical from association with other radicals. The chains of alternating cations and anions that occur in the crystal are shown at the bottom of Fig 5. A comparison similar to that performed in case of the 1,3,5-tris(diphenylamino)benzene crystal structure above notifies us that the counterion is, once again, $Ti^{IV}_2Cl_9^-$.
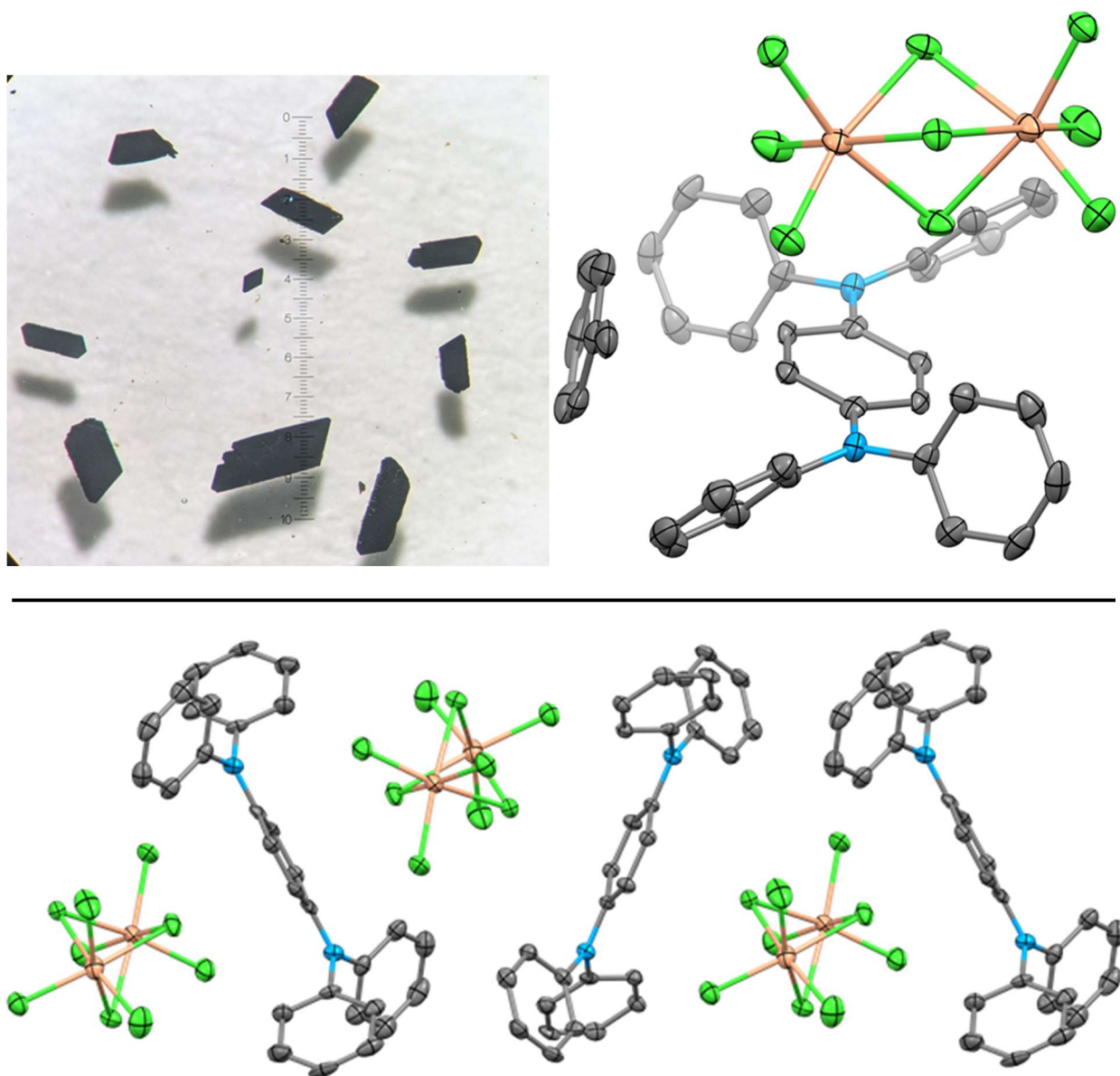
Fig 5. Top, the crystals (left) and structures and relative orientations of the independent constituents found in (N,N,N',N'-tetraphenyl-1,4-benzenediamine$^+$)(Ti$^{IV}_2$Cl$_9^-$)•toluene (right), portrayed to represent the correct cation-anion stoichiometry (although the asymmetric unit contains two half-molecules of the cation, one full cation is shown here). Bottom, a chain of alternating cations and anions in the solid. Color code: C, N, Cl, Ti. Hydrogen atoms have been omitted for clarity.

The Formation of Brown Black, Crystalline (N,N,N',N'-tetraphenyl-1,4-benzenediamine$^+$)(Ti$^{IV}_2$Br$_9^-$)•toluene from Neutral N,N,N',N'-tetraphenyl-1,4-benzenediamine.

Mixing of toluene solutions TiBr$_4$ with a toluene or acetonitrile solution of N,N,N',N'-tetraphenyl-1,4-benzenediamine produces intensely colored brown solutions. The toluene solution yields brown-black crystals of (N,N,N',N'-tetraphenyl-1,4-benzenediamine$^+$)(Ti$^{IV}_2$Br$_9^-$)•toluene over several days of standing. Although these crystals grow in the space group $P\bar{1}$, they are not isostructural with the chlorine-containing analogue, (N,N,N',N'-tetraphenyl-1,4-benzenediamine$^+$)(Ti$^{IV}_2$Cl$_9^-$)•toluene.   The asymmetric unit in (N,N,N',N'-tetraphenyl-1,4-benzenediamine$^+$)(Ti$^{IV}_2$Br$_9^-$)•toluene consists of one anion, one cation, and one toluene molecule, none of which have any crystallographically imposed symmetry. The structure of the cation is similar to that in (N,N,N',N'-tetraphenyl-1,4-benzenediamine$^+$)(Ti$^{IV}_2$Cl$_9^-$)•toluene. Both of the nitrogen atoms in (N,N,N',N'-tetraphenyl-1,4-benzenediamine$^+$)(Ti$^{IV}_2$Br$_9^-$)•toluene have planar geometry with the sum of the three C-N-C angles for N1 equal to 359.7 ° and the sum of the three C-N-C angles for N2 equal to 359.8 °. This particular anion (Ti$^{IV}_2$Br$_9^-$), has not been reported previously and appears to be analogous to Ti$^{IV}_2$Cl$_9^-$.
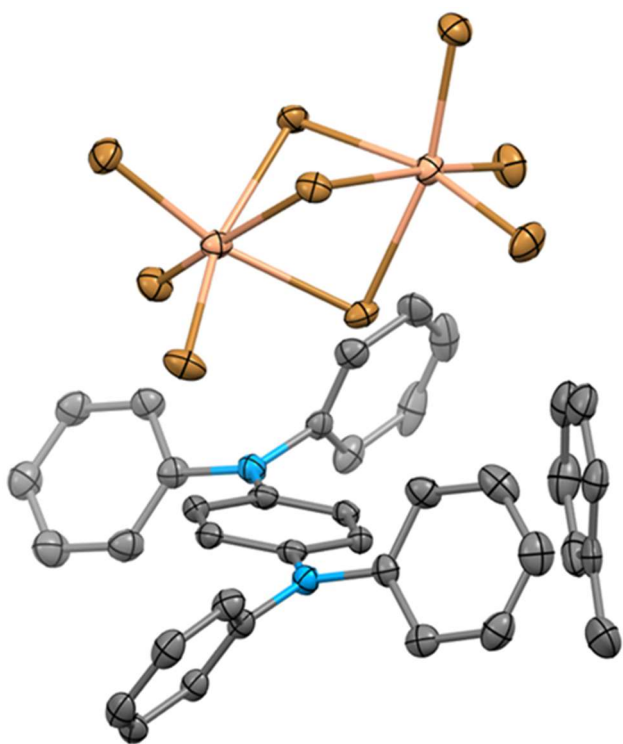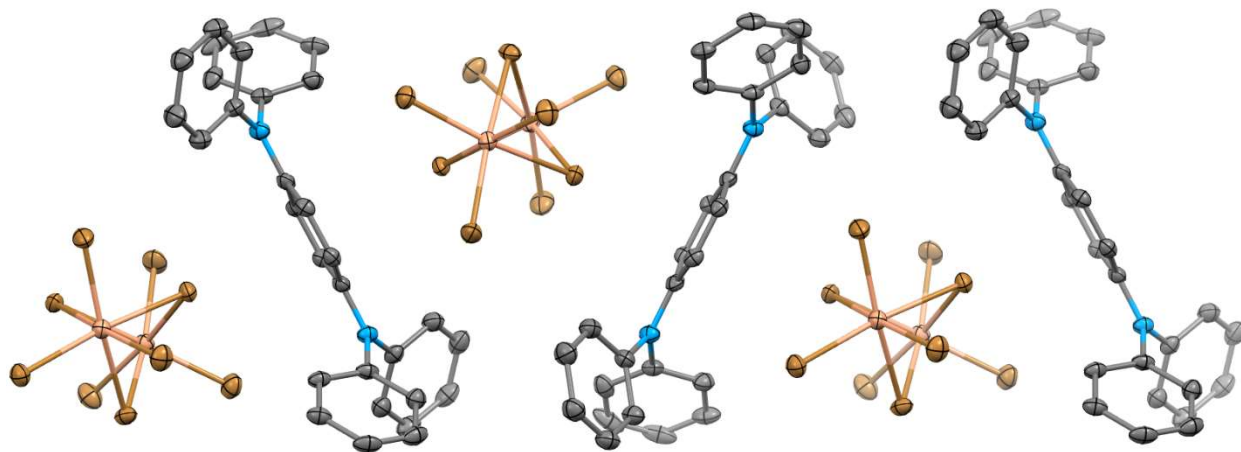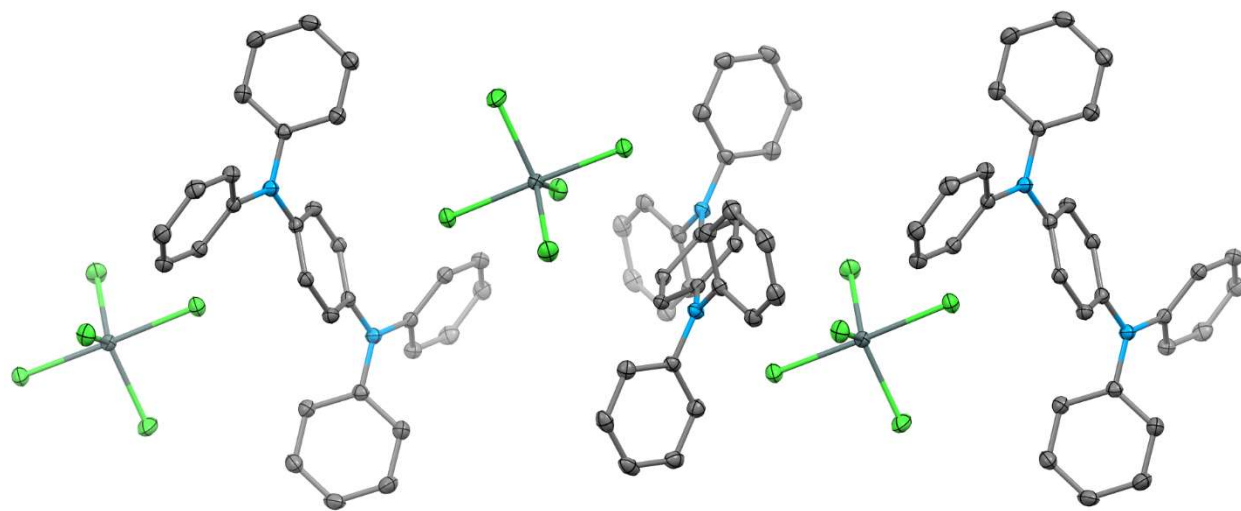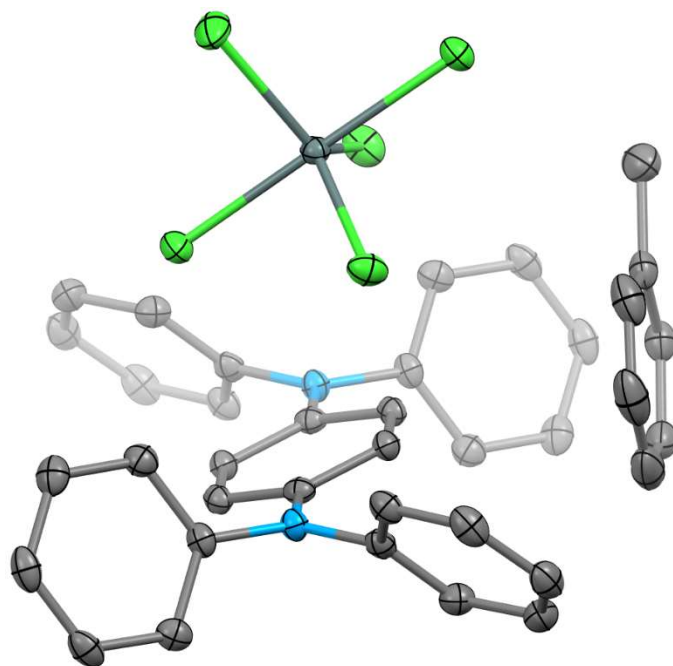
Fig 6. Crystals of (N,N,N',N'-tetraphenyl-1,4-benzenediamine$^+$)(Ti$^{IV}_2$Br$_9^-$)•toluene and the relative orientations of the independent components found in its crystal structure. The bottom view shows the chain of alternating anions and cations in the solid. Color code: C, N, Br, Ti.

The Formation of Green, Crystalline (N,N,N',N'-tetraphenyl-1,4-benzenediamine$^+$)(Sn^{IV}Cl$_5^-$)•toluene from Neutral N,N,N',N'-tetraphenyl-1,4-benzenediamine and Tin(IV) Tetrachloride

As discussed prior, comparing the behavior of early transition metal Ti with other closed shell Lewis acidic metal halides was a key objective of this project, and we chose SnCl$_4$ and SbCl$_5$ for this purpose. The addition of a solution of SnCl$_4$ in toluene to a solution of N,N,N',N'-tetraphenyl-1,4-benzenediamine in toluene produced a green solution which yielded rich green crystals over a period of a few days. The structure of the product, (N,N,N',N'-tetraphenyl-1,4-benzenediamine$^+$)(Sn^{IV}Cl$_5^-$)•toluene, is shown in Fig 7. The asymmetric unit consists of two half cations with the other half generated by reflection through centers of symmetry, one anion, and a toluene molecule. The sum of the three C-N-C angles at N1 is 359.91 °, and at N2, it is 359.95 °, indicating almost perfect planarity. The anion (Sn^{IV}Cl$_5^-$) has a trigonal bipyramidal geometry which has been observed in other salts of this ion.
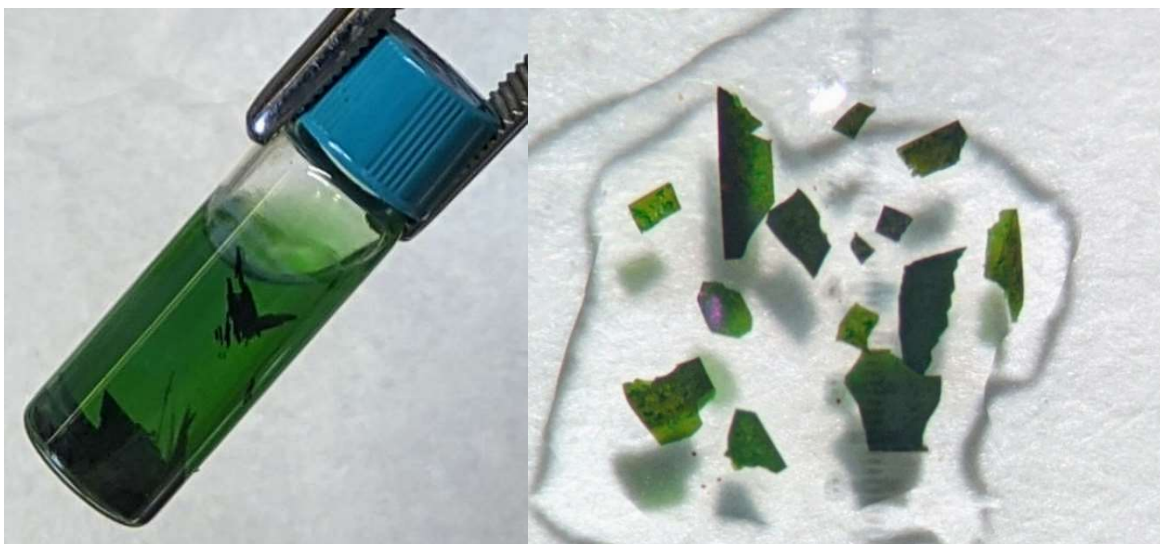
Fig 7. Top, the structures and relative orientations of the independent components found in crystalline (N,N,N',N'-tetraphenyl-1,4-benzenediamine$^+$)(Sn^{IV}Cl$_5^-$)•toluene, demonstrating accurate cation-anion stoichiometry (although the asymmetric unit contains two half-molecules of the cation, one full cation is shown here). Middle, the chains of alternating cations and anions present in the crystal. Color code: C, N, Cl, Sn. Bottom, the crystals growing in a toluene solution and as observed under a microscope.

The Formation of Greenish-black, crystalline (N,N,N',N'-tetraphenyl-1,4-benzenediamine$^+$)(Sb^{V}Cl$_6^-$)•toluene from N,N,N',N'-tetraphenyl-1,4-benzenediamine.

The reaction of SbCl$_5$ with N,N,N',N'-tetraphenyl-1,4-benzenediamine produced greenish black crystals with a golden luster containing (N,N,N',N'-tetraphenyl-1,4-benzenediamine$^+$)(Sb^{V}Cl$_6^-$)•toluene. A drawing showing the relative orientations and structures of the constituent ions in crystalline (N,N,N',N'-tetraphenyl-benzidine$^+$)(Sb^{V}Cl$_6^-$) is shown in Figure 8. The figure shows true stoichiometry, while the asymmetric unit contains half of each ion.
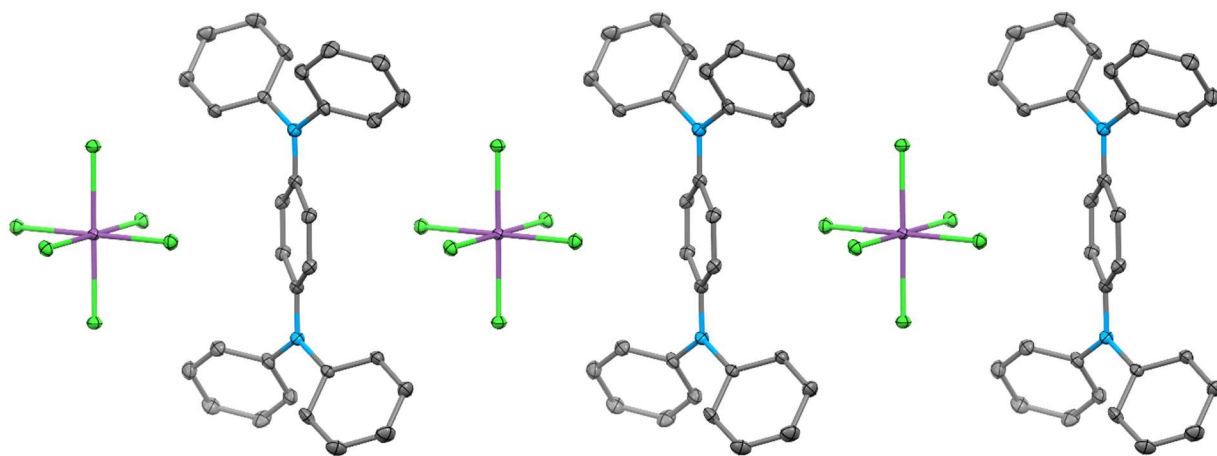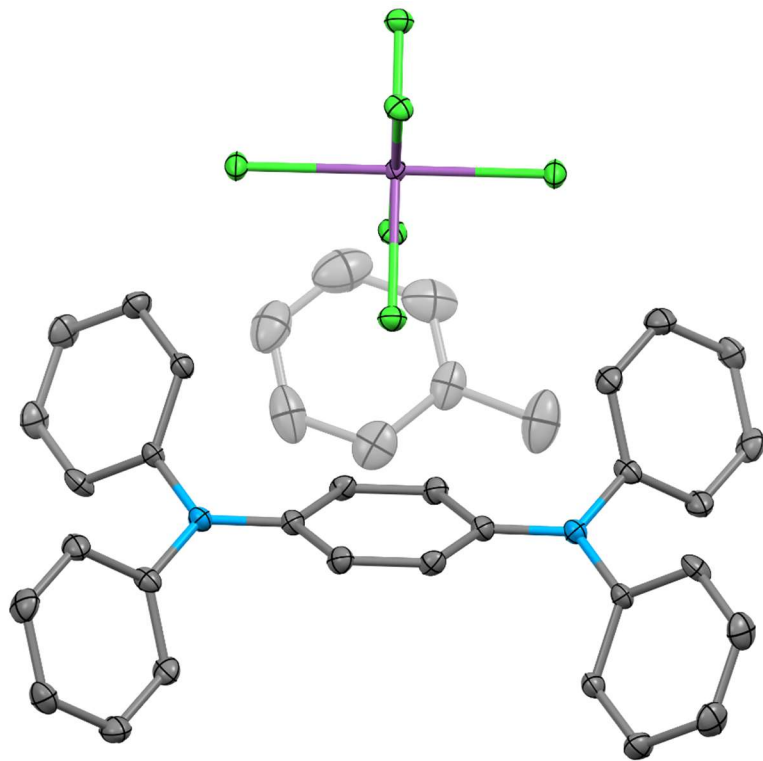
Fig 8. Top, the structures and relative orientations of the independent constituents found in crystalline (N,N,N',N'-tetraphenyl-1,4-benzenediamine$^+$)(Sb^{V}Cl$_6^-$)•(toluene). Middle, the alternating array of cations and anions that forms in the crystal. Color code: C, N, Cl, Sb. Bottom, the crystals under a microscope (the true color of the solid is not visible and only its golden luster is apparent).

The Formation of Greenish-Bronze, Crystalline (N,N,N',N'-tetraphenyl-benzidine$^+$)(Sb^{V}Cl$_6^-$) from Neutral N,N,N',N'-tetraphenyl-benzidine.

Oxidation of N,N,N',N'-tetraphenyl-benzidine with SbCl$_5$ in toluene produced greenish-bronze colored crystals of (N,N,N',N'-tetraphenyl-benzidine$^+$)(Sb^{V}Cl$_6^-$). The structure of the components of (N,N,N',N'-tetraphenyl-benzidine$^+$)(Sb^{V}Cl$_6^-$) and two of their relative orientations are shown in Figure 9. In one view, the benzidine radical appears to "stack" one upon the other in the specific direction of propagation, while the other view shows a different dimension of "crossed" stacking. Isomorphous crystals can be obtained by performing the reaction in dichloromethane, and in neither method do solvate molecules of toluene or dichloromethane make an appearance in the crystal structure.
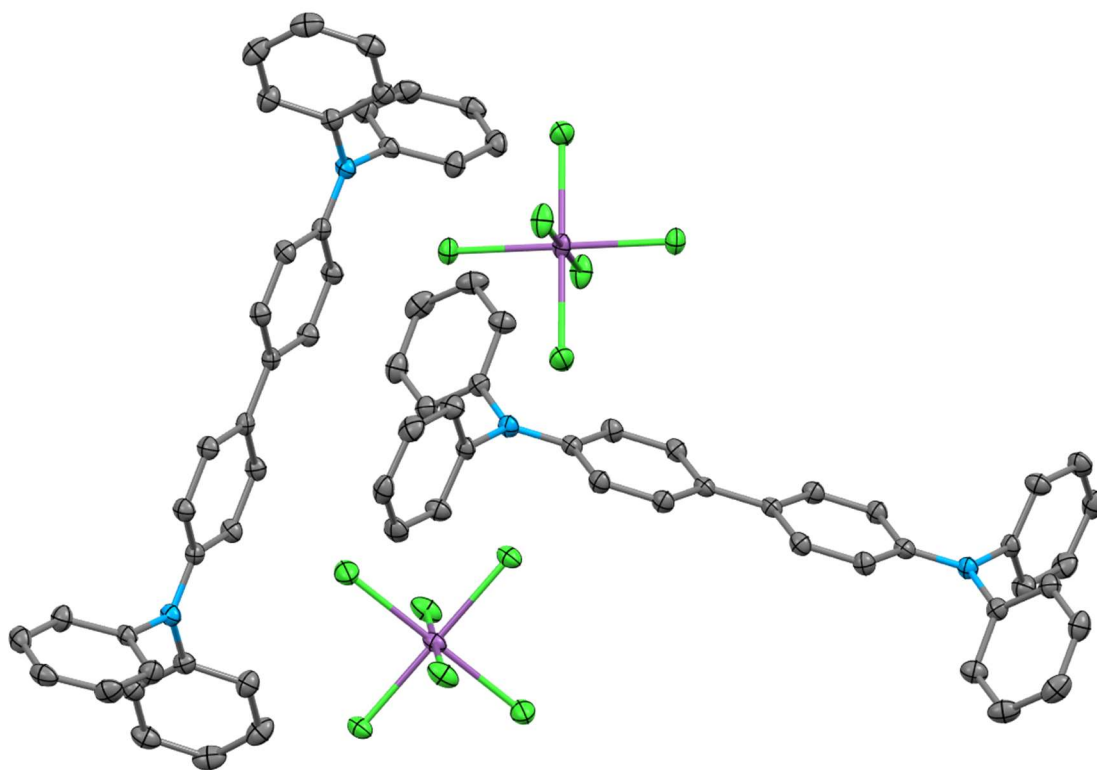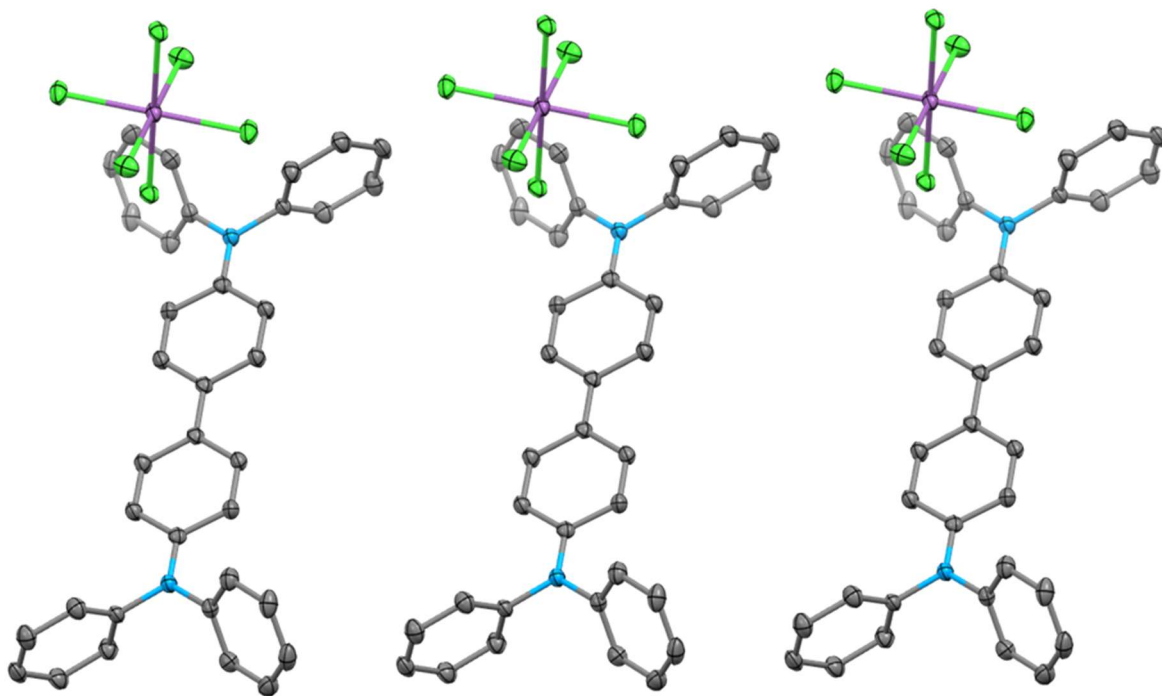
Fig 9. Two relative orientations of (N,N,N',N'-tetraphenyl-benzidine$^+$)(Sb^{V}Cl$_6^-$), exhibiting two modes of stacking for the benzidine radical. Bottom, dichroic crystals of the same. In this view of the crystal, the bronze sheen is not apparent.

The Formation of Reddish-brown, Crystalline (N,N,N',N'-tetraphenyl-benzidine^{2+})•2(Ti$_2^V$Cl$_9^-$)•CH$_2$Cl$_2$ from Neutral N,N,N',N'-tetraphenyl-benzidine and Titanium (IV) tetrachloride

Oxidation of N,N,N',N'-tetraphenyl-benzidine with TiCl$_4$ in dichloromethane produced an intensely-colored red solution, in which formed reddish-brown colored crystals of (N,N,N',N'-tetraphenyl-benzidine^{2+})•2(Ti$_2^V$Cl$_9^-$)•CH$_2$Cl$_2$ with a bronze sheen. The diamine species in this structure appears to be a dication; Figure 10 shows the accurate cation-anion stoichiometry, as well as the asymmetric unit. This species or the monocation could not be crystallized from toluene solutions prepared in the same manner. In both dichloromethane and toluene reaction mixtures,

the N,N,N',N'-tetraphenyl-benzidine radical species can be observed using EPR and UV/Vis/NIR spectra. Curiously, it is the dication that crystallizes with ease.
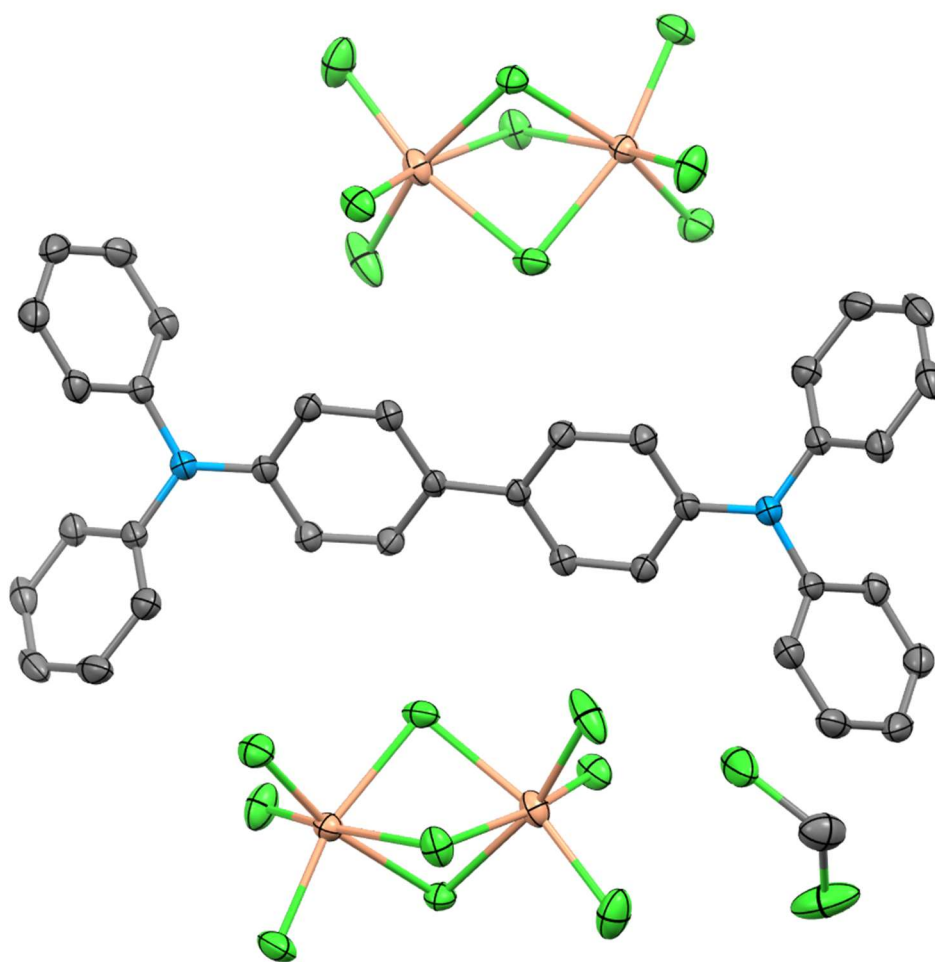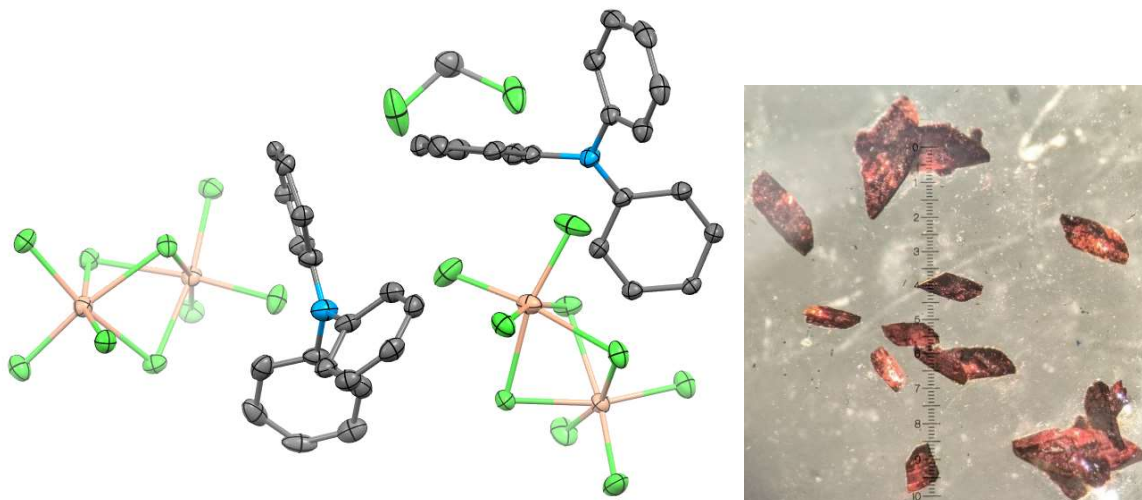
Fig 10. Top: asymmetric units in the crystals of (N,N,N',N'-tetraphenyl-benzidine^{2+}) 2(Ti$_2$^{V}Cl$_9$$^-$)•CH$_2Cl_2$ and the lustrous crystals themselves. Bottom: a whole cation and its two counterbalancing anions.

An overlay of the UV/Vis/NIR spectra of N,N,N',N'-tetraphenyl-benzidine and N,N,N',N'-tetraphenyl-1,4-benzenediamine radical cations, obtained in solution form (in dichloromethane) by isolating, washing, drying and then redissolving the crystalline samples of (N,N,N',N'-tetraphenyl-1,4-benzenediamine$^+$)(Sb^{V}Cl$_6$$^-$)•toluene and (N,N,N',N'-tetraphenyl-benzidine$^+$)(Sb^{V}Cl$_6$$^-$), can be seen below in Figure 11. As observed in previous literature, the appearance of the N,N,N',N'-tetraphenyl-1,4-benzenediamine radical is characterized by a single broad peak spanning the visible and NIR regions, while the N,N,N',N'-tetraphenyl-benzidine radical exhibits one visible peak and one broad peak in the farther NIR region, bathochromically shifted from the phenylene-bridged compound. This UV/Vis/NIR spectrum serves as a standard to compare with solution-state reaction aliquots where the two diamine products, N,N,N',N'-tetraphenyl-benzidine and N,N,N',N'-tetraphenyl-1,4-benzenediamine, are suspected to be formed in the radical state. The dashed red line indicates a direct aliquot of the reaction between TiCl$_4$ and N,N,N',N'-tetraphenyl-benzidine in dichloromethane. This trace is virtually identical to the solid red line exhibiting the N,N,N',N'-tetraphenyl-benzidine radical formed from SbCl$_5$ and isolated, yet Ti^{IV} and Sb^V yield different charged species in the crystalline form.
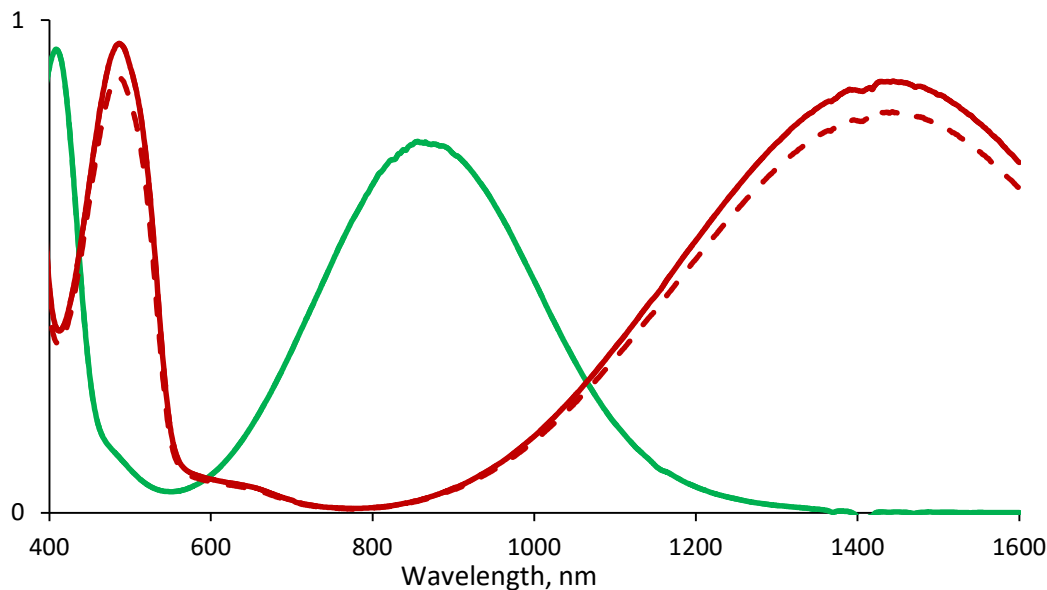
Figure 11: A comparison of the UV/vis/NIR spectra of (N,N,N',N'-tetraphenyl-benzidine+) (denoted in red) and (N,N,N',N'-tetraphenyl-1,4-benzenediamine+) (denoted in green) at room temperature in dichloromethane. The dashed red line represents a reaction aliquot from combining TiCl$_4$ with N,N,N',N'-tetraphenyl-benzidine in dichloromethane.

The electron paramagnetic resonance (EPR) spectra of the aforementioned diamines all exhibit five lines centered around a g value of approximately 2.005, as would be expected for an organic radical delocalized across two identical nitrogen centers through an aromatic bridge. These spectra hold much more meaning when compared with the coupling reactions we will discuss in the next chapter, where the diamines species serve as "standards".

References

(1)   Wang, X.; Zheng, X.; Wang, X.; Qiu, Y.; Li, Y.; Zhou, C.; Sui, Y.; Li, Y.; Ma, J. One-Electron Oxidation of an Organic Molecule by B(C$_6$F$_5$)$_3$; Isolation and Structures of Stable Non- Para -Substituted Triarylamine Cation Radical and Bis(Triarylamine) Dication

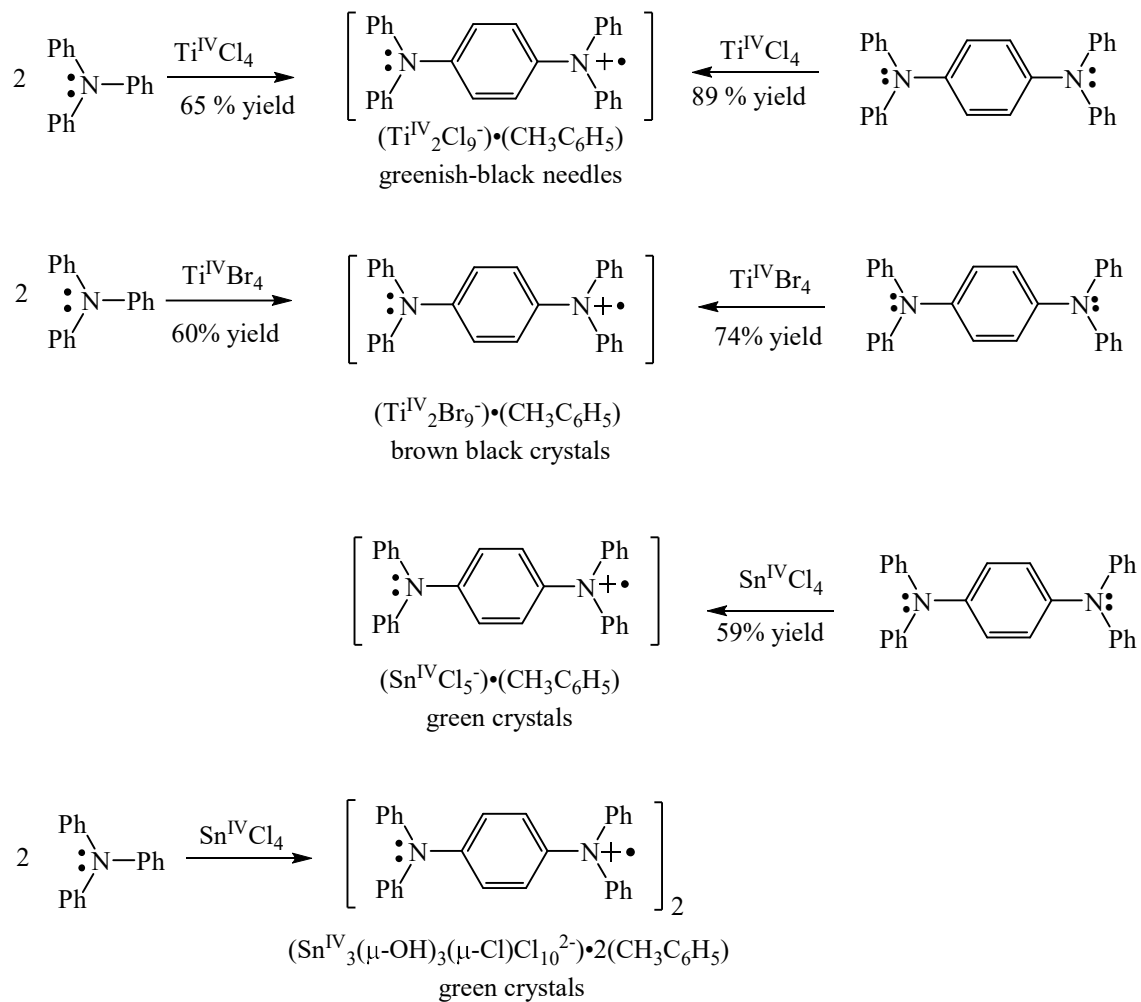Diradicaloid. *Journal of the American Chemical Society* **2013**, *135* (40). https://doi.org/10.1021/ja407318h.

(2)   Talipov, M. R.; Hossain, M. M.; Boddeda, A.; Thakur, K.; Rathore, R. A Search for Blues Brothers: X-Ray Crystallographic/Spectroscopic Characterization of the Tetraarylbenzidine Cation Radical as a Product of Aging of Solid Magic Blue. *Organic and Biomolecular Chemistry* **2016**, *14* (10). https://doi.org/10.1039/c6ob00140h.

(3)   Robé, E.; Daran, J. C.; Vincendeau, S.; Poli, R. A New Synthetic Method and Solution Equilibria for the Chlorotitanate(IV) Anions - Evidence for the Existence of a New Species: $[Ti_2Cl_{11}]^{3-}$. *European Journal of Inorganic Chemistry* **2004**, No. 20. https://doi.org/10.1002/ejic.200400293.

(4)   Chen, L.; Cotton, F. A. Synthesis, Reactivity, and X-Ray Structures of Face-Sharing Ti(III) Complexes; The New Trinuclear Ion, $[Ti_3Cl_{12}]^{3-}$. *Polyhedron* **1998**, *17* (21). https://doi.org/10.1016/s0277-5387(98)00171-5.

Chapter VI. The coupling of tertiary amine radical cations into *charged,* crystalline diamine species, and the evidence (spectroscopic or crystallographic) of these diamine products deviating from the expected C-C coupling scheme and forming unprecedented C-N bonds: Reactions of triphenylamine
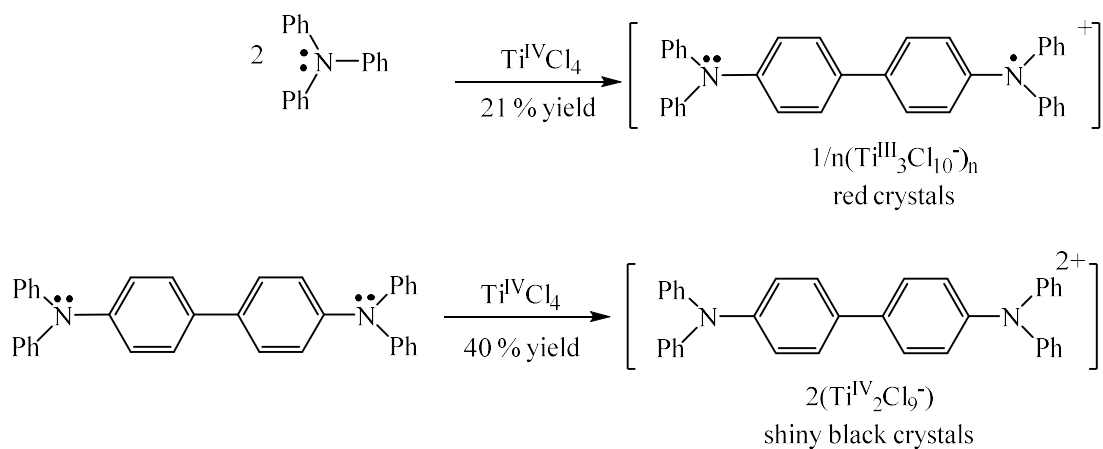
In this section we discuss the direct formation of charged diamine species from simpler, neutral tris-arylamines. As referenced before[1,2], neutral tetraphenylbenzidine can be synthesized through *p*-position coupling on one of the phenyl groups on each triphenylamine radical cation. However, a charged form of tetraphenylbenzidine has not been directly isolated from the neutral triphenylamine starting material in crystalline form – a phenomenon that also extends to other diamines formed from triarylamines. We have been able to demonstrate that using triphenylamine as starting material, we can both obtain benzidine radicals in crystalline form through the traditional *p*-position coupling, as well as form unconventional C-N bonds and capture the resultant tertiary diamine in its radical form. The formation of crystalline, isolable diamine species in this study can be summarized below in Scheme 1, while more detailed discussions of non-crystalline outcomes will follow.

Results and discussions

107

Crystallization from toluene solutions:

$$2 \; Ph_2N{-}Ph \xrightarrow[\text{65 \% yield}]{Ti^{IV}Cl_4} \left[Ph_2N{-}C_6H_4{-}N^+{\cdot}Ph_2 \right] \xleftarrow[\text{89 \% yield}]{Ti^{IV}Cl_4} Ph_2N{-}C_6H_4{-}NPh_2$$

$(Ti^{IV}_2Cl_9{}^-){\cdot}(CH_3C_6H_5)$
greenish-black needles

$$2 \; Ph_2N{-}Ph \xrightarrow[\text{60\% yield}]{Ti^{IV}Br_4} \left[Ph_2N{-}C_6H_4{-}N^+{\cdot}Ph_2 \right] \xleftarrow[\text{74\% yield}]{Ti^{IV}Br_4} Ph_2N{-}C_6H_4{-}NPh_2$$

$(Ti^{IV}_2Br_9{}^-){\cdot}(CH_3C_6H_5)$
brown black crystals

$$\left[Ph_2N{-}C_6H_4{-}N^+{\cdot}Ph_2 \right] \xleftarrow[\text{59\% yield}]{Sn^{IV}Cl_4} Ph_2N{-}C_6H_4{-}NPh_2$$

$(Sn^{IV}Cl_5{}^-){\cdot}(CH_3C_6H_5)$
green crystals

$$2 \; Ph_2N{-}Ph \xrightarrow{Sn^{IV}Cl_4} \left[Ph_2N{-}C_6H_4{-}N^+{\cdot}Ph_2 \right]_2$$

$(Sn^{IV}_3(\mu\text{-}OH)_3(\mu\text{-}Cl)Cl_{10}{}^{2-}){\cdot}2(CH_3C_6H_5)$
green crystals

Crystallization from dichloromethane solutions:

$$2 \quad Ph_2\ddot{N}-Ph \xrightarrow[\text{21 \% yield}]{Ti^{IV}Cl_4} \left[Ph_2\ddot{N} \text{—} \text{—} \dot{N}Ph_2 \right]^{+}$$

$1/n(Ti^{III}_3Cl_{10}^{-})_n$

red crystals

$$Ph_2\ddot{N}\text{—}\text{—}\ddot{N}Ph_2 \xrightarrow[\text{40 \% yield}]{Ti^{IV}Cl_4} \left[Ph_2N\text{—}\text{—}NPh_2 \right]^{2+}$$

$2(Ti^{IV}_2Cl_9^{-})$

shiny black crystals

Scheme 1. The formation of charged diamine species from neutral triphenylamine in toluene and dichloromethane solutions using TiCl$_4$, TiBr$_4$, SnCl$_4$ and SbCl$_5$.

Formation of C-C bond: Sb^V

The Formation of Greenish-Bronze, Crystalline (N,N,N',N'-tetraphenyl-benzidine$^+$)(Sb^{V}Cl$_6^-$) from Neutral Triphenylamine.

When triphenylamine is combined with SbCl$_5$ in toluene and dichloromethane, it is directly converted into the N,N,N',N'-tetraphenylbenzidine radical cation. The crystal structure for this compound can be seen below:
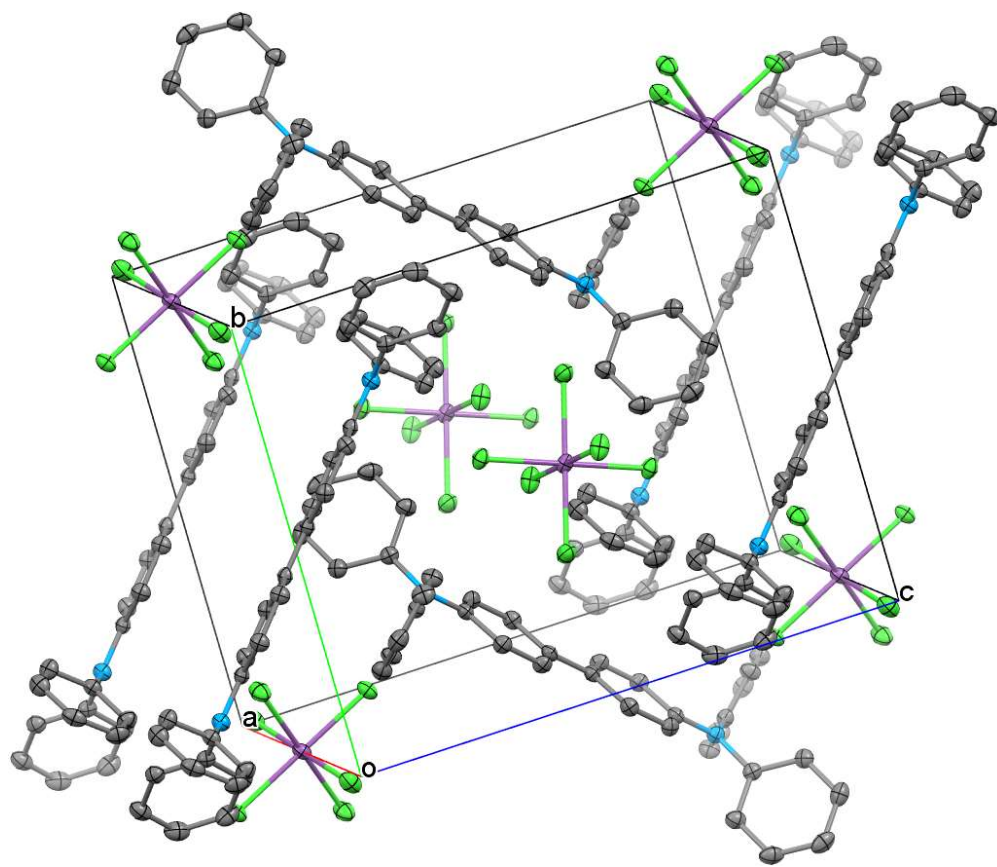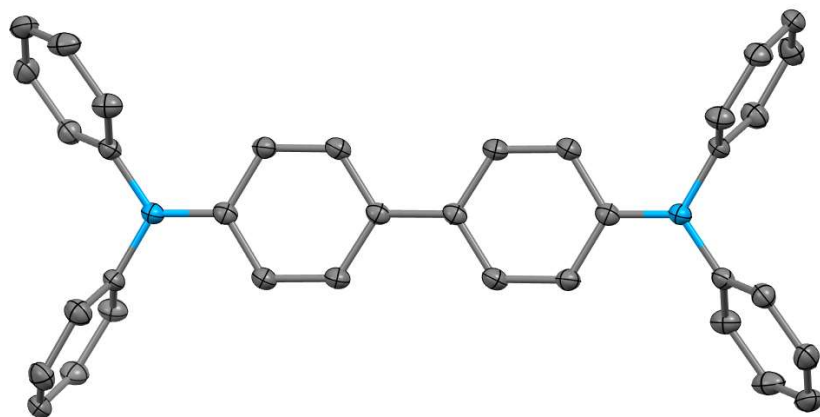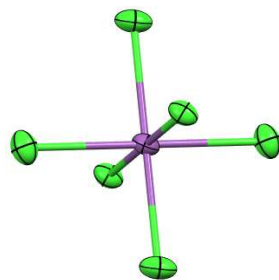
Fig 1. The crystal structure and packing diagram for (N,N,N',N'-tetraphenyl-benzidine$^+$)(Sb^{V}Cl$_6^-$) as formed from neutral triphenylamine and SbCl$_5$ in dichloromethane or toluene.

This crystalline material can be reproducibly made from triphenylamine, and is isomorphous to the crystal structure (N,N,N',N'-tetraphenylbenzidine)$^{•+}$ radical cation discussed in Part I which was obtained by performing one-electron oxidation on neutral N,N,N',N'-tetraphenylbenzidine itself. The isostructurality of the two crystal sources points towards a straightforward process for the coupling of triphenylamine species in the Sb^V mediated oxidation process. Shown in Figure 2 are optical spectra for the reaction between triphenylamine and SbCl$_5$, in toluene and dichloromethane. Both exhibit a combination of a 480 nm visible and a broad NIR peak, features together associated with the tetraphenylbenzidine radical, indicating almost instantaneous formation of the same. A 650 nm visible peak associated with triphenylamine in its radical state is also seen. However, in case of the spectrum collected in toluene one week after the day of reaction, the triphenylamine peak appears to be greater relative quantity than at the start of the reaction, indicating a certain degree of equilibrium between the charged mono-amine and diamine species.

SbCl$_5$ with NPh$_3$ in DCM
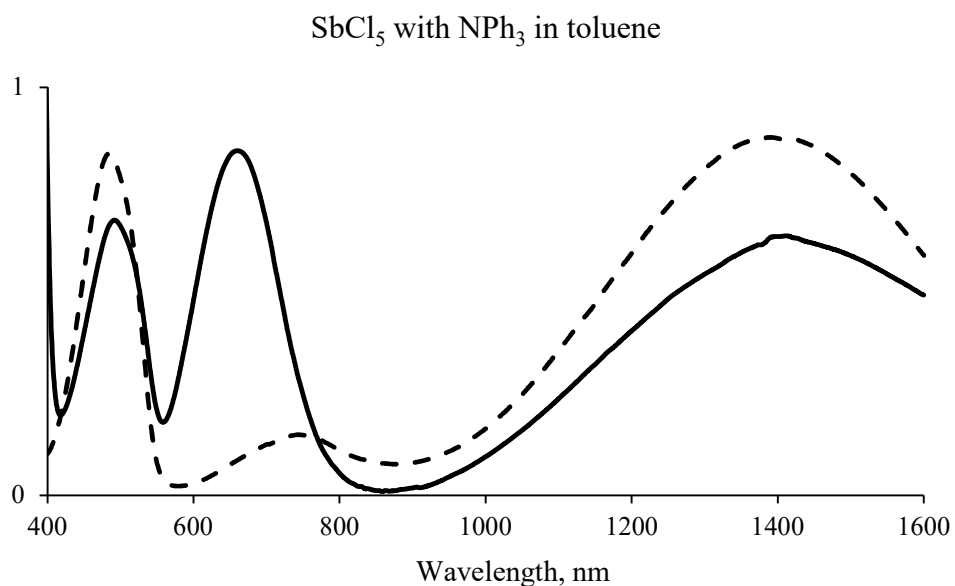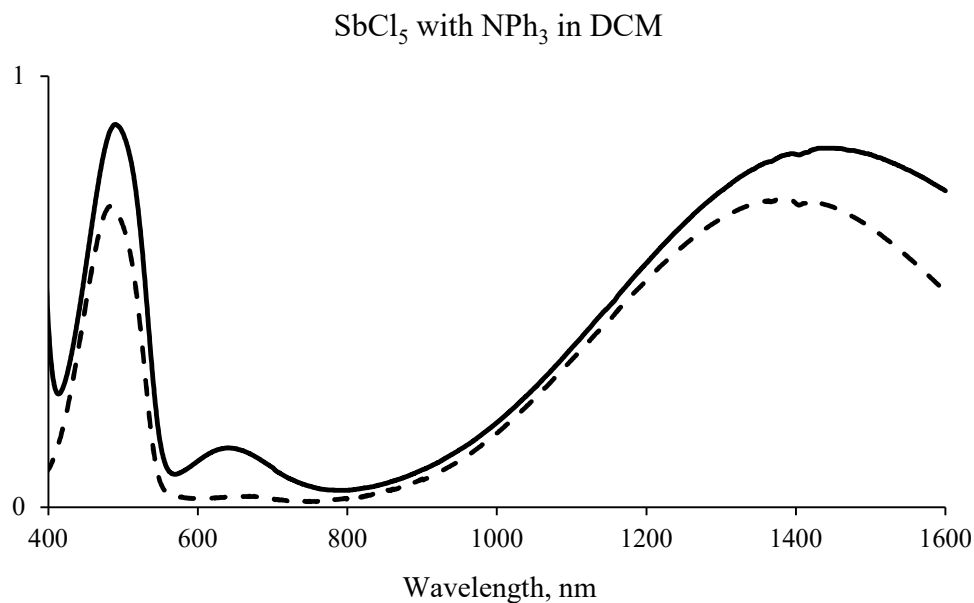

SbCl$_5$ with NPh$_3$ in toluene

Fig 2. UV/Vis/NIR spectra comparing aliquots from freshly prepared reaction mixtures (in dashed line) vs one week old reaction mixtures (in solid line). Top – reaction in dichloromethane, bottom – reaction in toluene.

When performing this reaction (between triphenylamine and SbCl$_5$) in acetonitrile, we see the appearance of simply the triphenylamine radical and not its dimer in the fresh reaction mixture,

and almost no change to the reaction mixture over the course of a week (Figure 3). This denotes significant dependence of the reaction progress on the solvent chosen. In later reactions involving other metal oxidants, we will see that performing the reaction in acetonitrile shows a deceleration of dimer formation, but not to the extent seen in case of antimony pentachloride.
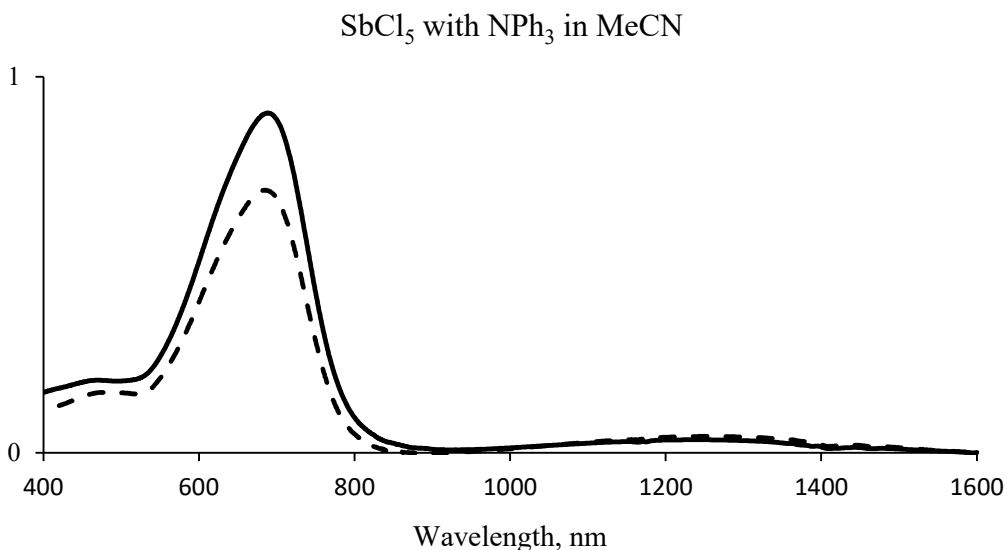
SbCl$_5$ with NPh$_3$ in MeCN

Fig 3. UV/Vis/NIR spectra for the reaction between triphenylamine and SbCl$_5$ in acetonitrile.

In addition to optical spectra, a solution-state room temperature EPR spectrum was collected for the reaction between SbCl$_5$ and triphenylamine in toluene instantly upon mixing. The spectrum contains 5 lines indicative of delocalization of the unpaired spin across two identical N-atoms, as would be expected from a tetraphenylbenzidine radical.
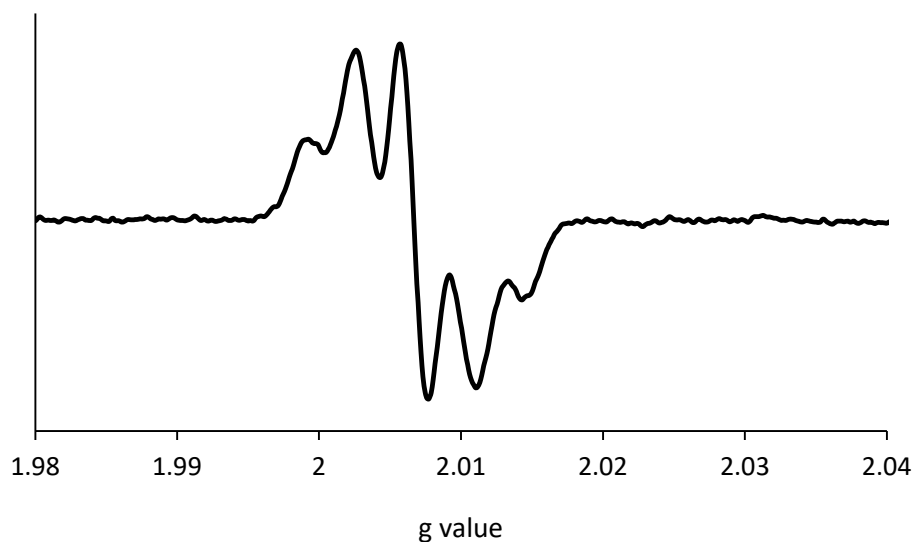
Fig 4. A five-line EPR Spectrum for the reaction between triphenylamine and SbCl₅

The delocalization evident from the EPR spectrum is further reinforced by closely observing the coplanarity of phenyl groups in the crystal structure of the benzidine radical. As compared to neutral benzidine, (N,N,N',N'-tetraphenylbenzidine)$^{\bullet+}$ shows significantly increased planarization of N-substituting phenyl groups with the benzidine "bridge". In the neutral amine, each N atom maintains roughly planar N-C bond geometry about itself, but the phenyl groups are visibly more offset from the benzidine unit as shown in Figure 5.
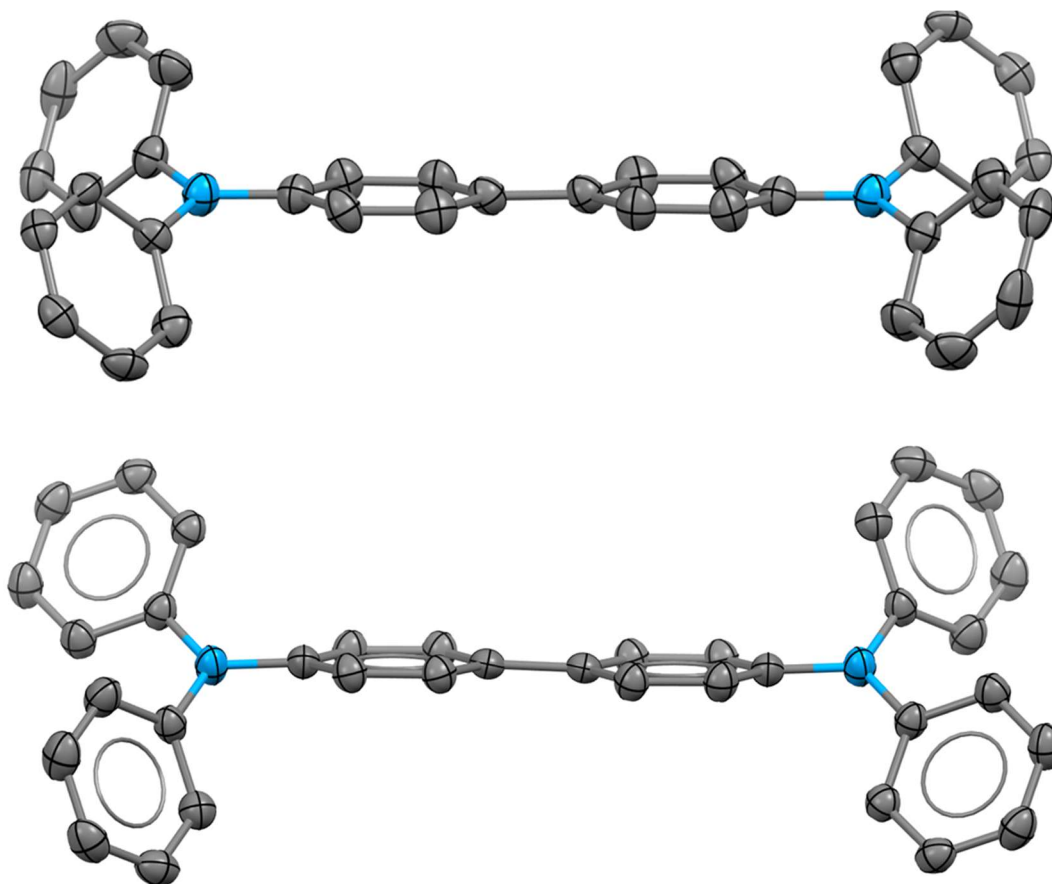
Fig 5. A sideways view of plane of the biphenyl moiety to help visualize the increased coplanarity of N-substituting phenyl groups with the benzidine "bridge" in case of the benzidine radical (top) and neutral benzidine (bottom). Crystal coordinates for the neutral tetraphenylbenzidine molecule were obtained from Ref 3[3].

Formation of C-N bond: Ti[IV] and Sn[IV]

When an attempt was made to oxidize triphenylamine with other metal halides, namely, titanium tetrachloride, titanium tetrabromide and tin tetrachloride, the results obtained were starkly different from the simple oxidative coupling observed in case of antimony pentachloride. The use of Ti[IV] and Sn[IV] as oxidants leads to radical coupling through the formation of a remarkable C-N bond and is discussed below.

The Formation of Green, Crystalline (N,N,N',N'-tetraphenyl-1,4-benzenediamine$^+$)(Ti$^{IV}_2$Cl$_9^-$)•toluene from Triphenylamine.

Mixing of toluene or acetonitrile solutions of TiCl$_4$ with solutions of triphenylamine in the same solvent produces deep green solutions corresponding to the radical cation of N,N,N',N'-tetraphenyl-1,4-benzenediamine (verified by EPR and optical spectroscopy). Upon standing, the toluene solutions produced deep green crystals of (N,N,N',N'-tetraphenyl-1,4-benzenediamine$^+$)(Ti$^{IV}_2$Cl$_9^-$)•toluene which form in the space group $P\bar{1}$, and is isostructural to the (N,N,N',N'-tetraphenyl-1,4-benzenediamine$^+$)(Ti$^{IV}_2$Cl$_9^-$)•toluene crystals obtained from oxidation of neutral N,N,N',N'-tetraphenyl-1,4-benzenediamin, which was discussed in Part I. In complete contrast to the analogous reactions conducted with SbCl$_5$ as oxidant, the product formed is not a cation of the tetraphenylbenzidine species proceeding through *p*-position coupling between two triphenylamines, but rather a cation of the N,N,N',N'-tetraphenyl-1,4-benzenediamine species proceeding through C-N bond formation and loss of one phenyl group. However, in one similarity with the analogous SbCl$_5$ reaction, the crystal structure formed from the triphenylamine reaction in toluene is isomorphous to that obtained when trying to oxidize the same neutral diamine – pointing towards very clear preference of one product over the other for the two reaction pathways mediated by different metal halides.
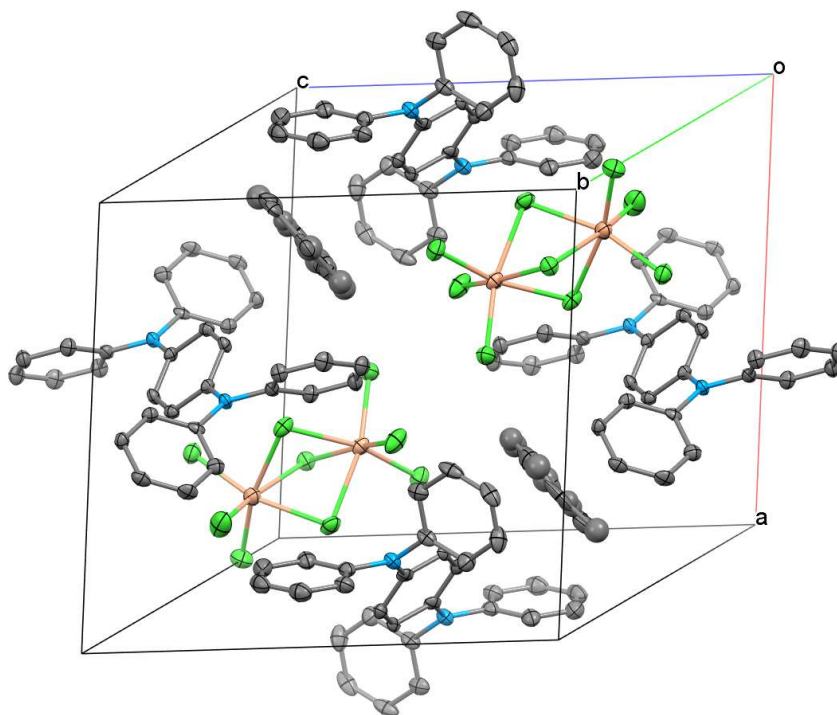
Fig 5. The unit cell contents of (N,N,N',N'-tetraphenyl-1,4-benzenediamine$^+$)(Ti$^{IV}_2$Cl$_9^-$)•toluene

The Formation of Brown Black, Crystalline (N,N,N',N'-tetraphenyl-1,4-benzenediamine$^+$)(Ti$^{IV}_2$Br$_9^-$)•toluene from Neutral Triphenylamine

In an analogous fashion to the TiCl$_4$ reaction described above, mixing of toluene/acetonitrile solutions of TiBr$_4$ with a toluene or acetonitrile solution of triphenylamine produces brown solutions identical to the reaction observed with neutral N,N,N',N'-tetraphenyl-1,4-benzenediamine. Shiny brown-black, dichroic crystals of (N,N,N',N'-tetraphenyl-1,4-benzenediamine$^+$)(Ti$^{IV}_2$Br$_9^-$)•toluene grew over several days of standing from solutions made from triphenylamine. Although these crystals grow in the in the space group $P\bar{1}$, they are not isostructural with the chlorine-containing analogue, (N,N,N',N'-tetraphenyl-1,4-benzenediamine$^+$)(Ti$^{IV}_2$Cl$_9^-$)•toluene (see figure below). However, they ARE isostructural with the

117

exact same compound obtained from the diamine standard (neutral N,N,N',N'-tetraphenyl-1,4-benzenediamine) – once again pointing to a clear product preference.
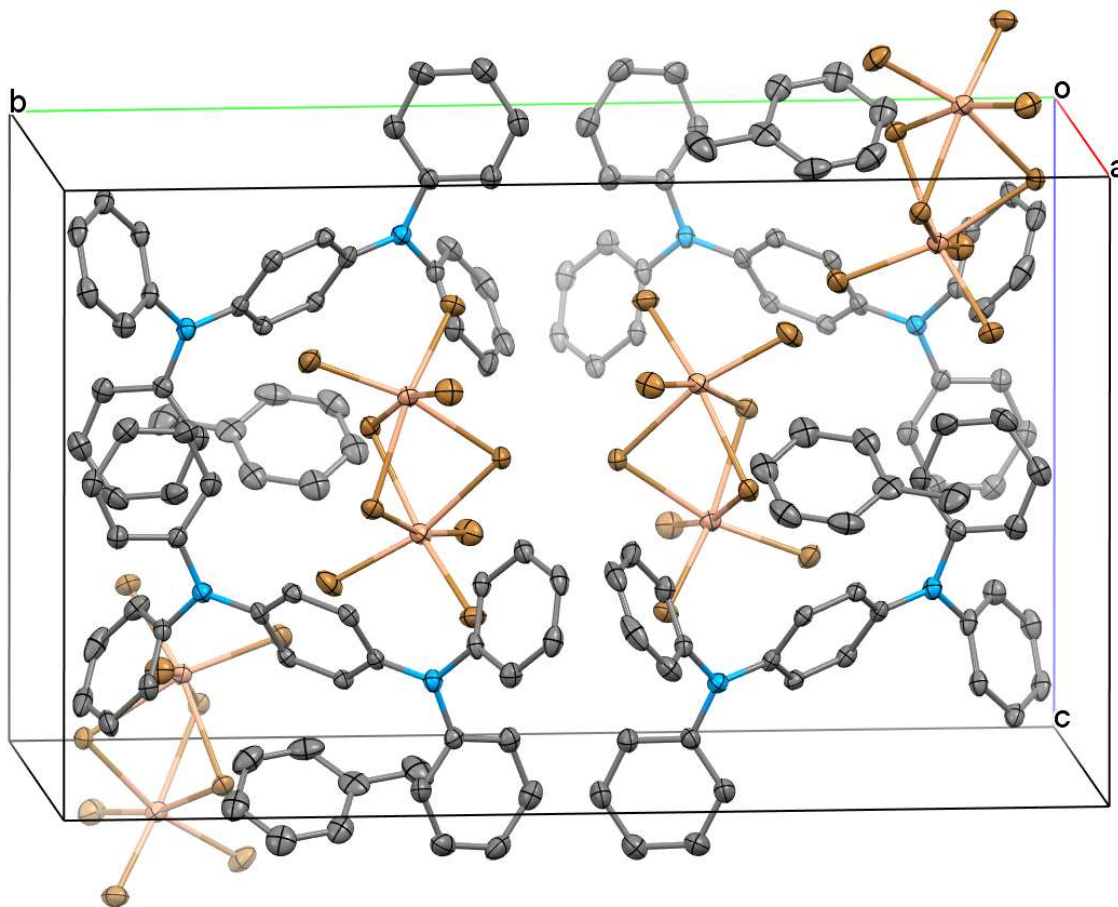

Fig 6. The unit cell contents of (N,N,N',N'-tetraphenyl-1,4-benzenediamine$^+$)(Ti$^{IV}_2$Br$_9^-$)•toluene

The reaction of Neutral Triphenylamine with Tin ^{IV} Chloride

Similar to the titanium halide reactions in toluene and acetonitrile, combining SnCl$_4$ with triphenylamine in toluene and acetonitrile results in immediate formation of a rich green solution containing N,N,N',N'-tetraphenyl-1,4-benzenediamine radical cation. However, unlike the titanium halide reactions, no crystals (isomorphous to the diamine standard or not) are formed

within a reasonable amount of fine. Optical and EPR spectra are used to confirm the presence of the N,N,N',N'-tetraphenyl-1,4-benzenediamine$^{\bullet+}$ species.

When a toluene solution of SnCl$_4$ and triphenylamine was left alone for a period of three to four months, green-black needles grew in it gradually. The crystalline sample had a disappointing yield of 11% but was crystallographically confirmed to contain the N,N,N',N'-tetraphenyl-1,4-benzenediamine radical cation, as shown below in Figure 6. The counterion appears to be a complex, disordered, hydrolyzed derivative of Tin^{IV} halide, with bridging hydroxyl groups that are likely formed from months of abandonment of the reaction mixture, leading to partial oxidation. The anion is modeled with and without crystallographic disorder.
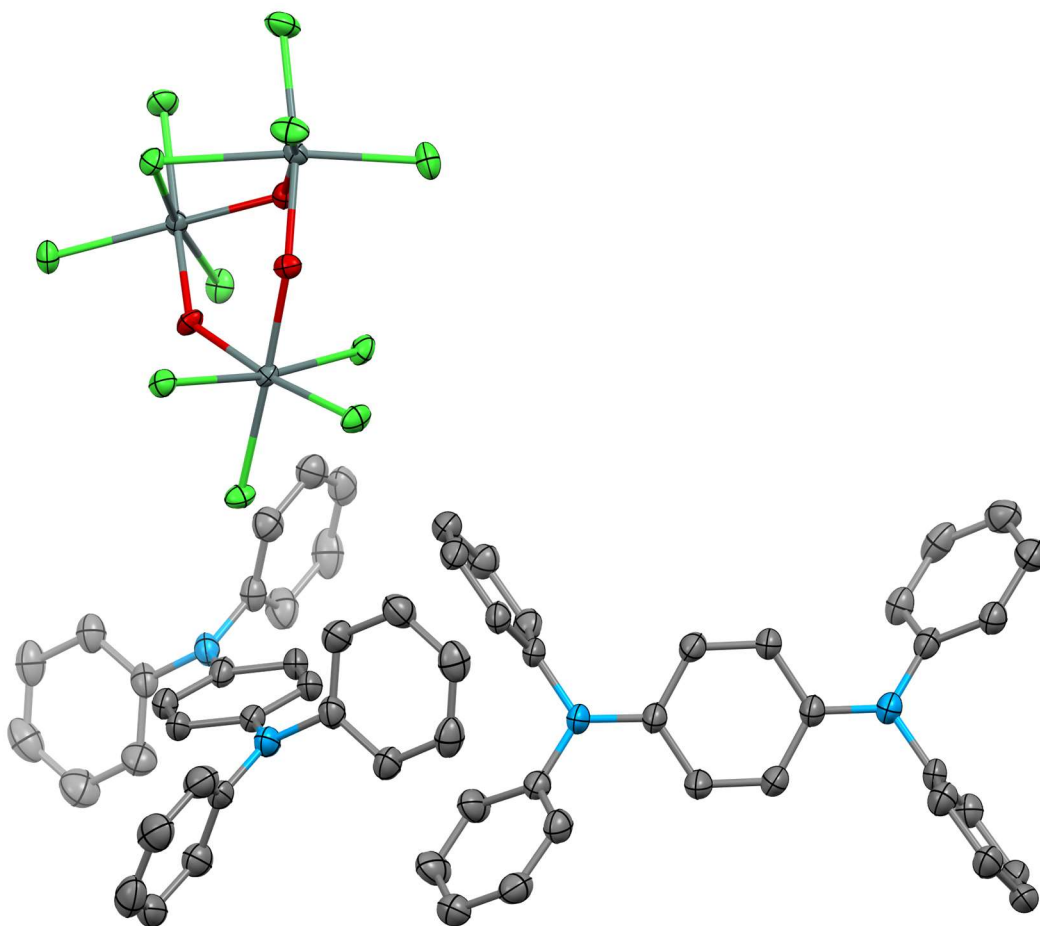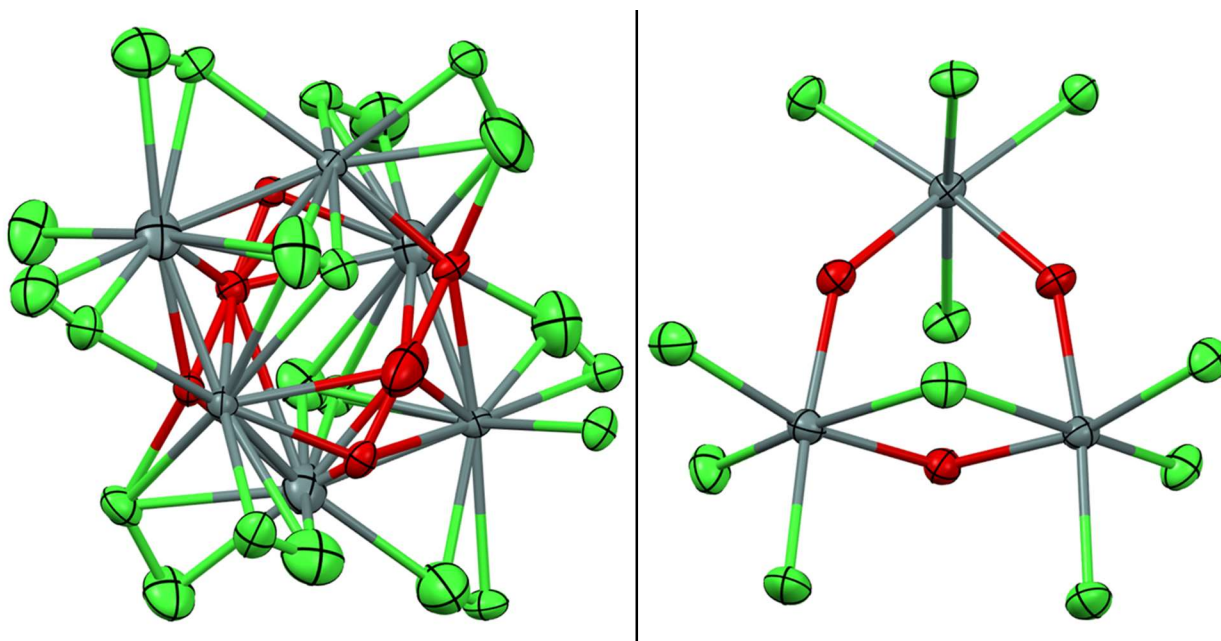
Fig 6. (Top) the structure of (N,N,N',N'-tetraphenyl-1,4-benzenediamine$^+$)$_2$ (Sn$^{IV}_3$(μ-OH)$_3$(μ-Cl)Cl$_{10}^{2-}$)•2toluene; (bottom) the counterion with and without disorder

In an odd departure from the Ti^{IV} and Sb^V mediated reactions, the Sn^{IV} case does not show isostructurality with crystals obtained from the parent diamine as this species could not be reproduced using neutral benzenediamine as starting material.

To take a closer look at the optical spectra, let us first familiarize ourselves with the two standards.
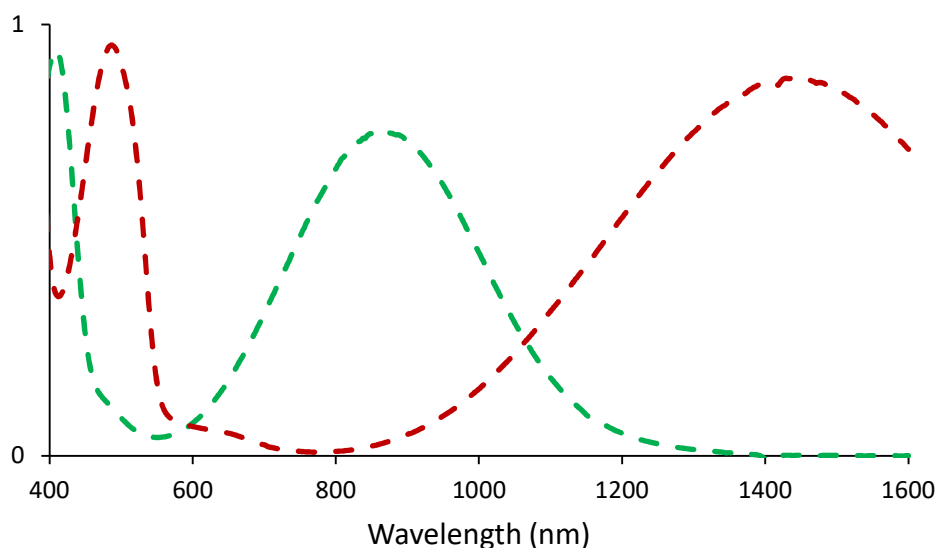
Fig 7. UV/Vis/NIR Spectra for the standard solutions made from neutral N,N,N',N'-tetraphenylbenzidine (red) and N,N,N',N'-tetraphenyl-1,4-benzenediamine (green)

The dashed red trace represents the N,N,N',N'-tetraphenylbenzidine radical cation and the dashed green trace represents the N,N,N',N'-tetraphenyl-1,4-benzenediamine radical cation. Both spectra were collected at room temperature in toluene, and are found to be consistent with literature findings. Moving forward with UV/Vis/NIR studies performed on the reactions between $SnCl_4$/$TiCl_4$/$SbCl_5$ and triphenylamine in toluene and acetonitrile, we will try to look out for the formation of a 600-1200 nm broad band to indicate the N,N,N',N'-tetraphenylbenzidine radical cation has been formed, while the combination of a sharp 500 nm peak and a broad band NIR stretching from 1000 nm into further low-energy regions of the IR can be thought of as the test for the formation of the N,N,N',N'-tetraphenylbenzidine radical cation species.

From Figure 8 below, we can see instantaneous formation of the N,N,N',N'-tetraphenyl-1,4-benzenediamine radical cation from neutral triphenylamine with both $SnCl_4$ and $TiCl_4$ in toluene and acetonitrile. The dashed black line indicates $TiCl_4$ reaction mixture while the dotted

black line indicates the SnCl$_4$ reaction mixture. Both spectra exhibit a shoulder around 1300 nm that is not linked to the N,N,N',N'-tetraphenyl-1,4-benzenediamine radical cation, and is more prominent in case of the Sn^{IV} reaction. The exact nature of this shoulder has not been identified.
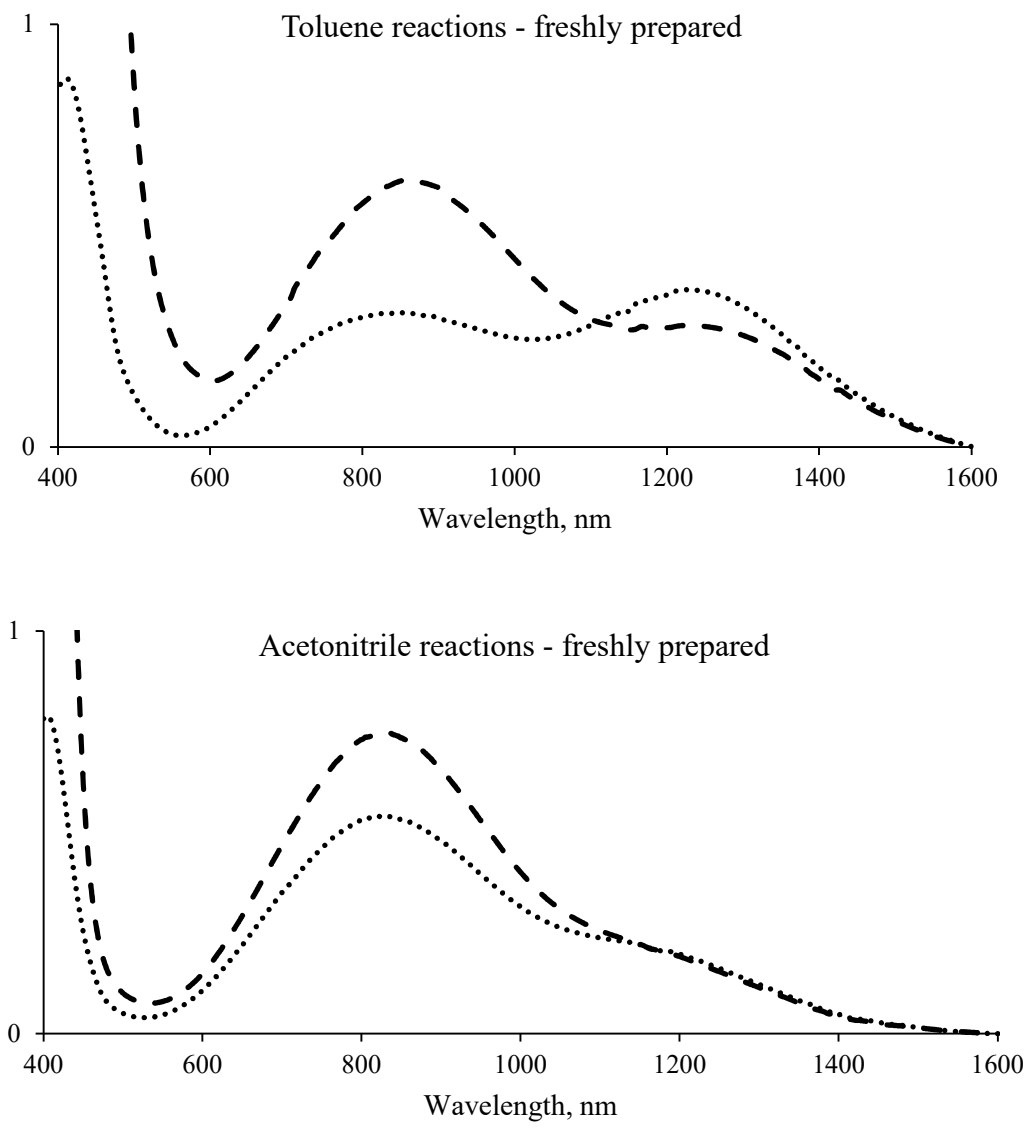

Fig 8. Reactions of TiCl$_4$ (large dashes) and SnCl$_4$ (dotted line) with triphenylamine in toluene (top) and acetonitrile (bottom)

A comparison between fresh vs aged samples of these reaction mixtures in toluene and acetonitrile shows that the unidentified shoulder gradually decreseases in relative quantity to give rise to a spectrum of mostly N,N,N',N'-tetraphenyl-1,4-benzenediamine radical cation. The $SnCl_4$ spectra in acetonitrile are shown below in Figure 9 (solid black line – spectrum after one week from reaction, dotted line – freshly collected spectrum).
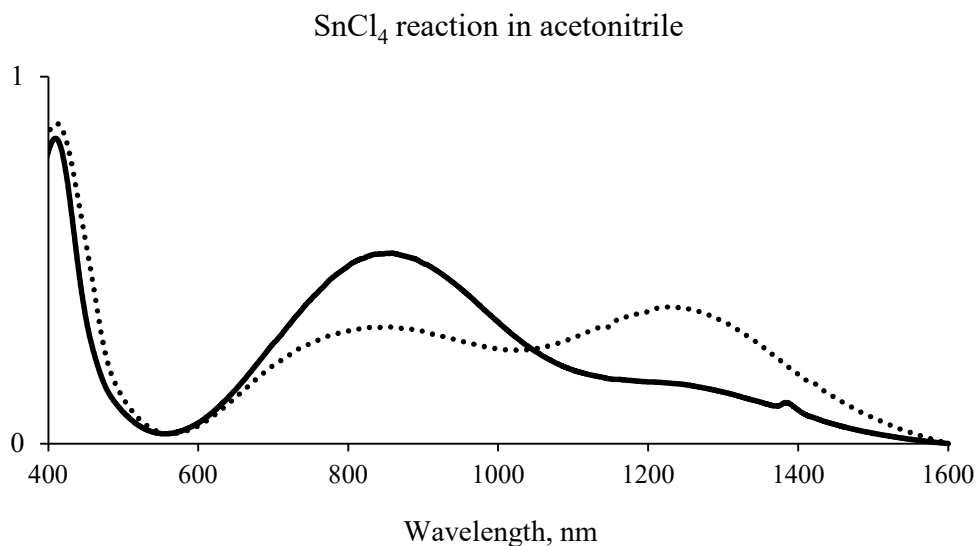
SnCl$_4$ reaction in acetonitrile

Fig 9. Comparing the UV/Vis/NIR spectra of freshly obtained aliquot (dotted black line) and a week-old aliquot (solid black line) from the reaction mixture of SnCl$_4$ and triphenylamine in acetonitrile.

EPR spectra collected from toluene and acetonitrile reactions of $TiCl_4$, $SnCl_4$ and $TiBr_4$ with triphenylamine strongly suggest the formation of N,N,N',N'-tetraphenyl-1,4-benzenediamine$^{\bullet+}$. In all cases, a five-line spectrum in the g-value region of an amine radical is observed, denoting that the unpaired spin is delocalized across 2 nitrogen-centers. However, a smaller hyperfine coupling constant can be expected for the N,N,N',N'-tetraphenylbenzidine radical cation than the N,N,N',N'-tetraphenyl-1,4-benzenediamine radical cation. If we look at the reaction between $TiCl_4$ and triphenylamine in toluene (shown in Figure 10 in yellow trace), we

can visually spot its similarity with N,N,N',N'-tetraphenyl-1,4-benzenediamine$^{\bullet+}$ (in green trace) rather than the N,N,N',N'-tetraphenylbenzidine$^{\bullet+}$ (in red trace).
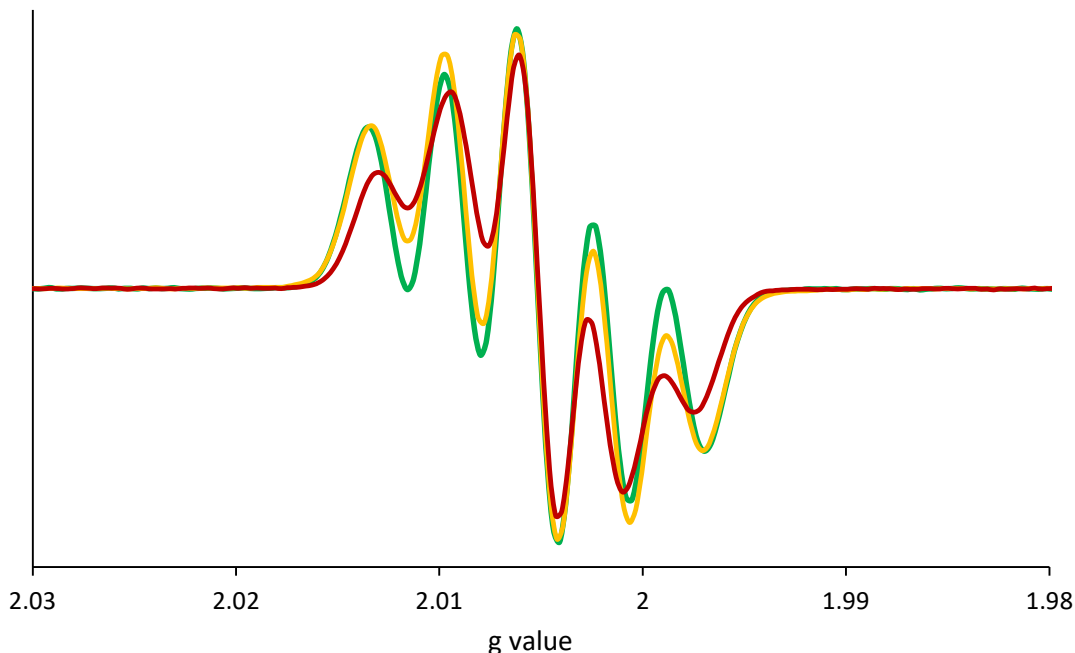

Fig 10. The EPR spectrum for a toluene solution of TiCl$_4$ and triphenylamine (yellow), contrasted with that of the benzenediamine standard (green) and benzidine standard (red), also in toluene.

This is confirmed by the hyperfine coupling constant for the triphenylamine-TiCl$_4$ reaction mixture. The benzenediamine standard (green trace) gives $a_N = 16.0\pm0.1$ MHz while the tetraphenylbenzidine standard (red trace) gives $a_N = 14.8\pm0.1$ MHz; the sample (yellow trace) gives $a_N = 15.9\pm0.1$ MHz, which is more in keeping with the benzenediamine standard. For the reaction between triphenylamine and TiBr$_4$, EPR spectra indicate *almost exclusive* formation of the benzenediamine radical as the a_N values for both sample and standard are 16.0 ± 0.1MHz.

While these results were internally consistent, there remained the question of explaining the redox process – assuming the metal halides are the oxidizing agents, the lack of appearance of a

paramagnetic Ti^{III} species in the above EPR spectrum was surprising. We postulated that any Ti^{III} formed in solution state would be better stabilized in the presence of a coordinating solvent and repeated the spectra using reaction aliquots from acetonitrile. The resulting spectrum is displayed in Figure 11.
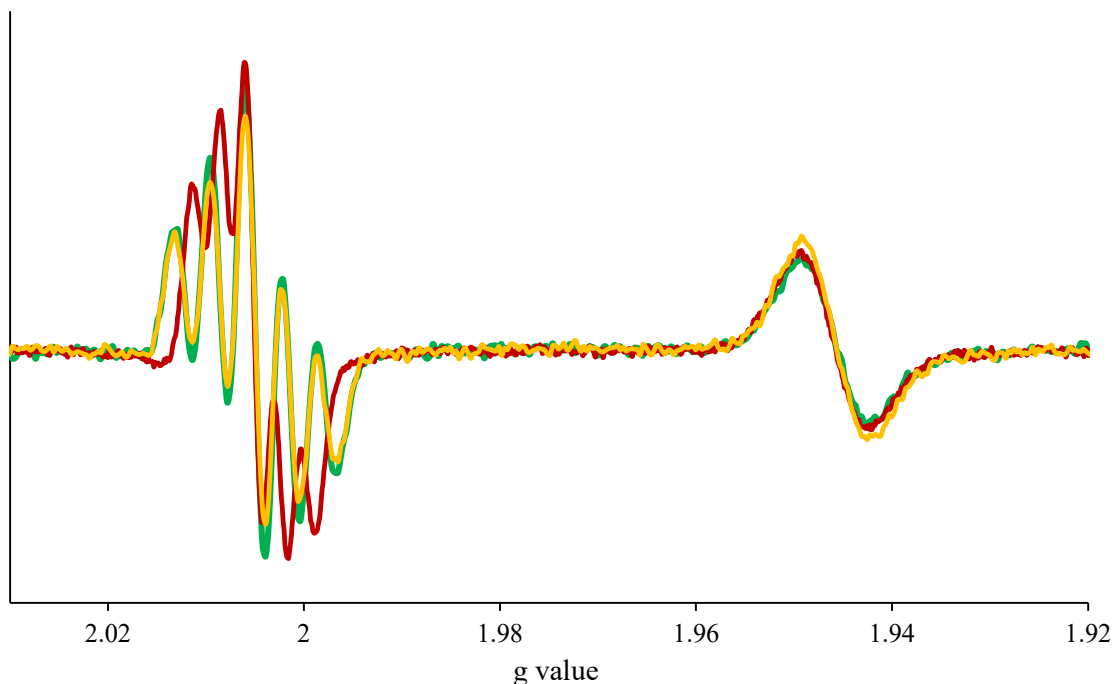

Fig 11. The EPR spectrum for an acetonitrile solution of $TiCl_4$ and triphenylamine (yellow), contrasted with that of the benzenediamine standard (green) and benzidine standard (red), also in acetonitrile.

In keeping with the color scheme followed before, the green, red and yellow traces denote benzenediamine standard, benzidine standard and triphenylamine reaction mixture respectively. It should be visually apparent that the reaction mixture, once again, forms the unexpected benzenediamine product rather than the benzidine product. The hyperfine coupling constants reinforce this belief, with the green trace (benzenediamine standard) and yellow trace (reaction aliquot) both fitting at $a_N = 16.0 \pm 0.1$ MHz, while the red trace (benzidine standard) fits at $a_N =$

11.7±0.1 MHz. Additionally, a second feature can be observed in this spectrum in the vicinity of g = 1.945. To verify that this species is indeed reduced titanium, a standard of $TiCl_3(MeCN)_3$ was also analyzed and is compared below with the spectrum of the reaction mixtures. The Ti^{III} standard (shown in dashed blue trace) exhibits a broad single line and similar g value to the suspected reduced metal signal from the reaction spectra.
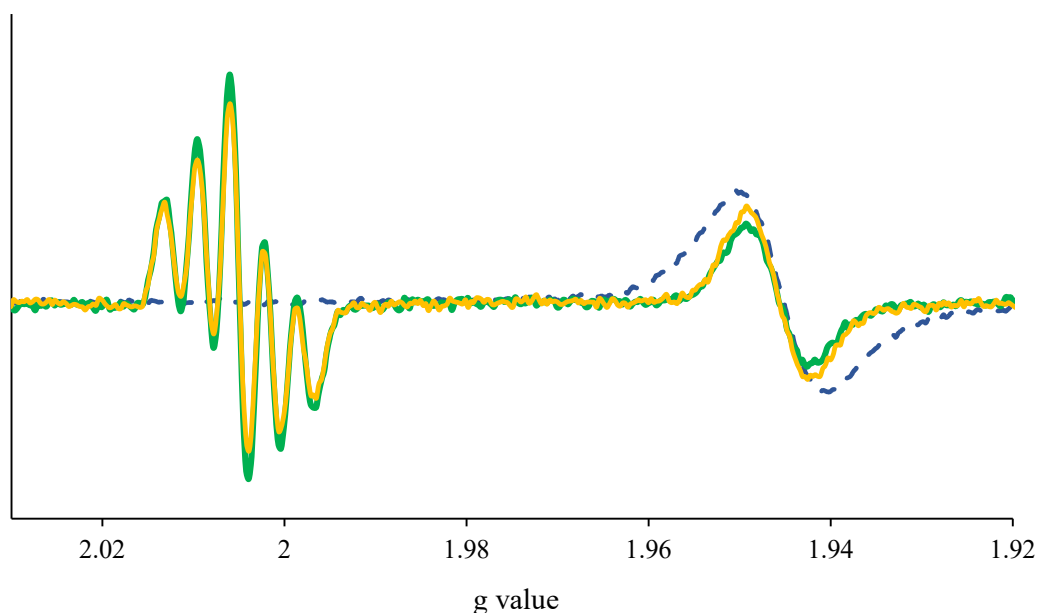

Fig 12. The EPR spectrum for acetonitrile solutions of $TiCl_4$ and triphenylamine (yellow) and $TiCl_4$ and benzenediamine standard (green), contrasted with $TiCl_3(NCCH_3)$ (dashed blue line).

Similarly, a comparison between the reactions of benzenediamine standard and triphenylamine with $TiBr_4$ in acetonitrile gives the following spectrum (the color scheme is kept consistent). A broader but nevertheless obvious appearance of the Ti^{III} signal confirms the reduction of the metal.
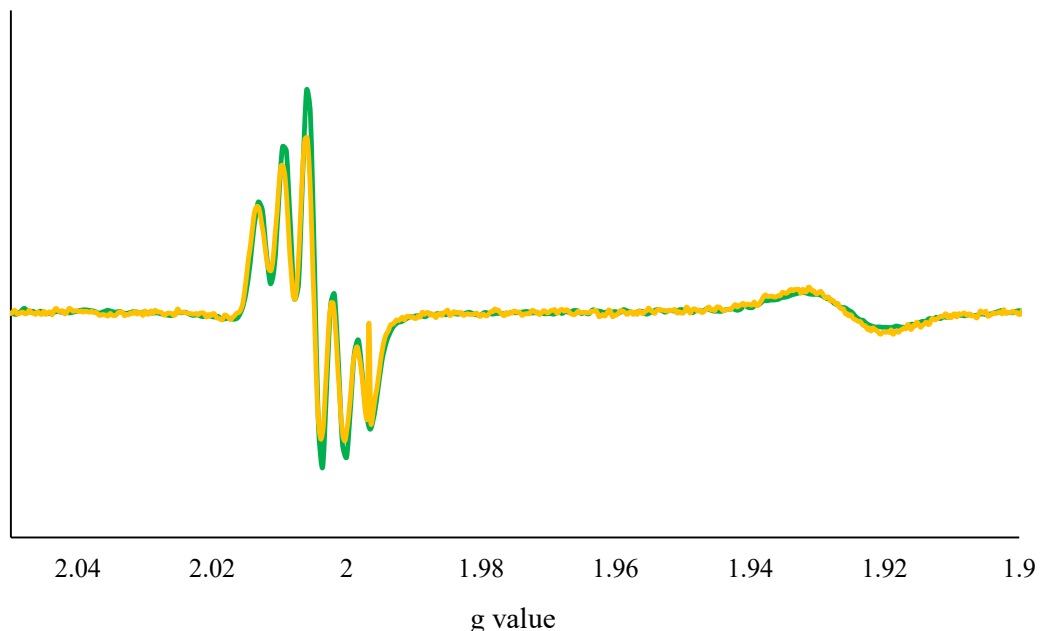
Fig 13. The EPR spectrum for an acetonitrile solution of TiBr$_4$ and triphenylamine (yellow), contrasted with TiBr$_4$ and the benzenediamine standard (green)

*Replication of C-C bond formation with Ti^{IV} and Sn^{IV}*

The unambiguous dominance of the benzenediamine product in Sn^{IV} and Ti^{IV} mediated reactions and its complete absence in the Sb(V) mediated reaction posed two crucial questions:

1. Can tetraphenylbenzidine, the historically more likely product, be made and isolated in its radical state using Ti or Sn?

2. Is this unprecedented C-N bond formation unique to the case of triphenylamine and two specific metals?

To answer the first question, we repeated all our previous experiments with TiCl$_4$ and SnCl$_4$ in dichloromethane. The results are presented below.

The Formation of Lustrous, Crystalline (N,N,N',N'-tetraphenylbenzidine$^+$)(Ti$^{III}_3$Cl$_{10}^-$) from Triphenylamine.

As mentioned earlier, in reactions of SbCl$_5$ conducted in both dichloromethane and toluene, crystals containing N,N,N',N'-tetraphenylbenzidine$^{•+}$ can be reproducibly obtained from both neutral tetraphenylbenzidine and neutral triphenylamine. In a glaring contrast, the reaction of triphenylamine with TiCl$_4$ in dichloromethane led to a complete departure from the toluene and acetonitrile reactions previously discussed, leading to the formation of the shiny reddish-black crystals with a green and bronze sheen to them. The crystals and the structure obtained from them are shown in Figure 14 and involve a tetraphenylbenzidine radical counterbalanced by a Ti$_x$Cl$_y$ anionic polymer whose simplest repeated unit can be formulated as (Ti$^{III}_3$Cl$_{10}$)$^-$. This anion is the only case where a Ti^{III} species can be crystallized alongside the radical product, and is a rare case where both the amine and the metal make an appearance in their oxidized and reduced forms respectively. The anion propagates in one dimension with each Ti^{III} center exhibiting six-coordinate geometry surrounded by chlorides bonded mostly in a bridging fashion, with the exception of one terminal Cl$^-$ ligand on every other Ti^{III} center. Charge balance or mathematical sense cannot be made when the Ti center is treated as having any other charge or mixed valence. Even so, we tried further experiments to confirm the presence of Ti^{III}.
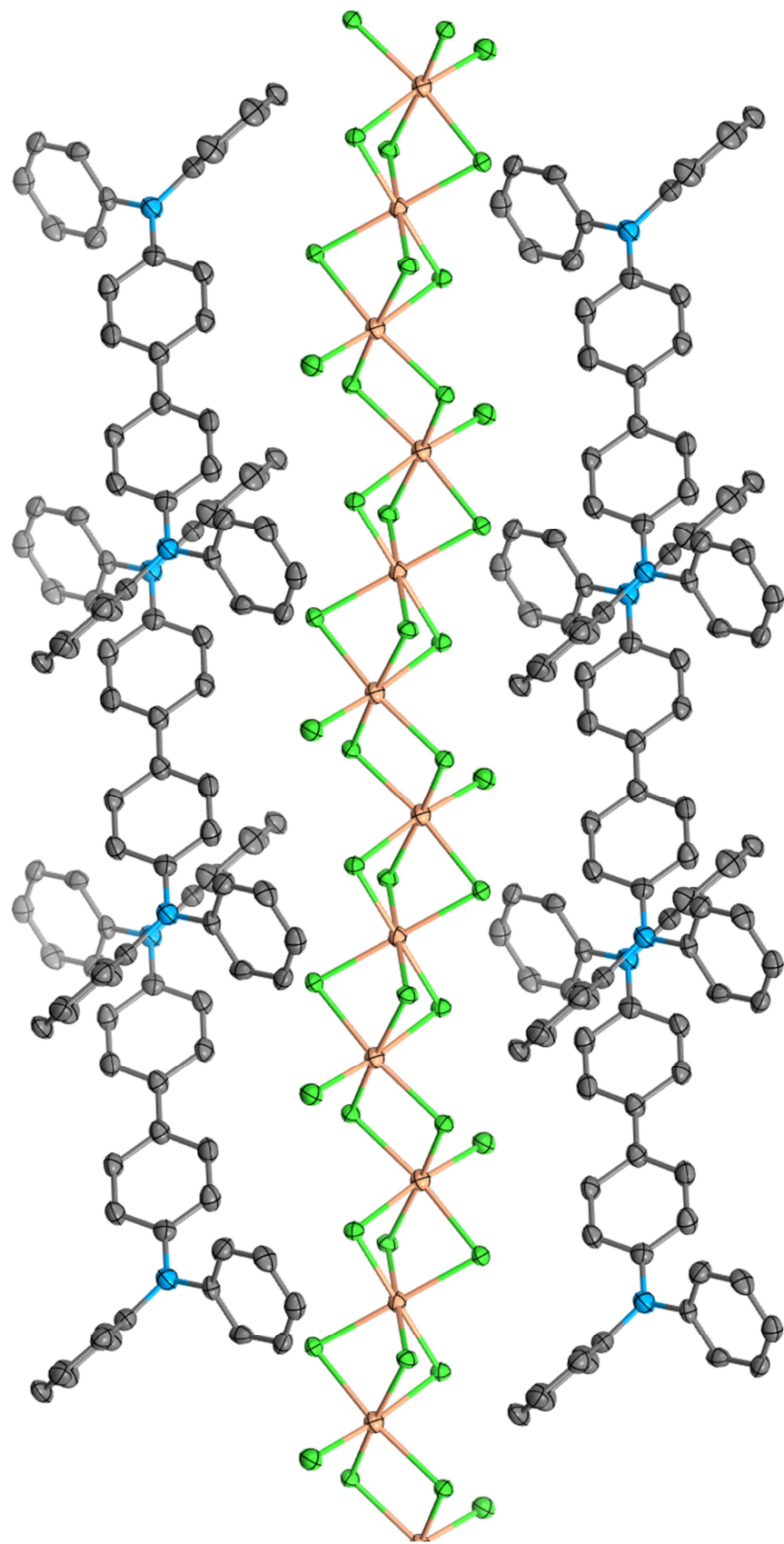
(A)

(B)
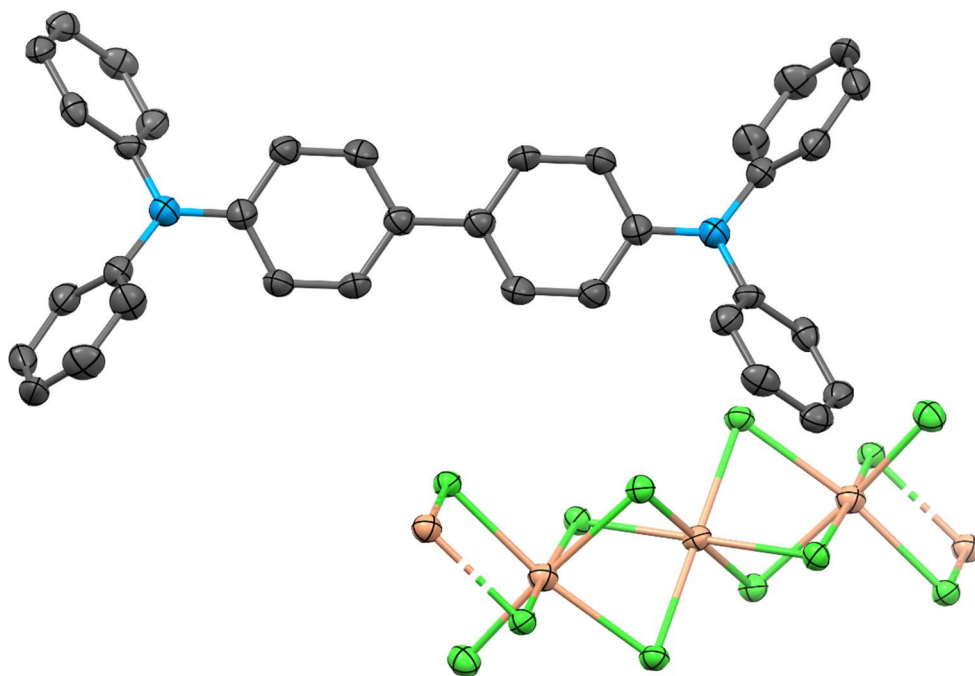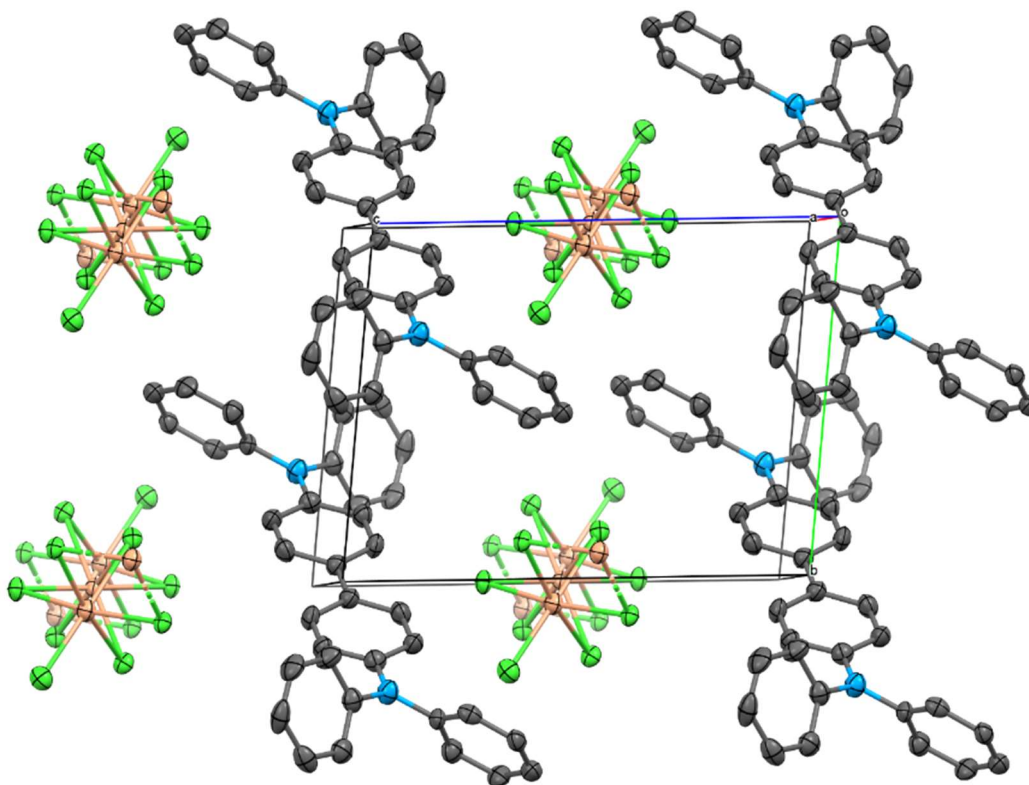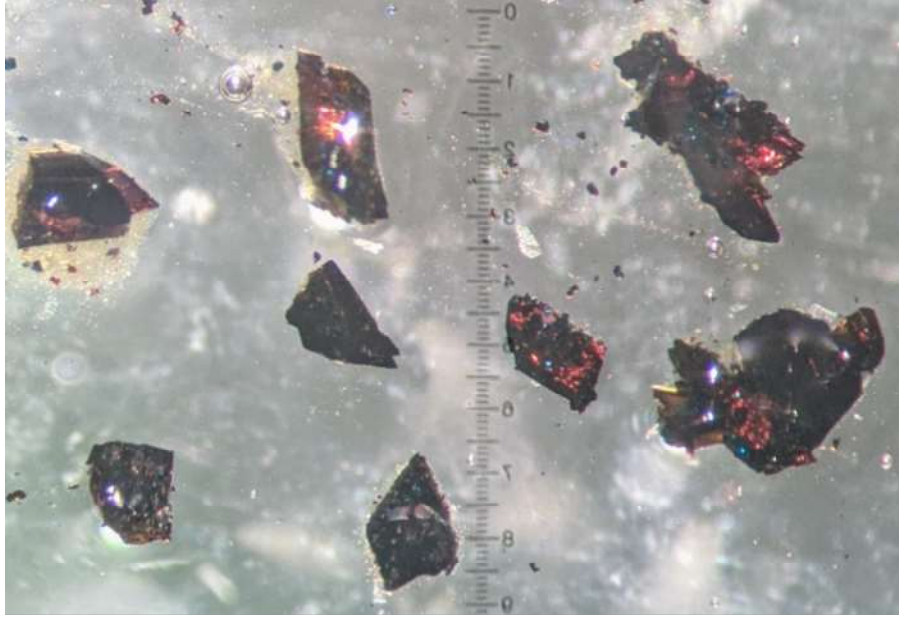
Fig 14. (A) A simplified crystal structure of the benzidine radical with a fraction of the non-coordinating anion; (B) the contents of the unit cell and the crystals themselves under a microscope and (C) an extended view of how the polymeric anion propagates.

A solid state EPR spectrum for these crystals was obtained by crushing them and washing with an antisolvent, and centering the crushed crystals in the cavity. It exhibited a signal at the expected g value of the diamine, although the peaks were not well-resolved in the solid state. A hint of a broad peak around g = 1.9 served as some basis for speculating the charge of each Ti cation in the polymeric counterion; however, in a configuration so closely packed, the Ti^{III} species may not be expected to give clear EPR signals in the solid state. A simple extraction was then performed where the crystals were dissolved in acetonitrile. We had previously found that the extraction of diamine-$Ti_2Cl_9^-$ crystals into acetonitrile causes rapid decolorization and disappearance of the radical species. However, while extraction of the above crystals into acetonitrile also causes some decolorization, the resulting solution is pale blue and can be analyzed by EPR to give a single-line spectrum consistent at g = 1.9545, consistent with our previous observations of Ti^{III}.
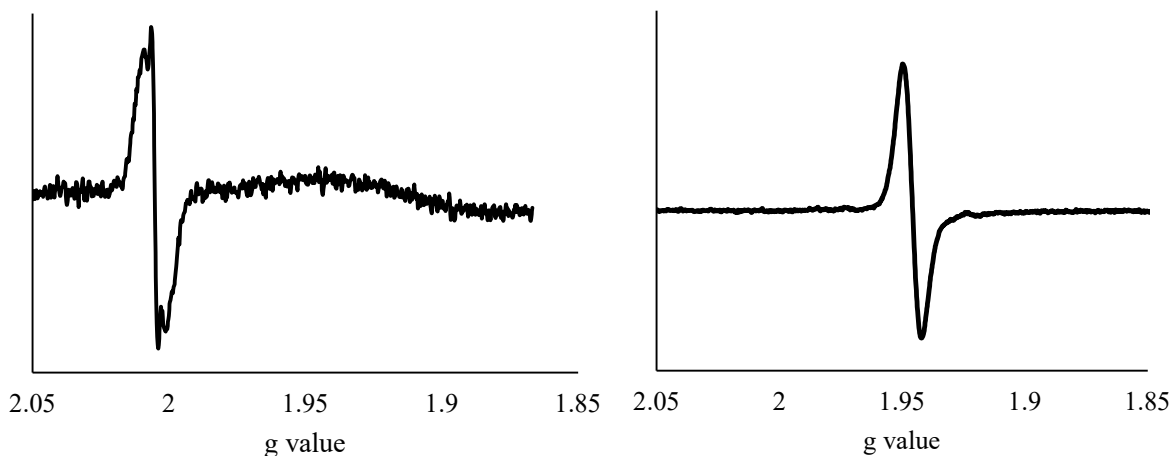
To further investigate the nature of these crystals, they were isolated, washed and then dissolved in a nonpolar solvent to preserve the integrity of the radical product. The resulting solution in toluene gave a UV/Vis/NIR spectrum shown below. The dashed lines represent radical standards (blue: triphenylamine and red: N,N,N',N'-tetraphenylbenzidine) while the solid yellow line represents redissolved crystals. It would appear that extraction into toluene preserves some of the N,N,N',N'-tetraphenylbenzidine$^+$ product but also reverts the compound into triphenylamine radical.
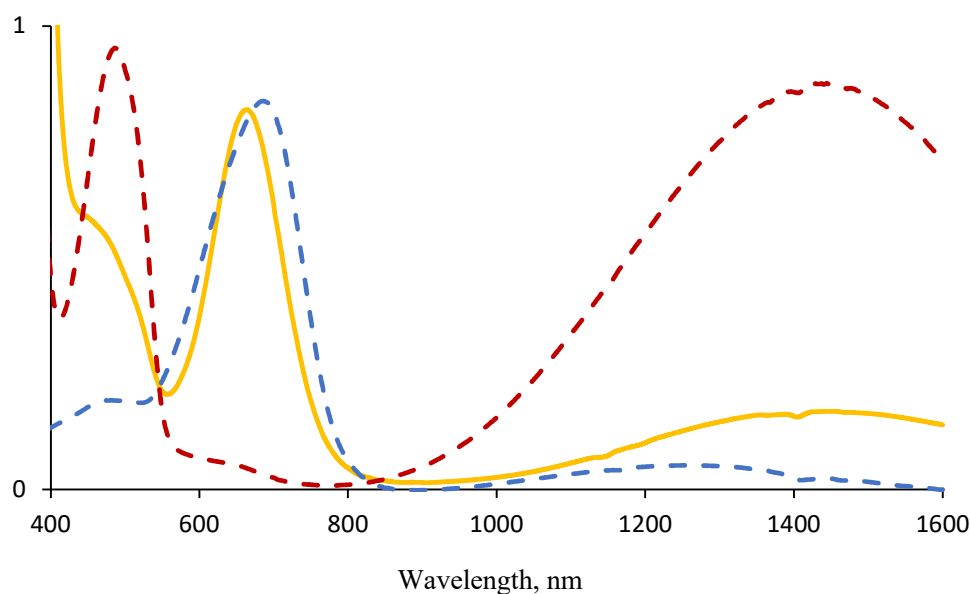

Fig 16. The UV/Vis/NIR spectrum for redissolved crystals of (N,N,N',N'-tetraphenylbenzidine$^+$)(Ti$^{III}_3$Cl$_{10}^-$) in toluene, shown in yellow trace, compared with triphenylamine radical (blue dashed line) and benzidine radical (red dashed line).

Spectroscopic investigations were conducted into the nature of the solution-state reaction between triphenylamine and the metal oxidants in dichloromethane. We have previously discussed

how this does not affect the preferred product in case of SbCl$_5$. In case of TiCl$_4$, optical spectra show the formation of both N,N,N',N'-tetraphenylbenzidine$^+$ and N,N,N',N'-tetraphenyl-1,4-benzenediamine in solution form (in addition to the purely visible peak for triphenylamine$^+$) when a fresh reaction aliquot is studied. However, over time there seems to be a disappearance of the N,N,N',N'-tetraphenyl-1,4-benzenediamine$^+$ species and formation of mostly N,N,N',N'-tetraphenylbenzidine$^+$. An EPR spectrum of the reaction between TiCl$_4$ and triphenylamine in dichloromethane exhibits a$_N$ = 11.7 ± 0.1 MHz, and conforms much more closely to the N,N,N',N'-tetraphenylbenzidine standard than the N,N,N',N'-tetraphenyl-1,4-benzenediamine standard. Both figures are shown below.

NPh$_3$ with TiCl$_4$ in DCM

(A)
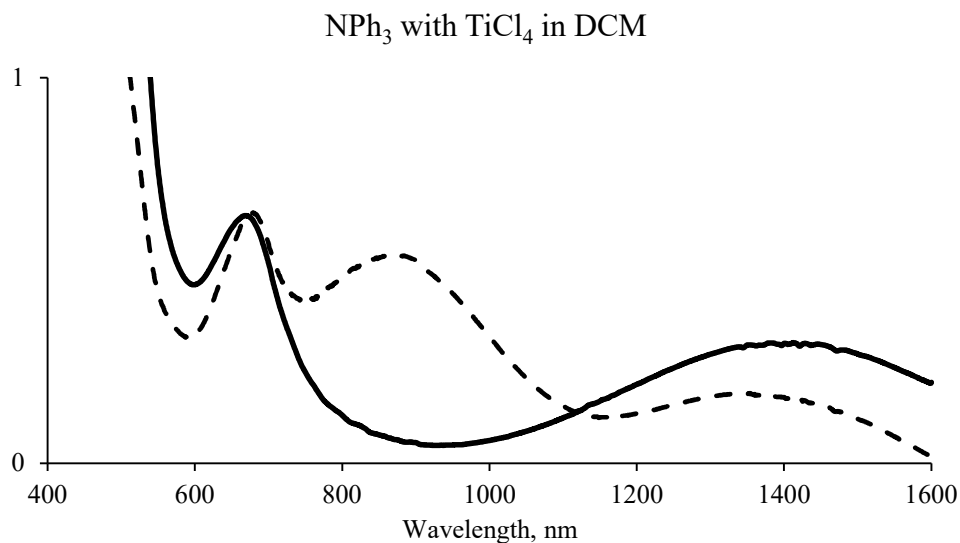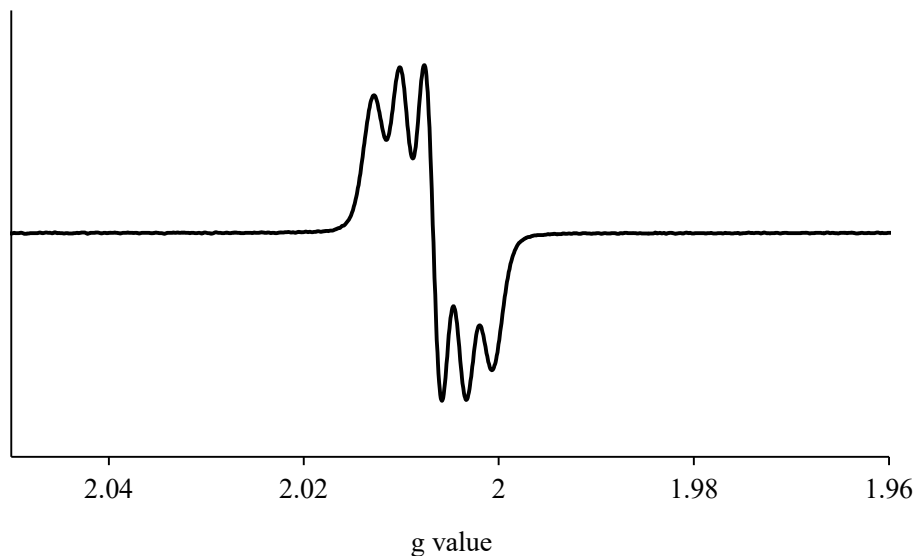
(B)

Fig 17. (A) the UV/Vis/NIR spectrum of a freshly prepared mixture of triphenylamine and TiCl$_4$ in dichloromethane (dashed line) vs a week-old mixture, also in dichloromethane (solid line); (B) an EPR spectrum of this reaction mixture containing a five-line signal about g = 2.0070, a$_N$ = 11.8±0.1 MHz (matching the a$_N$ value from a separate spectrum taken with tetraphenylbenzidine as standard).

In case of SnCl$_4$, it appears that the reaction begins with the formation of mostly the benzenediamine product, while, over time, the benzidine product begins to predominate. The change is rather drastic in comparison with TiCl$_4$, but maintains the same trend and can be seen below in a figure (dashed line – freshly prepared reaction mixture; solid line – one week old sample). No crystals of the benzidine or benzenediamine product was obtained from any dichloromethane reactions involving SnCl$_4$.
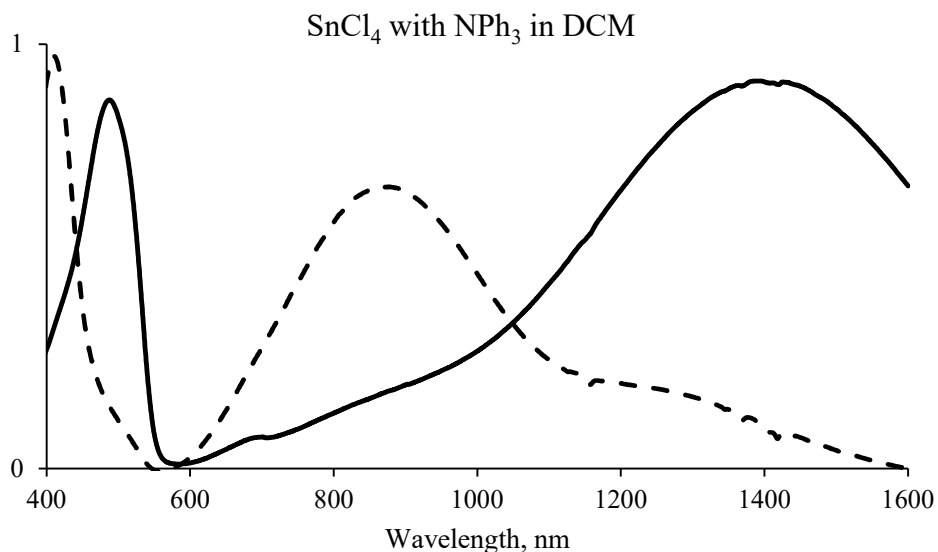
SnCl$_4$ with NPh$_3$ in DCM

Wavelength, nm

Fig 18. The UV/Vis/NIR spectrum of a freshly prepared dichloromethane solution of SnCl$_4$ and triphenylamine (dashed line) contrasted with the same mixture aged by one week (solid black line).

Following the observations made from the series of triphenylamine reactions discussed above, a few key statements were surmised. Firstly, there is tremendous dependence of the preferred diamine product on the metal halide used to perform oxidation. To reiterate, a reproducible formation of the N,N,N',N'-tetraphenyl-1,4-benzenediamine radical cation, an unprecedented oxidative coupling product, may be accomplished using TiCl$_4$, TiBr$_4$ and SnCl$_4$ and is amply evidenced by solution state spectra and analysis of crystalline material. In the Ti^{IV} cases, this reproducibility goes so far as to manifest itself as isostructurality of crystals when obtained from coupling of triphenylamine versus when obtained from simple oxidation of the diamine standard. However, by using SbCl$_5$ as oxidant under several conditions, and by using Ti^{IV} or Sn^{IV} as oxidant exclusively in the cases where the reactions are performed in dichloromethane, we may obtain the N,N,N',N'-tetraphenylbenzidine radical, although not all cases result in the formation of isolable crystals.

136

This leads us to turn our attention to a question posed some time ago in this story: whether this unique C-N bond-forming radical coupling pathway is restricted to triphenylamine, or whether the phenomenon may be extended to its substituted forms. The reactions between some of the metal halides previously studied with triphenylamine, and substituted tris-arylamines will be examined in Chapter VII.

References

(1) Ling, X.; Xiong, Y.; Huang, R.; Zhang, X.; Zhang, S.; Chen, C. Synthesis of Benzidine Derivatives via $FeCl_3 \cdot 6H_2O$-Promoted Oxidative Coupling of Anilines. *Journal of Organic Chemistry* **2013**, *78* (11). https://doi.org/10.1021/jo4002504.

(2) Svejstrup, T. D.; Ruffoni, A.; Juliá, F.; Aubert, V. M.; Leonori, D. Synthesis of Arylamines via Aminium Radicals. *Angewandte Chemie - International Edition* **2017**, *56* (47). https://doi.org/10.1002/anie.201708693.

(3) Shao, X.; Asahi, K.; Yamauchi, T.; Sugimoto, T.; Shiro, M. A New Crystal Phase of *N,N,N′,N′*-Tetraphenyl-1,1′-Biphenyl-4,4′-Diamine. *Acta Crystallographica Section E Structure Reports Online* **2009**, *65* (6). https://doi.org/10.1107/S1600536809016389.

Chapter VII. The reactions of substituted triphenylamine with previously discussed oxidants and the formation of C-C vs C-N radical coupling products

Premise

To study the solution-state chemistry of substituted triphenylamines with each metal halide oxidant, we can first make a few assumptions about the nature of the product, i.e., whether we observe the formation of a C-N bond or a C-C bond can be reasonably inferred from the UV/Vis spectra. The tetrakis *p*-substituted tetraphenylbenzenediamine radical usually exhibits a broad band that begins in the visible, in the region of 600 nm, and ending around 1200 nm. In contrast, tetraphenylbenzidine derivatives tend to exhibit a sharp visible peak and a broad peak further out into the NIR, extending as far out as 2200 nm in some cases. Figure 1A, borrowed from Ref 1[1], displays this phenomenon for tetrakis *p*-bromo substituted tetraphenylbenzidine species, which we may abbreviate henceforth as TAB$^+$ (short for tetra-arylbenzidine to encompass all substituents). Figure 1B shows the UV/Vir/NIR spectrum for a standard solution of (N,N,N',N'-tetraphenyl-1,4-benzenediamine$^+$) where the broad band stretches from 600 to 1200 nm, while Figure 1C, adapted from Ref 2, displays the spectra for various substituted *p*-phenylenediamine species, which we may abbreviate as TAPD$^+$ (short for tetra-aryl *p*-phenylene diamine).[2] It may be noted that the range of the broad band, when converted from wavenenumbers (cm-^{1}) to wavelength (nm), represents a similar range.
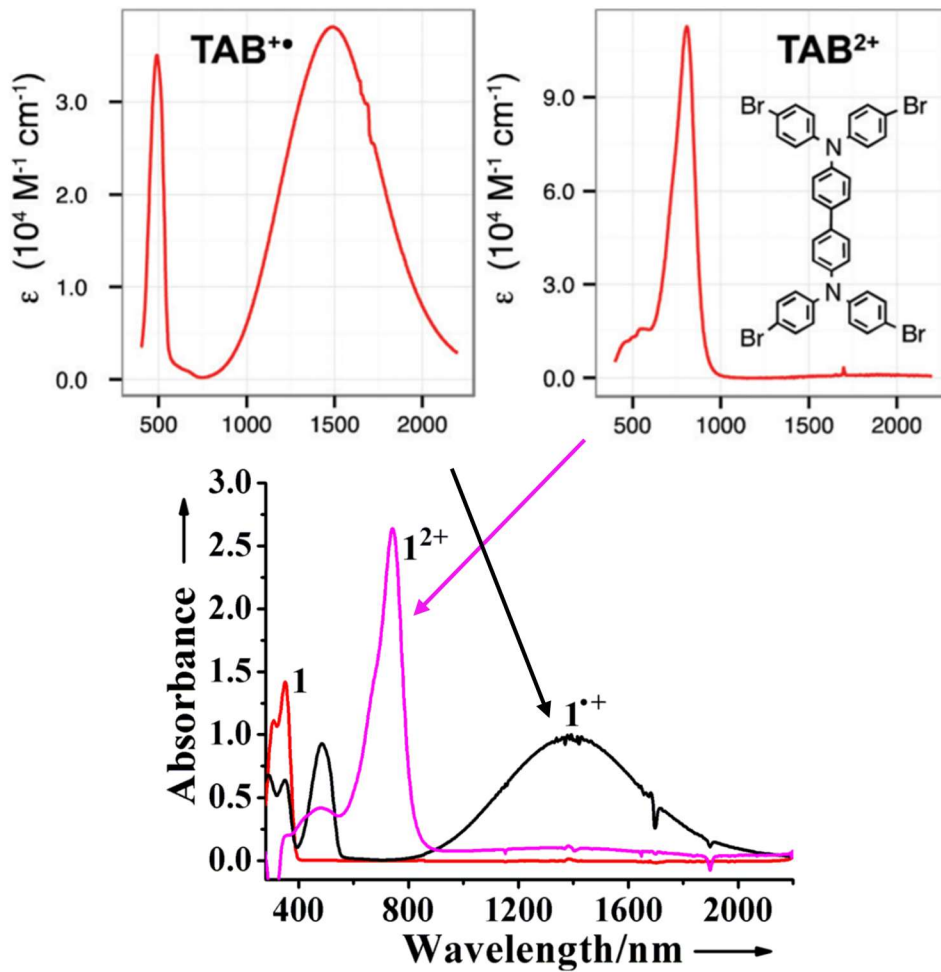
(A)
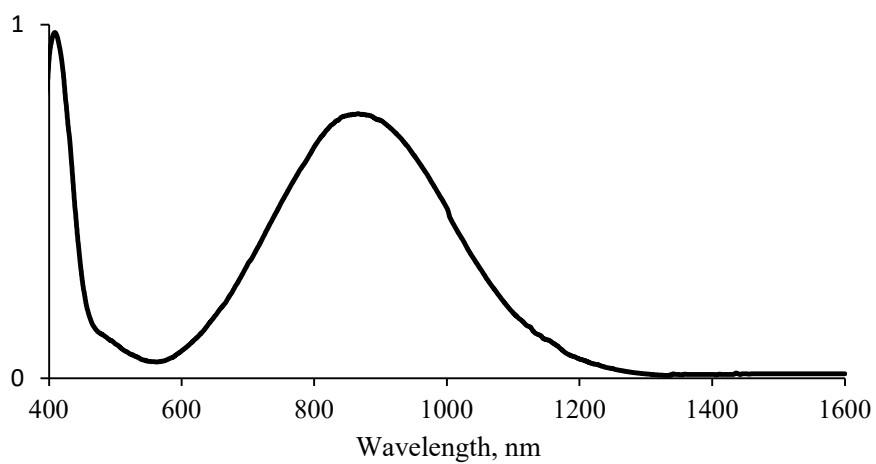
(B)

©
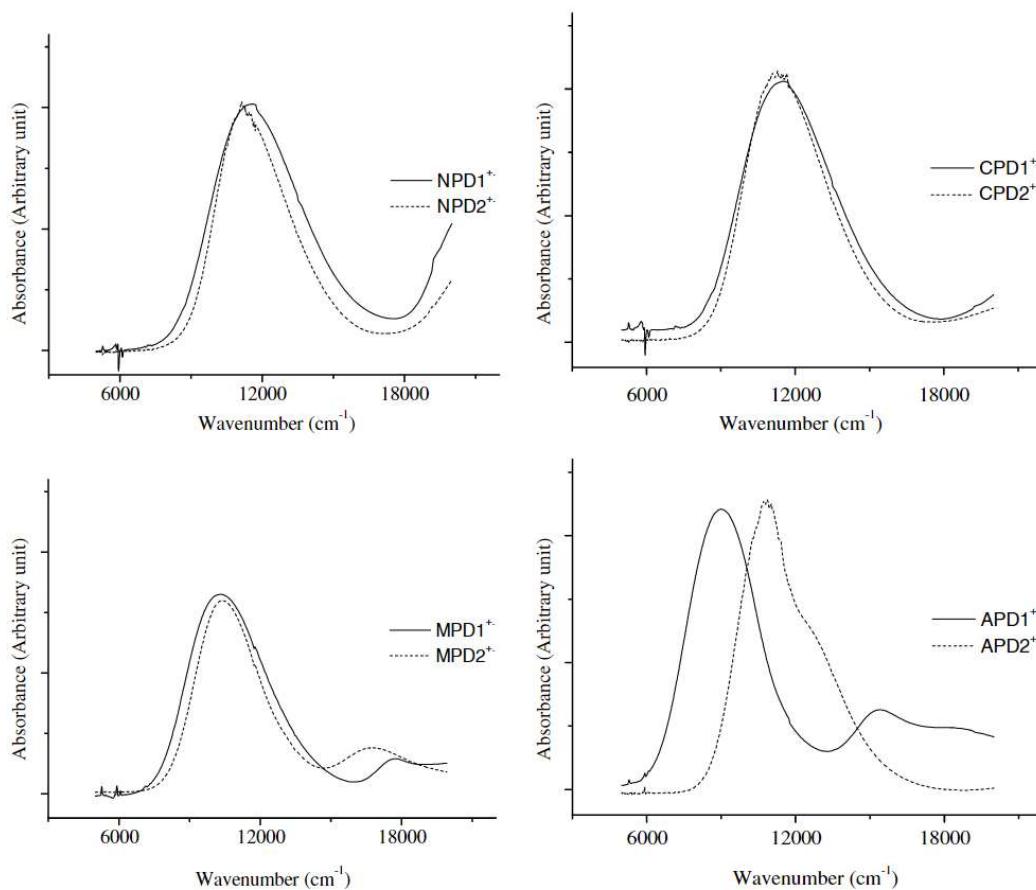
Fig 1. (A) The UV/Vis/NIR spectra of tetrakis(*p*-bromophenyl) benzidine in its cation and dication state, adapted from Ref 1. This figure serves as a "standard" for detecting the TAB$^+$ and TAB^{2+} species in the following discussion. The symbols 1$^+$ and 1^{2+} refer to this same diamine in its two cationic states **(B)** A spectrum for a standard solution of N,N,N',N'-tetraphenyl-1,4-benzenediamine$^+$ obtained using our method of oxidation by Ti^{IV}. **(C)** Various TAPD$^+$ species from Ref 2 (the start and end of the broad band are around 6000-8000 cm^{-1} and 12000-16000 cm^{-1}, which correspond to 1666.67 -1250 nm and 833 -625 nm respectively and are consistent with our methods).

Results and Discussion

Reactions of tris(p-bromophenyl)amine

Tris(*p*-bromophenyl)amine has all three of its *p*-positions substituted. Nevertheless, the radical cation of this amine has been shown to undergo slow dimerization accompanied by loss of one mole of Br_2 to form the diamine radical shown below.
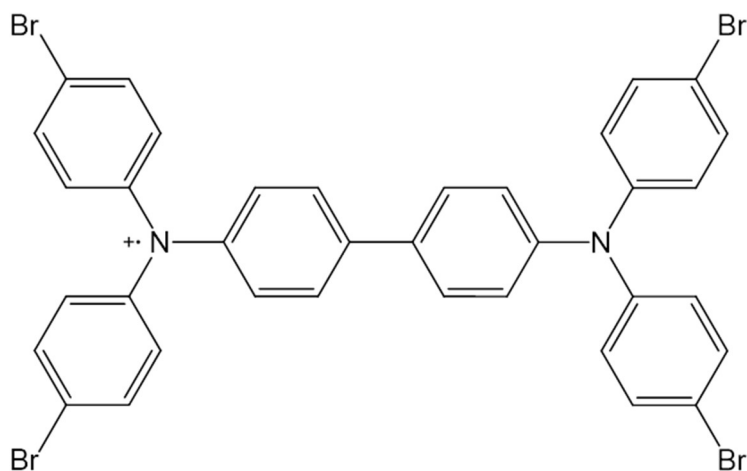

Fig 2. The product representing the major component of aged magic blue, responsible for the broad diamine signal in its optical spectra.

The process occurs automatically through aging of the commercial reagent "Magic Blue" and has been established using mass spectrometry studies and optical spectroscopy of aged samples of magic blue. However, the conversion of neutral tris(*p*-bromophenyl)amine to the above diamine has, to date, not been performed directly unlike unsubstituted tetraphenylbenzidine, nor been captured in its cationic form. The spectroscopic results of reactions between tris(*p*-bromophenyl)amine and metal halides is discussed below.

When $TiCl_4$ is allowed to oxidize tris(*p*-bromophenyl)amine or $(BrPh)_3N$, the reaction mixture exhibits the following spectra (where black lines denote the $TiCl_4$ reactions). The dashed blue line represents true "Magic Blue" as a standard, i.e., $(BrPh)_3N^{\bullet+}$ (freshly prepared from the

neutral amine using SbCl$_5$). The dashed black line shows the signal for an aliquot of the TiCl$_4$-(BrPh)$_3$N reaction mixture promptly after combination.
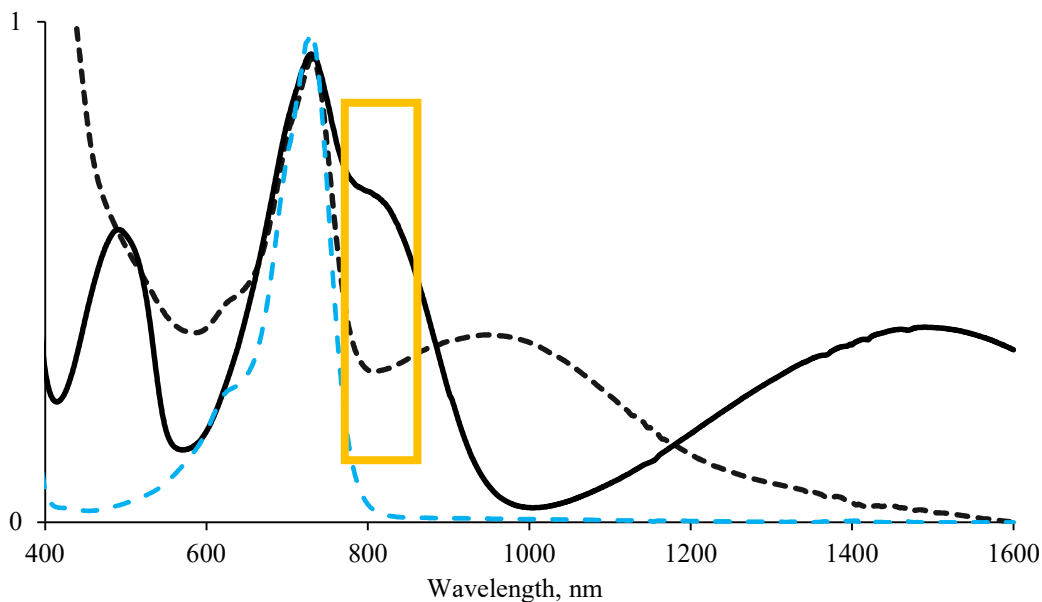

Fig 3. Optical spectra for magic blue (dashed, blue), contrasted with a fresh aliquot from the reaction between TiCl$_4$ and (BrPh)$_3$N (dashed black) and a week-old aliquot of the same (solid black). Yellow box: denotes

In addition to the ~ 660 nm signal for (BrPh)$_3$N$^{\bullet+}$, the broad visible-NIR band is strongly suggestive of the formation of a C-N bonded radical coupling product or a TAPD$^+$ species. One can reasonably hypothesize that the TAPD$^+$ species that could be formed from C-N bond formation in this case would be:
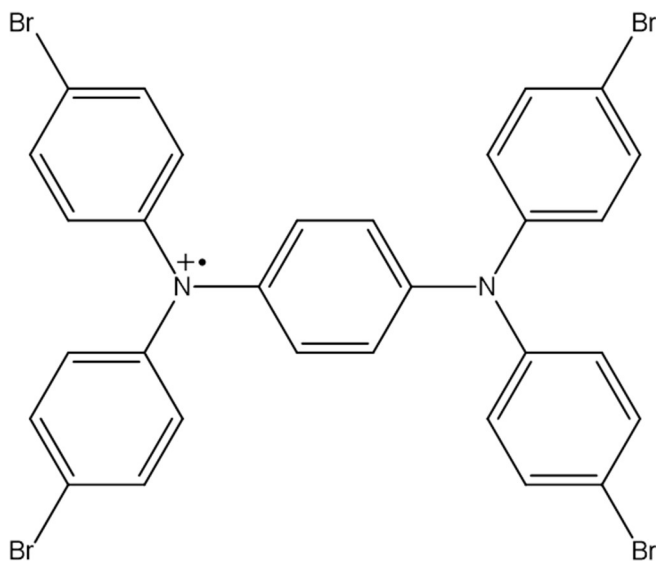
Fig 4. Speculated temporary product in the reaction between TiCl₄ and (BrPh)₃N

The solid black line represents the same reaction mixture after being allowed to rest for one week. All traces of the broad ~1000 nm band appear to have disappeared and the spectrum now shows the tell-tale signs for the formation of N,N,N',N'-tetrakis(*p*-bromophenyl)benzidine or a TAB⁺ species. In addition, a new signal around 800 nm appears in the aged spectrum.

Our excitement at this result was short-lived as we were unable to obtain any X-Ray quality crystals of TAB⁺ or TAPD⁺ species from the reaction between TiCl₄ and (BrPh)₃N. However, beautifully lustrous, layered crystals of TAB²⁺ (Fiure 5D) were obtained from these reactions, as shown below. The asymmetric unit consists of one-half of the N,N,N',N'-tetrakis(*p*-bromophenyl)benzidine species and one full Ti₂Cl₉⁻ anion (Figure 5B), which ratio can be better visualized when examining contents of each unit cell in the packing diagram (Figure 5C). This TAB²⁺ species could be seen in Figure 4 as an ~800 nm shoulder on the (BrPh)₃N•⁺ radical (refer to Figure 1 for another instance of this spectrum). It is interesting to note that this species, as opposed to TAB⁺, is preferentially crystallized from toluene (and reproducibly so).
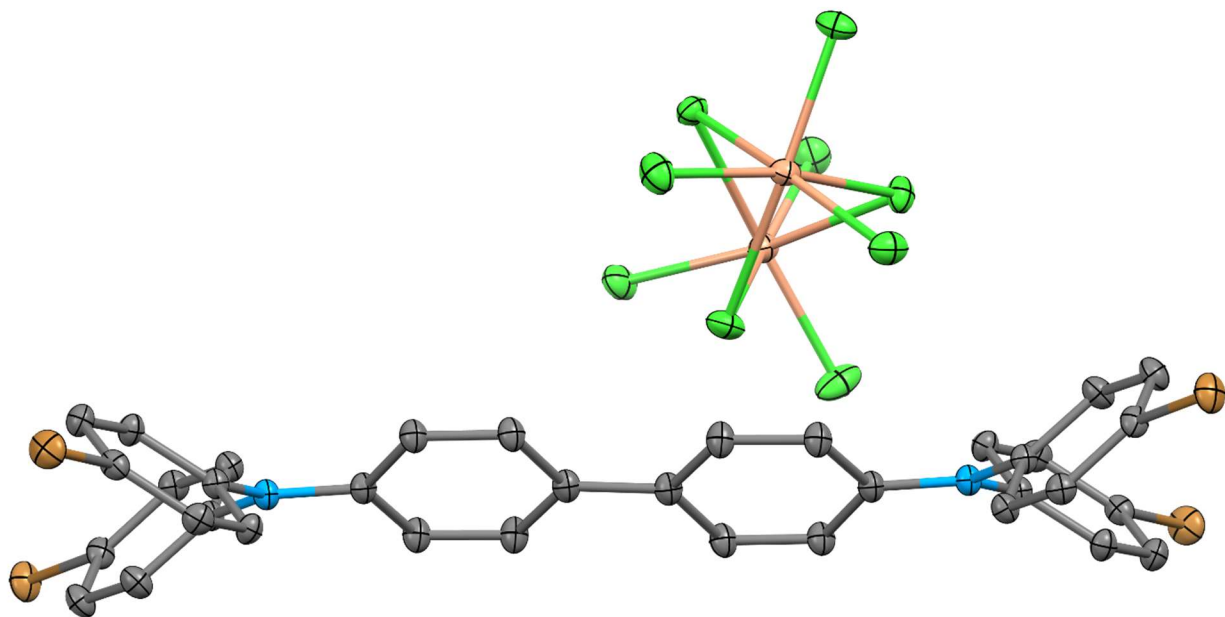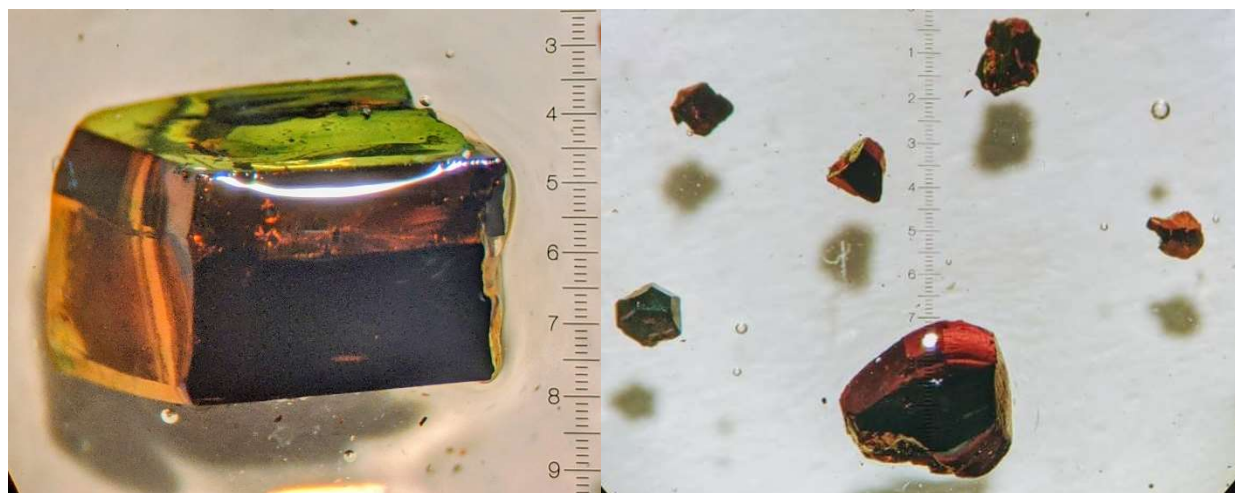
(A)
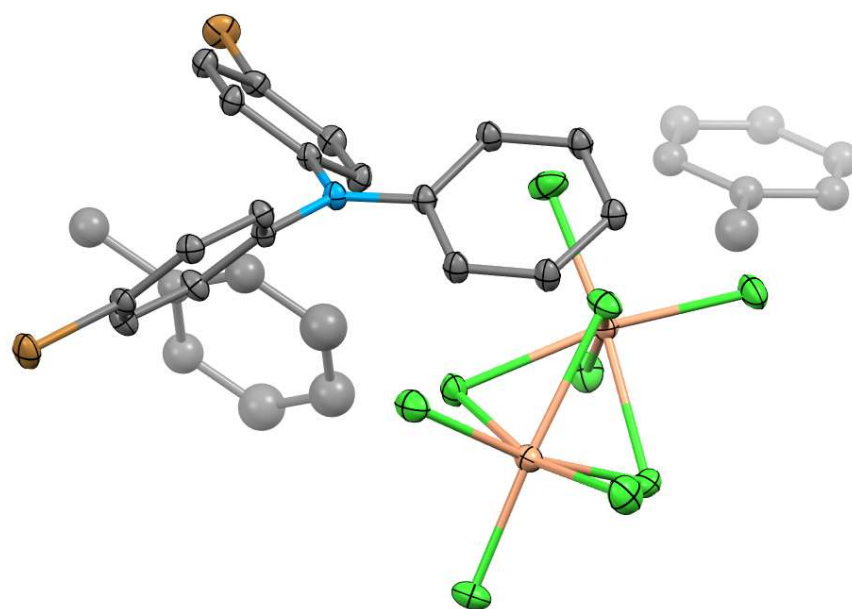
(B)
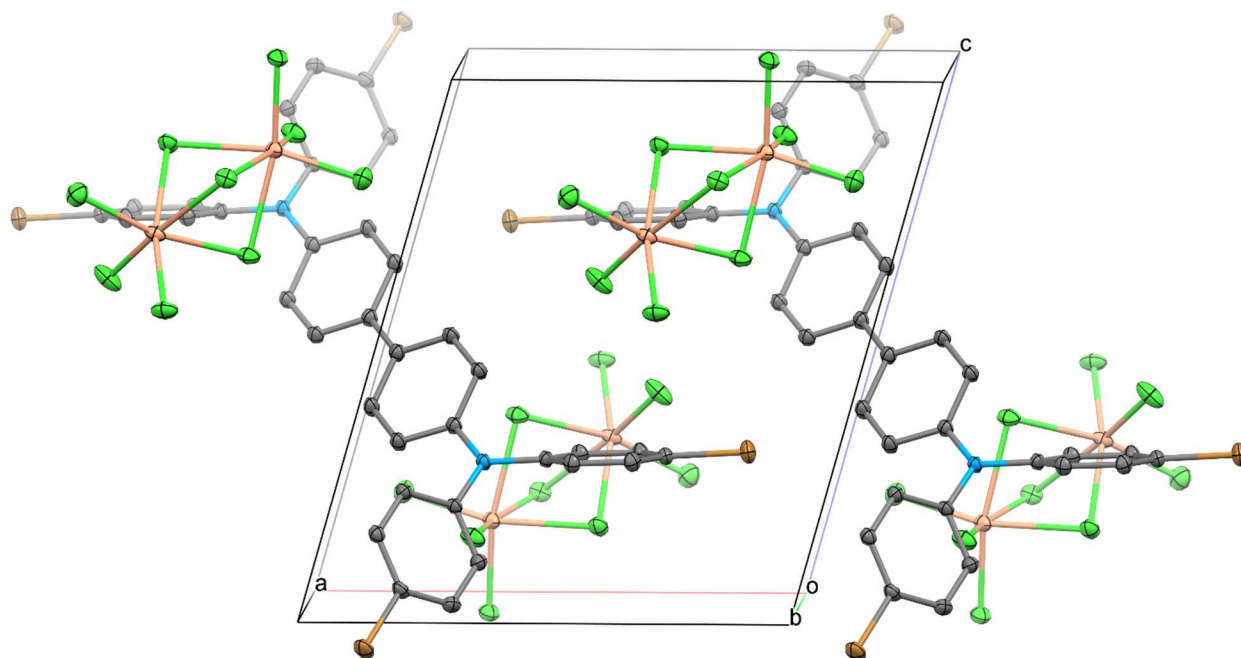
(C)

(D)

Fig 5. (A) The structure of the full dication of tetrakis(*p*-bromophenyl) benzidine, or TAB^{2+},

accompanied by the anion. (B) The asymmetric unit denoting the true cation-anion stoichiometry.

(C) Contents of one unit cell of this crystal structure. (D) the lustrous, metallic-looking crystals

obtained

This Ti^{IV}-mediated reaction is remarkable because both diamine products have their own pedagogical and methodological significance. While decomposition of magic blue has been extensively studied, the direct conversion of $(BrPh)_3N^{\bullet+}$ to its dimer has not been performed before, nor has neutral $(BrPh)_3N$ been dimerized into a new C-C bonded product the same way as its unsubstituted benzidine analogue. In the reactions performed with Ti^{IV} and Sn^{IV}, the direct conversion of *neutral* $(BrPh)_3N$ to charged TAB^+ and TAB^{2+} can be demonstrated (and, in the case of TAB^{2+}, isolated as crystalline solid). However, perhaps even more remarkable is the formation, however fleeting, of the C-N bonded product in case of this tri-substituted triphenylamine.

The same time-dependent product selection effect (seen in case of Ti^{IV}) can be observed, to an even more dramatic degree, when combining neutral $(BrPh)_3N$ with $SnCl_4$. In Figure 6A, a dashed black line, representing a reaction aliquot instantly after combination, shows *mostly* the $TAPD^+$ product along with some $(BrPh)_3N^+$. An aged reaction mixture (solid black line) shows complete disappearance of the $TAPD^+$ product, and what appears to be an equilibrium between $(BrPh)_3N^{\bullet+}$ and its C-C bonded dimer cation. It is interesting to note that the dimerization process is considerably slower in case of Sn^{IV} than Ti^{IV}. Figure 6B shows an EPR spectrum of a week-old reaction mixture of $SnCl_4$ and $(BrPh)_3N$ in toluene (solid black line) compared with freshly prepared reaction aliquots from $SnCl_4$ and $(BrPh)_3N$ in toluene (dotted black line) and $TiCl_4$ and $(BrPh)_3N$ in toluene (dashed green line). The large singlet signal represented by the dotted black line represents uncoupled $(BrPh)_3N^{\bullet+}$ while we see the beginnings of a five-line signal. In comparison, the one-week signal for the same reaction shows a more robust quintuplet, which, in case of the Ti^{IV} reaction, can be seen immediately upon combination.
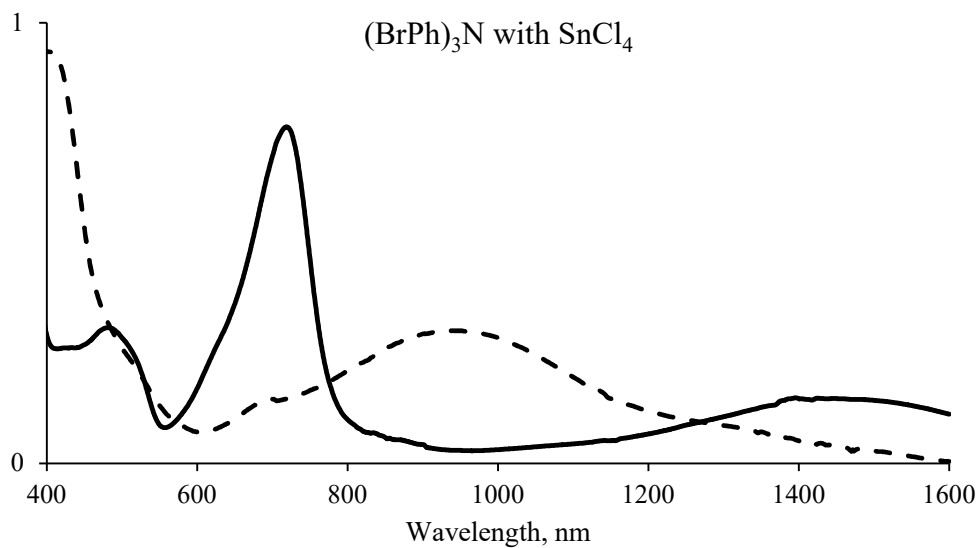
(A)
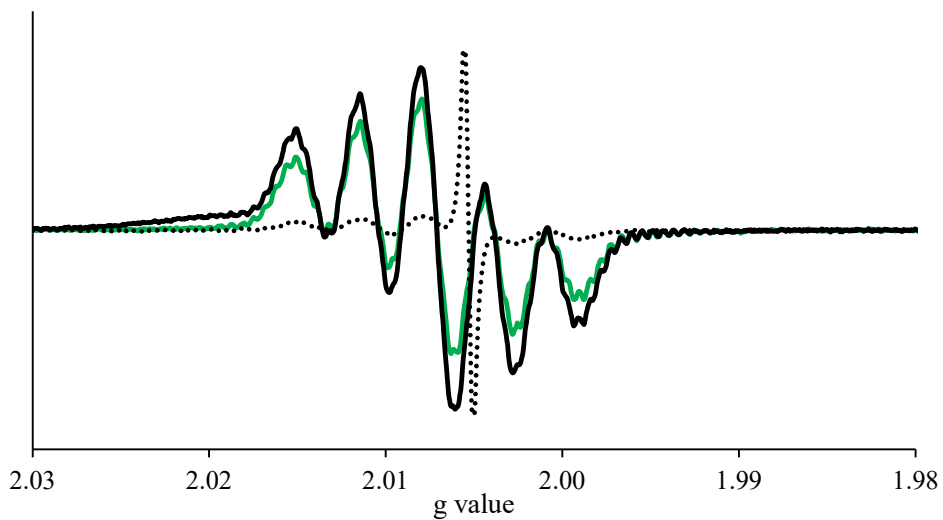
(B)

Fig 6. (A) The UV/Vis/NIR spectra of a freshly prepared mixture of SnCl₄ and (BrPh)₃N (dashed black line) and the same mixture aged about one week (solid black line). (B) The EPR spectrum comparing mixtures of SnCl₄ and (BrPh)₃N in toluene, freshly made (dotted black line) and one week old (solid black line), in addition to TiCl₄ and (BrPh)₃N also in toluene, freshly made (solid green line).

In keeping with the Sb^V mediated coupling of unsubstituted triphenylamine, the reaction of (BrPh)$_3$N with SbCl$_5$ results in no formation of the TAPD$^+$ product! A fresh reaction aliquot, to no one's great surprise, shows simply the "magic blue" signal while with aging one sees the TAB$^+$ product begin to appear (Figure 7). No crystals containing TAB$^+$ could be isolated from reactions mediated by Sb^V as the overwhelmingly crystalline magic blue species selectively precipitates out in the time it takes for conversion to the TAB$^+$ product.
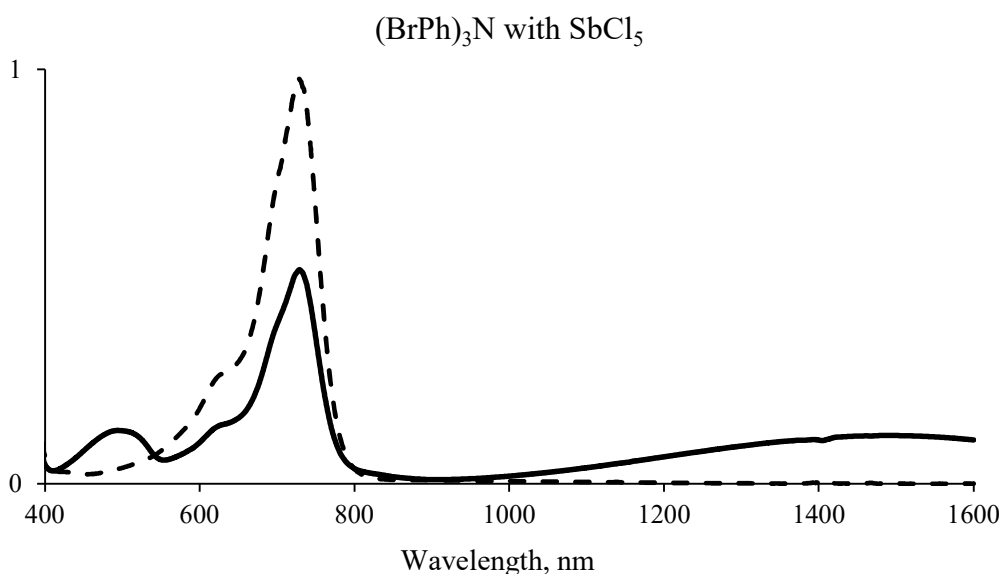

(BrPh)$_3$N with SbCl$_5$

Wavelength, nm

Fig 7. The UV/Vis/NIR spectra of a freshly prepared mixture of SbCl$_5$ and (BrPh)$_3$N (dashed black line) and the same mixture aged about one week (solid black line)

Sb^V and the use of a different starting material

Although never synthesized from magic blue itself, the TAB$^+$ species formed above has been previosuly crystallized in accompaniment with SbCl$_6^-$ by simple oxidation of the TAB, i.e., by taking tetrakis(*p*-bromophenyl) benzidine and performing one-electron oxidation using SbCl$_5$. The structure of a DCM-solvate of this compound is shown below:
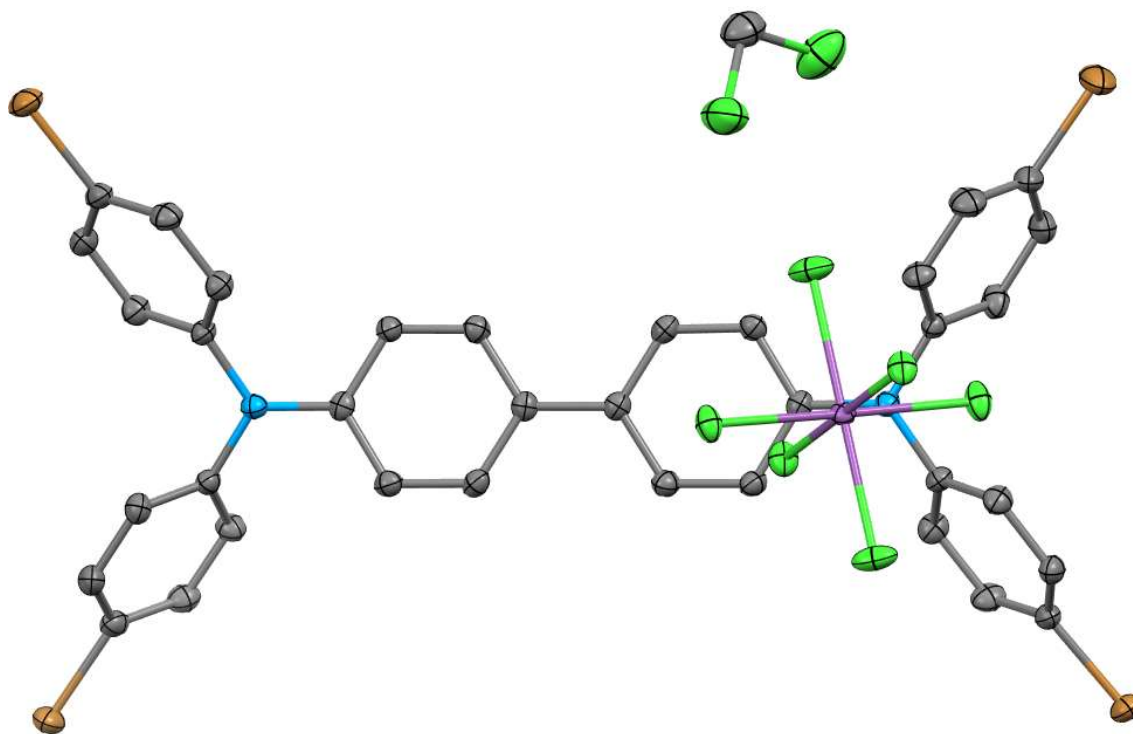
148

Fig 8. The crystal structure of the radical cation of tetrakis(*p*-bromophenyl) benzidine counterbalanced by hexachloroantimonate (coordinates imported from Ref 1).

However, we *can* readily crystallize the tetrakis(p-bromophenyl) benzidine radical with the help of SbCl₅ – using a different, partly substituted arylamine shown below in Scheme 1. Using 4,4'-dibromotriphenylamine and SbCl₅ as oxidant, shiny brown crystals of the same substance as in Figure 8 can be obtained overnight. The crystals have a blue sheen to them that disappears when crushed and appears to be unrelated to the true color of the compound.
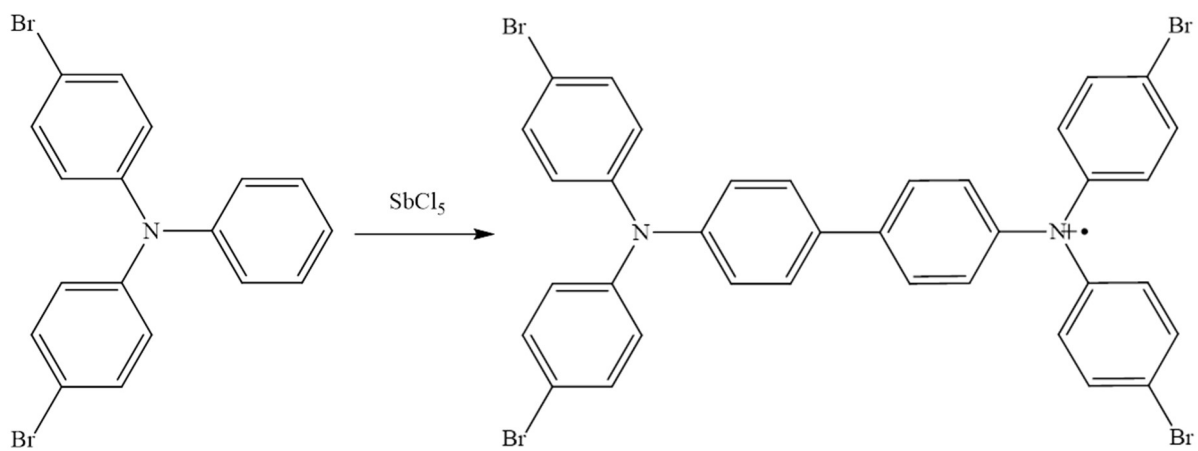
Scheme 1. Coupling reaction for 4,4'-dibromotriphenylamine

(A)

150
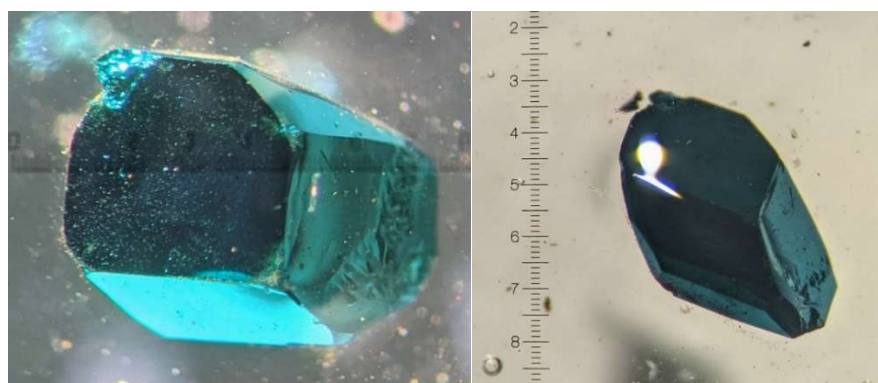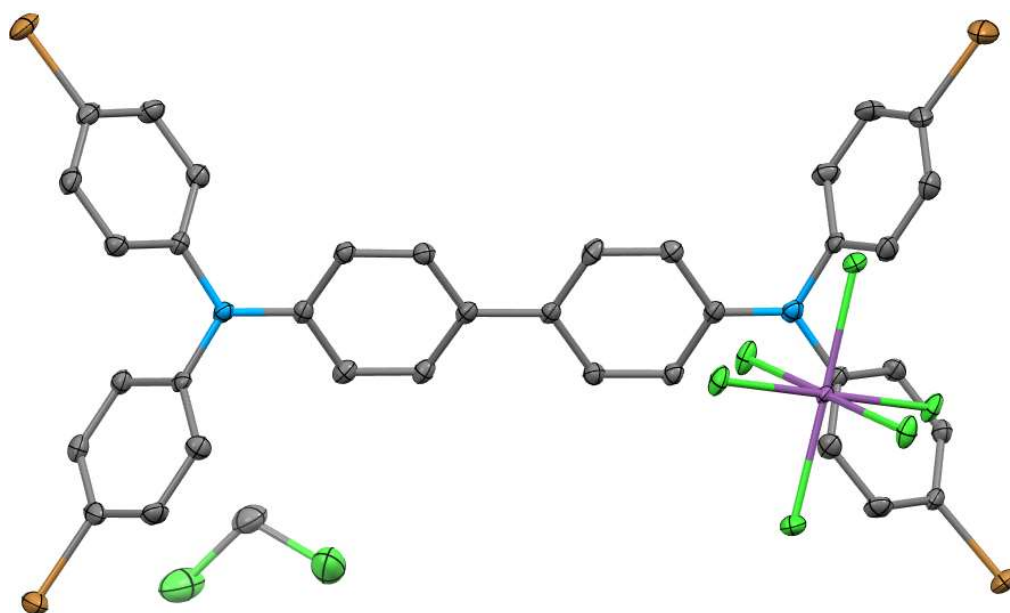
(B)

Fig 9. (A) Crystals of (tetrakis(p-bromophenyl)benzidine⁺)SnCl₆⁻ (B) A structure of (tetrakis(p-bromophenyl)benzidine⁺)SnCl₆⁻

Crystal sample	(tetrakis(p-bromophenyl)benzidine$^+$) SbCl₆ •CH₂Cl₂ (from CSD code LACRUF, Ref 1)	(tetrakis(p-bromophenyl)benzidine$^+$) SbCl₆ •CH₂Cl₂ from 4,4'-dibromo triphenylamine
a (Å)	15.37545(18)	15.3444(6)
b (Å)	14.15367(14)	14.1590(5
c (Å)	19.4760(2)	19.4757(7)
α	90°	90°
β	91.4952(10) °	91.542(2)°
γ	90°	90°
Volume (Å³)	4236.91	4229.78
Space Group	$P2_1/n$	$P2_1/n$

Table 1. Comparing the structures of (tetrakis(p-bromophenyl)benzidine⁺) obtained from two different amines

The optical spectrum of the reaction between 4,4'-dibromotriphenylamine and SbCl₅ in dichloromethane is shown below in Figure 10, in a solid black line. The dashed green line shows the reaction between tris(p-bromophenyl)amine and SbCl₅ in dichloromethane. The uncoupled triarylamine signal for both amines (BrPh)₃N$^{•+}$ and (BrPh)₂PhN$^{•+}$ appear around 660 nm. The features of TAB$^{•+}$ are present in both spectra. In addition, the dibromotriphenylamine reaction shows a familiar 800nm peak we have seen before in the Ti^{IV} mediated dimerization – the TAB^{2+} peak, indicated with a yellow box around it. The identical nature of coupling and dimerization in case of the two amines, (BrPh)₃N and (BrPh)₂PhN, helps shed light on the mechanistic possibilities

151

for reactions such as these. We might speculate that the loss of bromine and activation of the *p*-position precedes any association chemistry.
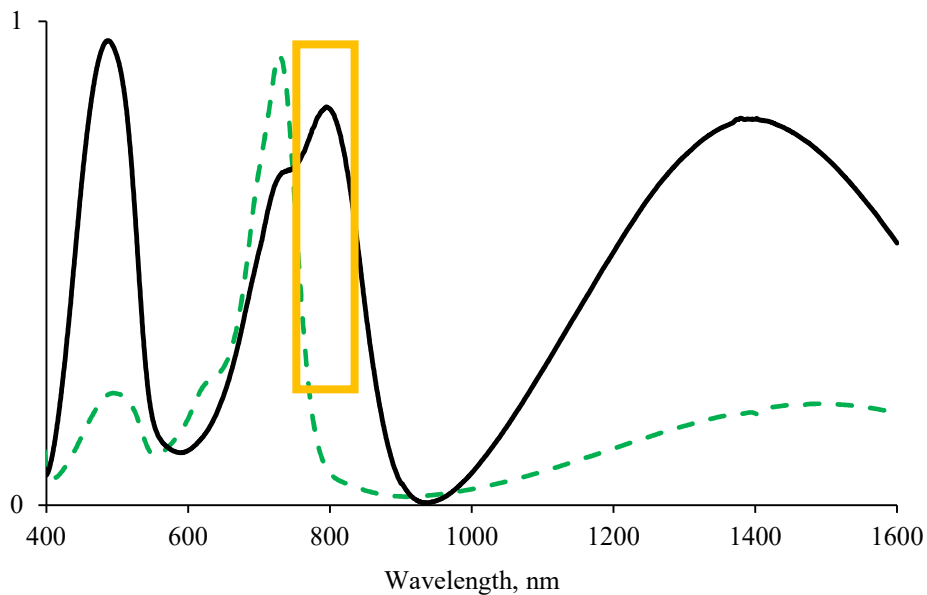

Fig 10. Spectra for the Sb^V mediated reactions of (BrPh)$_3$N (dashed green line) and (BrPh)$_2$PhN (solid black line), with the yellow rectangle highlighting TAB^{2+} band.

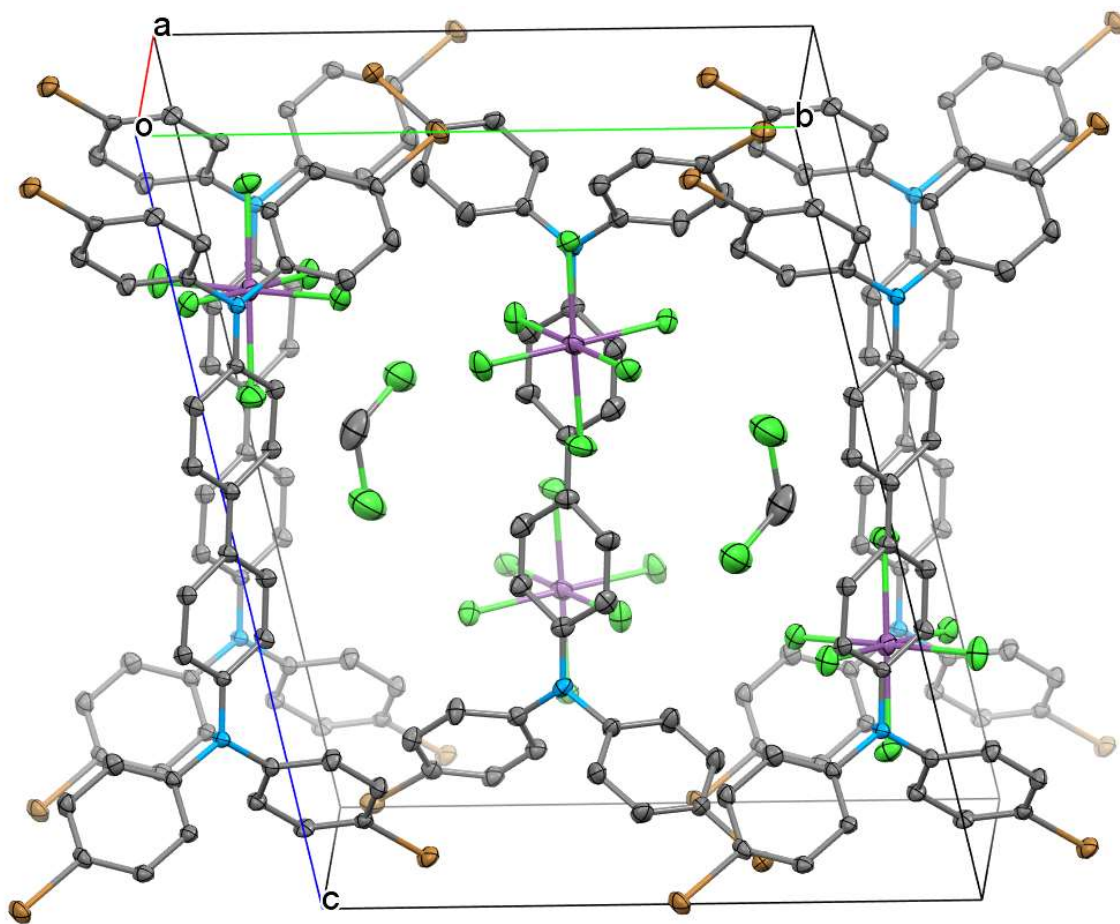Using a prolonged reaction at 5x dilution and a slower crystallization technique, this TAB^{2+} species can be isolated in crystalline form. The crystal structure of (tetrakis(*p*-bromophenyl) benzidine^{2+})(SbCl$_6^-$)•CH$_2$Cl$_2$ is shown below in Figure 11. Examining the asymmetric unit (11B) and the contents of a unit cell (11C) assures us of the cation-anion stoichiometry.
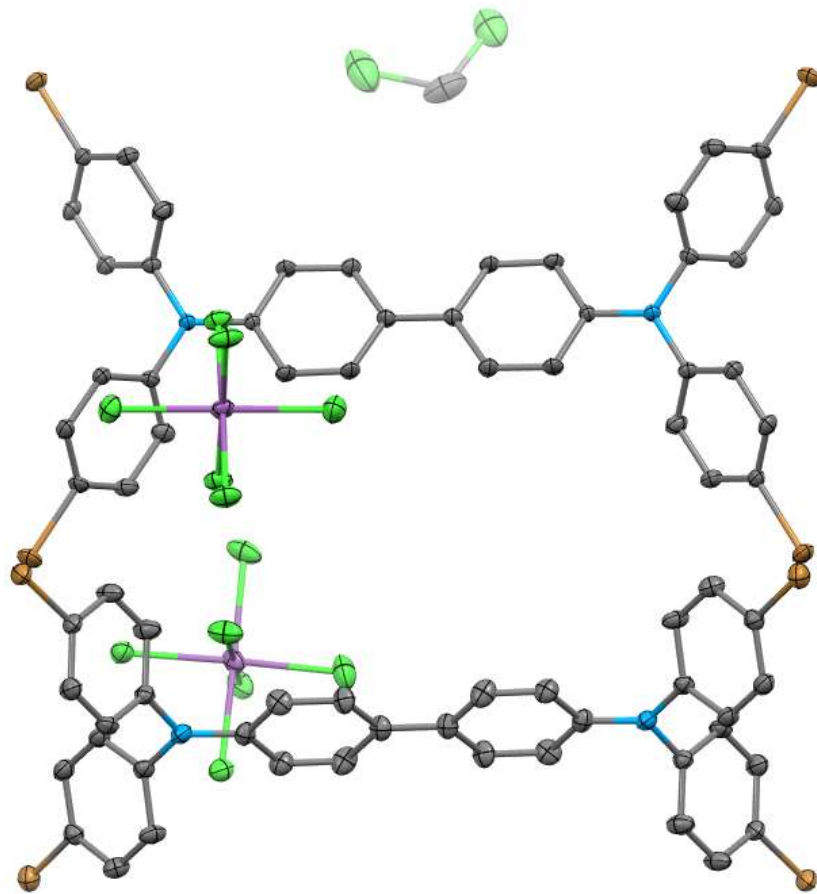
(A)
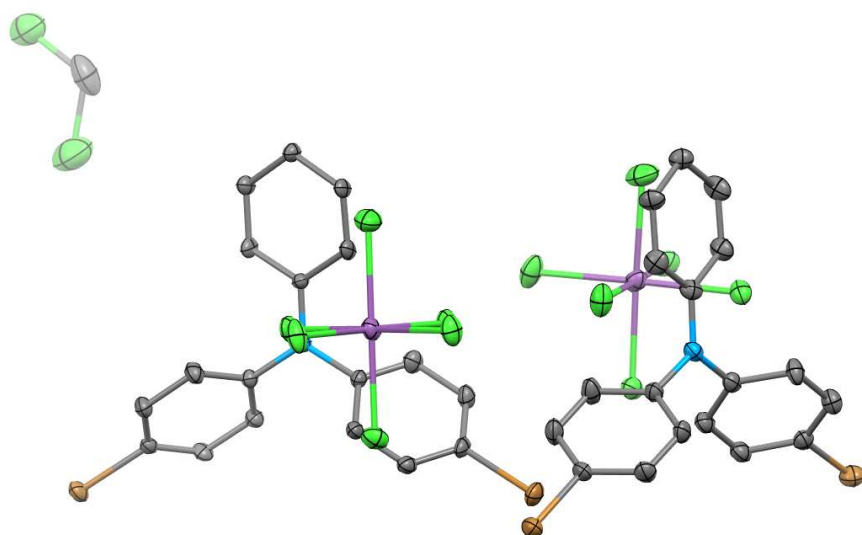
(B)

(C)

Fig 11. (A) The crystal structure of (tetrakis(*p*-bromophenyl) benzidine^{2+})(SbCl$_6^-$)•CH$_2$Cl$_2$ exhibiting two full cations and two anions, instead of accurate stoichiometry. (B) the asymmetric unit of this structure, this time representing correct anion-cation stoichiometry and (C) the contents of a single unit cell of this compound.

Ti^{IV} and Sn^{IV} reactions of 4,4'-dibromotriphenylamine

The Ti^{IV} or Sn^{IV} mediated reactions of 4,4'-dibromotriphenylamine are of little interest to us as no isolable material was obtained in crystalline form. However, a cursory glance at the UV/Vis/NIR spectrum of an aliquot from a freshly combined mixture of TiCl$_4$ and 4,4'-dibromotriphenylamine (black solid line in Figure 12A below) reveals some key features. Fig 12A

154

also shows a fresh reaction mixture containing $(BrPh)_3N$ and $TiCl_4$ which we have previously examined, and as highlighted in the green box, both spectra contain the 800-1200 nm broad peak representative of $TAPD^+$ species. In addition, we have the usual ~660 nm uncoupled triarylamine peak, and what appears to be the 800 nm shoulder attributed to the TAB^{2+} product. Figure 12B shows a bewildering EPR spectrum for the same reaction aliquot (solid black line). While it has the loose features of a five-line signal corresponding to a delocalized diamine, what is more distinctive is its similarity to the signal obtained from a mixture of unsubstituted triphenylamine and $TiCl_4$ in dichloromethane (dashed green line) – a mixture, we may recall, resulted in the simultaneous formation of TAB^+ and $TAPD^+$ species.
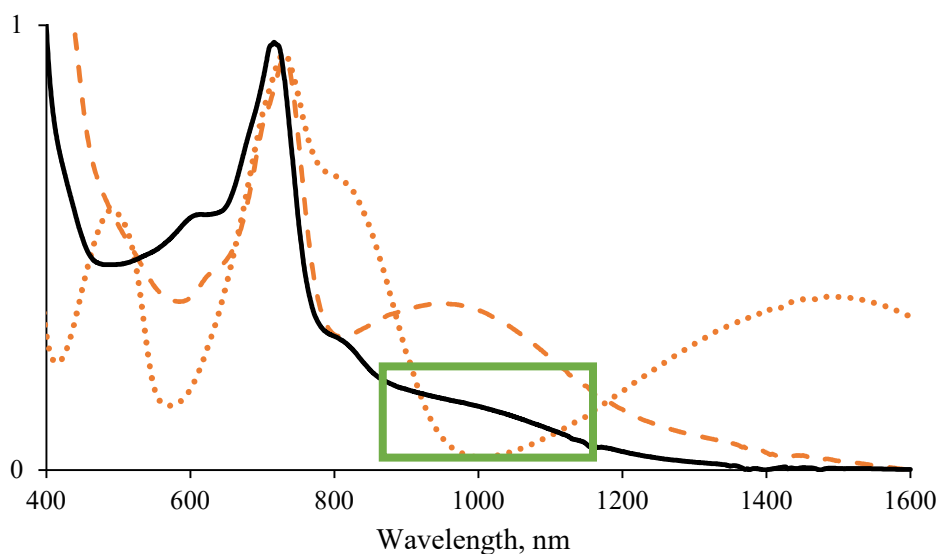
(A)
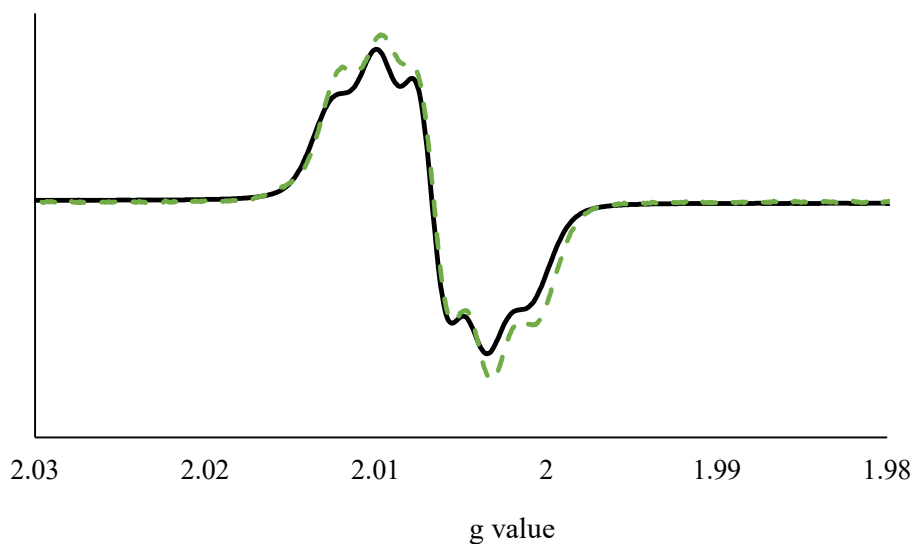
(B)

Fig 12. (A) The UV/Vis/NIR spectra of aliquots from reactions between TiCl₄ and 4,4'-dibromotriphenylamine (solid black trace), (BrPh)₃N, freshly prepared (dashed orange line) and (BrPh₃N), aged over a week (dotted orange line). (B) The EPR signal from a reaction between TiCl4 and 4,4'-dibromotriphenylamine (solid black line) and that between TiCl₄ and triphenylamine (dashed green line).

Through our study of the above bromo-substituted amines, it became gradually apparent that bromine substituents on triphenylamine affected coupling reactions in a few key ways that make them distinct from the unsubstituted amine, while maintaining similarities in some other ways. First, a ready dissociation of the *p*-bromo group and its carbon seat must be occurring facilely once the radical amine is formed. Second, this radical species, now short one Br-group, is subject to the same Ti^{IV} vs Sb^V discrimination of product. The Sb^V oxidant does not allow for formation of a $TAPD^+$ product, however fleeting, while in case of the Ti^{IV} aided reactions, a new C-N bond and hence, a $TAPD^+$ product, appears to be forming. This much is in keeping with the chemistry we saw triphenylamine perform. However, unlike in the case of triphenylamine, the

156

solvent-dependent selectivity of the TAPD$^+$ product and its subsequent crystallization in high yield does not occur in case of the bromo-substituted triphenylamines, and any C-N bonded product is swiftly replaced with the TAB$^+$ and/or TAB^{2+} species, the second of which can be more reliably crystallized, possibly due to it being more "terminal" in terms of oxidation state.

Methyl substitution

To conclude this study and supply a more final takeaway regarding the reactivity of substituted arylamines, we examine one final set of substituted amines, 4-methyltriphenylamine and 4,4'-dimethyltriphenylamine, shown in Figure 13.
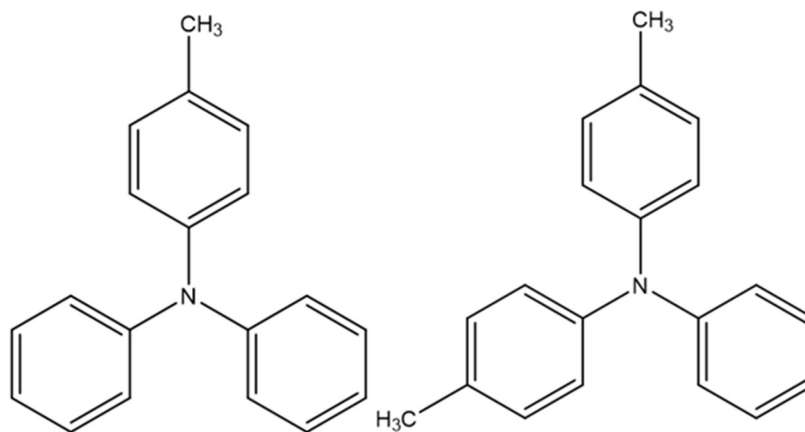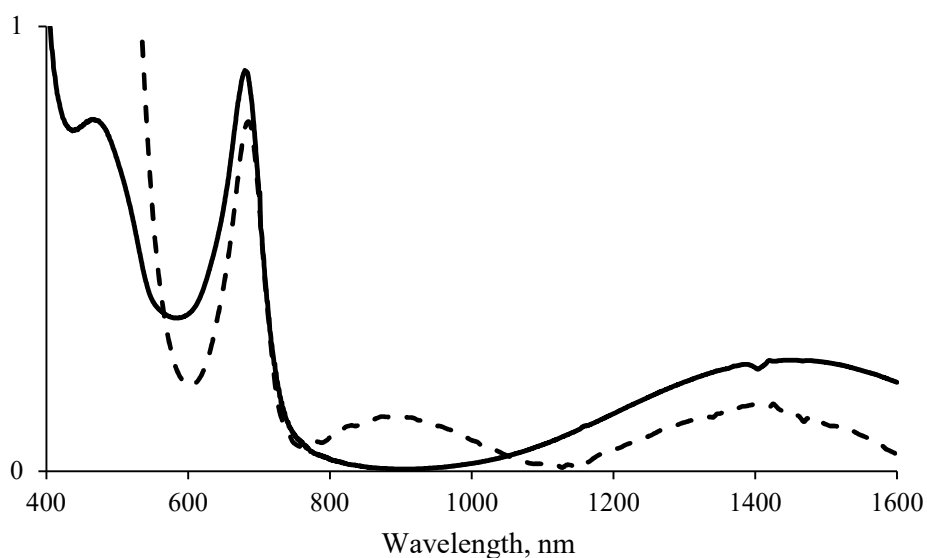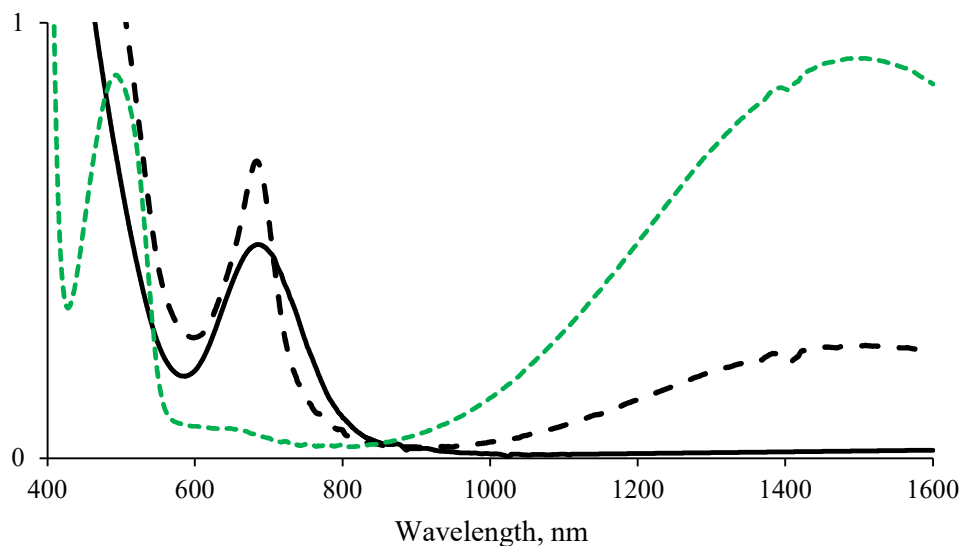

Fig 13. 4-methyltriphenylamine and 4,4'-dimethyltriphenylamine

Figure 14A shows an optical spectrum of a reaction between 4-methyltriphenylamine and TiCl$_4$, freshly combined (dashed black line), and a day old (solid black line). As can be predicted by now, the fresh aliquot contains the visible band for uncoupled arylamine, the Vis-NIR band for the TAPD$^+$ product, and the NIR band for the TAB$^+$ product. The day-old spectrum appears to be a mixture of simply the uncoupled amine and TAB$^+$ product. Figure 14B shows the spectrum for reactions between 4,4'dimethyltriphenylamine and SnCl$_4$ immediately after combining (dashed green line) and the spectra for reactions between the same amine and TiCl$_4$, promptly after mixing

(dashed black line) and at equilibrium (solid black line). This is a curious set of spectra. The green trace, or Sn^{IV} reaction, shows unmistakable TAB^+ product, which the freshly-combined Ti^{IV} reaction mixture also exhibits. However, it appears that prolonged standing causes the Ti^{IV} reaction to revert to what resembles mostly the uncoupled amine radical. This reaction contains no trace of the $TAPD^+$ product, not even immediately after combining, or in case of the Sn^{IV}-mediated reaction where $TAPD^+$ product has usually been detected exclusively upon immediate reaction.

(A)

(B)

Figure 14. (A) The reactions of 4-methyltriphenylamine with TiCl₄, immediately after combining (dashed black line) vs two days old (solid black line). (B) The reactions of 4,4'-dimethyltriphenylamine, with SnCl₄ (dashed green line) and TiCl₄ (dashed black line) both promptly after combination, as well as with TiCl₄ after equilibrating (solid black line).

To get a sense of the locations of the signals of each triarylamine radical and its TAB⁺ dimer, we may look at the comparison in Figure 15. The blue trace represents an equilibrated reaction mixture of (BrPh)₃N and SbCl₅ (or, a slightly aged "magic blue" solution; the red trace indicates 4,4'-dibromotriphenylamine (and Sb^V), and the yellow and green trace indicate 4-methyltriphenylamine and 4,4'-dimethyltriphenylamine respectively, with Ti^{IV} as oxidant. A dashed black line shows the Sb^V mediated triphenylamine dimerization as a reference. The absorption for Br-containing amine radicals (uncoupled, as a single N center) occur at higher wavelength than the uncoupled amine radicals for the methyl-containing amines. Based on the location of the uncoupled, unsubstituted triphenylamine absorption band, the substituents cause a bathochromic shift of the triarylamine signal (Br more so than CH₃) However, we cannot

159

determine a clear trend as to the λ_{max} for the NIR band in any of these cases, nor contrast it with tetraphenylbenzidine itself.
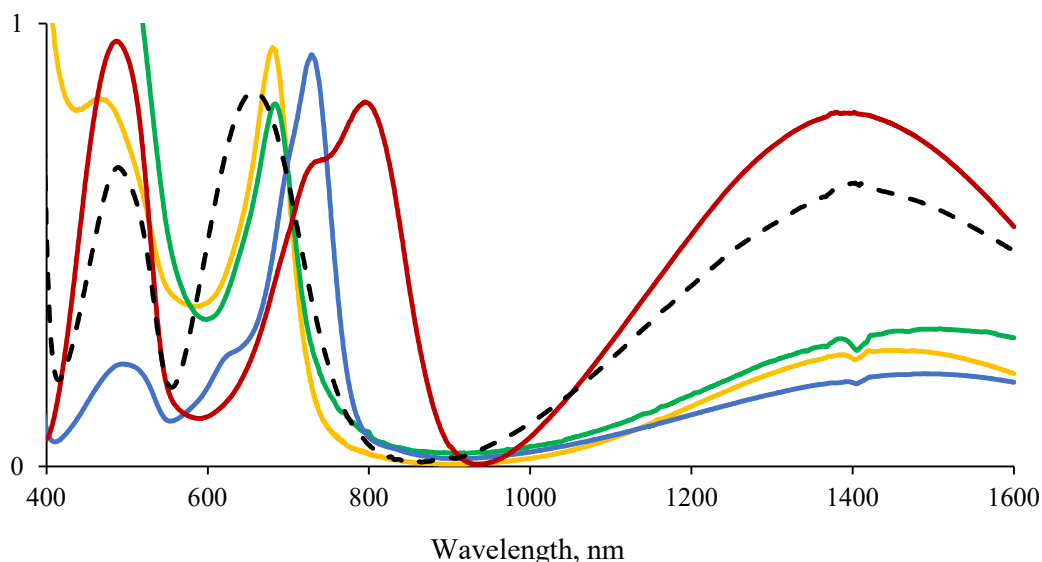

Fig 15. Comparing the triarylamine and TAB$^+$ bands for the reactions of 4-methyltripenylamine (yellow), 4,4'-dimethyltriphenylamine (green), tris(p-bromophenyl)amine (blue), 4,4'-dibromotriphenylamine (red) and triphenylamine (black, dashed).

The only crystalline product to be isolated from the methyl-substituted triphenylamine reactions is shown below in Figure 16. The radical product is N,N,N',N'-tetrakis(p-tolyl)benzidine$^+$, counterbalanced by the previously observed Ti$^{III}_3$Cl$_{10}^-$ subunit of the (Ti$^{III}_3$Cl$_{10}$)$_n^{n-}$ polymeric anion. As in the case of the tetraphenylbenzidine$^+$ crystal structure, the asymmetric unit consists of the half cation. However, unlike in case of the analogous tetraphenylbenzidine compound, an optical spectrum of the redissolved crystal shows TAB$^+$ signal exclusively and no reverting to triphenylamine$^+$.
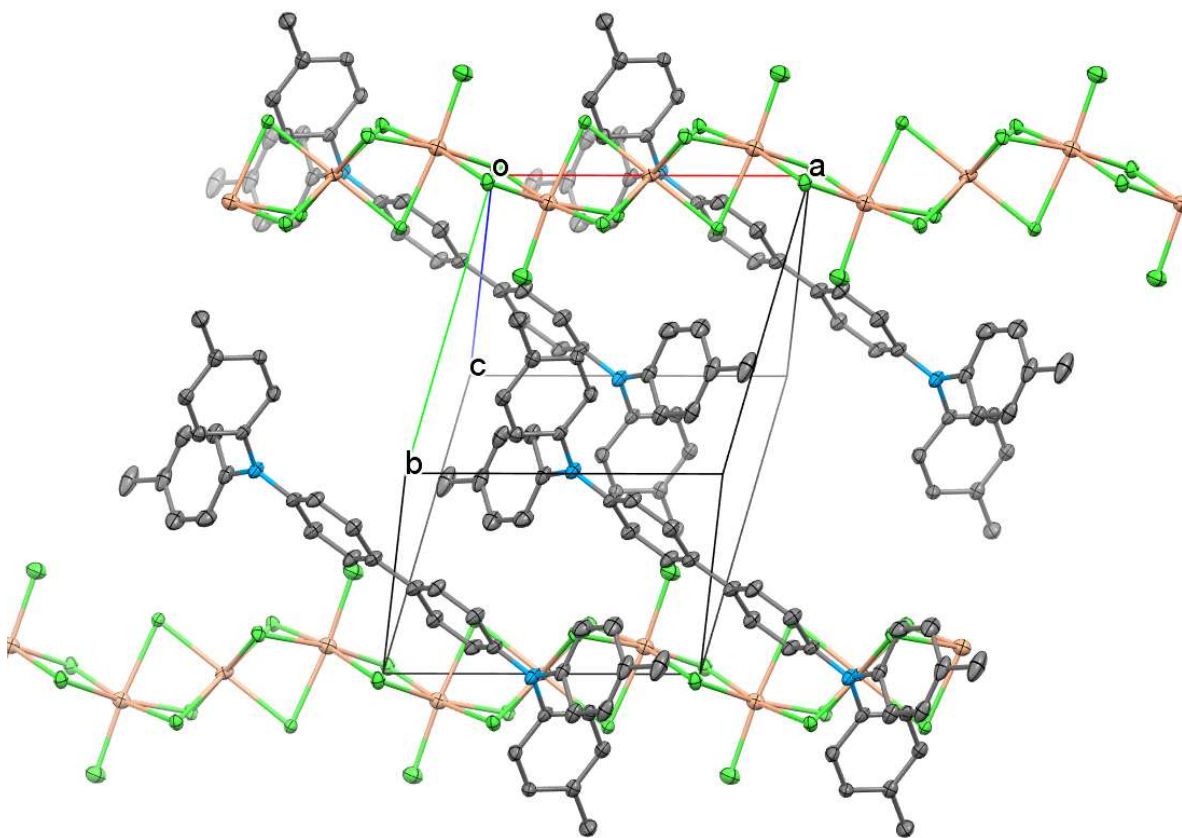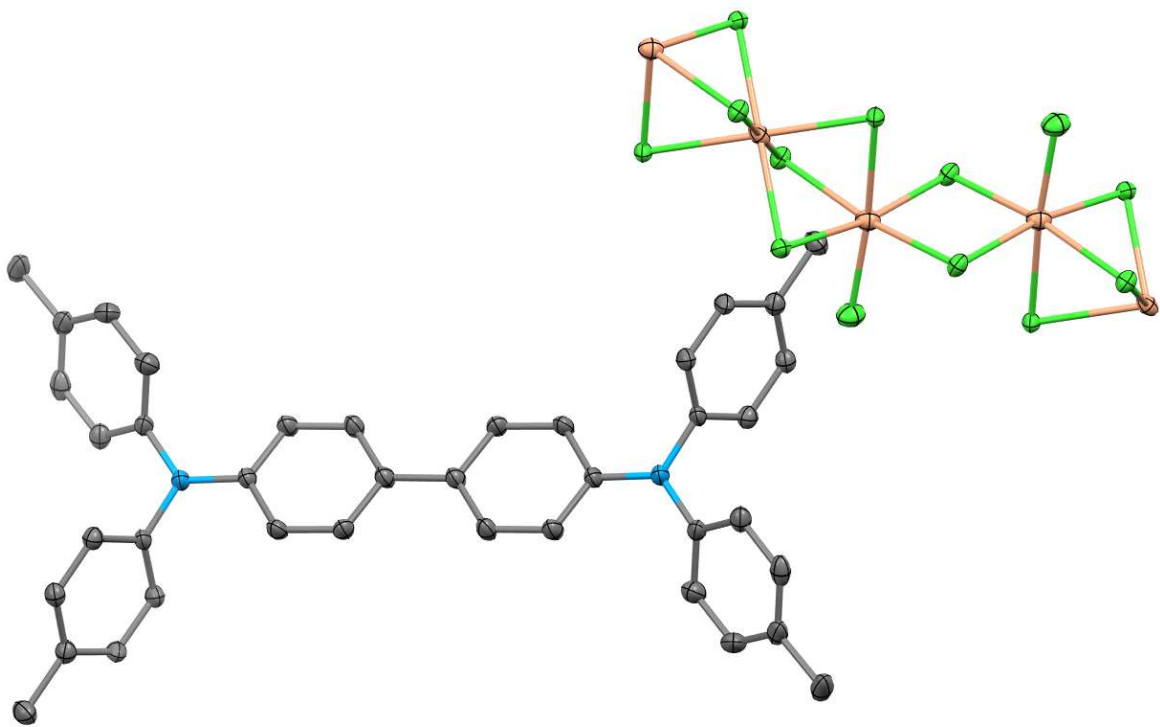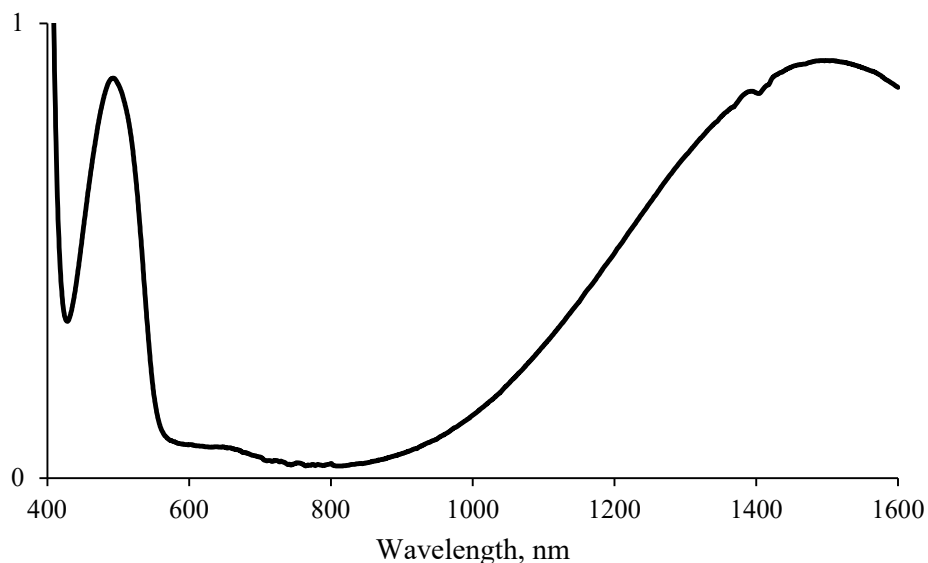
Fig 16. Top – a view of the full radical cation of N,N,N',N'-tetrakis(*p*-tolyl)benzidine[+] accompanied by a part of the polymer chain. Middle – a look at one packed unit cell. Bottom – an optical spectrum of the redissolved crystals.

Conclusion

All of the substituted and unsubstituted diamine species listed in this discussion of amine coupling may be thought of as belonging to Class III of the Robin-Day Classification[3] due to thorough delocalization of the unpaired electron across 2 identical nitrogen atoms. This type of "bridged" intervalent species are of particular interest in the design of tunable optoelectronic materials where bridge length may be used as a parameter to control charge-transfer properties.4,[5] While both π-bridged diamines[6] and triphenylamine derivatives7,[8] have been separately evaluated as candidates for charge-transport, not many studies have successfully explored the possibility of their existence in tandem or the conversion of one to the other – which process might already be contributing to the charge-transport behavior of these systems. By supplying a detailed look into the controlled coupling of triarylamines in-situ, establishing pathways for reagent-selected tuning

of the π-bridge, and characterizing the products of our study structurally, we open up a new door into future detailed electronic and mechanistic studies that would further the workings of triphenylamine-derived optoelectronic systems.

Our study shows a dependence of preferred product on the metal halide. It is interesting to note that $TiCl_4$, a one-electron oxidant, and $SnCl_4$, a two-electron oxidant, behave similarly by forming the phenylene product in all cases, but particularly in the case of triphenylamine where the phenylene product is crystallized as a radical cation salt. In contrast, $SbCl_5$, another two-electron oxidant, reacts with triphenylamine to generate the benzidine product. A *proposed* and *entirely speculative* mechanism for the formation of (N,N,N',N'-tetraphenyl-1,4-benzenediamine$^+$)(Ti$^{IV}_2$Cl$_9^-$) is presented in Scheme 2. The reaction starts with the oxidation of triphenylamine to its radical cation and the reduction of $TiCl_4$ to $TiCl_3$ – however it may not be in the form of discrete $TiCl_3$ molecules since the instances where a Ti^{III} counterion crystallized involved formation of a Ti^{III} chloride polymer. The EPR spectra taken in acetonitrile confirm the formation of Ti^{III} during this process. Computations involving the triphenylamine radical cation have shown that the unpaired electron is largely localized on the nitrogen atom.[9] Subsequently, the triphenylamine radical cation can react with a triphenylamine molecule to form the crucial C-N bond. This bond forming reaction is followed by the loss of benzene and the formation of the salt, (N,N,N',N'-tetraphenyl-1,4-benzenediamine$^+$)(Ti$^{IV}_2$Cl$_9^-$)•toluene. A similar mechanism with altered stoichiometry can be operating for the oxidations with the two-electron oxidant tin(IV) tetrachloride, with two equivalents of amine oxidized to the radical state for each tin(IV) reduced. In contrast, the oxidation of triphenylamine with $SbCl_5$ produced the tetraphenylbenzidine radical cation in form of a crystalline salt. Thus, the nature of the Lewis acid oxidant influences the outcome of triphenylamine oxidation in a manner not previously recognized. It is possible that the

differences in behavior of these different Lewis acid oxidants may be attributed to fleeting coordination of the Lewis acidic metal-center with the amine, a situation which may alter the amine reactivity and account for the metal-dependent nature of these crystallization outcomes. For example, in the case of titanium tetrachloride, the adduct could exist as a coordination compound, $Ph_3NTi^{IV}Cl_4$, or as an ion pair, $(Ph_3N^{\bullet}+)(Ti^{III}Cl_4^-)$ with each providing altered reactivity of the amine.
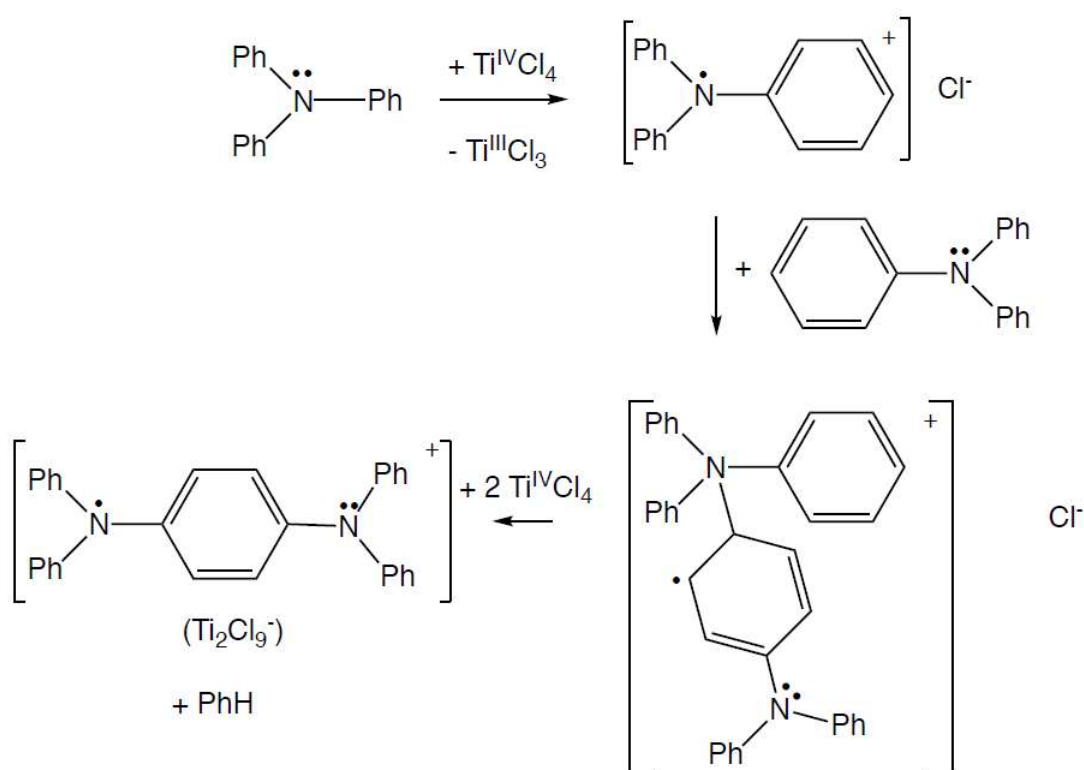
Scheme 2. Proposed mechanism for the formation of (N,N,N',N'-tetraphenyl-1,4-benzenediamine$^+$)(Ti$^{IV}_2$Cl$_9^-$)

References

(1)   Talipov, M. R.; Hossain, M. M.; Boddeda, A.; Thakur, K.; Rathore, R. A Search for Blues Brothers: X-Ray Crystallographic/Spectroscopic Characterization of the Tetraarylbenzidine Cation Radical as a Product of Aging of Solid Magic Blue. *Organic and Biomolecular Chemistry* **2016**, *14* (10). https://doi.org/10.1039/c6ob00140h.

(2)   Chiu, K. Y.; Su, T. H.; Huang, C. W.; Liou, G. S.; Cheng, S. H. Substituent Effects on the Electrochemical and Spectral Characteristics of N,N,N',N'-Tetraaryl-p-Phenylenediamine Derivatives. *Journal of Electroanalytical Chemistry* **2005**, *578* (2). https://doi.org/10.1016/j.jelechem.2005.01.010.

(3)   Robin, M. B.; Day, P. Mixed Valence Chemistry-A Survey and Classification. *Advances in Inorganic Chemistry and Radiochemistry* **1968**, *10* (C). https://doi.org/10.1016/S0065-2792(08)60179-X.

(4)   Lambert, C.; Nöll, G. The Class II/III Transition in Triarylamine Redox Systems. *Journal of the American Chemical Society* **1999**, *121* (37). https://doi.org/10.1021/ja991264s.

(5)   Bailey, S. E.; Zink, J. I.; Nelsen, S. F. Contributions of Symmetric and Asymmetric Normal Coordinates to the Intervalence Electronic Absorption and Resonance Raman Spectra of a Strongly Coupled *P*-Phenylenediamine Radical Cation. *Journal of the American Chemical Society* **2003**, *125* (19). https://doi.org/10.1021/ja021343v.

(6)   Ganzorig, C.; Suga, K.; Fujihira, M. P-Type Semiconductors of Aromatic Diamines Doped with $SbCl_5$. *Chemistry Letters* **2000**, No. 9. https://doi.org/10.1246/cl.2000.1032.

(7)   Coropceanu, V.; Lambert, C.; Nöll, G.; Brédas, J. L. Charge-Transfer Transitions in Triarylamine Mixed-Valence Systems: The Effect of Temperature. *Chemical Physics Letters* **2003**, *373* (1–2). https://doi.org/10.1016/S0009-2614(03)00553-0.

(8)   Liang, M.; Chen, J. Arylamine Organic Dyes for Dye-Sensitized Solar Cells. *Chemical Society Reviews* **2013**, *42* (8). https://doi.org/10.1039/c3cs35372a.

(9)   Pacansky, J.; Waltman, R. J.; Seki, H. Ab Initio Computational Studies on the Structures and Energetics of Hole Transport Molecules: Triphenylamine. *Bulletin of the Chemical Society of Japan* **1997**, *70* (1). https://doi.org/10.1246/bcsj.70.55.

List of Publications

1. Gralinski, S. R., Roy, M., Baldauf, L. M., Olmstead, M. M., Balch, A. L. Introduction of a $(Ph_3P)_2Pt$ group into the rim of an open-cage fullerene by breaking a carbon–carbon bond. *Chemical Communications*, **2021**, *57*(79), 10218-10221.

2. Roy, M.; Diaz Morillo, I. D.; Carroll, X. B.; Olmstead, M. M.; Balch, A. L. Solvent and Solvate Effects on the Cocrystallization of C_{60} with $Co^{II}(OEP)$ or $Zn^{II}(OEP)$ (OEP = Octaethylporphyrin). *Crystal Growth and Design* **2020**, *20*(8).

3. Stevenson, S.; Rothgeb, A. J.; Tepper, K. R.; Duchamp, J.; Dorn, H. C.; Powers, X. B.; Roy, M.; Olmstead, M. M.; Balch, A. L. Isolation and Crystallographic Characterization of Two, Nonisolated Pentagon Endohedral Fullerenes: $Ho_3N@C_2(22010)$-C_{78} and $Tb_3N@C_2(22010)$-C_{78}. *Chemistry - A European Journal* **2019**, *25* (54).

4. Roy, M.; Olmstead, M. M.; Balch, A. L. Metal Ion Effects on Fullerene/Porphyrin Cocrystallization. *Crystal Growth and Design* **2019**, *19* (11). https://doi.org/10.1021/acs.cgd.9b01092.

5. Roy, M.; Walton, J. H.; Fettinger, J. C.; Balch. A. L. Carbon-Nitrogen Bond Formation and Direct Crystallization of Diamine Radical Cations from the Reactions of Triphenylamine with Titanium(IV) Chloride, Titanium(IV) Bromide, Tin(IV) Tetrachloride but not with Antimony(V) Pentachloride. *Submitted.*

6. Roy, M.; Walton, J. H.; Fettinger, J. C.; Balch. A. L. Carbon-Nitrogen Bond Formation and Direct Crystallization of Diamine Radical Cations from the Reactions of Substituted Triphenylamine. *(manuscript in preparation)*